IN-34

143 P

(NASA-TM-4479) SCHLIEREN PHOTOGRAPHS AND INTERNAL PRESSURE DISTRIBUTIONS FOR THREE-DIMENSIONAL SIDEWALL-COMPRESSION SCRAMJET INLETS AT A MACH NUMBER OF 6 IN CF4 (NASA) 143 p

N94-10644

Unclas

H1/34 0179684

NASA Technical Memorandum 4479

Schlieren Photographs and Internal Pressure Distributions for Three-Dimensional Sidewall-Compression Scramjet Inlets at a Mach Number of 6 in CF_4

Scott D. Holland
Langley Research Center
Hampton, Virginia

National Aeronautics and
Space Administration
Office of Management
Scientific and Technical
Information Program
1993

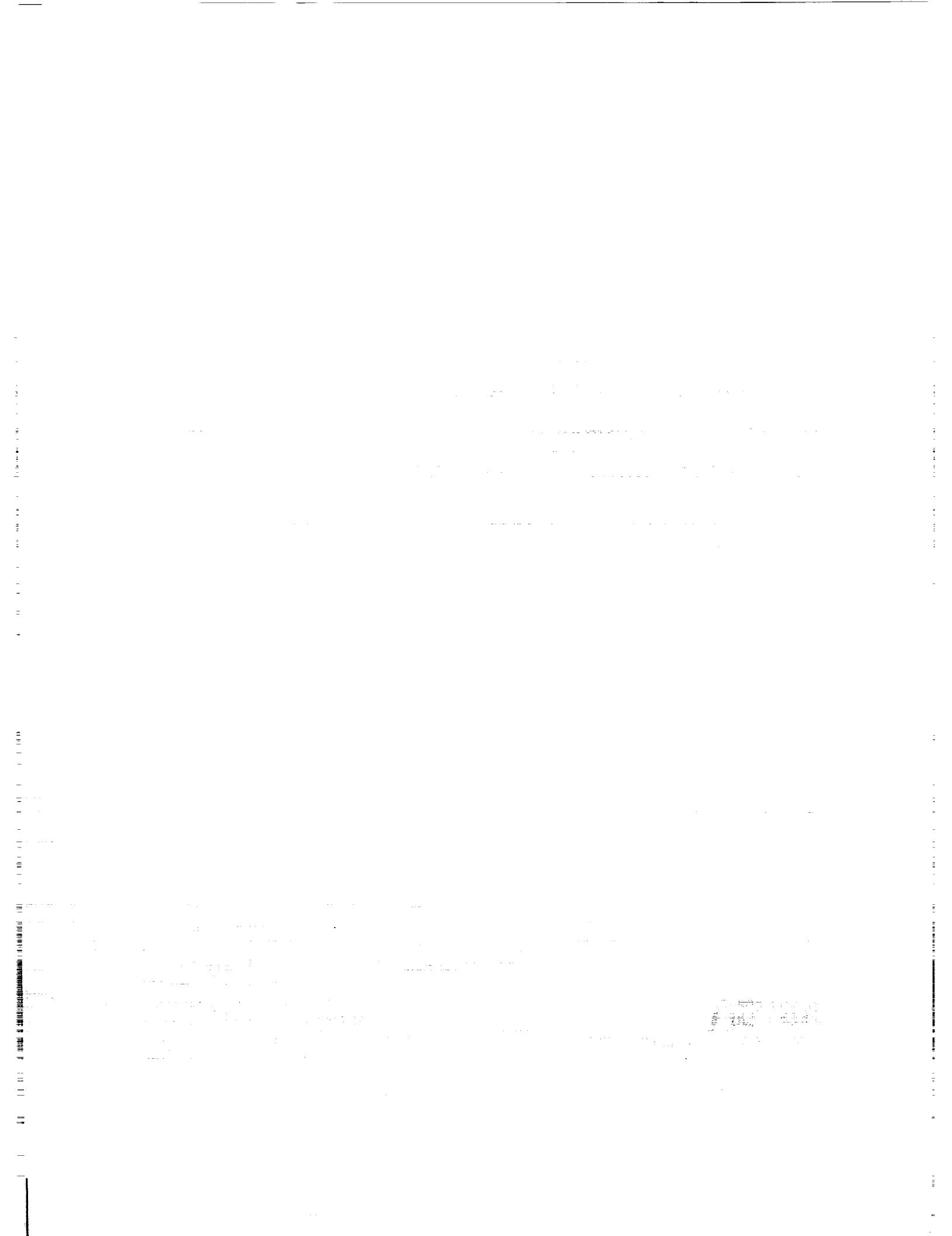

Abstract

Three-dimensional sidewall-compression scramjet inlets with leading-edge sweeps of 30° and 70° have been tested in the Langley Hypersonic CF_4 Tunnel at a Mach number of 6 and a free-stream ratio of specific heats of 1.2. The parametric effects of leading-edge sweep, cowl position, contraction ratio, and Reynolds number were investigated. The models were instrumented with static pressure orifices distributed on the sidewalls, baseplate, and cowl. Schlieren movies were made of selected tunnel runs for flow visualization of the entrance plane and cowl region. Although these movies could not show the internal flow, the effect of the internal flow on the external flow was evident by way of spillage. The purpose of the present report is to provide a preliminary data release for the investigation. The models, facility, and testing methods are described, and the test matrix and a tabulation of tunnel runs are provided. Line plots highlighting the stated parametric effects and a representative set of schlieren photographs are presented without analysis.

Introduction

Hypersonic cruise vehicles such as the National Aero-Space Plane (X-30) have been reported to make use of supersonic combustion ramjets for high Mach number propulsion (refs. 1 and 2). Such propulsion systems are highly integrated with the airframe to exploit the compression caused by the forebody bow shock. (The advantages of propulsion-airframe integration have been well recognized for many years (ref. 3).) The precompression of the flow in the vertical direction upstream of the engine inlet is demonstrated in figure 1. The boundary layer at the inlet entrance on a full-scale hypersonic vehicle can be large with respect to the inlet height. (Computational results have been presented in ref. 4 for inflow boundary layers as large as 20 percent of the inlet height.) As a result, further turning in the vertical direction, as in two-dimensional inlets, greatly increases the probability of large-scale separation regions at the entrance of the inlet because of the shock/boundary-layer interaction. The scale and nature of these interactions depend strongly upon the state of the boundary layer (i.e., whether laminar, transitional, or turbulent); for this series of tests, the boundary layer entering the inlet is laminar.

The sidewall-compression inlet (fig. 2) represents a three-dimensional configuration wherein further flow compression is accomplished in the horizontal direction by wedge-shaped sidewalls that reduce the total vertical turning that the flow must encounter to obtain the desired pressure rise. The leading edges of these sidewalls are swept both to reduce aerothermal loads, hence cooling requirements on the leading edge, and to increase inlet flow spillage to aid in starting the fixed-geometry inlet at the lower Mach numbers. The aft sweep has the effect of turning the flow away from the forebody plane (spilling out ahead of the cowl); as the Mach number is increased, the sidewall shock angles become smaller, thus effectively reducing the spillage window and increasing the mass capture (ref. 5).

Three-dimensional sidewall-compression scramjet inlet models with leading-edge sweeps of 30° and 70° have been tested in the Langley Hypersonic CF_4 Tunnel at a Mach number of 6 with a free-stream ratio of specific heats of 1.2. The models were instrumented with static pressure orifices distributed on the sidewalls, baseplate, and cowl to quantify the effects of leading-edge sweep, cowl position, contraction ratio, and Reynolds number. Schlieren movies were made for flow visualization.

This report identifies inlet characteristics in tetrafluoromethane (CF_4) as a first step toward obtaining a characterization of simulated real-gas effects on inlet flow fields. Traditionally, CF_4 has been used for blunt body research (refs. 6–8) to simulate the decrease in the ratio of specific heats (γ) that occurs within a dissociating shock layer surrounding a vehicle that is reentering the atmosphere. The direct effect of a decreased γ is an increase in the normal-shock density ratio, which has been shown to be a primary factor in determining the inviscid characteristics of the hypersonic flow surrounding a reentering vehicle. Midden and Miller (ref. 9) point out that for relatively slender bodies and lifting bodies, the simulation of low γ effects is approximate because of the variation of γ within the shock layer along or around a reentering vehicle, which is in contrast to the nearly constant γ within the shock layer in CF_4. In spite of this effect, they note the importance of such tests in

providing a lower bound for the assessment of γ effects, which cannot be obtained in other ground test facilities.

In order to obtain the explicit effects of low γ, the model must be tested in both CF_4 and air. This report is a first step toward that end. Further, these tests may be considered exploratory because these models were the largest tested to date in the CF_4 facility. Therefore, it was not known if the tunnel could remain started once the model was injected into the flow. Finally, although the instrumentation density in these tests was insufficient for a true computational fluid dynamics (CFD) validation, this test in CF_4 (a virial gas) provides a set of data that may be used to compare with CFD calculations for which the assumption of a perfect gas is not valid. This report provides a preliminary data release for the investigation. The models, facility, and testing methods are described, and the test matrix and a tabulation of tunnel runs are provided. Line plots highlighting the stated parametric effects and a representative set of schlieren photographs are presented without analysis.

Symbols and Abbreviations

Values are given in the U.S. Customary Units, but they are occasionally given in SI Units or in both where considered useful.

C_p	pressure coefficient, $\left(\frac{2}{\gamma_1 M_1}\right)\left(\frac{p}{p_1}-1\right)$
C'_x	distance from throat entrance to cowl leading edge, in.
CR	contraction ratio, W/g
g	throat gap (see fig. 4), in.
H	height of inlet, 2.75 in.
h	enthalpy, J/kg (Btu/lbm)
I.D.	inside diameter
M	Mach number
N_{Pr}	Prandtl number
N_{Re}	Reynolds number
p	static pressure, N/m^2 (psia)
q	dynamic pressure, N/m^2 (psia)
T	static temperature, K (°R)
T_x	distance from baseplate leading edge to inlet throat (see fig. 4), in.
T'_x	distance from sidewall leading edge to inlet throat (see fig. 4), 5.04 in.
u	velocity, m/sec (ft/sec)
W	inlet width at sidewall leading edge, in.
x	axial distance measured from baseplate leading edge (see fig. 4), in.
x'	local axial distance measured from sidewall leading edge (see fig. 4), in.
y	vertical distance from baseplate, in.
Z	compressibility factor
z	lateral distance from inlet plane of symmetry, in.
γ	ratio of specific heats
δ	sidewall-compression angle, deg
Λ	leading-edge sweep angle, deg
μ	viscosity, N-sec/m^2 (lbm/ft-sec)
ρ	density, kg/m^3 (lbm/ft^3)

Subscripts:

t	total conditions
1	wind-tunnel free-stream conditions
2	postshock conditions

Experimental Methods

Model Description

The generic, three-dimensional sidewall-compression inlets used in the present report have been under study for several years. (In ref. 10 Northam and Anderson traced the development of scramjet research at the Langley Research Center.) Much of the early work on this type of inlet was performed by Trexler in references 11–15, and his notation is used in the present investigation. Photographs of the inlet models are shown in figure 3, and sketches are presented in figure 4. Sidewall leading-edge sweeps of 30° and 70° were selected to represent both moderately and highly swept models. As a result of a trade study (ref. 13), the sidewall compression angle was fixed at 6°. This angle was a compromise between larger compression angles (leading to stronger internal shocks with increased probability of boundary-layer separation) and smaller compression angles (leading to weaker internal shocks but requiring the inlet to be longer to obtain the same compression, and thus imposing a size and weight penalty on the inlet).

The models were 2.75 in. tall and were machined of aluminum; the sidewalls had leading-edge diameters of 0.010 in., and the baseplate and cowl each had a leading-edge diameter of 0.015 in. and 10° of external compression. The models were injected into the tunnel in an inverted orientation, with the cowl on top. The vehicle forebody plane was represented by a flat plate and is referred to as the *baseplate*. The model was uncooled. Because the forebody boundary layer was not modeled, the configuration was said to be "uninstalled."

The 30° sidewall model was originally designed for a parametric study of inlet starting performance (ref. 14) and was instrumented only to the extent necessary to determine if unstart had occurred. A number of pressure taps were added to the 30° model, a 70° leading-edge-sweep model was fabricated, and then both were tested in the 22-inch aerodynamics leg of the Langley Hypersonic Helium Tunnel at Mach numbers of 18.1 and 21.6 (ref. 15). Because these models were adapted from previous test programs, the number and location of the instrumentation were not optimal. Static orifices (with 0.040-in. inside diameter) were arranged in single arrays located along the centerlines of the baseplate, sidewall, and cowl, and also on the sidewall at $y/H = 0.13$ (near the baseplate) and $y/H = 0.87$ (near the cowl), as shown in figure 4.

The contraction ratio is defined as the ratio of the inlet entrance area to the throat area. Because the present configuration is characterized by a constant height, the contraction ratio reduces to the ratio of the inlet entrance width (W) to the throat gap (g). (See fig. 4.) This W/g ratio can be varied between the runs by laterally moving the sidewalls. The cowl position can also be changed between runs. For the present study, the cowl was placed at the throat (referred to as *0-percent cowl*) and forward of the throat 25 percent of the distance between the throat and the sidewall leading edge (referred to as *25-percent cowl*).

Facility Description

Since the time that these tests were made, the Langley Hypersonic CF_4 Tunnel has undergone major upgrades. A description of the present upgraded facility is presented in reference 16, and a detailed description of the facility as it existed at the time of these tests is presented in reference 9. The important features of the original tunnel that pertain to these tests are noted herein. Figure 5 presents a schematic of the original tunnel illustrating the major components.

The high-pressure supply system consisted of a CF_4 storage trailer rated for 2500 psia, a compressor capable of 5000 psia, a 5000-psia bottlefield with a storage volume of 120 ft^3, and an externally loaded dome pressure regulator to control the operating pressure of the tunnel. After compression, the gas was heated to a maximum temperature of 1500°R as it flowed through 44 spirally wound stainless steel tubes immersed in two parallel lead-bath heaters. Particles larger than 10 μm were removed from the flow by an in-line filter located between the heater and the settling chamber. The flow was then expanded through a contoured, axisymmetric nozzle with a 0.446-in-diameter throat that was designed to create an $M = 6$ flow at the nozzle exit (approximately 20 in. in diameter). The flow exhausted into an open-jet test section approximately 6 ft in length and 5 ft in diameter, was collected by a diffuser, and was then cooled by a water-cooled heat exchanger before being dumped into vacuum spheres. The spheres had a combined total volume of 72 000 ft^3. These spheres were then evacuated into a reclaimer system.

Prior to a run, the test section, nozzle, settling chamber, and vacuum spheres were evacuated to approximately 0.01 psia. The dome loader was set to the desired reservoir pressure, and the heaters were set to the desired flow temperature. An automated sequencer opened and closed appropriate valves and also controlled the injection and retraction of the model. Although run times up to 30 sec are possible, a run time of 15 sec was found to be adequate for these tests.

Instrumentation

The settling chamber (reservoir) pressure ($p_{t,1}$) was measured with strain gauge pressure transducers having full-scale ratings of either 3000 or 300 psia, depending on the operating condition of the tunnel. The settling chamber (reservoir) temperature ($T_{t,1}$) was measured with two chromel-alumel thermocouples inserted through the wall of the settling chamber and positioned near the center of the chamber. The pitot pressure of the flow in the test section ($p_{t,2}$) was measured by a flat-faced cylindrical probe that was mounted in the test section and linked to an electronically scanned pressure (ESP) silicon sensor module. A second ESP module was used to measure the surface pressures on the model. Each 2.5-psid ESP module contained 32 sensors and was located at the base of the model strut to minimize the tubing length between the pressure orifices on the model and the module. The pressure tubing and ESP modules were insulated to prevent thermal shift of the ESP calibration. The *in situ* calibration consisted

of applying three known pressures (vacuum levels) that were chosen to span the range of the expected measured pressures. A sample rate of 20 samples per second was obtained for the 64 channels.

Schlieren movies were made for flow visualization in the region of the entrance plane and cowl, and they were recorded on 16-mm video news film. The movies, which were shot at 128 frames per second, allowed the flow to be observed on an 8-msec time scale.

Test Conditions

Tests were performed at a nominal Mach number of 6 for reservoir pressures of 300, 1000, and 2000 psia at a reservoir temperature of 1200°R. The test matrix for both models is given in tables 1 and 2. Free-stream and postnormal-shock flow properties were calculated using a procedure outlined in reference 9. The nominal free-stream Reynolds numbers obtained under these conditions were 0.89×10^5, 2.85×10^5, and 5.50×10^5 per foot, respectively. Free-stream static pressures were quite low: 0.01 psia, 0.03 psia, and 0.05 psia, respectively. The free-stream ratio of specific heats was 1.2. Tables 3–5 present free-stream and postnormal-shock flow conditions for the three Reynolds numbers. A listing of tunnel runs correlating the test conditions, model configurations, and run numbers is given in table 6.

Pitot-rake surveys of the flow in the test section were performed previously for reservoir pressures ranging from 100 to 400 psia and 1000 to 2500 psia (ref. 9). Each of the surveys showed a uniform core but with a centerline disturbance. At the lower reservoir pressures, a second disturbance was located at a radius of 4 in. from the centerline. Because the model was only 2.75 in. tall, it was injected 1 in. above the centerline, thereby avoiding injestion of either disturbance. The diameter of the core varied weakly with reservoir pressure from 14 in. at 300 psia to 15 in. at 2000 psia. In each case, the model was completely immersed in the core, free from tunnel boundary-layer interference.

Test Medium

In 1969 Jones and Hunt (ref. 6) pointed out that the purpose of the CF_4 Tunnel was to provide a conventional wind tunnel that could simulate the increased normal-shock density ratios (from 10 to 20) and the decreased ratio of specific heats (to as low as 1.1) encountered in hypervelocity flight because of the chemical dissociation of the postshock flow. In 1981 Sutton (ref. 17) indicated that conventional air or nitrogen tunnels are limited to $\gamma = 1.4$ and a density ratio of approximately 6 and that helium tunnels are limited to $\gamma = 1.67$ and a normal-shock density ratio of 4; however, he showed that the CF_4 Tunnel provides a normal-shock density ratio of 12 with $\gamma < 1.4$. The thermodynamic and transport properties of CF_4 may be found in Chari (ref. 18), Hunt and Boney (ref. 19), and Talcott (ref. 20), and relations are presented in a form amenable to flow field computer codes in Sutton (ref. 17). Although the relations must generally account for intermolecular force effects and high-temperature effects, in the test section the gas has been expanded to such a low pressure that intermolecular force effects and high-temperature effects are negligible in both the free stream and behind a normal shock. For these tests, therefore, CF_4 can be treated as thermally perfect ($Z = 1$) and calorically imperfect, with the specific heats given as functions of temperature only (ref. 17).

Data Reduction and Uncertainty

Measured values of $p_{t,1}$ and $T_{t,1}$ are believed to be accurate to within 2 percent (ref. 9). Values of p/p_1 are estimated to be accurate to within 4 percent, based on manufacturer's specifications for the given pressure levels. Run-to-run repeatability was examined for two configurations. The mean absolute deviation of the set of measured pressures for both configurations was less than 4 percent and hence was less than the uncertainty of the measurement.

Results and Discussion

The purpose of the present report is to provide a preliminary data release for the investigation. Selected sets of schlieren photographs are presented first. Then, line plots of the pressure data are presented that highlight the parametric effects of contraction ratio, cowl position, Reynolds number, and leading-edge sweep. Line plots demonstrating run-to-run repeatability for each of the two configurations are also presented.

Schlieren Movies

Schlieren movies of the entrance plane and cowl region showed that the flow was steady on an 8-msec time scale. When combined with the pressure measurements, these movies indicated that the inlet started for each configuration tested and remained started for the duration of the test. Although these movies could not detail the internal flow features, the effects of the internal flow on the external flow were evident by way of spillage. (A small quantity of silicone sealant was placed on the external surface of the cowl to protect the pressure tubing leading from

the cowl. A bow shock is visible because of the silicone sealant, but it is located far enough downstream of the cowl lip that it does not appear to interfere with the flow into the inlet.) The view, which is a profile of the inlet, is shown in an inverted (relative to flight) orientation with the cowl on top. Note that the schlieren photographs present an integrated view across the span of the inlet. Two-dimensional features (i.e., features that are constant across the width of the inlet), such as the shocks on the underside of the baseplate, appear in sharp detail. Because of the horizontal orientation of the knife edge in the schlieren system, increases in density (shocks) appear dark in the top half of the frame. Interpretation of the schlieren image in the region above the inlet is complicated by the fact that the shock waves are skewed relative to the plane of the schlieren.

Photographs of enlarged frames from the schlieren movies are presented in figure 6 for selected $\Lambda = 30°$ models and in figure 7 for selected $\Lambda = 70°$ models. Because of the process involved in transferring a 16-mm video frame into a print for inclusion in this report, considerable degradation of the original image occurs. Fine details in the originals have, in many cases, been lost.

Pressure Data

Tables 7–33 provide the absolute magnitude of p, p/p_1, and C_p for each pressure orifice for each of the tunnel runs. Line plots that highlight the effects of contraction ratio, cowl position, Reynolds number, and leading-edge sweep are presented. Plots that superimpose the pressure distributions on all surfaces of a given configuration are designated "configuration-complete" plots and are presented to indicate the overall flow structure. Configuration-complete plots for the $\Lambda = 30°$ and $70°$ models are presented in figures 8 and 9, respectively.

The effects of varying a given parameter for a number of model configurations can be studied. For example, contraction ratio effects can be examined for three cowl positions and two leading-edge sweep angles. Although this examination leads to a large number of plots, each of the possible plot combinations are presented so that the effects of one parameter can be studied over a broad range of configurations, and a listing of the parameters for each plot is provided in table 34.

Contraction ratio effects for the $\Lambda = 30°$ model at $N_{Re} = 5.50 \times 10^5$ per foot for 0-percent cowl, 25-percent cowl, and no cowl are presented in figures 10, 11, and 12, respectively. Likewise, figures 13, 14, and 15 document the same effects for the $\Lambda = 70°$ model. The effects of cowl position are presented for the $\Lambda = 30°$ model at $N_{Re} = 5.50 \times 10^5$ per foot for CR = 3, 5, and 9 in figures 16, 17, and 18, respectively, and for the $\Lambda = 70°$ model in figures 19, 20, and 21, respectively. The effects of Reynolds number are presented for the $\Lambda = 30°$ model at CR = 3 with 0-percent cowl in figure 22 and for the $\Lambda = 70°$ model at CR = 9 with 25-percent cowl in figure 23. Leading-edge sweep effects at $N_{Re} = 5.50 \times 10^5$ per foot for CR = 3, 5, and 9 are given in figures 24, 25, and 26, respectively, for the 0-percent cowl position; in figures 27, 28, and 29, respectively, for the 25-percent cowl position; and in figures 30, 31, and 32, respectively, for the no-cowl configuration. Leading-edge sweep effects are also presented for CR = 3 with 0-percent cowl at $N_{Re} = 0.89 \times 10^5$ per foot in figure 33. The two conditions that were used as a measure of repeatability involved the 0- and 25-percent cowl positions of the $\Lambda = 70°$ model at CR = 3 and $N_{Re} = 5.50 \times 10^5$ per foot. These plots are presented in figures 34 and 35, respectively. The data are given in tables 21 and 25 for the 0-percent cowl position and in tables 22 and 24 for the 25-percent cowl position.

Concluding Remarks

The present report has presented the experimental results of tests of three-dimensional sidewall-compression scramjet inlets with leading-edge sweeps of 30° and 70° in the Langley Hypersonic CF_4 Tunnel at a nominal Mach number of 6 and a free-stream ratio of specific heats of 1.2. The parametric effects of leading-edge sweep, cowl position, contraction ratio, and Reynolds number were investigated. Schlieren movies were made of each test for flow visualization of the entrance plane and cowl region. Although these movies could not show the internal flow, the effect of the internal flow on the external flow was evident by way of spillage. Enlarged frames from selected schlieren movies have been presented. For each configuration tested, the inlets were observed to start and remain started for the duration of the test. The flow was also observed to be steady on an 8-msec time scale. The models were instrumented with static pressure orifices distributed on the sidewalls, baseplate, and cowl. Line plots of axial pressure distributions highlighting the stated parametric effects have been presented. The models, facility, and testing methods were described, and the test matrix and a tabulation of tunnel runs were provided.

NASA Langley Research Center
Hampton, VA 23681-0001
May 27, 1993

References

1. Williams, Robert M.: National Aero-Space Plane: Technology for America's Future. *Aerosp. America,* vol. 24, no. 11, Nov. 1986, pp. 18–22.

2. Kandebo, Stanley W.: Researchers Pursue X-30 Spaceplane Technologies for 1990 Evaluation. *Aviation Week & Space Technol.,* vol. 129, no. 6, Aug. 8, 1988, pp. 49–53.

3. Henry, John R.; and Anderson, Griffin Y.: *Design Considerations for the Airframe Integrated Scramjet.* NASA TM X-2895, 1973.

4. Kumar, Ajay; Singh, D. J.; and Trexler, Carl A.: Numerical Study of the Effects of Reverse Sweep on Scramjet Inlet Performance. *J. Propuls. & Power,* vol. 8, no. 3, May–June 1992, pp. 714–719.

5. Holland, Scott D.; and Perkins, John N.: Internal Shock Interactions in Propulsion/Airframe Integrated Three-Dimensional Sidewall Compression Scramjet Inlets. AIAA-92-3099, July 1992.

6. Jones, Robert A.; and Hunt, James L. (appendix A by James L. Hunt, Kathryn A. Smith, and Robert B. Reynolds and appendix B by James L. Hunt and Lillian R. Boney): *Use of Tetrafluoromethane To Simulate Real-Gas Effects on the Hypersonic Aerodynamics of Blunt Vehicles.* NASA TR R-312, 1969.

7. Miller, Charles G., III: *Measured Pressure Distributions, Aerodynamic Coefficients, and Shock Shapes on Blunt Bodies at Incidence in Hypersonic Air and CF_4.* NASA TM-84489, 1982.

8. Micol, John R.: Simulation of Real-Gas Effects on Pressure Distributions for a Proposed Aeroassist Flight Experiment Vehicle and Comparison to Prediction. AIAA-87-2368, Aug. 1987.

9. Midden, Raymond E.; and Miller, Charles G., III: *Description and Calibration of the Langley Hypersonic CF_4 Tunnel A Facility for Simulating Low γ Flow as Occurs for a Real Gas.* NASA TP-2384, 1985.

10. Northam, G. Burton; and Anderson, G. Y.: Supersonic Combustion Ramjet Research at Langley. AIAA-86-0159, Jan. 1986.

11. Trexler, Carl A.: Performance of an Inlet for an Integrated Scramjet Concept. *J. Aircr.,* vol. 11, no. 9, Sept. 1974, pp. 589–591.

12. Trexler, Carl A.: Inlet Performance of the Integrated Langley Scramjet Module (Mach 2.3 to 7.6). AIAA Paper No. 75-1212, Sept.–Oct. 1975.

13. Trexler, Carl A.; and Souders, Sue W.: *Design and Performance at a Local Mach Number of 6 of an Inlet for an Integrated Scramjet Concept.* NASA TN D-7944, 1975.

14. Trexler, Carl A.: Inlet Starting Predictions for Sidewall-Compression Scramjet Inlets. AIAA-88-3257, July 1988.

15. Trexler, Carl A.: *Tests of Two Sidewall-Compression Scramjet Inlets at Mach 18.1 to 21.6 in Helium.* NASP TM-1018, 1988.

16. Micol, John R.; Midden, Raymond E.; and Miller, Charles G., III: Langley 20-Inch Hypersonic CF_4 Tunnel: A Facility for Simulating Real-Gas Effects. AIAA-92-3939, July 1992.

17. Sutton, Kenneth: *Relations for the Thermodynamic and Transport Properties in the Testing Environment of the Langley Hypersonic CF_4 Tunnel.* NASA TM-83220, 1981.

18. Chari, Nallan Chakravartula Satyanarayana: Thermodynamic Properties of Carbon Tetrafluoride. Ph.D. Thesis, Univ. of Mich., 1960.

19. Hunt, James L.; and Boney, Lillian R.: *Thermodynamic and Transport Properties of Gaseous Tetrafluoromethane in Chemical Equilibrium.* NASA TN D-7181, 1973.

20. Talcott, Noel A., Jr.: *Thermodynamic Properties of Gaseous Fluorocarbons and Isentropic Equilibrium Expansions of Two Binary Mixtures of Fluorocarbons and Argon.* NASA TN D-8405, 1977.

Table 1. Test Matrix for $\Lambda = 30°$ Model

Contraction ratio (CR)	Reynolds number per foot at each cowl position—		
	0 percent	25 percent	No cowl
3	0.89×10^5 2.85 5.50	5.50×10^5	5.50×10^5
5	5.50×10^5	5.50×10^5	5.50×10^5
9	5.50×10^5	5.50×10^5	5.50×10^5

Table 2. Test Matrix for $\Lambda = 70°$ Model

Contraction ratio (CR)	Reynolds number per foot at each cowl position—		
	0 percent	25 percent	No cowl
3	0.89×10^5 2.85 5.50	5.50×10^5	5.50×10^5
5	5.50×10^5	5.50×10^5	5.50×10^5
9	5.50×10^5	0.89×10^5 2.85 5.50	5.50×10^5

Table 3. Free-Stream and Postnormal-Shock Flow Conditions for $N_{Re} = 0.89 \times 10^5$ Per Foot

[CF_4 Tunnel; run 2289; Time = 7 sec]

Reservoir stagnation conditions:	
$p_{t,1}$, N/m^2 (psia)	0.1853E+07 (0.2687E+03)
$T_{t,1}$, K (°R)	0.6317E+03 (0.1137E+04)
$\rho_{t,1}$, kg/m^3 (lbm/ft^3)	0.3083E+02 (0.1924E+01)
$Z_{t,1}$	0.1007E+01
$h_{t,1}$, J/kg (Btu/lbm)	0.6298E+06 (0.2709E+03)
Free-stream conditions (flow not saturated):	
p_1, N/m^2 (psia)	0.5165E+02 (0.7491E–02)
T_1, K (°R)	0.1623E+03 (0.2921E+03)
ρ_1, kg/m^3 (lbm/ft^3)	0.3369E 02 (0.2103E–03)
q_1, N/m^2 (psia)	0.1245E+04 (0.1805E+00)
h_1, J/kg (Btu/lbm)	0.2603E+06 (0.1120E+03)
u_1, m/sec (ft/sec)	0.8596E+03 (0.2820E+04)
$N_{Re,1}$, m^{-1} (ft^{-1})	0.2912E+06 (0.8877E+05)
μ_1, N-sec/m^2 (lbm/ft-sec)	0.9945E–05 (0.6683E–05)
M_1	0.6237E+01
Z_1	0.1000E+01
γ_1	0.1239E+01
$N_{Pr,1}$	0.8511E+00
Static conditions behind normal shock:	
p_2, N/m^2 (psia)	0.2328E+04 (0.3376E+00)
T_2, K (°R)	0.6275E+03 (0.1129E+04)
ρ_2, kg/m^3 (lbm/ft^3)	0.3926E–01 (0.2451E–02)
u_2, m/sec (ft/sec)	0.7376E+02 (0.2420E+03)
h_2, J/kg (Btu/lbm)	0.6270E+06 (0.2697E+03)
$N_{Re,2}$ m^{-1} (ft^{-1})	0.9370E+05 (0.2856E+05)
Z_2	0.1000E+01
M_2	0.2881E+00
γ_2	0.1106E+01
$N_{Pr,2}$	0.7574E+00
Stagnation conditions behind normal shock:	
$p_{t,2}$, N/m^2 (psia)	0.2437E+04 (0.3534E+00)
$T_{t,2}$, K (°R)	0.6302E+03 (0.1134E+04)
$\rho_{t,2}$, kg/m^3 (lbm/ft^3)	0.4092E–01 (0.2555E–02)
$Z_{t,2}$	0.1000E+01
$h_{t,2}$, J/kg (Btu/lbm)	0.6297E+06 (0.2709E+03)
$\gamma_{t,2}$	0.1106E+01

Table 4. Free-Stream and Postnormal-Shock Flow Conditions for $N_{Re} = 2.85 \times 10^5$ Per Foot

[CF_4 Tunnel; run 2290; Time = 7 sec]

Reservoir stagnation conditions:	
$p_{t,1}$, N/m^2 (psia)	0.6607E+07 (0.9583E+03)
$T_{t,1}$, K (°R)	0.6511E+03 (0.1172E+04)
$\rho_{t,1}$, kg/m^3 (lbm/ft^3)	0.1042E+03 (0.6504E+01)
$Z_{t,1}$	0.1031E+01
$h_{t,1}$, J/kg (Btu/lbm)	0.6462E+06 (0.2780E+03)
Free-stream conditions (flow not saturated):	
p_1, N/m^2 (psia)	0.1761E+03 (0.2555E-01)
T_1, K (°R)	0.1688E+03 (0.3038E+03)
ρ_1, kg/m^3 (lbm/ft^3)	0.1105E-01 (0.6897E-03)
q_1, N/m^2 (psia)	0.4228E+04 (0.6132E+00)
h_1, J/kg (Btu/lbm)	0.2636E+06 (0.1134E+03)
u_1, m/sec (ft/sec)	0.8749E+03 (0.2870E+04)
N_{Re}, m^{-1} (ft^{-1})	0.9348E+06 (0.2849E+06)
μ_1, N-sec/m^2 (lbm/ft-sec)	0.1034E-04 (0.6948E-05)
M_1	0.6240E+01
Z_1	0.1000E+01
γ_1	0.1233E+01
$N_{Pr,1}$	0.8330E+00
Static conditions behind normal shock:	
p_2, N/m^2 (psia)	0.7914E+04 (0.1148E+01)
T_2, K (°R)	0.6441E+03 (0.1159E+04)
ρ_2, kg/m^3 (lbm/ft^3)	0.1300E+00 (0.8119E-02)
u_2, m/sec (ft/sec)	0.7432E+02 (0.2438E+03)
h_2, J/kg (Btu/lbm)	0.6435E+06 (0.2768E+03)
$N_{Re,2}$ m^{-1} (ft^{-1})	0.3070E+06 (0.9357E+05)
Z_2	0.1000E+01
M_2	0.2866E+00
γ_2	0.1105E+01
$N_{Pr,2}$	0.7541E+00
Stagnation conditions behind normal shock:	
$p_{t,2}$, N/m^2 (psia)	0.8280E+04 (0.1201E+01)
$T_{t,2}$, K (°R)	0.6469E+03 (0.1164E+04)
$\rho_{t,2}$, kg/m^3 (lbm/ft^3)	0.1355E+00 (0.8458E-02)
$Z_{t,2}$	0.1000E+01
$h_{t,2}$, J/kg (Btu/lbm)	0.6462E+06 (0.2780E+03)
$\gamma_{t,2}$	0.1105E+01

Table 5. Free-Stream and Postnormal-Shock Flow Conditions for $N_{Re} = 5.50 \times 10^5$ Per Foot

[CF_4 Tunnel; run 2284; Time = 7 sec]

Reservoir stagnation conditions:	
$p_{t,1}$, N/m^2 (psia)	0.1380E+08 (0.2002E+04)
$T_{t,1}$, K (°R)	0.6711E+03 (0.1208E+04)
$\rho_{t,1}$, kg/m^3 (lbm/ft^3)	0.2023E+03 (0.1263E+02)
$Z_{t,1}$	0.1076E+01
$h_{t,1}$, J/kg (Btu/lbm)	0.6634E+06 (0.2854E+03)
Free-stream conditions (flow not saturated):	
p_1, N/m^2 (psia)	0.3630E+03 (0.5265E–01)
T_1, K (°R)	0.1760E+03 (0.3168E+03)
ρ_1, kg/m^3 (lbm/ft^3)	0.2184E–01 (0.1363E–02)
q_1, N/m^2 (psia)	0.8652E+04 (0.1255E+01)
h_1, J/kg (Btu/lbm)	0.2672E+06 (0.1150E+03)
u_1, m/sec (ft/sec)	0.8902E+03 (0.2921E+04)
N_{Re}, m^{-1} (ft^{-1})	0.1804E+07 (0.5499E+06)
μ_1, N-sec/m^2 (lbm/ft-sec)	0.1077E–04 (0.7240E–05)
M_1	0.6233E+01
Z_1	0.9999E+00
γ_1	0.1227E+01
$N_{Pr,1}$	0.8170E+00
Static conditions behind normal shock:	
p_2, N/m^2 (psia)	0.1621E+05 (0.2351E+01)
T_2, K (°R)	0.6613E+03 (0.1190E+04)
ρ_2, kg/m^3 (lbm/ft^3)	0.2595E+00 (0.1620E–01)
u_2, m/sec (ft/sec)	0.7492E+02 (0.2458E+03)
h_2, J/kg (Btu/lbm)	0.6606E+06 (0.2842E+03)
$N_{Re,2}$ m^{-1} (ft^{-1})	0.6062E+06 (0.1848E+06)
Z_2	0.1000E+01
M_2	0.2852E+00
γ_2	0.1104E+01
$N_{Pr,2}$	0.7507E+00
Stagnation conditions behind normal shock:	
$p_{t,2}$, N/m^2 (psia)	0.1695E+05 (0.2459E+01)
$T_{t,2}$, K (°R)	0.6641E+03 (0.1195E+04)
$\rho_{t,2}$, kg/m^3 (lbm/ft^3)	0.2702E+00 (0.1687E–01)
$Z_{t,2}$	0.1000E+01
$h_{t,2}$, J/kg (Btu/lbm)	0.6634E+06 (0.2854E+03)
$\gamma_{t,2}$	0.1104E+01

Table 6. Listing of Tunnel Runs

Run	CR			Cowl position			Reynolds number per foot		
	3	5	9	0%	25%	No	5.50×10^5	2.85×10^5	0.89×10^5
$\Lambda = 30°$ model									
[a]2262	x			x			x		
2263	x					x		x	
2264	x					x	x		
2265	x			x					x
2266	x			x				x	
[a]2267	x				x		x		
2268		x			x		x		
[a]2270		x		x			x		
2271		x				x	x		
[a]2272			x	x			x		
[a]2273			x		x		x		
[a]2274			x			x	x		
$\Lambda = 70°$ model									
2275	x			x					x
2276	x			x				x	
[a]2277	x			x			x		
2278	x				x		x		
2279	x					x	x		
2280	x				x		x		
2281	x			x			x		
[a]2282		x		x			x		
2284		x			x		x		
[a]2285		x				x	x		
2286			x			x	x		
[a]2287			x	x			x		
2288			x		x		x		
2289			x		x				x
2290			x		x			x	

[a]Schlieren photograph included in this report.

Table 7. Pressure Distributions for Run 2262 for $\Lambda = 30°$ Model

[CF_4 Tunnel; CR = 3; 0-percent cowl; $N_{Re} = 5.50 \times 10^5$ per foot]

Orifice	x'/T'_x	p, psia	p/p_1	C_p
Baseplate centerline				
20	0.190	0.056	1.056	0.0024
21	.448	.089	1.665	.0283
22	.567	.100	1.881	.0374
23	.686	.124	2.327	.0564
24	.845	.166	3.111	.0898
25	1.003	.219	4.111	.1323
26	1.150	.246	4.618	.1538
27	1.348	.209	3.917	.1240
28	1.547	.213	3.996	.1274
29	1.810	.161	3.014	.0856
30	2.009	.092	1.720	.0306
30° sidewall centerline ($y/H = 0.50$)				
1	0.378	0.118	2.211	0.0515
14	.572	.117	2.194	.0508
15	.765	.117	2.202	.0511
16	.867	.161	3.012	.0856
3	.954	.265	4.976	.1690
4	1.046	.242	4.548	.1509
5	1.231	.228	4.284	.1396
6	1.415	.276	5.186	.1780
7	1.653	.101	1.902	.0384
8	2.050	.124	2.330	.0565
30° sidewall ($y/H = 0.87$)				
17	0.776	0.102	1.908	0.0386
18	.865	.148	2.785	.0759
2	.954	.193	3.615	.1112
34	1.049	.185	3.469	.1050
30° sidewall ($y/H = 0.13$)				
10	0.657	0.111	2.080	0.0459
11	.756	.119	2.229	.0522
12	.855	.130	2.440	.0612
13	.954	.225	4.229	.1373
30° cowl centerline				
39	1.099	0.356	6.675	0.2413
40	1.198	.313	5.867	.2069
41	1.297	.296	5.549	.1934

Table 8. Pressure Distributions for Run 2263 for $\Lambda = 30°$ Model

[CF_4 Tunnel; CR = 3; no cowl; $N_{Re} = 2.85 \times 10^5$ per foot]

Orifice	x'/T'_x	p, psia	p/p_1	C_p
Baseplate centerline				
20	0.190	0.030	1.145	0.0060
21	.448	.049	1.880	.0366
22	.567	.058	2.199	.0498
23	.686	.066	2.515	.0630
24	.845	.082	3.132	.0886
25	1.003	.123	4.705	.1540
26	1.150	.129	4.909	.1624
27	1.348	.111	4.233	.1344
28	1.547	.117	4.464	.1440
29	1.810	.078	2.996	.0829
30	2.009	.052	1.983	.0408
30° sidewall centerline ($y/H = 0.50$)				
1	0.378	0.063	2.396	0.0580
14	.572	.063	2.391	.0578
15	.765	.064	2.429	.0594
16	.867	.093	3.555	.1062
3	.954	.169	6.469	.2273
4	1.046	.133	5.062	.1688
5	1.231	.119	4.560	.1480
6	1.415	.147	5.607	.1915
7	1.653	.053	2.014	.0422
8	2.050	.055	2.117	.0464
30° sidewall ($y/H = 0.87$)				
17	0.776	0.056	2.136	0.0472
18	.865	.082	3.125	.0883
2	.954	.117	4.474	.1444
34	1.049	.099	3.765	.1149
30° sidewall ($y/H = 0.13$)				
10	0.657	0.059	2.235	0.0513
11	.756	.067	2.545	.0642
12	.855	.076	2.894	.0787
13	.954	.128	4.887	.1615

Table 9. Pressure Distributions for Run 2264 for $\Lambda = 30°$ Model

[CF_4 Tunnel; CR = 3; no cowl; $N_{Re} = 5.50 \times 10^5$ per foot]

Orifice	x'/T'_x	p, psia	p/p_1	C_p
Baseplate centerline				
20	0.190	0.058	1.049	0.0021
21	.448	.092	1.676	.0286
22	.567	.104	1.886	.0374
23	.686	.130	2.361	.0575
24	.845	.174	3.172	.0918
25	1.003	.227	4.125	.1321
26	1.150	.253	4.609	.1525
27	1.348	.212	3.859	.1208
28	1.547	.219	3.983	.1261
29	1.810	.170	3.085	.0881
30	2.009	.095	1.725	.0307
30° sidewall centerline ($y/H = 0.50$)				
1	0.378	0.124	2.257	0.0531
14	.572	.123	2.242	.0525
15	.765	.124	2.257	.0531
16	.867	.166	3.016	.0852
3	.954	.270	4.913	.1654
4	1.046	.248	4.517	.1486
5	1.231	.232	4.230	.1365
6	1.415	.280	5.104	.1735
7	1.653	.105	1.912	.0385
8	2.050	.117	2.130	.0477
30° sidewall ($y/H = 0.87$)				
17	0.776	0.108	1.966	0.0408
18	.865	.156	2.837	.0777
2	.954	.198	3.596	.1097
34	1.049	.190	3.452	.1036
30° sidewall ($y/H = 0.13$)				
10	0.657	0.113	2.062	0.0449
11	.756	.122	2.215	.0514
12	.855	.134	2.440	.0609
13	.954	.228	4.141	.1327

Table 10. Pressure Distributions for Run 2265 for $\Lambda = 30°$ Model

[CF_4 Tunnel; CR = 3; 0-percent cowl; $N_{Re} = 0.89 \times 10^5$ per foot]

Orifice	x'/T'_x	p, psia	p/p_1	C_p
Baseplate centerline				
20	0.190	0.008	0.909	−0.0037
21	.448	.020	2.409	.0580
22	.567	.021	2.558	.0641
23	.686	.024	2.913	.0787
24	.845	.028	3.382	.0980
25	1.003	.045	5.487	.1845
26	1.150	.048	5.859	.1999
27	1.348	.043	5.257	.1751
28	1.547	.044	5.348	.1788
29	1.810	.029	3.457	.1010
30	2.009	.018	2.229	.0505
30° sidewall centerline ($y/H = 0.50$)				
1	0.378	0.021	2.503	0.0618
14	.572	.021	2.548	.0637
15	.765	.028	3.391	.0983
16	.867	.045	5.404	.1811
3	.954	.069	8.324	.3013
4	1.046	.051	6.150	.2118
5	1.231	.050	6.073	.2086
6	1.415	.051	6.234	.2153
7	1.653	.022	2.692	.0696
8	2.050	.022	2.646	.0677
30° sidewall ($y/H = 0.87$)				
17	0.776	0.028	3.345	0.0964
18	.865	.034	4.062	.1259
2	.954	.045	5.424	.1820
34	1.049	.039	4.710	.1526
30° sidewall ($y/H = 0.13$)				
10	0.657	0.022	2.638	0.0674
11	.756	.029	3.484	.1022
12	.855	.030	3.652	.1091
13	.954	.046	5.599	.1892
30° cowl centerline				
39	1.099	0.072	8.686	0.3161
40	1.198	.083	10.085	.3737
41	1.297	.074	8.915	.3256

Table 11. Pressure Distributions for Run 2266 for $\Lambda = 30°$ Model

[CF_4 Tunnel; CR = 3; 0-percent cowl; $N_{Re} = 2.85 \times 10^5$ per foot]

Orifice	x'/T'_x	p, psia	p/p_1	C_p
Baseplate centerline				
20	0.190	0.030	1.118	0.0050
21	.448	.052	1.945	.0396
22	.567	.058	2.153	.0484
23	.686	.067	2.513	.0635
24	.845	.086	3.220	.0931
25	1.003	.124	4.626	.1521
26	1.150	.131	4.896	.1634
27	1.348	.113	4.219	.1351
28	1.547	.118	4.400	.1427
29	1.810	.081	3.022	.0849
30	2.009	.052	1.940	.0394
30° sidewall centerline ($y/H = 0.50$)				
1	0.378	0.062	2.313	0.0551
14	.572	.063	2.354	.0568
15	.765	.065	2.431	.0600
16	.867	.093	3.484	.1042
3	.954	.172	6.406	.2268
4	1.046	.133	4.956	.1660
5	1.231	.123	4.570	.1498
6	1.415	.148	5.530	.1901
7	1.653	.053	1.959	.0402
8	2.050	.065	2.425	.0598
30° sidewall ($y/H = 0.87$)				
17	0.776	0.059	2.186	0.0498
18	.865	.084	3.147	.0901
2	.954	.120	4.476	.1459
34	1.049	.099	3.704	.1134
30° sidewall ($y/H = 0.13$)				
10	0.657	0.060	2.239	0.0520
11	.756	.068	2.553	.0652
12	.855	.076	2.829	.0767
13	.954	.130	4.846	.1614
30° cowl centerline				
39	1.099	0.181	6.758	0.2416
40	1.198	.179	6.688	.2387
41	1.297	.178	6.648	.2370

Table 12. Pressure Distributions for Run 2267 for $\Lambda = 30°$ Model

[CF_4 Tunnel; CR = 3; 25-percent cowl; $N_{Re} = 5.50 \times 10^5$ per foot]

Orifice	x'/T'_x	p, psia	p/p_1	C_p
Baseplate centerline				
20	0.190	0.055	1.042	0.0018
21	.448	.088	1.675	.0285
22	.567	.099	1.879	.0372
23	.686	.123	2.336	.0565
24	.845	.167	3.171	.0918
25	1.003	.217	4.128	.1322
26	1.150	.244	4.629	.1534
27	1.348	.208	3.945	.1245
28	1.547	.211	4.003	.1270
29	1.810	.162	3.084	.0881
30	2.009	.091	1.734	.0310
30° sidewall centerline ($y/H = 0.50$)				
1	0.378	0.117	2.216	0.0514
14	.572	.116	2.197	.0506
15	.765	.116	2.206	.0510
16	.867	.160	3.041	.0863
3	.954	.260	4.942	.1667
4	1.046	.243	4.615	.1528
5	1.231	.226	4.291	.1392
6	1.415	.276	5.230	.1788
7	1.653	.105	2.001	.0423
8	2.050	.127	2.403	.0593
30° sidewall ($y/H = 0.87$)				
17	0.776	0.153	2.895	0.0801
18	.865	.185	3.513	.1062
2	.954	.214	4.062	.1294
34	1.049	.239	4.535	.1495
30° sidewall ($y/H = 0.13$)				
10	0.657	0.111	2.106	0.0468
11	.756	.117	2.218	.0515
12	.855	.129	2.453	.0614
13	.954	.222	4.218	.1360
30° cowl centerline				
39	0.841	0.241	4.572	0.1510
40	.940	.356	6.751	.2431
41	1.039	.375	7.128	.2591

Table 13. Pressure Distributions for Run 2268 for $\Lambda = 30°$ Model

[CF_4 Tunnel; CR = 5; 25-percent cowl; $N_{Re} = 5.50 \times 10^5$ per foot]

Orifice	x'/T'_x	p, psia	p/p_1	C_p
Baseplate centerline				
20	0.190	0.061	1.148	0.0062
21	.448	.100	1.880	.0371
22	.567	.126	2.378	.0580
23	.686	.164	3.104	.0886
24	.845	.229	4.326	.1400
25	1.003	.372	7.030	.2539
26	1.150	.373	7.041	.2544
27	1.348	.388	7.329	.2665
28	1.547	.378	7.145	.2587
29	1.810	.177	3.350	.0989
30	2.009	.121	2.288	.0542
30° sidewall centerline ($y/H = 0.50$)				
1	0.378	0.123	2.319	0.0555
14	.572	.122	2.313	.0553
15	.765	.206	3.883	.1214
16	.867	.377	7.120	.2577
3	.954	.415	7.844	.2882
4	1.046	.305	5.770	.2009
5	1.231	.423	7.993	.2945
6	1.415	.469	8.867	.3313
7	1.653	.241	4.548	.1494
8	2.050	.079	1.488	.0206
30° sidewall ($y/H = 0.87$)				
17	0.776	0.188	3.561	0.1078
18	.865	.314	5.925	.2074
2	.954	.441	8.324	.3084
34	1.049	.490	9.262	.3479
30° sidewall ($y/H = 0.13$)				
10	0.657	0.118	2.236	0.0521
11	.756	.171	3.227	.0938
12	.855	.310	5.852	.2043
13	.954	.358	6.756	.2424
30° cowl centerline				
39	0.841	0.428	8.085	0.2983
40	.940	.654	12.363	.4785
41	1.039	.650	12.286	.4752

Table 14. Pressure Distributions for Run 2270 for $\Lambda = 30°$ Model

[CF_4 Tunnel; CR = 5; 0-percent cowl; $N_{Re} = 5.50 \times 10^5$ per foot]

Orifice	x'/T'_x	p, psia	p/p_1	C_p
Baseplate centerline				
20	0.190	0.062	1.176	0.0074
21	.448	.101	1.921	.0389
22	.567	.124	2.369	.0578
23	.686	.162	3.103	.0888
24	.845	.226	4.318	.1402
25	1.003	.365	6.965	.2520
26	1.150	.369	7.051	.2556
27	1.348	.384	7.338	.2677
28	1.547	.373	7.127	.2588
29	1.810	.175	3.347	.0991
30	2.009	.120	2.285	.0543
30° sidewall centerline ($y/H = 0.50$)				
1	0.378	0.123	2.352	0.0571
14	.572	.122	2.338	.0565
15	.765	.206	3.944	.1244
16	.867	.372	7.116	.2584
3	.954	.406	7.754	.2853
4	1.046	.305	5.836	.2043
5	1.231	.417	7.964	.2941
6	1.415	.458	8.750	.3274
7	1.653	.233	4.454	.1459
8	2.050	.075	1.437	.0185
30° sidewall ($y/H = 0.87$)				
17	0.776	0.190	3.622	0.1108
18	.865	.308	5.890	.2066
2	.954	.364	6.954	.2515
34	1.049	.426	8.148	.3019
30° sidewall ($y/H = 0.13$)				
10	0.657	0.117	2.238	0.0523
11	.756	.168	3.214	.0935
12	.855	.307	5.863	.2054
13	.954	.354	6.757	.2432
30° cowl centerline				
39	1.099	0.830	15.852	0.6274
40	1.198	.605	11.554	.4458
41	1.297	.749	14.313	.5623

Table 15. Pressure Distributions for Run 2271 for $\Lambda = 30°$ Model

[CF_4 Tunnel; CR = 5; no cowl; $N_{Re} = 5.50 \times 10^5$ per foot]

Orifice	x'/T'_x	p, psia	p/p_1	C_p
Baseplate centerline				
20	0.190	0.061	1.163	0.0068
21	.448	.102	1.923	.0385
22	.567	.125	2.366	.0570
23	.686	.165	3.127	.0888
24	.845	.229	4.332	.1391
25	1.003	.370	7.010	.2509
26	1.150	.373	7.067	.2533
27	1.348	.391	7.400	.2672
28	1.547	.380	7.186	.2582
29	1.810	.179	3.396	.1000
30	2.009	.121	2.298	.0542
30° sidewall centerline ($y/H = 0.50$)				
1	0.378	0.124	2.345	0.0562
14	.572	.124	2.347	.0562
15	.765	.206	3.903	.1212
16	.867	.375	7.105	.2549
3	.954	.414	7.843	.2857
4	1.046	.309	5.846	.2023
5	1.231	.425	8.048	.2943
6	1.415	.466	8.814	.3262
7	1.653	.237	4.489	.1457
8	2.050	.063	1.184	.0077
30° sidewall ($y/H = 0.87$)				
17	0.776	0.187	3.533	0.1058
18	.865	.313	5.924	.2056
2	.954	.371	7.032	.2518
34	1.049	.310	5.872	.2034
30° sidewall ($y/H = 0.13$)				
10	0.657	0.118	2.243	0.0519
11	.756	.166	3.151	.0898
12	.855	.312	5.903	.2047
13	.954	.361	6.831	.2434

Table 16. Pressure Distributions for Run 2272 for $\Lambda = 30°$ Model

[CF_4 Tunnel; CR = 9; 0-percent cowl; $N_{Re} = 5.50 \times 10^5$ per foot]

Orifice	x'/T'_x	p, psia	p/p_1	C_p
Baseplate centerline				
20	0.190	0.068	1.281	0.0119
21	.448	.110	2.074	.0453
22	.567	.145	2.745	.0736
23	.686	.190	3.600	.1098
24	.845	.315	5.966	.2096
25	1.003	.718	13.582	.5311
26	1.150	.798	15.096	.5951
27	1.348	.761	14.385	.5650
28	1.547	.759	14.357	.5638
29	1.810	.234	4.419	.1443
30	2.009	.128	2.421	.0600
30° sidewall centerline ($y/H = 0.50$)				
1	0.378	0.113	2.137	0.0480
14	.572	.126	2.379	.0582
15	.765	.362	6.841	.2466
16	.867	.462	8.743	.3269
3	.954	.721	13.643	.5337
4	1.046	.919	17.374	.6912
5	1.231	1.001	18.937	.7572
6	1.415	.908	17.178	.6829
7	1.653	.219	4.142	.1326
8	2.050	.104	1.975	.0412
30° sidewall ($y/H = 0.87$)				
17	0.776	0.328	6.195	0.2193
18	.865	.434	8.209	.3043
2	.954	.571	10.798	.4136
34	1.049	.655	12.384	.4806
30° sidewall ($y/H = 0.13$)				
10	0.657	0.153	2.885	0.0796
11	.756	.292	5.517	.1907
12	.855	.340	6.434	.2294
13	.954	.732	13.842	.5421
30° cowl centerline				
39	1.099	1.521	28.768	1.1722
40	1.198	1.524	28.821	1.1744
41	1.297	1.507	28.495	1.1607

Table 17. Pressure Distributions for Run 2273 for $\Lambda = 30°$ Model

[CF_4 Tunnel; CR = 9; 25-percent cowl; $N_{Re} = 5.50 \times 10^5$ per foot]

Orifice	x'/T'_x	p, psia	p/p_1	C_p
Baseplate centerline				
20	0.190	0.070	1.305	0.0130
21	.448	.113	2.096	.0466
22	.567	.148	2.756	.0746
23	.686	.194	3.605	.1107
24	.845	.320	5.956	.2107
25	1.003	.723	13.462	.5297
26	1.150	.805	14.981	.5943
27	1.348	.769	14.322	.5663
28	1.547	.767	14.283	.5646
29	1.810	.236	4.395	.1443
30	2.009	.131	2.440	.0612
30° sidewall centerline ($y/H = 0.50$)				
1	0.378	0.115	2.132	0.0481
14	.572	.131	2.440	.0612
15	.765	.367	6.826	.2476
16	.867	.477	8.886	.3352
3	.954	.726	13.520	.5322
4	1.046	.928	17.271	.6916
5	1.231	1.011	18.827	.7578
6	1.415	.918	17.091	.6840
7	1.653	.219	4.084	.1311
8	2.050	.110	2.051	.0447
30° sidewall ($y/H = 0.87$)				
17	0.776	0.332	6.183	0.2203
18	.865	.524	9.757	.3722
2	.954	.822	15.302	.6079
34	1.049	.848	15.786	.6285
30° sidewall ($y/H = 0.13$)				
10	0.657	0.157	2.931	0.0821
11	.756	.296	5.512	.1918
12	.855	.345	6.415	.2302
13	.954	.739	13.754	.5422
30° cowl centerline				
39	0.841	1.013	18.847	0.7586
40	.940	1.293	24.060	.9802
41	1.039	1.769	32.923	1.3570

Table 18. Pressure Distributions for Run 2274 for $\Lambda = 30°$ Model

[CF_4 Tunnel; CR = 9; no cowl; $N_{Re} = 5.50 \times 10^5$ per foot]

Orifice	x'/T'_x	p, psia	p/p_1	C_p
Baseplate centerline				
20	0.190	0.064	1.202	0.0085
21	.448	.110	2.081	.0453
22	.567	.144	2.715	.0719
23	.686	.191	3.606	.1092
24	.845	.312	5.880	.2045
25	1.003	.726	13.681	.5314
26	1.150	.806	15.185	.5944
27	1.348	.764	14.394	.5613
28	1.547	.764	14.403	.5617
29	1.810	.235	4.433	.1439
30	2.009	.126	2.369	.0574
30° sidewall centerline ($y/H = 0.50$)				
1	0.378	0.110	2.073	0.0450
14	.572	.124	2.340	.0561
15	.765	.363	6.844	.2449
16	.867	.453	8.535	.3158
3	.954	.723	13.614	.5286
4	1.046	.920	17.339	.6847
5	1.231	1.006	18.952	.7523
6	1.415	.911	17.168	.6775
7	1.653	.217	4.092	.1296
8	2.050	.086	1.623	.0261
30° sidewall ($y/H = 0.87$)				
17	0.776	0.331	6.238	0.2195
18	.865	.438	8.258	.3042
2	.954	.576	10.852	.4129
34	1.049	.666	12.553	.4841
30° sidewall ($y/H = 0.13$)				
10	0.657	0.148	2.795	0.0752
11	.756	.298	5.611	.1932
12	.855	.343	6.454	.2285
13	.954	.730	13.746	.5341

Table 19. Pressure Distributions for Run 2275 for $\Lambda = 70°$ Model

[CF_4 Tunnel; CR = 3; 0-percent cowl; $N_{Re} = 0.89 \times 10^5$ per foot]

Orifice	x'/T'_x	p, psia	p/p_1	C_p
Baseplate centerline				
20	0.190	0.012	1.414	0.0170
21	.448	.016	1.829	.0341
22	.567	.017	2.039	.0427
23	.686	.018	2.121	.0461
24	.845	.023	2.675	.0688
25	1.003	.026	3.097	.0861
26	1.150	.030	3.580	.1060
28	1.547	.029	3.415	.0992
29	1.810	.029	3.390	.0982
30	2.009	.028	3.267	.0931
70° sidewall centerline ($y/H = 0.50$)				
2	0.590	0.027	3.201	0.0904
4	.994	.041	4.808	.1565
5	1.075	.033	3.941	.1208
6	1.256	.035	4.171	.1303
7	1.436	.031	3.669	.1096
8	1.611	.029	3.415	.0992
9	1.796	.031	3.692	.1106
10	1.979	.019	2.205	.0495
70° sidewall ($y/H = 0.87$)				
34	0.782	0.044	5.237	0.1741
13	.991	.050	5.855	.1995
35	1.067	.043	5.052	.1665
36	1.234	.034	4.043	.1250
70° sidewall ($y/H = 0.13$)				
14	0.673	0.022	2.562	0.0642
15	.772	.024	2.870	.0768
16	.871	.028	3.304	.0947
17	.970	.029	3.450	.1006

Table 20. Pressure Distributions for Run 2276 for $\Lambda = 70°$ Model

[CF_4 Tunnel; CR = 3; 0-percent cowl; $N_{Re} = 2.85 \times 10^5$ per foot]

Orifice	x'/T'_x	p, psia	p/p_1	C_p
Baseplate centerline				
20	0.190	0.032	1.182	0.0076
21	.448	.041	1.508	.0212
22	.567	.048	1.779	.0326
23	.686	.051	1.894	.0374
24	.845	.061	2.264	.0529
25	1.003	.073	2.713	.0716
26	1.150	.091	3.381	.0996
28	1.547	.075	2.783	.0746
29	1.810	.075	2.800	.0753
30	2.009	.076	2.836	.0768
70° sidewall centerline ($y/H = 0.50$)				
2	0.590	0.072	2.665	0.0696
4	.994	.110	4.079	.1288
5	1.075	.095	3.537	.1061
6	1.256	.101	3.750	.1150
7	1.436	.073	2.725	.0721
8	1.611	.081	3.013	.0842
9	1.796	.080	2.976	.0827
10	1.979	.046	1.711	.0298
70° sidewall ($y/H = 0.87$)				
34	0.782	0.117	4.342	0.1398
13	.991	.122	4.511	.1469
35	1.067	.118	4.391	.1418
36	1.234	.101	3.758	.1154
70° sidewall ($y/H = 0.13$)				
14	0.673	0.057	2.111	0.0465
15	.772	.064	2.374	.0575
16	.871	.071	2.635	.0684
17	.970	.083	3.070	.0866

Table 21. Pressure Distributions for Run 2277 for $\Lambda = 70°$ Model

[CF_4 Tunnel; CR = 3; 0-percent cowl; $N_{Re} = 5.50 \times 10^5$ per foot]

Orifice	x'/T'_x	p, psia	p/p_1	C_p
Baseplate centerline				
20	0.190	0.058	1.084	0.0035
21	.448	.077	1.420	.0177
22	.567	.087	1.615	.0260
23	.686	.095	1.769	.0325
24	.845	.117	2.165	.0492
25	1.003	.145	2.686	.0713
26	1.150	.165	3.055	.0869
28	1.547	.140	2.604	.0678
29	1.810	.142	2.628	.0688
30	2.009	.140	2.603	.0677
70° sidewall centerline ($y/H = 0.50$)				
2	0.590	0.124	2.306	0.0552
4	.994	.210	3.902	.1226
5	1.075	.182	3.376	.1004
6	1.256	.202	3.746	.1161
7	1.436	.138	2.558	.0658
8	1.611	.154	2.860	.0786
9	1.796	.148	2.750	.0740
10	1.979	.079	1.469	.0198
70° sidewall ($y/H = 0.87$)				
34	0.782	0.207	3.840	0.1200
13	.991	.267	4.958	.1673
35	1.067	.205	3.794	.1181
36	1.234	.209	3.886	.1220
70° sidewall ($y/H = 0.13$)				
14	0.673	0.102	1.902	0.0381
15	.772	.114	2.114	.0471
16	.871	.127	2.354	.0572
17	.970	.155	2.880	.0795

Table 22. Pressure Distributions for Run 2278 for $\Lambda = 70°$ Model

[CF_4 Tunnel; CR = 3; 25-percent cowl; $N_{Re} = 5.50 \times 10^5$ per foot]

Orifice	x'/T'_x	p, psia	p/p_1	C_p
Baseplate centerline				
20	0.190	0.058	1.066	0.0028
21	.448	.077	1.410	.0174
22	.567	.087	1.594	.0252
23	.686	.095	1.748	.0317
24	.845	.117	2.145	.0486
25	1.003	.144	2.653	.0702
26	1.150	.165	3.030	.0862
28	1.547	.140	2.568	.0666
29	1.810	.142	2.612	.0684
30	2.009	.140	2.585	.0673
70° sidewall centerline ($y/H = 0.50$)				
2	0.590	0.125	2.292	0.0548
4	.994	.212	3.895	.1229
5	1.075	.183	3.370	.1006
6	1.256	.202	3.718	.1154
7	1.436	.139	2.563	.0663
8	1.611	.153	2.821	.0773
9	1.796	.148	2.727	.0733
10	1.979	.084	1.547	.0232
70° sidewall ($y/H = 0.87$)				
34	0.782	0.206	3.794	0.1186
13	.991	.267	4.918	.1663
35	1.067	.240	4.426	.1454
36	1.234	.286	5.262	.1809
70° sidewall ($y/H = 0.13$)				
14	0.673	0.102	1.881	0.0374
15	.772	.113	2.085	.0460
16	.871	.127	2.335	.0567
17	.970	.155	2.859	.0789

Table 23. Pressure Distributions for Run 2279 for $\Lambda = 70°$ Model

[CF_4 Tunnel; CR = 3; no cowl; $N_{Re} = 5.50 \times 10^5$ per foot]

Orifice	x'/T'_x	p, psia	p/p_1	C_p
Baseplate centerline				
20	0.190	0.054	1.018	0.0008
21	.448	.070	1.323	.0136
22	.567	.082	1.541	.0227
23	.686	.091	1.708	.0297
24	.845	.110	2.071	.0450
25	1.003	.139	2.626	.0683
26	1.150	.158	2.973	.0829
28	1.547	.133	2.497	.0629
29	1.810	.135	2.550	.0651
30	2.009	.136	2.555	.0653
70° sidewall centerline ($y/H = 0.50$)				
2	0.590	0.119	2.237	0.0520
4	.994	.205	3.861	.1202
5	1.075	.178	3.345	.0985
6	1.256	.196	3.691	.1130
7	1.436	.131	2.474	.0619
8	1.611	.147	2.772	.0744
9	1.796	.141	2.662	.0698
10	1.979	.074	1.401	.0169
70° sidewall ($y/H = 0.87$)				
34	0.782	0.198	3.735	0.1149
13	.991	.259	4.885	.1632
35	1.067	.200	3.767	.1162
36	1.234	.203	3.822	.1185
70° sidewall ($y/H = 0.13$)				
14	0.673	0.098	1.840	0.0353
15	.772	.109	2.051	.0441
16	.871	.120	2.268	.0533
17	.970	.150	2.835	.0771

Table 24. Pressure Distributions for Run 2280 for $\Lambda = 70°$ Model

[CF_4 Tunnel; CR = 3; 25-percent cowl; $N_{Re} = 5.50 \times 10^5$ per foot]

Orifice	x'/T'_x	p, psia	p/p_1	C_p
Baseplate centerline				
20	0.190	0.054	1.023	0.0010
21	.448	.072	1.356	.0151
22	.567	.083	1.564	.0239
23	.686	.091	1.705	.0299
24	.845	.112	2.103	.0467
25	1.003	.140	2.625	.0689
26	1.150	.159	2.991	.0844
28	1.547	.134	2.516	.0643
29	1.810	.137	2.569	.0665
30	2.009	.135	2.536	.0651
70° sidewall centerline ($y/H = 0.50$)				
2	0.590	0.120	2.247	0.0529
4	.994	.205	3.858	.1211
5	1.075	.178	3.351	.0996
6	1.256	.196	3.690	.1140
7	1.436	.133	2.495	.0634
8	1.611	.147	2.765	.0748
9	1.796	.143	2.682	.0713
10	1.979	.080	1.506	.0214
70° sidewall ($y/H = 0.87$)				
34	0.782	0.200	3.765	0.1172
13	.991	.259	4.863	.1637
35	1.067	.242	4.552	.1505
36	1.234	.275	5.166	.1765
70° sidewall ($y/H = 0.13$)				
14	0.673	0.098	1.848	0.0359
15	.772	.109	2.053	.0446
16	.871	.122	2.295	.0549
17	.970	.150	2.813	.0768

Table 25. Pressure Distributions for Run 2281 for $\Lambda = 70°$ Model

[CF_4 Tunnel; CR = 3; 0-percent cowl; $N_{Re} = 5.50 \times 10^5$ per foot]

Orifice	x'/T'_x	p, psia	p/p_1	C_p
Baseplate centerline				
20	0.190	0.056	1.032	0.0013
21	.448	.074	1.378	.0160
22	.567	.085	1.581	.0246
23	.686	.093	1.717	.0304
24	.845	.113	2.106	.0469
25	1.003	.142	2.639	.0695
26	1.150	.161	2.991	.0844
28	1.547	.136	2.534	.0650
29	1.810	.138	2.571	.0666
30	2.009	.138	2.559	.0661
70° sidewall centerline ($y/H = 0.50$)				
2	0.590	0.121	2.252	0.0531
4	.994	.208	3.860	.1212
5	1.075	.180	3.333	.0989
6	1.256	.198	3.681	.1137
7	1.436	.135	2.503	.0637
8	1.611	.151	2.794	.0761
9	1.796	.145	2.685	.0714
10	1.979	.076	1.406	.0172
70° sidewall ($y/H = 0.87$)				
34	0.782	0.203	3.775	0.1177
13	.991	.262	4.861	.1637
35	1.067	.203	3.770	.1174
36	1.234	.207	3.847	.1207
70° sidewall ($y/H = 0.13$)				
14	0.673	0.099	1.841	0.0356
15	.772	.111	2.055	.0447
16	.871	.123	2.291	.0547
17	.970	.151	2.809	.0767

Table 26. Pressure Distributions for Run 2282 for $\Lambda = 70°$ Model

[CF_4 Tunnel; CR = 5; 0-percent cowl; $N_{Re} = 5.50 \times 10^5$ per foot]

Orifice	x'/T'_x	p, psia	p/p_1	C_p
Baseplate centerline				
20	0.190	0.055	1.029	0.0012
21	.448	.079	1.492	.0206
22	.567	.093	1.745	.0312
23	.686	.106	2.008	.0423
24	.845	.147	2.766	.0741
25	1.003	.206	3.882	.1209
26	1.150	.208	3.923	.1226
28	1.547	.210	3.958	.1240
29	1.810	.212	4.002	.1259
30	2.009	.217	4.086	.1294
70° sidewall centerline ($y/H = 0.50$)				
2	0.590	0.158	2.987	0.0833
4	.994	.426	8.044	.2954
5	1.075	.333	6.290	.2219
6	1.256	.234	4.419	.1434
7	1.436	.229	4.315	.1390
8	1.611	.222	4.184	.1335
9	1.796	.225	4.243	.1360
10	1.979	.117	2.215	.0509
70° sidewall ($y/H = 0.87$)				
34	0.782	0.393	7.421	0.2693
13	.991	.455	8.576	.3177
35	1.067	.345	6.508	.2310
36	1.234	.281	5.295	.1801
70° sidewall ($y/H = 0.13$)				
14	0.673	0.113	2.137	0.0477
15	.772	.157	2.965	.0824
16	.871	.209	3.942	.1234
17	.970	.274	5.165	.1747

Table 27. Pressure Distributions for Run 2284 for $\Lambda = 70°$ Model

[CF_4 Tunnel; CR = 5; 25-percent cowl; $N_{Re} = 5.50 \times 10^5$ per foot]

Orifice	x'/T'_x	p, psia	p/p_1	C_p
Baseplate centerline				
20	0.190	0.061	1.136	0.0058
21	.448	.085	1.596	.0252
22	.567	.097	1.823	.0349
23	.686	.114	2.132	.0479
24	.845	.152	2.847	.0782
25	1.003	.211	3.963	.1255
26	1.150	.210	3.942	.1246
28	1.547	.216	4.049	.1291
29	1.810	.217	4.062	.1297
30	2.009	.223	4.173	.1344
70° sidewall centerline ($y/H = 0.50$)				
2	0.590	0.164	3.071	0.0877
4	.994	.431	8.076	.2997
5	1.075	.338	6.329	.2257
6	1.256	.238	4.466	.1468
7	1.436	.234	4.383	.1433
8	1.611	.227	4.250	.1377
9	1.796	.231	4.326	.1409
10	1.979	.144	2.708	.0723
70° sidewall ($y/H = 0.87$)				
34	0.782	0.396	7.428	0.2722
13	.991	.457	8.567	.3205
35	1.067	.349	6.540	.2346
36	1.234	.368	6.893	.2496
70° sidewall ($y/H = 0.13$)				
14	0.673	0.117	2.198	0.0507
15	.772	.163	3.047	.0867
16	.871	.214	4.008	.1274
17	.970	.281	5.261	.1805

Table 28. Pressure Distributions for Run 2285 for $\Lambda = 70°$ Model

[CF_4 Tunnel; CR = 5; no cowl; $N_{Re} = 5.50 \times 10^5$ per foot]

Orifice	x'/T'_x	p, psia	p/p_1	C_p
Baseplate centerline				
20	0.190	0.060	1.133	0.0057
21	.448	.085	1.600	.0255
22	.567	.098	1.835	.0355
23	.686	.113	2.122	.0476
24	.845	.151	2.830	.0777
25	1.003	.211	3.955	.1254
26	1.150	.210	3.935	.1246
28	1.547	.215	4.038	.1289
29	1.810	.218	4.083	.1309
30	2.009	.223	4.177	.1348
70° sidewall centerline ($y/H = 0.50$)				
2	0.590	0.165	3.085	0.0885
4	.994	.432	8.085	.3007
5	1.075	.338	6.340	.2266
6	1.256	.239	4.487	.1480
7	1.436	.235	4.408	.1447
8	1.611	.228	4.277	.1391
9	1.796	.231	4.332	.1414
10	1.979	.123	2.311	.0557
70° sidewall ($y/H = 0.87$)				
34	0.782	0.398	7.453	0.2739
13	.991	.457	8.567	.3211
35	1.067	.350	6.549	.2355
36	1.234	.283	5.309	.1829
70° sidewall ($y/H = 0.13$)				
14	0.673	0.117	2.190	0.0505
15	.772	.162	3.037	.0864
16	.871	.214	4.003	.1275
17	.970	.280	5.250	.1804

Table 29. Pressure Distributions for Run 2286 for $\Lambda = 70°$ Model

[CF_4 Tunnel; CR = 9; no cowl; $N_{Re} = 5.50 \times 10^5$ per foot]

Orifice	x'/T'_x	p, psia	p/p_1	C_p
Baseplate centerline				
20	0.190	0.062	1.172	0.0072
21	.448	.091	1.722	.0301
22	.567	.105	1.985	.0411
23	.686	.128	2.421	.0593
24	.845	.205	3.864	.1195
25	1.003	.310	5.851	.2024
26	1.150	.322	6.083	.2121
28	1.547	.346	6.526	.2306
29	1.810	.345	6.507	.2298
30	2.009	.351	6.628	.2349
70° sidewall centerline ($y/H = 0.50$)				
2	0.590	0.199	3.762	0.1153
4	.994	.659	12.432	.4771
5	1.075	.442	8.341	.3064
6	1.256	.356	6.716	.2386
7	1.436	.353	6.662	.2363
8	1.611	.346	6.521	.2304
9	1.796	.347	6.546	.2315
10	1.979	.186	3.504	.1045
70° sidewall ($y/H = 0.87$)				
34	0.782	0.640	12.068	0.4619
13	.991	.576	10.861	.4116
35	1.067	.434	8.188	.3000
36	1.234	.363	6.854	.2443
70° sidewall ($y/H = 0.13$)				
14	0.673	0.146	2.753	0.0732
15	.772	.212	3.993	.1249
16	.871	.312	5.889	.2040
17	.970	.486	9.180	.3414

Table 30. Pressure Distributions for Run 2287 for $\Lambda = 70°$ Model

[CF_4 Tunnel; CR = 9; 0-percent cowl; $N_{Re} = 5.50 \times 10^5$ per foot]

Orifice	x'/T'_x	p, psia	p/p_1	C_p
Baseplate centerline				
20	0.190	0.064	1.192	0.0081
21	.448	.090	1.691	.0292
22	.567	.106	1.987	.0417
23	.686	.129	2.407	.0595
24	.845	.204	3.815	.1190
25	1.003	.305	5.718	.1994
26	1.150	.321	6.017	.2121
28	1.547	.345	6.450	.2304
29	1.810	.344	6.433	.2297
30	2.009	.350	6.551	.2346
70° sidewall centerline ($y/H = 0.50$)				
2	0.590	0.200	3.748	0.1162
4	.994	.657	12.291	.4773
5	1.075	.441	8.246	.3063
6	1.256	.355	6.649	.2388
7	1.436	.352	6.589	.2363
8	1.611	.347	6.502	.2326
9	1.796	.348	6.505	.2327
10	1.979	.186	3.489	.1052
70° sidewall ($y/H = 0.87$)				
34	0.782	0.635	11.886	0.4602
13	.991	.573	10.724	.4111
35	1.067	.434	8.115	.3008
36	1.234	.364	6.820	.2460
70° sidewall ($y/H = 0.13$)				
14	0.673	0.146	2.725	0.0729
15	.772	.211	3.954	.1249
16	.871	.312	5.847	.2049
17	.970	.486	9.090	.3420

Table 31. Pressure Distributions for Run 2288 for $\Lambda = 70°$ Model

[CF_4 Tunnel; CR = 9; 25-percent cowl; $N_{Re} = 5.50 \times 10^5$ per foot]

Orifice	x'/T'_x	p, psia	p/p_1	C_p
Baseplate centerline				
20	0.190	0.063	1.188	0.0080
21	.448	.091	1.715	.0303
22	.567	.106	1.993	.0421
23	.686	.128	2.409	.0598
24	.845	.203	3.814	.1194
25	1.003	.301	5.663	.1979
26	1.150	.319	6.011	.2126
28	1.547	.343	6.449	.2312
29	1.810	.340	6.404	.2293
30	2.009	.348	6.541	.2351
70° sidewall centerline ($y/H = 0.50$)				
2	0.590	0.199	3.749	0.1166
4	.994	.649	12.205	.4754
5	1.075	.436	8.211	.3060
6	1.256	.354	6.655	.2399
7	1.436	.350	6.588	.2371
8	1.611	.345	6.498	.2333
9	1.796	.397	7.468	.2745
10	1.979	.276	5.190	.1778
70° sidewall ($y/H = 0.87$)				
34	0.782	0.626	11.785	0.4577
13	.991	.569	10.707	.4119
35	1.067	.526	9.896	.3775
36	1.234	.924	17.384	.6952
70° sidewall ($y/H = 0.13$)				
14	0.673	0.145	2.728	0.0733
15	.772	.210	3.946	.1250
16	.871	.311	5.861	.2062
17	.970	.479	9.009	.3398

Table 32. Pressure Distributions for Run 2289 for $\Lambda = 70°$ Model

[CF_4 Tunnel; CR = 9; 25-percent cowl; $N_{Re} = 0.89 \times 10^5$ per foot]

Orifice	x'/T'_x	p, psia	p/p_1	C_p
Baseplate centerline				
20	0.190	0.012	1.629	0.0261
21	.448	.018	2.349	.0559
22	.567	.020	2.680	.0696
23	.686	.025	3.275	.0942
24	.845	.033	4.420	.1417
25	1.003	.051	6.808	.2405
26	1.150	.061	8.117	.2948
28	1.547	.075	10.040	.3744
29	1.810	.077	10.231	.3823
30	2.009	.076	10.182	.3803
70° sidewall centerline ($y/H = 0.50$)				
2	0.590	0.042	5.548	0.1883
4	.994	.093	12.392	.4718
5	1.075	.078	10.437	.3909
6	1.256	.077	10.216	.3817
7	1.436	.076	10.088	.3764
8	1.611	.074	9.829	.3657
9	1.796	.105	13.987	.5379
10	1.979	.046	6.144	.2130
70° sidewall ($y/H = 0.87$)				
34	0.782	0.093	12.342	0.4697
13	.991	.088	11.770	.4460
35	1.067	.111	14.838	.5731
36	1.234	.168	22.400	.8863
70° sidewall ($y/H = 0.13$)				
14	0.673	0.032	4.276	0.1357
15	.772	.045	5.959	.2054
16	.871	.054	7.144	.2544
17	.970	.064	8.523	.3116

Table 33. Pressure Distributions for Run 2290 for $\Lambda = 70°$ Model

[CF_4 Tunnel; CR = 9; 25-percent cowl; $N_{Re} = 2.85 \times 10^5$ per foot]

Orifice	x'/T'_x	p, psia	p/p_1	C_p
Baseplate centerline				
20	0.190	0.035	1.358	0.0149
21	.448	.048	1.880	.0368
22	.567	.055	2.167	.0487
23	.686	.064	2.484	.0620
24	.845	.102	4.002	.1254
25	1.003	.152	5.953	.2069
26	1.150	.169	6.587	.2333
28	1.547	.185	7.212	.2594
29	1.810	.177	6.932	.2477
30	2.009	.182	7.117	.2555
70° sidewall centerline ($y/H = 0.50$)				
2	0.590	0.113	4.420	0.1428
4	.994	.309	12.082	.4628
5	1.075	.213	8.312	.3053
6	1.256	.188	7.331	.2644
7	1.436	.185	7.224	.2599
8	1.611	.184	7.177	.2580
9	1.796	.246	9.601	.3592
10	1.979	.150	5.874	.2036
70° sidewall ($y/H = 0.87$)				
34	0.782	0.299	11.681	0.4461
13	.991	.277	10.808	.4096
35	1.067	.289	11.272	.4290
36	1.234	.508	19.839	.7867
70° sidewall ($y/H = 0.13$)				
14	0.673	0.079	3.074	0.0866
15	.772	.112	4.370	.1407
16	.871	.174	6.798	.2421
17	.970	.213	8.317	.3055

Table 34. Listing of Parameters for Each Plot

Figure 6: Schlieren photographs for $\Lambda = 30°$ model at $N_{Re} = 5.50 \times 10^5$ per foot.
(a) Run 2262. CR = 3; 0-percent cowl.
(b) Run 2267. CR = 3; 25-percent cowl.
(c) Run 2270. CR = 5; 0-percent cowl.
(d) Run 2272. CR = 9; 0-percent cowl.
(e) Run 2273. CR = 9; 25-percent cowl.
(f) Run 2274. CR = 9; no cowl.

Figure 7: Schlieren photographs for $\Lambda = 70°$ model at $N_{Re} = 5.50 \times 10^5$ per foot.
(a) Run 2277. CR = 3; 0-percent cowl.
(b) Run 2282. CR = 5; 0-percent cowl.
(c) Run 2285. CR = 5; no cowl.
(d) Run 2287. CR = 9; 0-percent cowl.

Figure 8: Configuration-complete plots for $\Lambda = 30°$ model at various Reynolds numbers.
(a) Run 2262. CR = 3; 0-percent cowl; $N_{Re} = 5.50 \times 10^5$ per foot.
(b) Run 2263. CR = 3; no cowl; $N_{Re} = 2.85 \times 10^5$ per foot.
(c) Run 2264. CR = 3; no cowl; $N_{Re} = 5.50 \times 10^5$ per foot.
(d) Run 2265. CR = 3; 0-percent cowl; $N_{Re} = 0.89 \times 10^5$ per foot.
(e) Run 2266. CR = 3; 0-percent cowl; $N_{Re} = 2.85 \times 10^5$ per foot.
(f) Run 2267. CR = 3; 25-percent cowl; $N_{Re} = 5.50 \times 10^5$ per foot.
(g) Run 2268. CR = 5; 25-percent cowl; $N_{Re} = 5.50 \times 10^5$ per foot.
(h) Run 2270. CR = 5; 0-percent cowl; $N_{Re} = 5.50 \times 10^5$ per foot.
(i) Run 2271. CR = 5; no cowl; $N_{Re} = 5.50 \times 10^5$ per foot.
(j) Run 2272. CR = 9; 0-percent cowl; $N_{Re} = 5.50 \times 10^5$ per foot.
(k) Run 2273. CR = 9; 25-percent cowl; $N_{Re} = 5.50 \times 10^5$ per foot.
(l) Run 2274. CR = 9; no cowl; $N_{Re} = 5.50 \times 10^5$ per foot.

Figure 9: Configuration-complete plots for $\Lambda = 70°$ model at various Reynolds numbers.
(a) Run 2275. CR = 3; 0-percent cowl; $N_{Re} = 0.89 \times 10^5$ per foot.
(b) Run 2276. CR = 3; 0-percent cowl; $N_{Re} = 2.85 \times 10^5$ per foot.
(c) Run 2277. CR = 3; 0-percent cowl; $N_{Re} = 5.50 \times 10^5$ per foot.
(d) Run 2278. CR = 3; 25-percent cowl; $N_{Re} = 5.50 \times 10^5$ per foot.
(e) Run 2279. CR = 3; no cowl; $N_{Re} = 5.50 \times 10^5$ per foot.
(f) Run 2280. CR = 3; 25-percent cowl; $N_{Re} = 5.50 \times 10^5$ per foot.
(g) Run 2281. CR = 3; 0-percent cowl; $N_{Re} = 5.50 \times 10^5$ per foot.
(h) Run 2282. CR = 5; 0-percent cowl; $N_{Re} = 5.50 \times 10^5$ per foot.
(i) Run 2284. CR = 5; 25-percent cowl; $N_{Re} = 5.50 \times 10^5$ per foot.
(j) Run 2285. CR = 5; no cowl; $N_{Re} = 5.50 \times 10^5$ per foot.
(k) Run 2286. CR = 9; no cowl; $N_{Re} = 5.50 \times 10^5$ per foot.
(l) Run 2287. CR = 9; 0-percent cowl; $N_{Re} = 5.50 \times 10^5$ per foot.
(m) Run 2288. CR = 9; 25-percent cowl; $N_{Re} = 5.50 \times 10^5$ per foot.
(n) Run 2289. CR = 9; 25-percent cowl; $N_{Re} = 0.89 \times 10^5$ per foot.
(o) Run 2290. CR = 9; 25-percent cowl; $N_{Re} = 2.85 \times 10^5$ per foot.

Table 34. Continued

Figure 10: Contraction ratio effects on pressure distributions of $\Lambda = 30°$ model with 0-percent cowl and $N_{Re} = 5.50 \times 10^5$ per foot.
(a) Baseplate centerline.
(b) Sidewall at $y/H = 0.13$.
(c) Sidewall centerline.
(d) Sidewall at $y/H = 0.87$.
(e) Cowl centerline.

Figure 11: Contraction ratio effects on pressure distributions of $\Lambda = 30°$ model with 25-percent cowl and $N_{Re} = 5.50 \times 10^5$ per foot.
(a) Baseplate centerline.
(b) Sidewall at $y/H = 0.13$.
(c) Sidewall centerline.
(d) Sidewall at $y/H = 0.87$.
(e) Cowl centerline.

Figure 12: Contraction ratio effects on pressure distributions of $\Lambda = 30°$ model with no cowl and $N_{Re} = 5.50 \times 10^5$ per foot.
(a) Baseplate centerline.
(b) Sidewall at $y/H = 0.13$.
(c) Sidewall centerline.
(d) Sidewall at $y/H = 0.87$.

Figure 13: Contraction ratio effects on pressure distributions of $\Lambda = 70°$ model with 0-percent cowl and $N_{Re} = 5.50 \times 10^5$ per foot.
(a) Baseplate centerline.
(b) Sidewall at $y/H = 0.13$.
(c) Sidewall centerline.
(d) Sidewall at $y/H = 0.87$.
(e) Cowl centerline.

Figure 14: Contraction ratio effects on pressure distributions of $\Lambda = 70°$ model with 25-percent cowl and $N_{Re} = 5.50 \times 10^5$ per foot.
(a) Baseplate centerline.
(b) Sidewall at $y/H = 0.13$.
(c) Sidewall centerline.
(d) Sidewall at $y/H = 0.87$.
(e) Cowl centerline.

Figure 15: Contraction ratio effects on pressure distributions of $\Lambda = 70°$ model with no cowl and $N_{Re} = 5.50 \times 10^5$ per foot.
(a) Baseplate centerline.
(b) Sidewall at $y/H = 0.13$.
(c) Sidewall centerline.
(d) Sidewall at $y/H = 0.87$.

Table 34. Continued

Figure 16: Cowl position effects on pressure distributions of $\Lambda = 30°$ model with CR = 3 and $N_{Re} = 5.50 \times 10^5$ per foot.
(a) Baseplate centerline.
(b) Sidewall at $y/H = 0.13$.
(c) Sidewall centerline.
(d) Sidewall at $y/H = 0.87$.
(e) Cowl centerline.

Figure 17: Cowl position effects on pressure distributions of $\Lambda = 30°$ model with CR = 5 and $N_{Re} = 5.50 \times 10^5$ per foot.
(a) Baseplate centerline.
(b) Sidewall at $y/H = 0.13$.
(c) Sidewall centerline.
(d) Sidewall at $y/H = 0.87$.
(e) Cowl centerline.

Figure 18: Cowl position effects on pressure distributions of $\Lambda = 30°$ model with CR = 9 and $N_{Re} = 5.50 \times 10^5$ per foot.
(a) Baseplate centerline.
(b) Sidewall at $y/H = 0.13$.
(c) Sidewall centerline.
(d) Sidewall at $y/H = 0.87$.
(e) Cowl centerline.

Figure 19: Cowl position effects on pressure distributions of $\Lambda = 70°$ model with CR = 3 and $N_{Re} = 5.50 \times 10^5$ per foot.
(a) Baseplate centerline.
(b) Sidewall at $y/H = 0.13$.
(c) Sidewall centerline.
(d) Sidewall at $y/H = 0.87$.
(e) Cowl centerline.

Figure 20: Cowl position effects on pressure distributions of $\Lambda = 70°$ model with CR = 5 and $N_{Re} = 5.50 \times 10^5$ per foot.
(a) Baseplate centerline.
(b) Sidewall at $y/H = 0.13$.
(c) Sidewall centerline.
(d) Sidewall at $y/H = 0.87$.
(e) Cowl centerline.

Figure 21: Cowl position effects on pressure distributions of $\Lambda = 70°$ model with CR = 9 and $N_{Re} = 5.50 \times 10^5$ per foot.
(a) Baseplate centerline.
(b) Sidewall at $y/H = 0.13$.
(c) Sidewall centerline.
(d) Sidewall at $y/H = 0.87$.
(e) Cowl centerline.

Table 34. Continued

Figure 22: Reynolds number effects on pressure distributions of $\Lambda = 30°$ model with CR = 3 and 0-percent cowl.
(a) Baseplate centerline.
(b) Sidewall at $y/H = 0.13$.
(c) Sidewall centerline.
(d) Sidewall at $y/H = 0.87$.
(e) Cowl centerline.

Figure 23: Reynolds number effects on pressure distributions of $\Lambda = 70°$ model with CR = 9 and 25-percent cowl.
(a) Baseplate centerline.
(b) Sidewall at $y/H = 0.13$.
(c) Sidewall centerline.
(d) Sidewall at $y/H = 0.87$.
(e) Cowl centerline.

Figure 24: Leading-edge sweep effects on pressure distributions of both models with CR = 3, 0-percent cowl, and $N_{Re} = 5.50 \times 10^5$ per foot.
(a) Baseplate centerline.
(b) Sidewall at $y/H = 0.13$.
(c) Sidewall centerline.
(d) Sidewall at $y/H = 0.87$.

Figure 25: Leading-edge sweep effects on pressure distributions of both models with CR = 5, 0-percent cowl, and $N_{Re} = 5.50 \times 10^5$ per foot.
(a) Baseplate centerline.
(b) Sidewall at $y/H = 0.13$.
(c) Sidewall centerline.
(d) Sidewall at $y/H = 0.87$.

Figure 26: Leading-edge sweep effects on pressure distributions of both models with CR = 9, 0-percent cowl, and $N_{Re} = 5.50 \times 10^5$ per foot.
(a) Baseplate centerline.
(b) Sidewall at $y/H = 0.13$.
(c) Sidewall centerline.
(d) Sidewall at $y/H = 0.87$.

Figure 27: Leading-edge sweep effects on pressure distributions of both models with CR = 3, 25-percent cowl, and $N_{Re} = 5.50 \times 10^5$ per foot.
(a) Baseplate centerline.
(b) Sidewall at $y/H = 0.13$.
(c) Sidewall centerline.
(d) Sidewall at $y/H = 0.87$.
(e) Cowl centerline.

Table 34. Continued

Figure 28: Leading-edge sweep effects on pressure distributions of both models with CR = 5, 25-percent cowl, and $N_{Re} = 5.50 \times 10^5$ per foot.
(a) Baseplate centerline.
(b) Sidewall at $y/H = 0.13$.
(c) Sidewall centerline.
(d) Sidewall at $y/H = 0.87$.
(e) Cowl centerline.

Figure 29: Leading-edge sweep effects on pressure distributions of both models with CR = 9, 25-percent cowl, and $N_{Re} = 5.50 \times 10^5$ per foot.
(a) Baseplate centerline.
(b) Sidewall at $y/H = 0.13$.
(c) Sidewall centerline.
(d) Sidewall at $y/H = 0.87$.
(e) Cowl centerline.

Figure 30: Leading-edge sweep effects on pressure distributions of both models with CR = 3, no cowl, and $N_{Re} = 5.50 \times 10^5$ per foot.
(a) Baseplate centerline.
(b) Sidewall at $y/H = 0.13$.
(c) Sidewall centerline.
(d) Sidewall at $y/H = 0.87$.

Figure 31: Leading-edge sweep effects on pressure distributions of both models with CR = 5, no cowl, and $N_{Re} = 5.50 \times 10^5$ per foot.
(a) Baseplate centerline.
(b) Sidewall at $y/H = 0.13$.
(c) Sidewall centerline.
(d) Sidewall at $y/H = 0.87$.

Figure 32: Leading-edge sweep effects on pressure distributions of both models with CR = 9, no cowl, and $N_{Re} = 5.50 \times 10^5$ per foot.
(a) Baseplate centerline.
(b) Sidewall at $y/H = 0.13$.
(c) Sidewall centerline.
(d) Sidewall at $y/H = 0.87$.

Figure 33: Leading-edge sweep effects on pressure distributions of both models with CR = 3, 0-percent cowl, and $N_{Re} = 0.89 \times 10^5$ per foot.
(a) Baseplate centerline.
(b) Sidewall at $y/H = 0.13$.
(c) Sidewall centerline.
(d) Sidewall at $y/H = 0.87$.

Table 34. Concluded

Figure 34: Repeatability effects on pressure distributions of $\Lambda = 70°$ model with CR = 3, 0-percent cowl, and $N_{Re} = 5.50 \times 10^5$ per foot.
(a) Baseplate centerline.
(b) Sidewall at $y/H = 0.13$.
(c) Sidewall centerline.
(d) Sidewall at $y/H = 0.87$.

Figure 35: Repeatability effects on pressure distributions of $\Lambda = 70°$ model with CR = 3, 25-percent cowl, and $N_{Re} = 5.50 \times 10^5$ per foot.
(a) Baseplate centerline.
(b) Sidewall at $y/H = 0.13$.
(c) Sidewall centerline.
(d) Sidewall at $y/H = 0.87$.

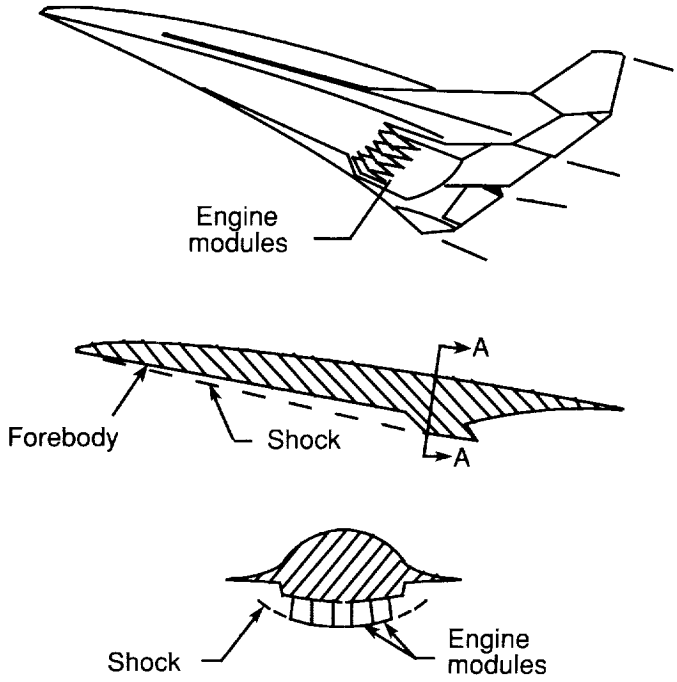

Figure 1. Propulsion airframe integration.

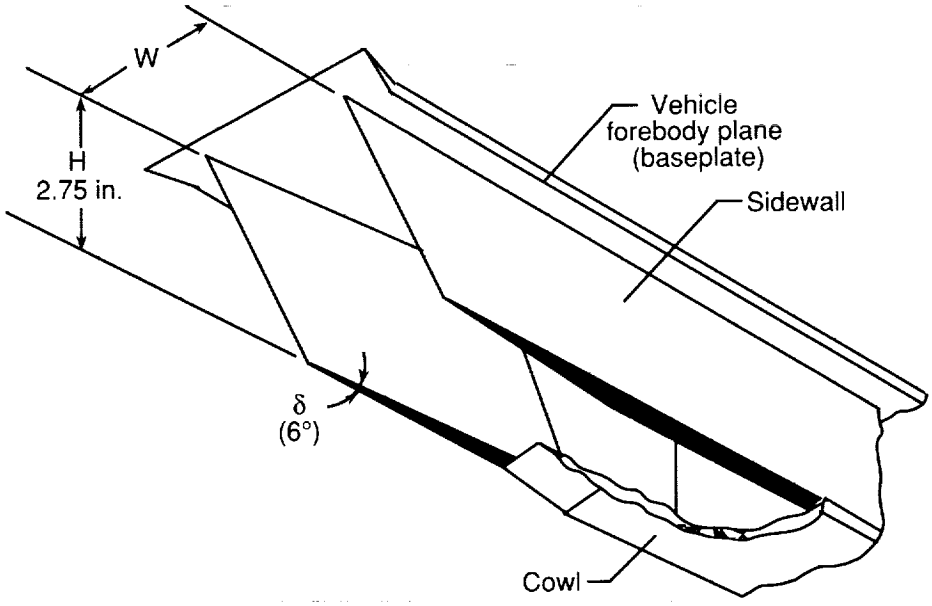

Figure 2. Modular engine construction for airframe integration scramjet inlet.

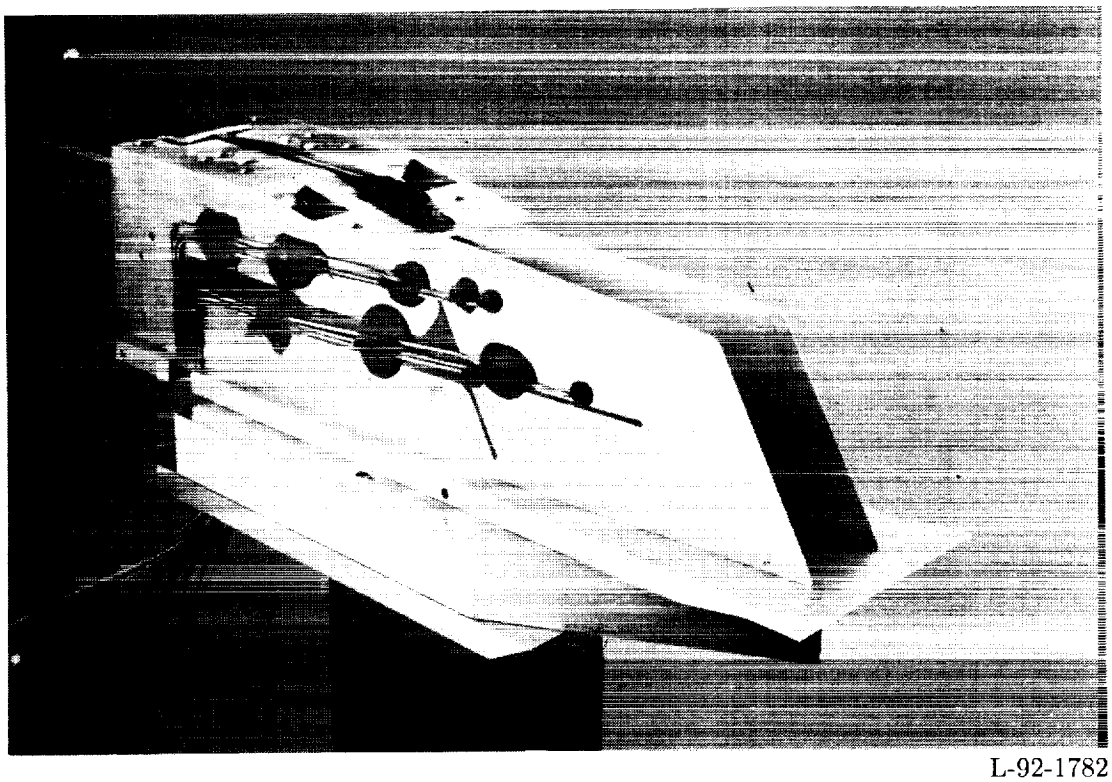

L-92-1782

(a) $\Lambda = 30°$ model.

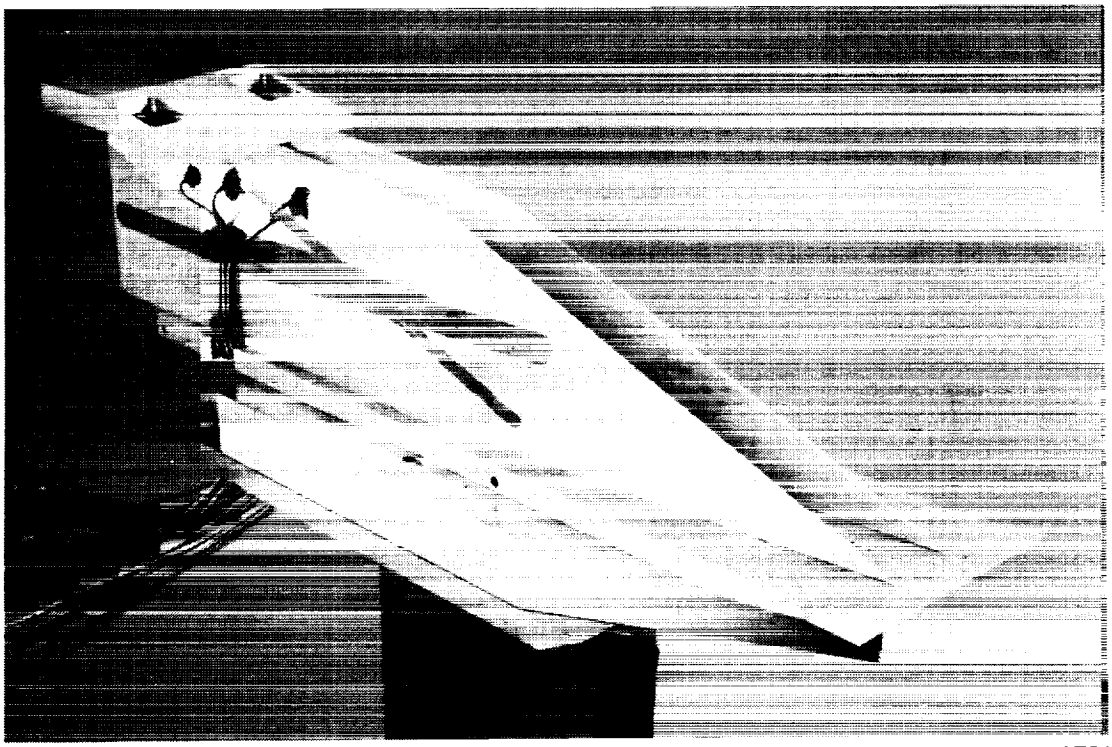

L-92-1781

(b) $\Lambda = 70°$ model.

Figure 3. Photographs of scramjet inlet models.

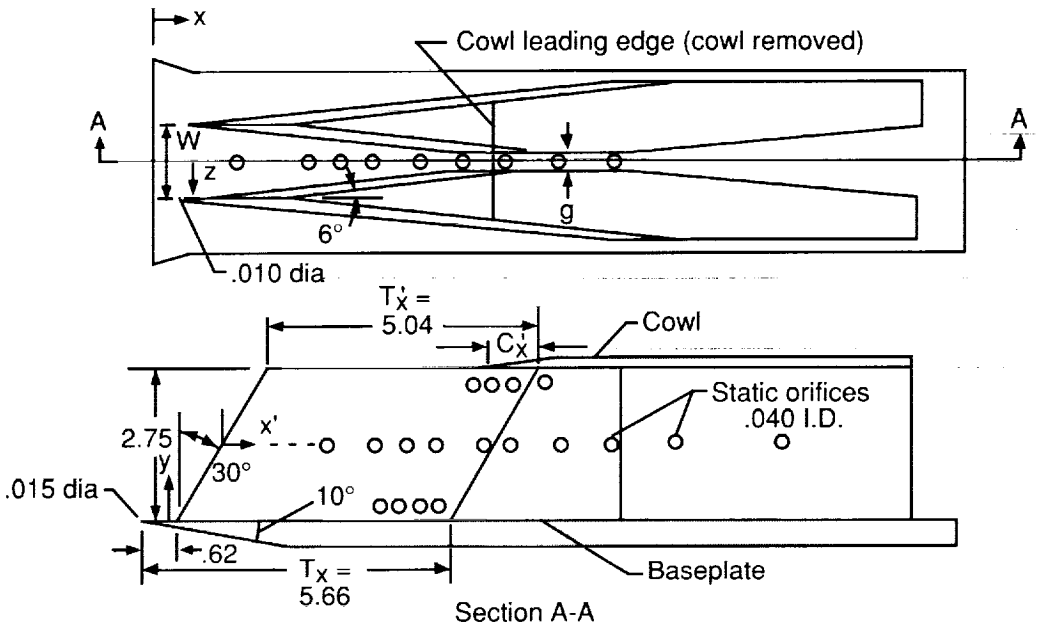

(a) 30° model.

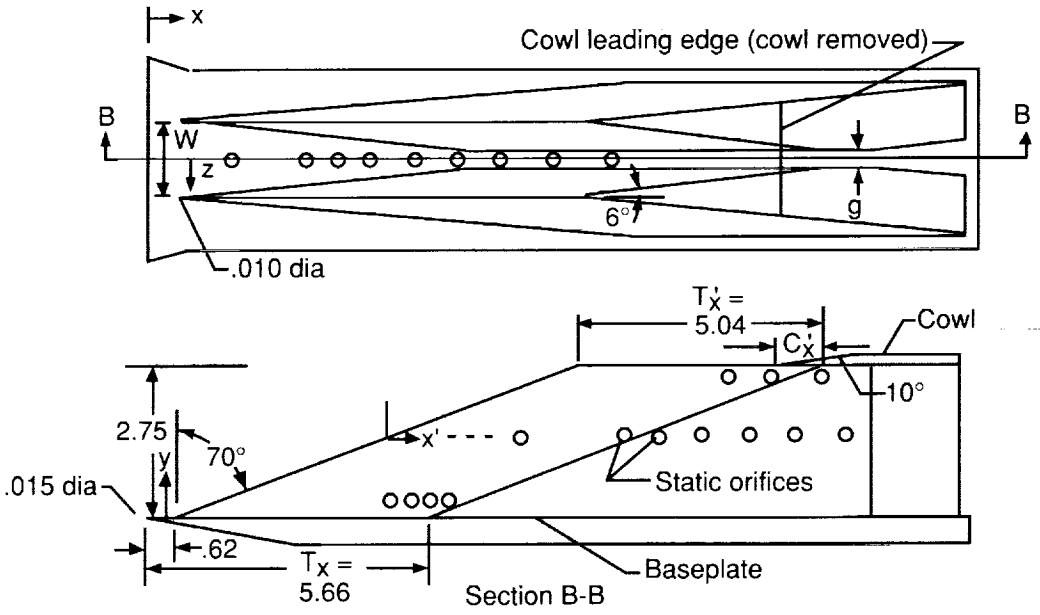

(b) 70° model.

Figure 4. Sketches of inlet models having 30° and 70° leading-edge sweep. Linear dimensions are given in inches.

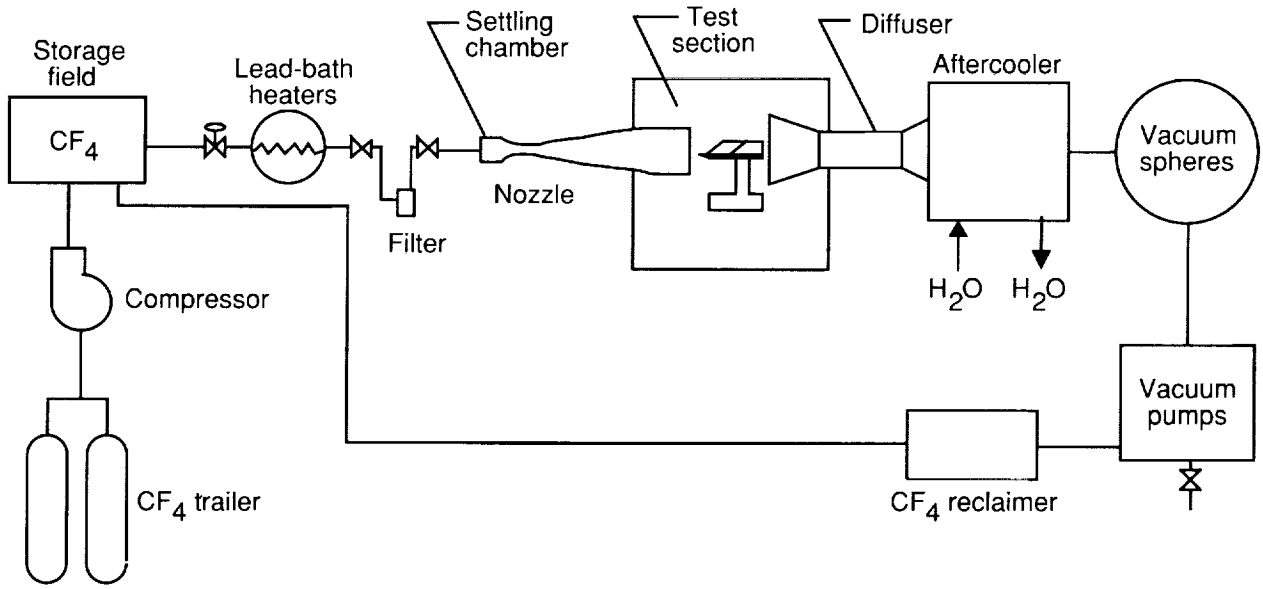

Figure 5. Schematic drawing of the Langley Hypersonic CF_4 Tunnel.

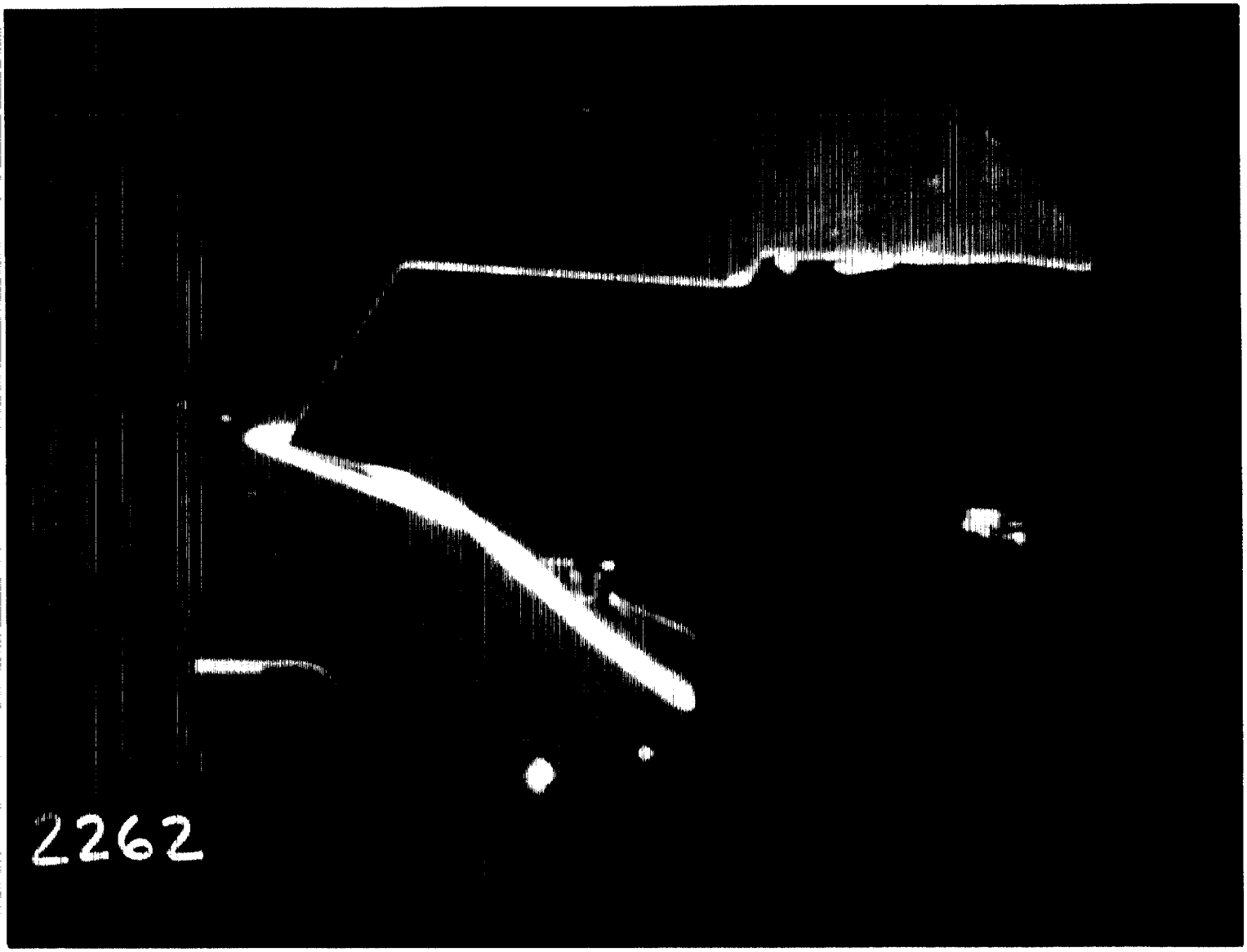

(a) Run 2262. CR = 3; 0-percent cowl.

Figure 6. Photographs of enlarged frames from schlieren movies of $\Lambda = 30°$ model at $N_{Re} = 5.50 \times 10^5$ per foot.

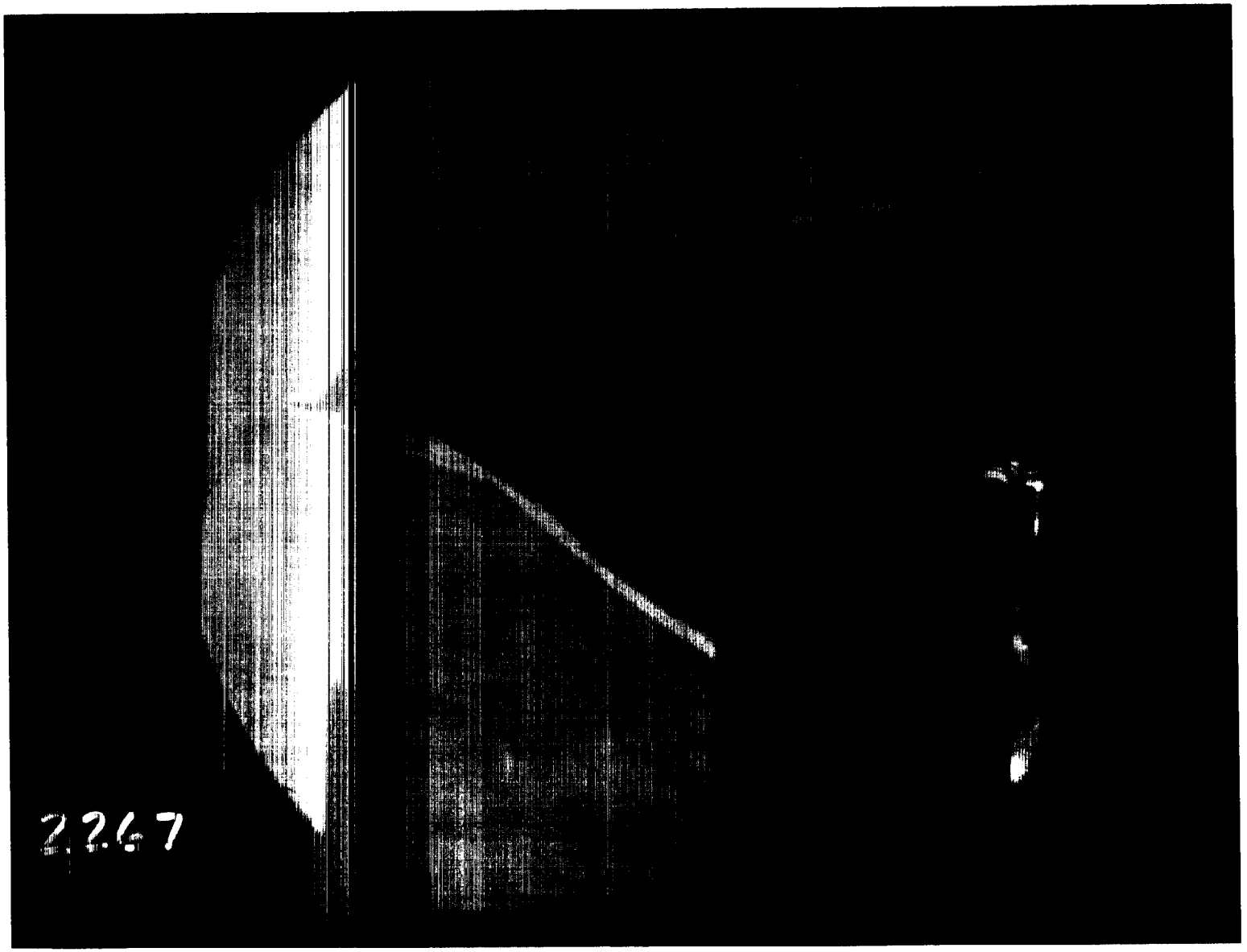

(b) Run 2267. CR = 3; 25-percent cowl.

Figure 6. Continued.

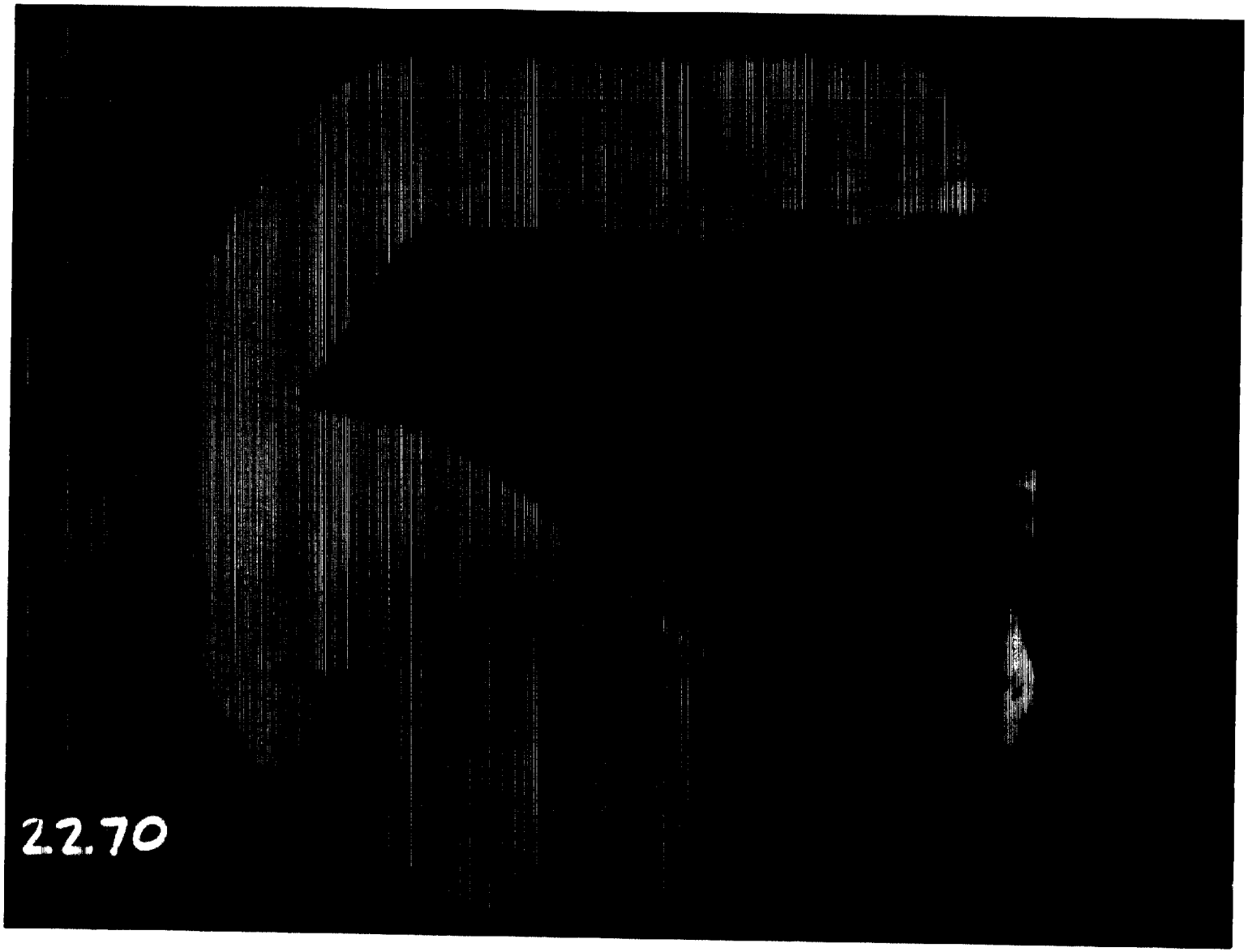

(c) Run 2270. CR = 5; 0-percent cowl.

Figure 6. Continued.

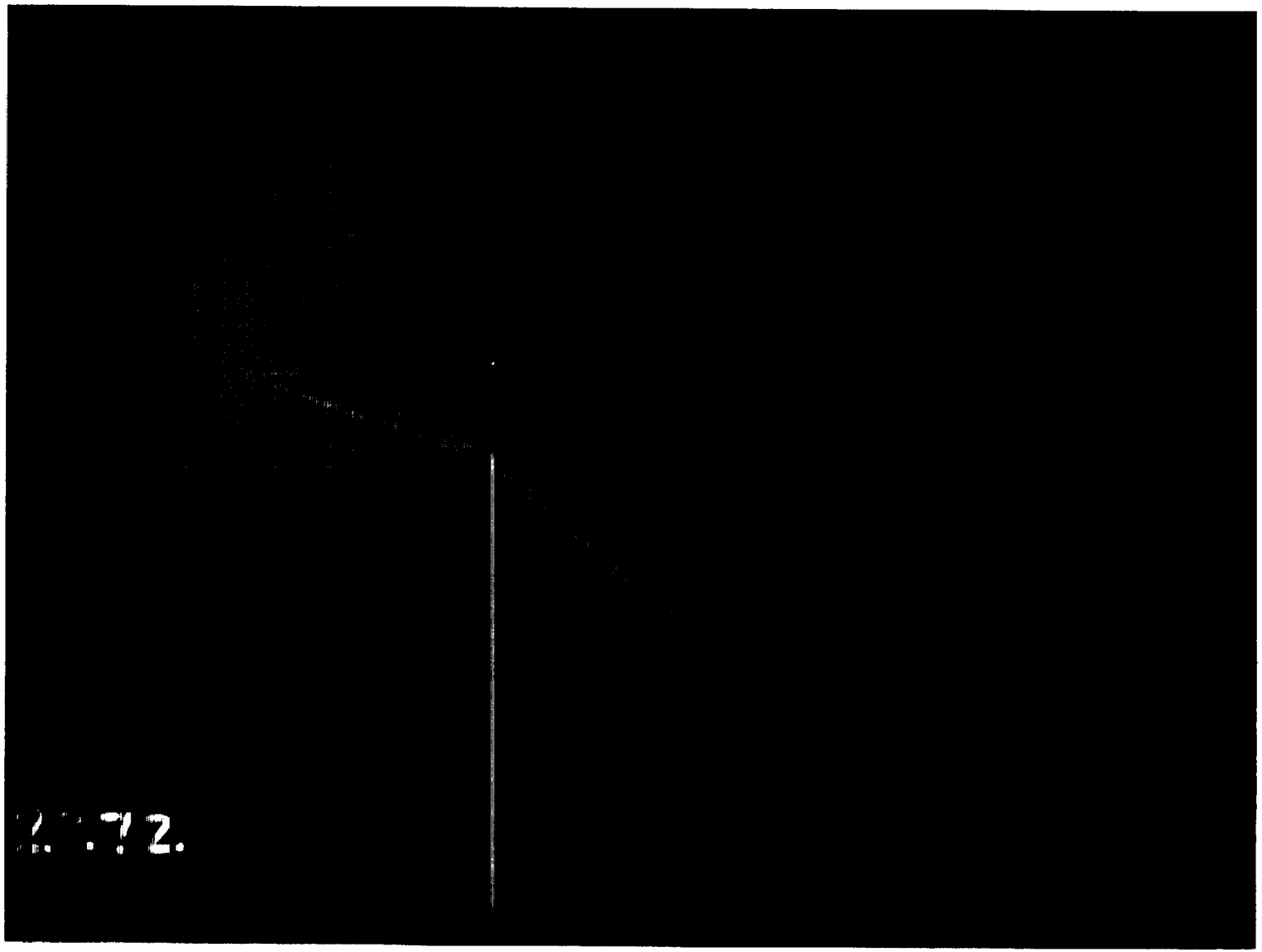

(d) Run 2272. CR = 9; 0-percent cowl.

Figure 6. Continued.

(e) Run 2273. CR = 9; 25-percent cowl.

Figure 6. Continued.

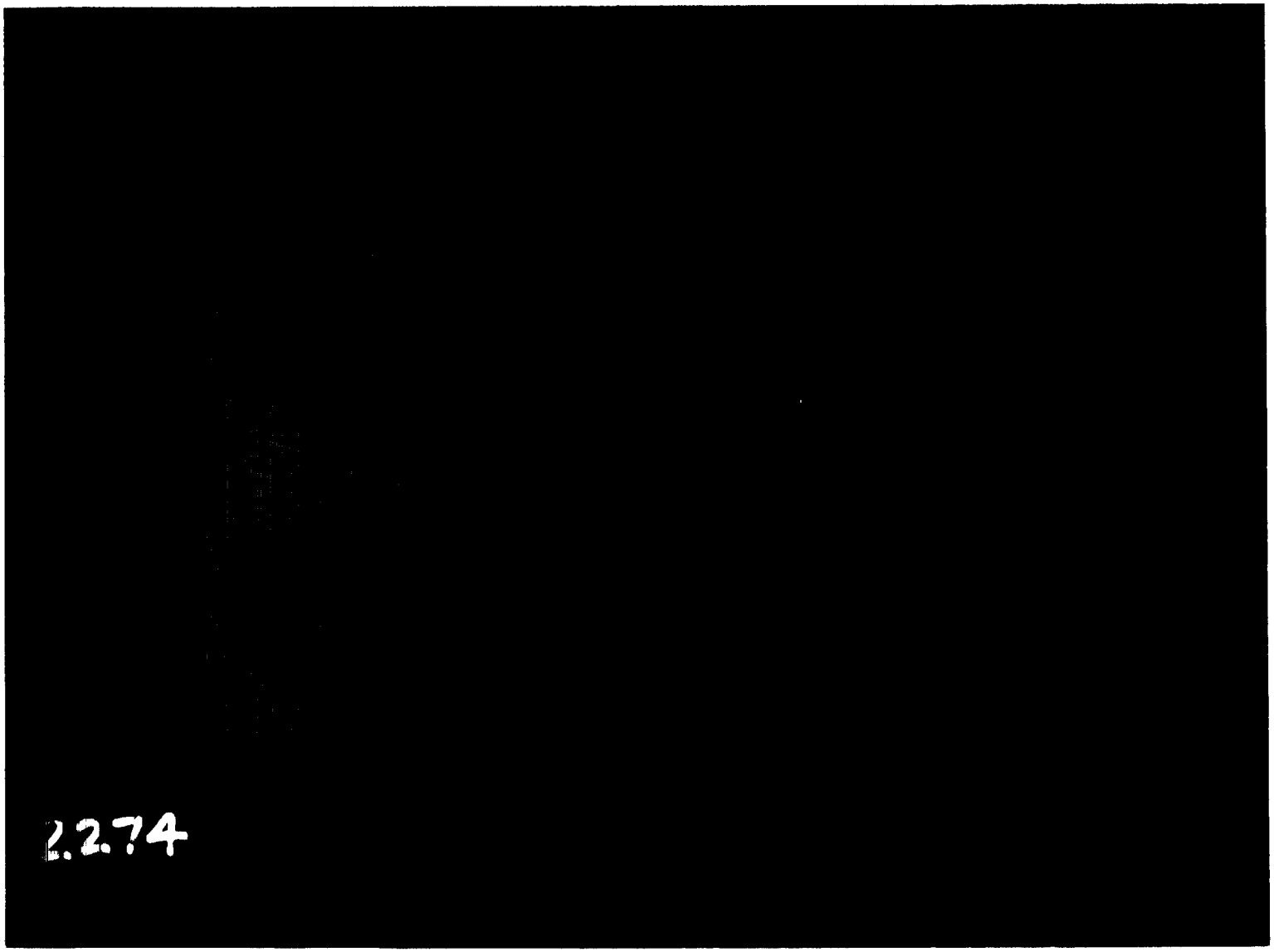

(f) Run 2274. CR = 9; no cowl.

Figure 6. Concluded.

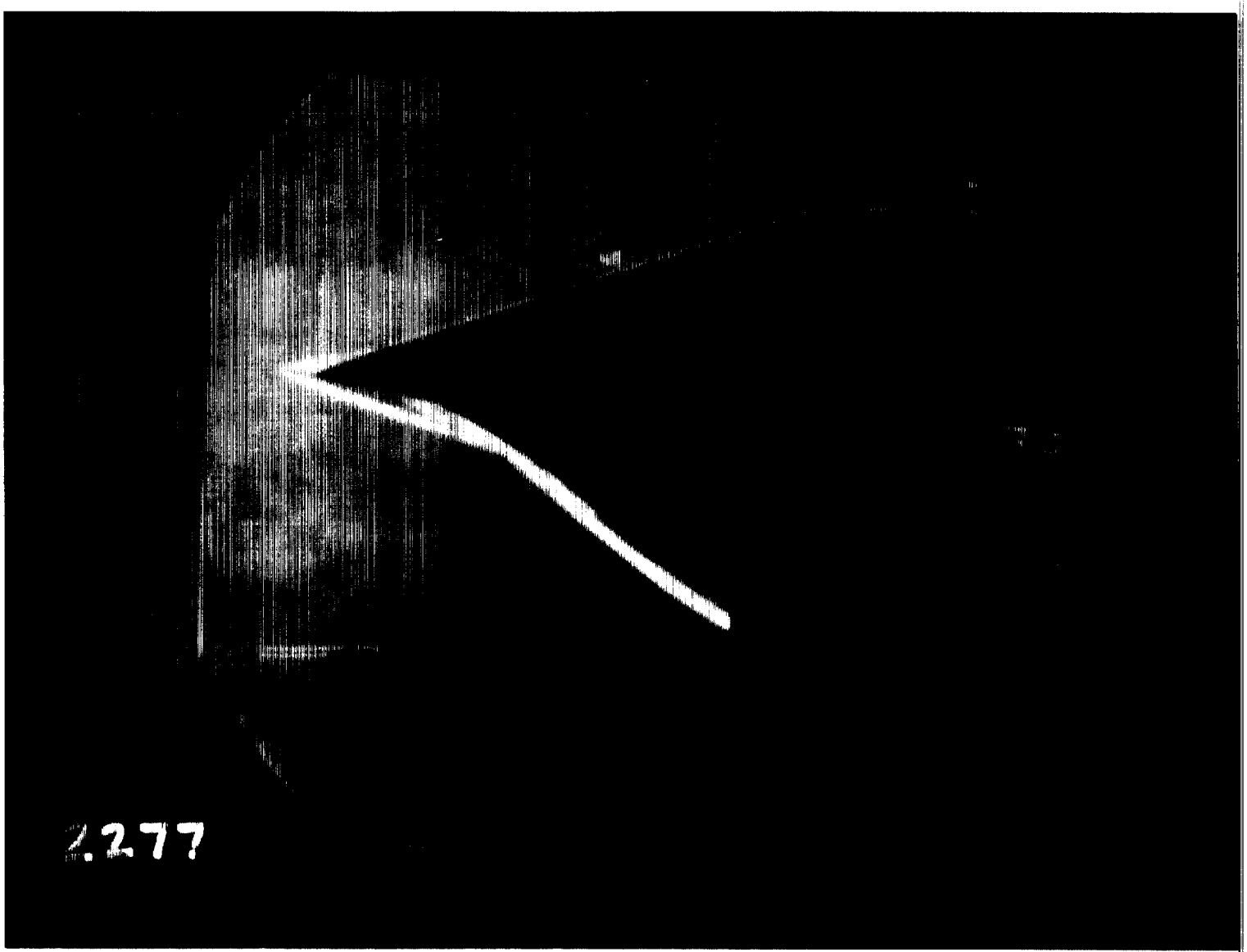

(a) Run 2277. CR = 3; 0-percent cowl.

Figure 7. Photographs of enlarged frames from schlieren movies of $\Lambda = 70°$ model at $N_{Re} = 5.50 \times 10^5$ per foot.

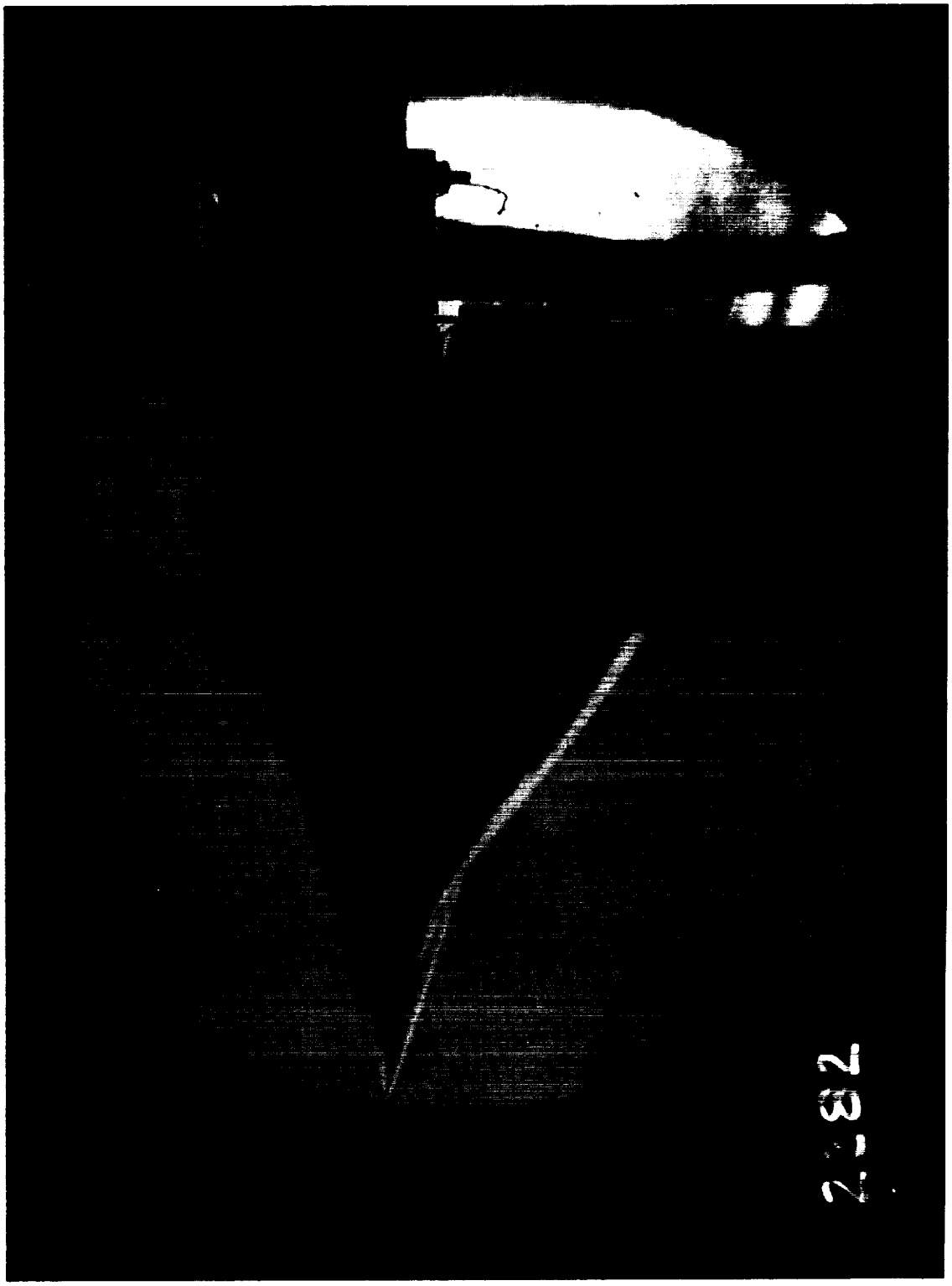

(b) Run 2282. CR = 5; 0-percent cowl.

Figure 7. Continued.

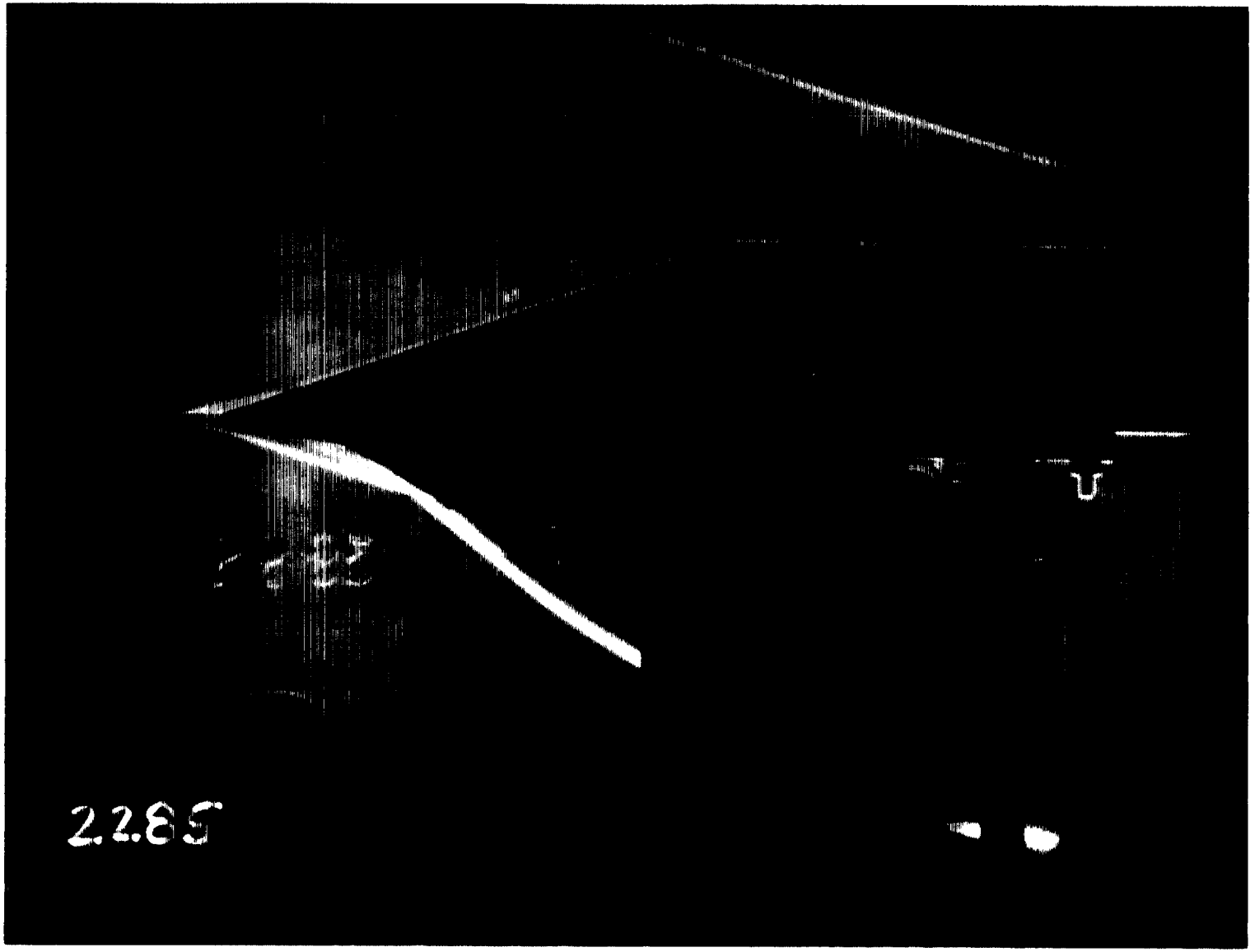

(c) Run 2285. CR = 5; no cowl.

Figure 7. Continued.

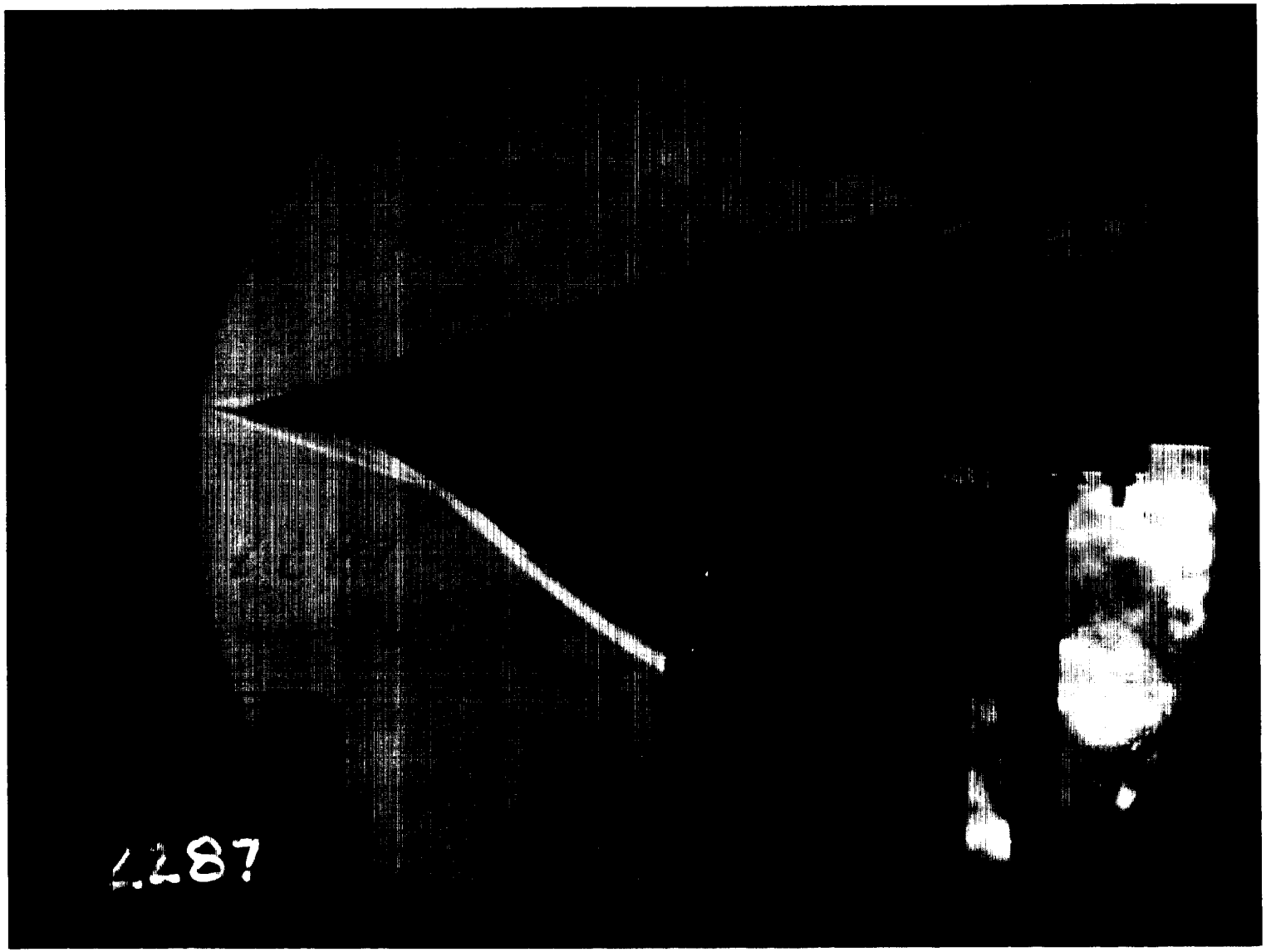

(d) Run 2287. CR = 9; 0-percent cowl.

Figure 7. Concluded.

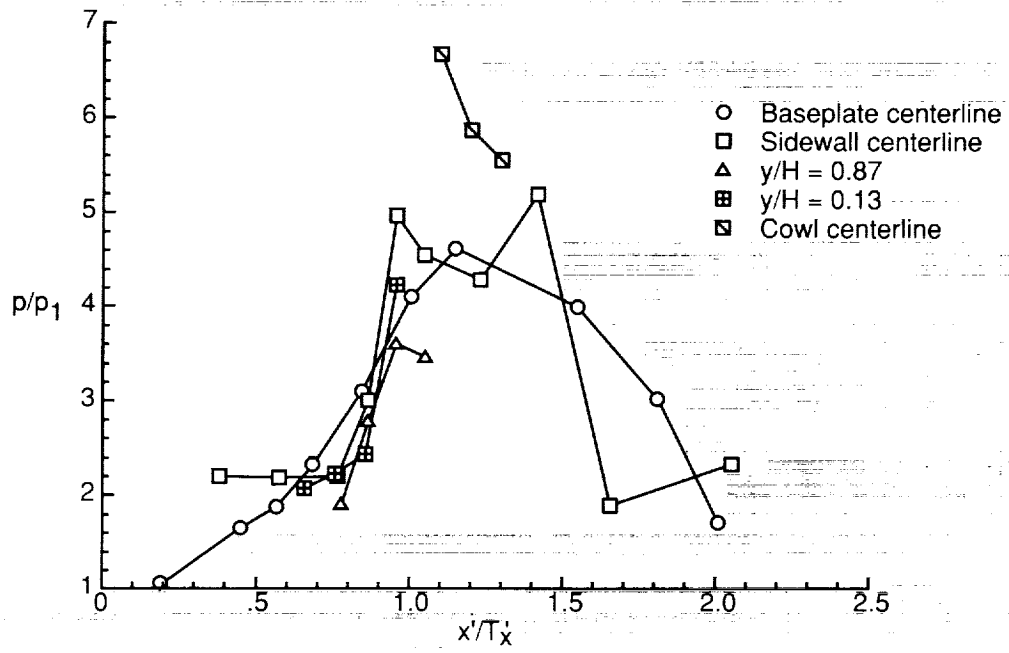

(a) Run 2262. CR = 3; 0-percent cowl; $N_{Re} = 5.50 \times 10^5$ per foot.

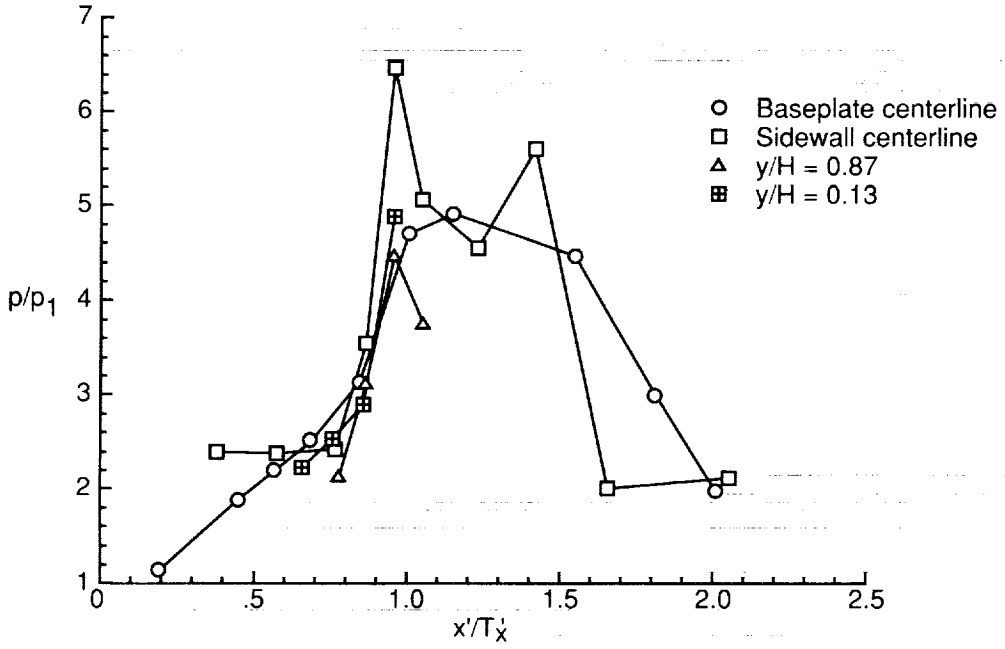

(b) Run 2263. CR = 3; no cowl; $N_{Re} = 2.85 \times 10^5$ per foot.

Figure 8. Configuration-complete plots for $\Lambda = 30°$ model.

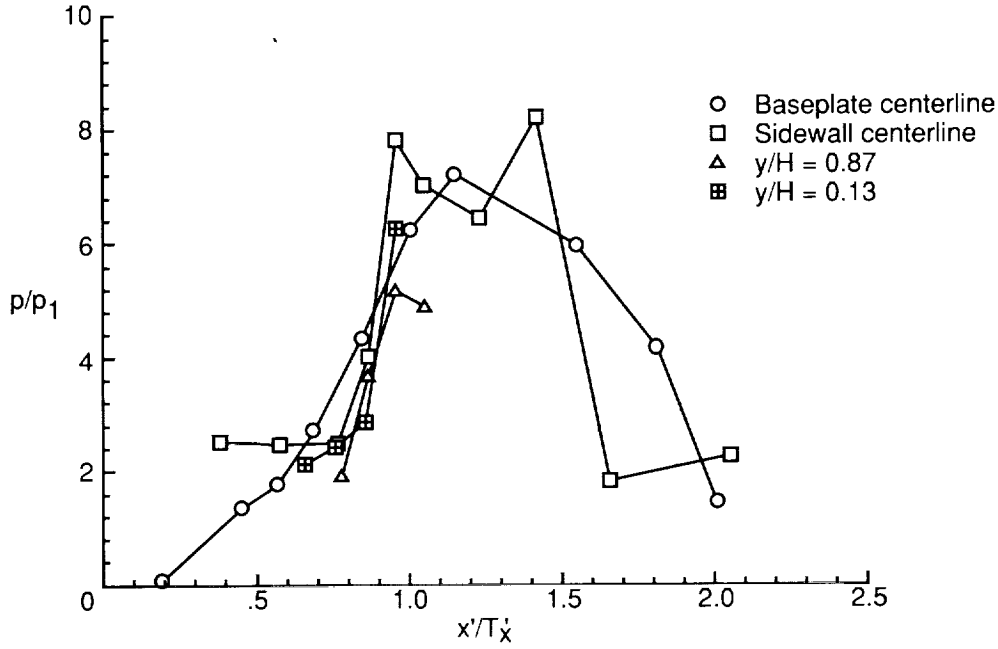

(c) Run 2264. CR = 3; no cowl; $N_{Re} = 5.50 \times 10^5$ per foot.

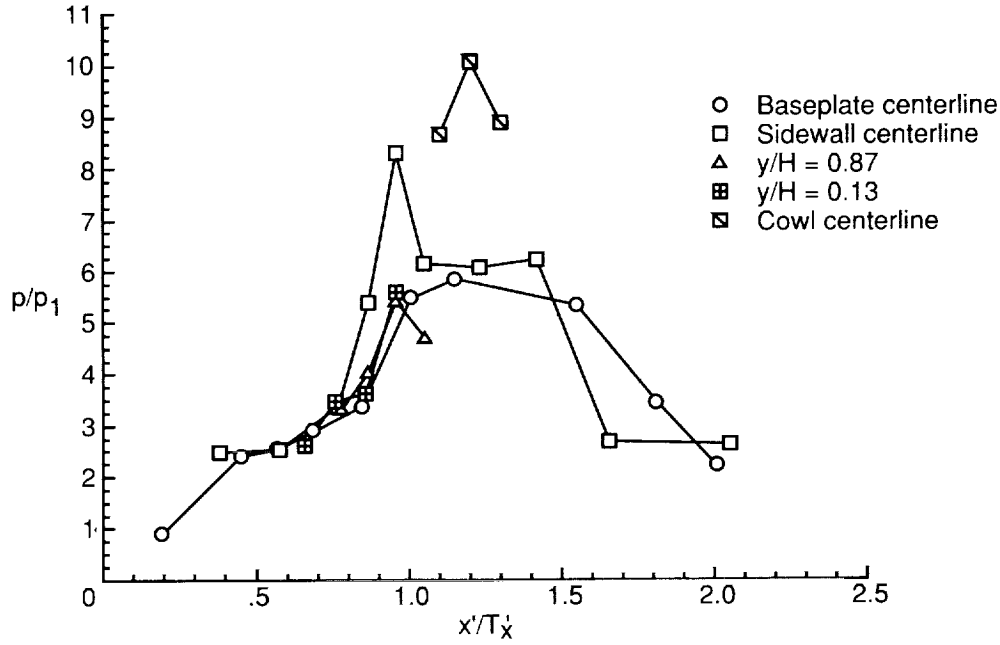

(d) Run 2265. CR = 3; 0-percent cowl; $N_{Re} = 0.89 \times 10^5$ per foot.

Figure 8. Continued.

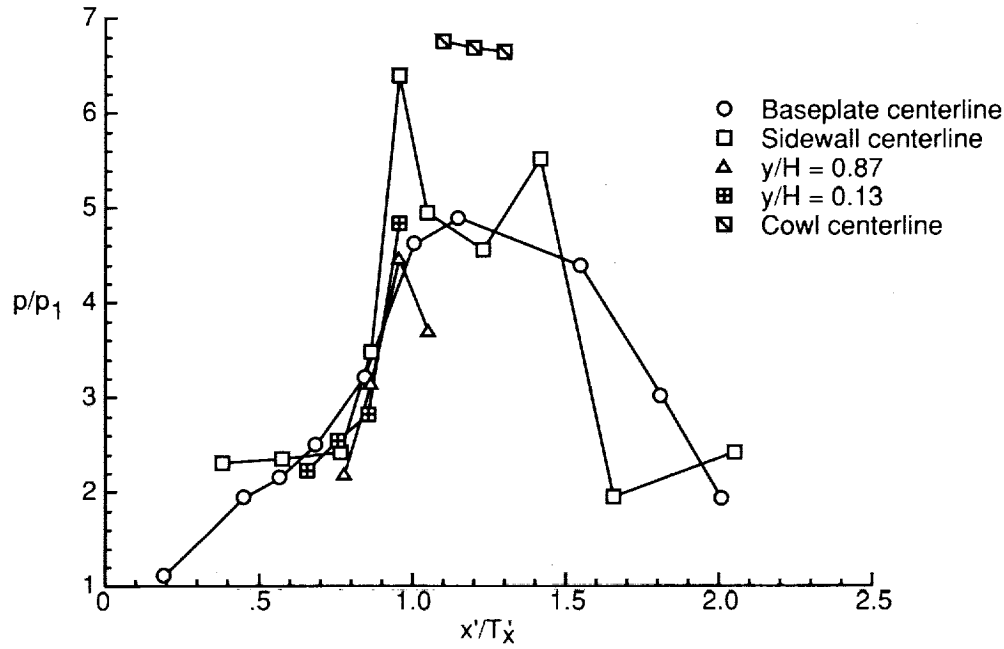

(e) Run 2266. CR = 3; 0-percent cowl; $N_{Re} = 2.85 \times 10^5$ per foot.

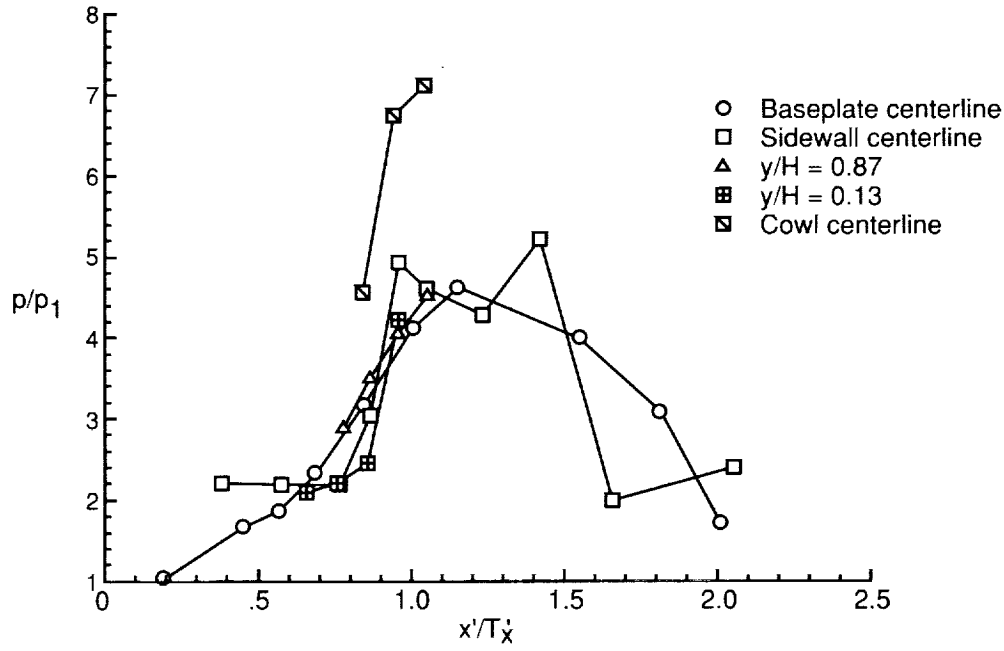

(f) Run 2267. CR = 3; 25-percent cowl; $N_{Re} = 5.50 \times 10^5$ per foot.

Figure 8. Continued.

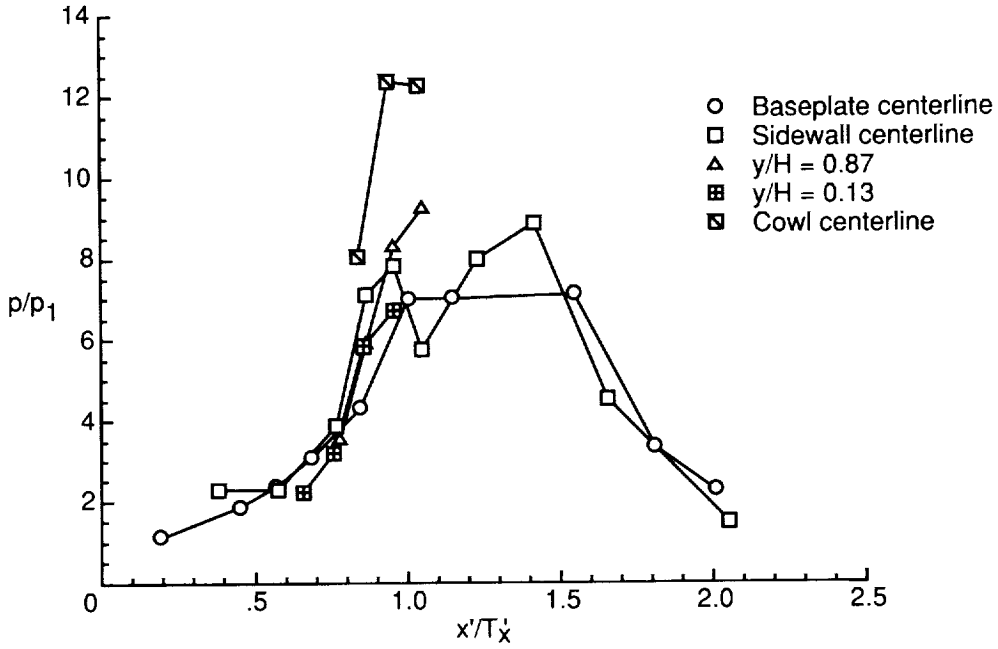

(g) Run 2268. CR = 5; 25-percent cowl; $N_{Re} = 5.50 \times 10^5$ per foot.

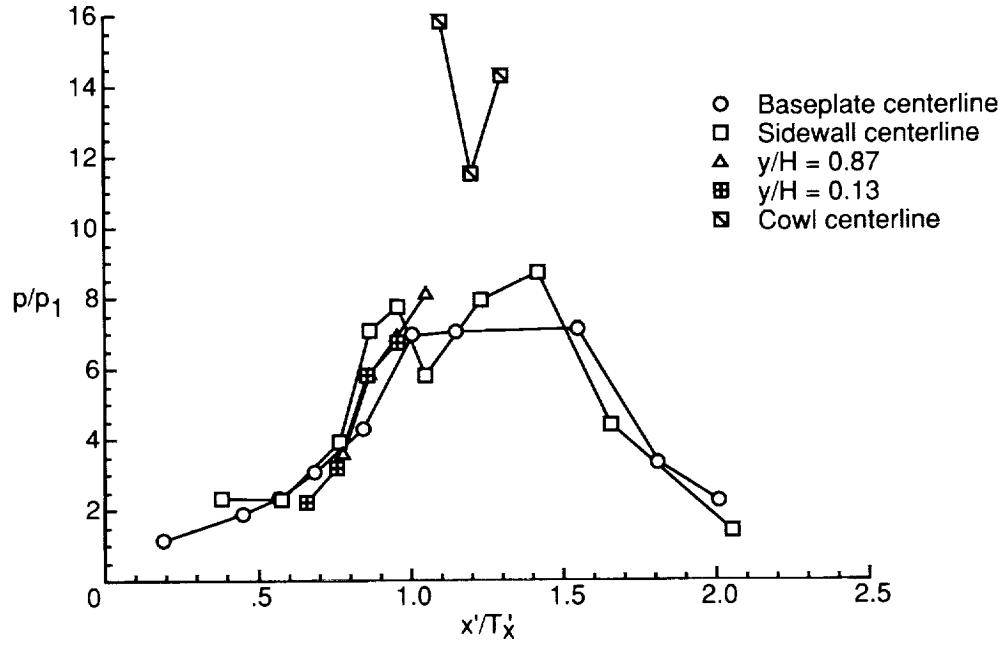

(h) Run 2270. CR = 5; 0-percent cowl; $N_{Re} = 5.50 \times 10^5$ per foot.

Figure 8. Continued.

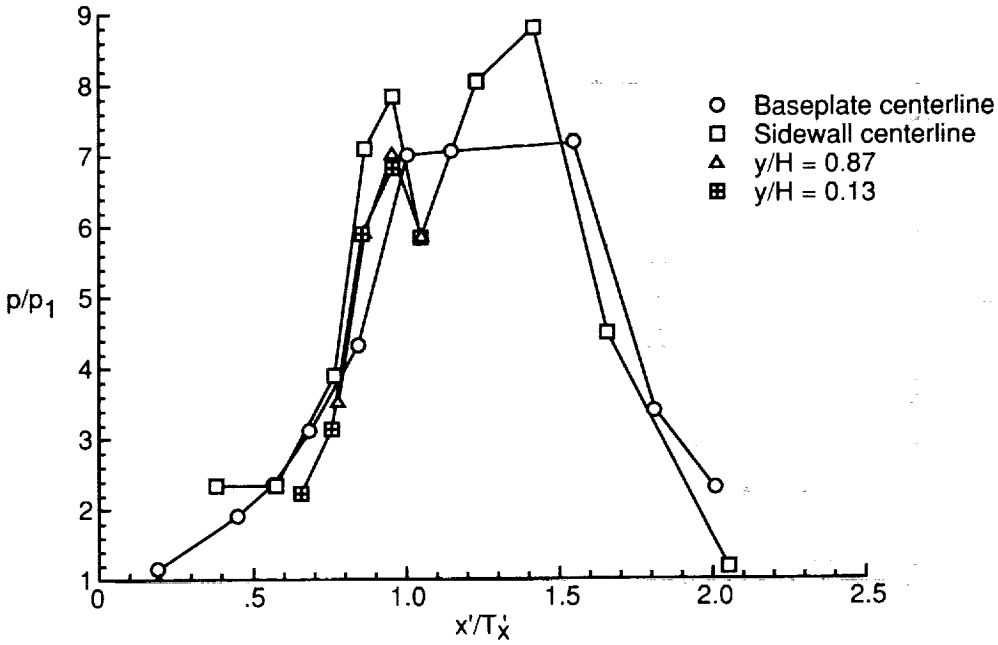

(i) Run 2271. CR = 5; no cowl; $N_{Re} = 5.50 \times 10^5$ per foot.

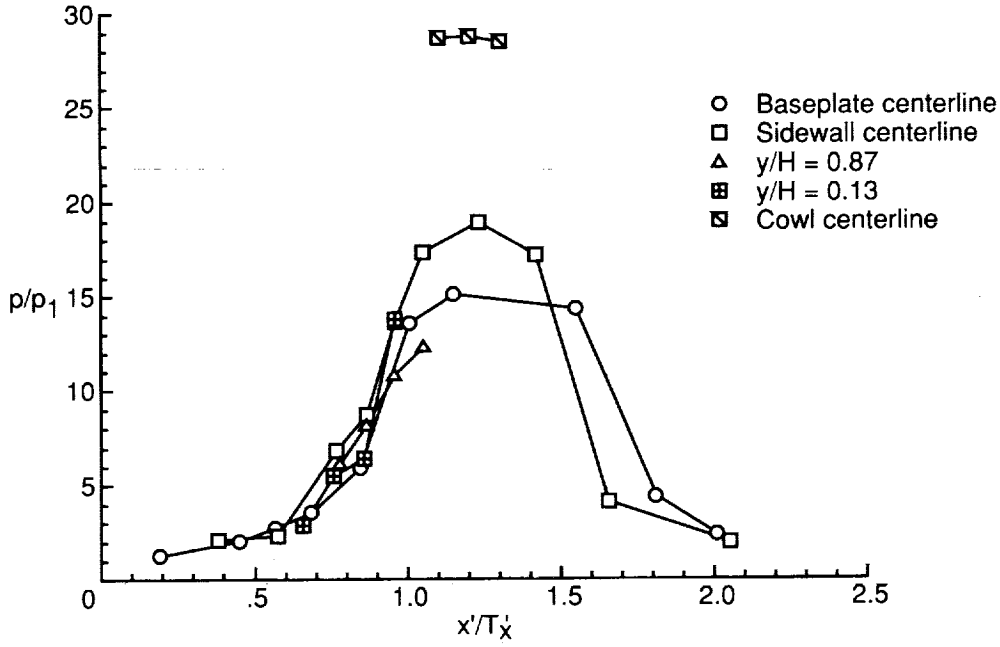

(j) Run 2272. CR = 9; 0-percent cowl; $N_{Re} = 5.50 \times 10^5$ per foot.

Figure 8. Continued.

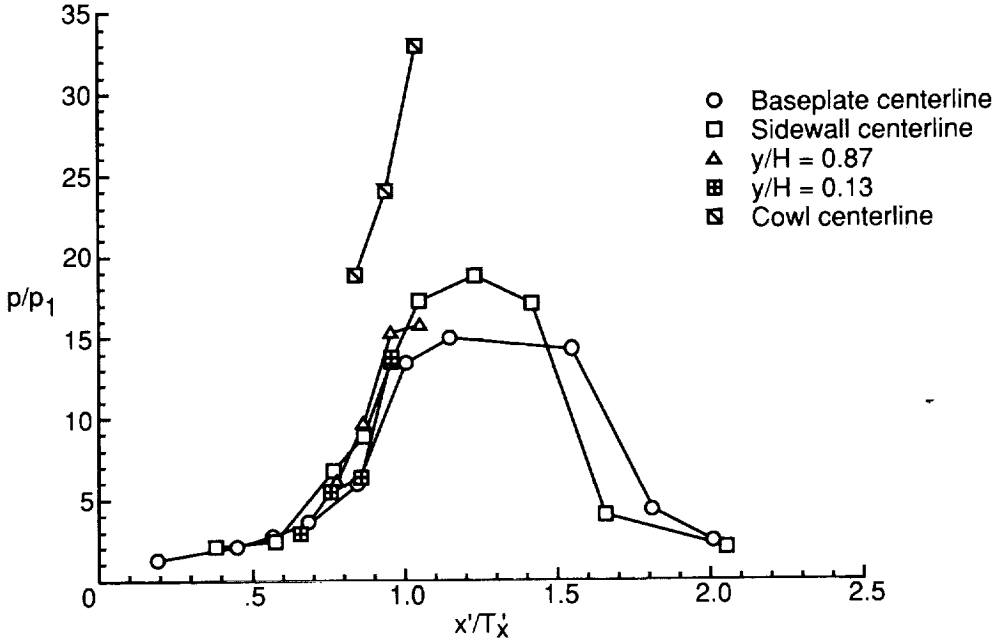

(k) Run 2273. CR = 9; 25-percent cowl; $N_{Re} = 5.50 \times 10^5$ per foot.

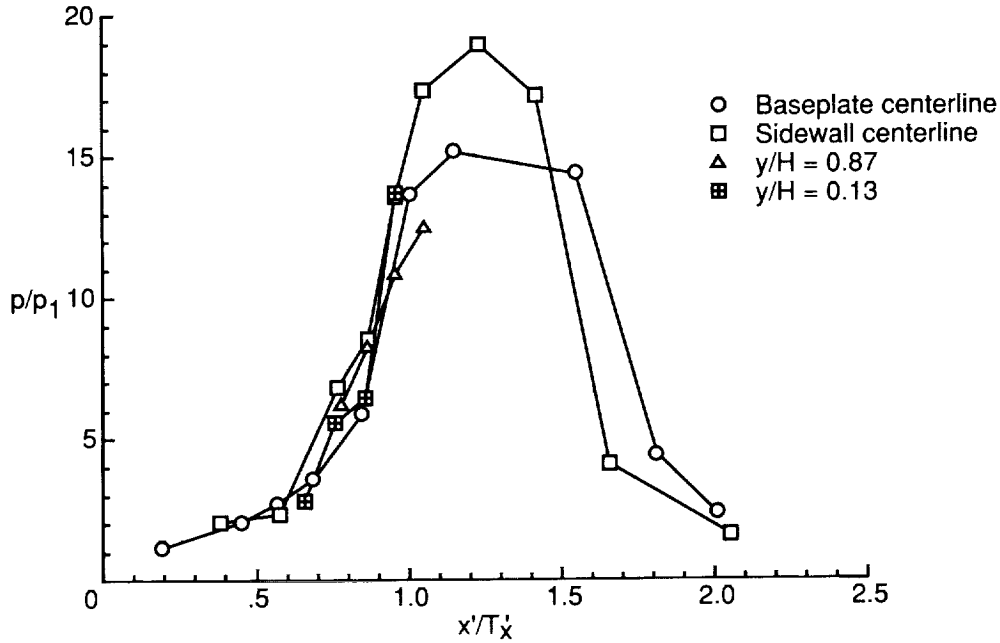

(l) Run 2274. CR = 9; no cowl; $N_{Re} = 5.50 \times 10^5$ per foot.

Figure 8. Concluded.

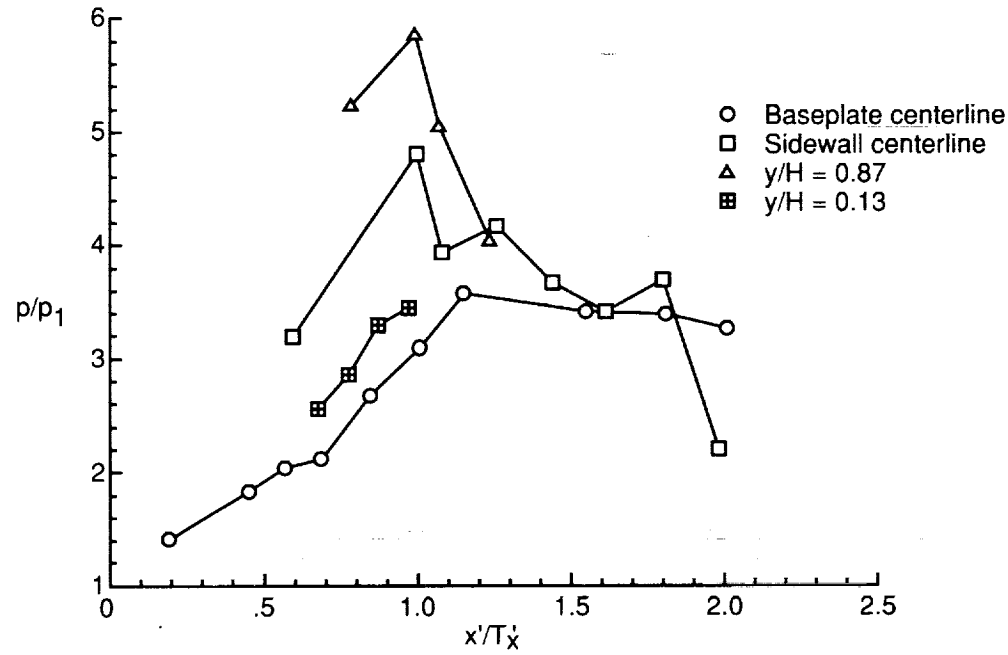

(a) Run 2275. CR = 3; 0-percent cowl; $N_{Re} = 0.89 \times 10^5$ per foot.

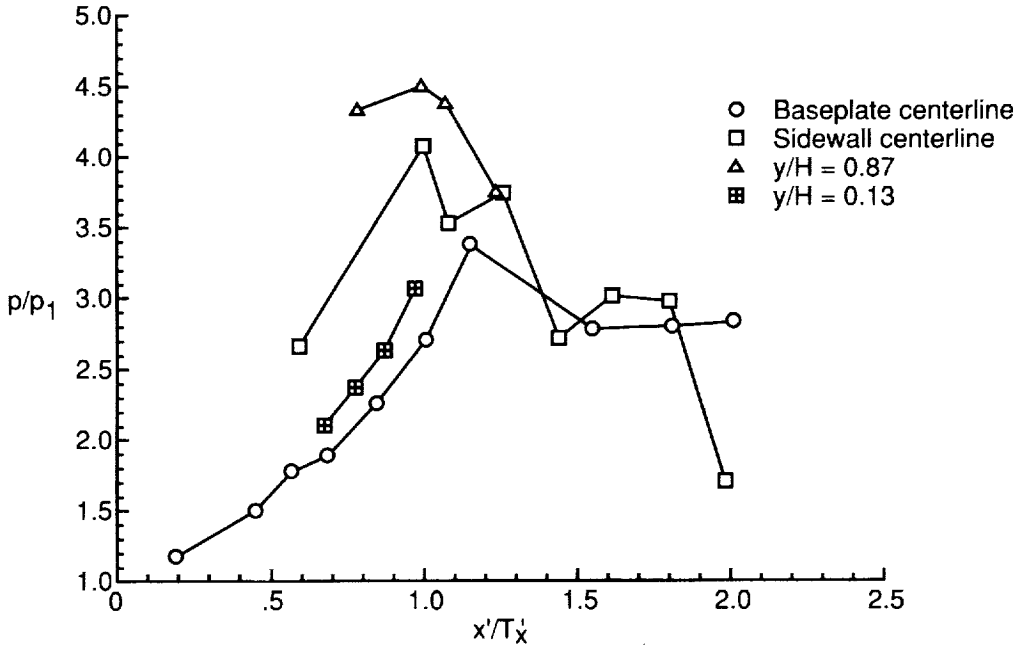

(b) Run 2276. CR = 3; 0-percent cowl; $N_{Re} = 2.85 \times 10^5$ per foot.

Figure 9. Configuration-complete plots for $\Lambda = 70°$ model.

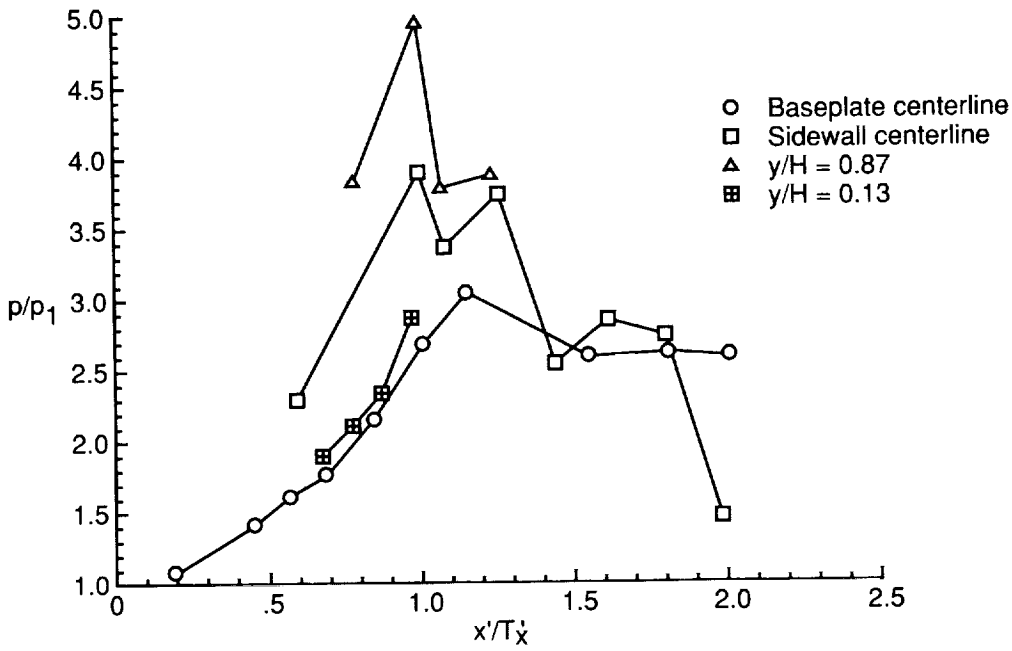

(c) Run 2277. CR = 3; 0-percent cowl; $N_{Re} = 5.50 \times 10^5$ per foot.

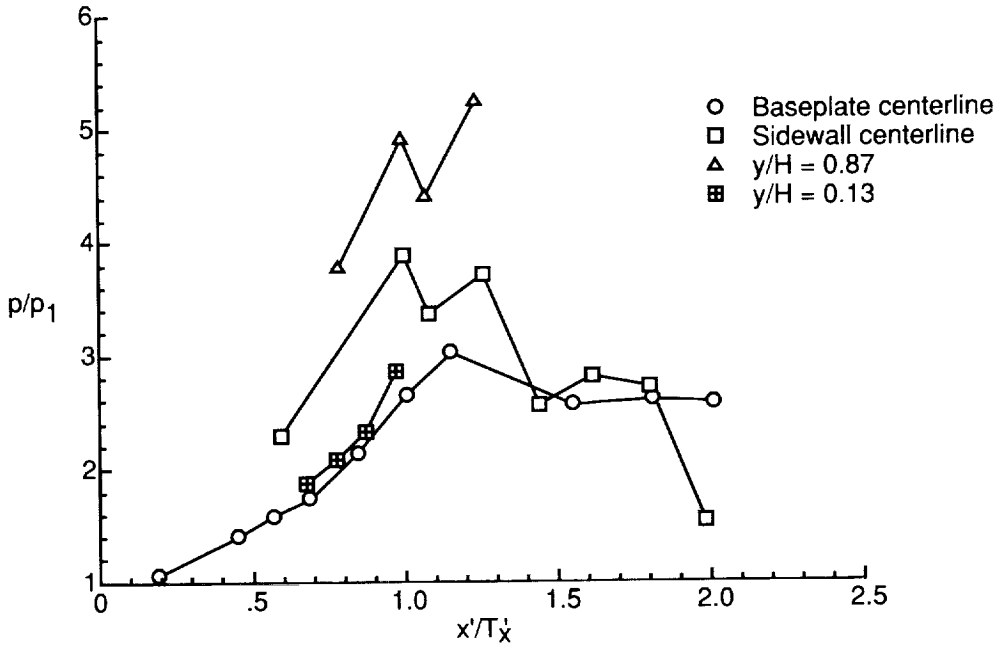

(d) Run 2278. CR = 3; 25-percent cowl; $N_{Re} = 5.50 \times 10^5$ per foot.

Figure 9. Continued.

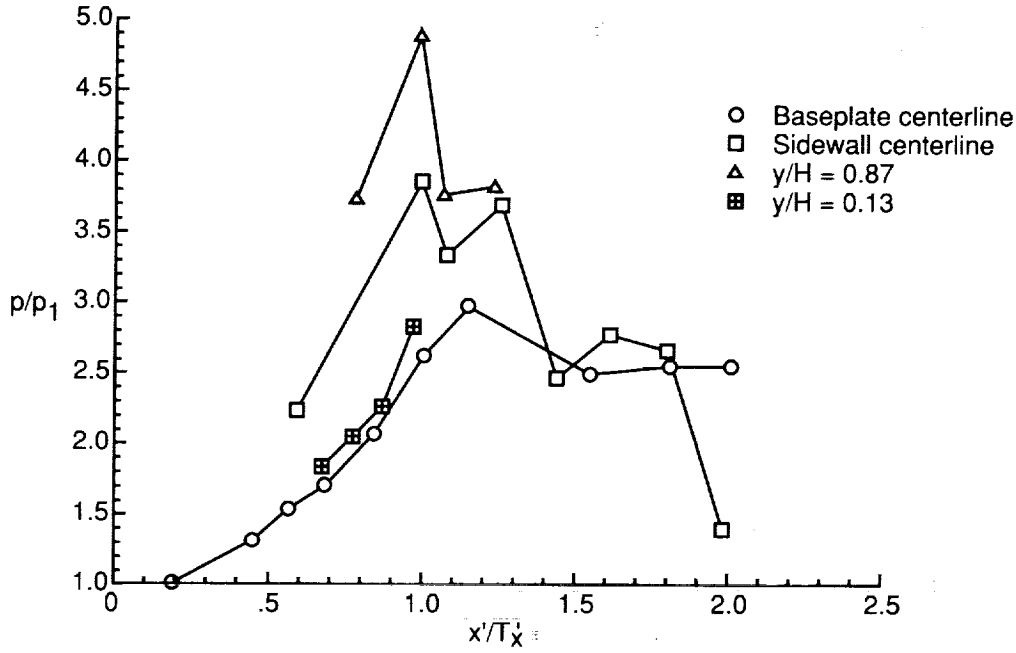

(e) Run 2279. CR = 3; no cowl; $N_{Re} = 5.50 \times 10^5$ per foot.

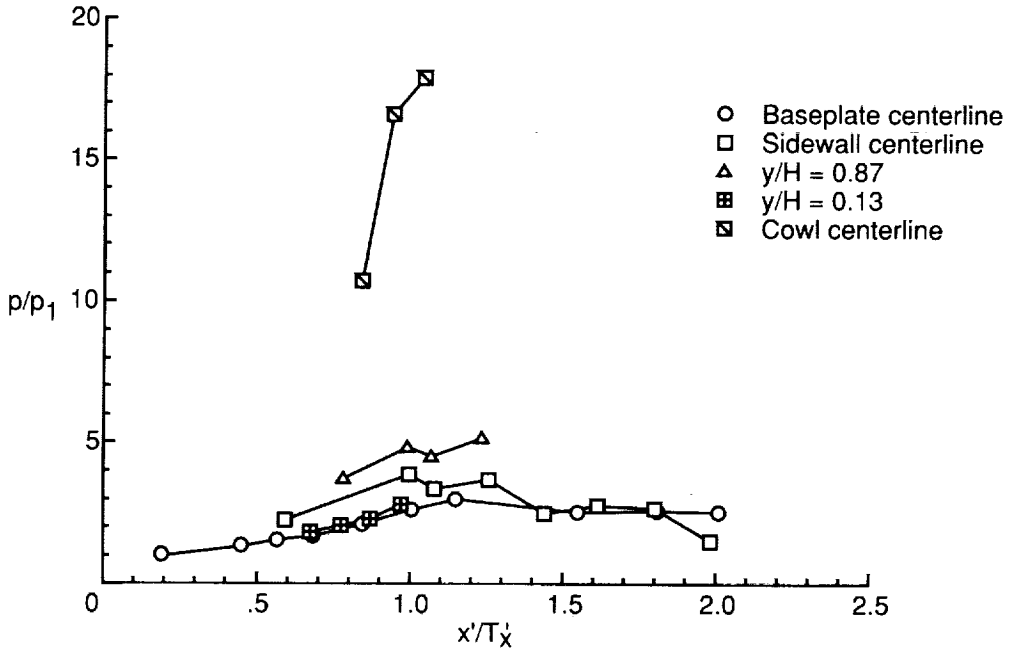

(f) Run 2280. CR = 3; 25-percent cowl; $N_{Re} = 5.50 \times 10^5$ per foot.

Figure 9. Continued.

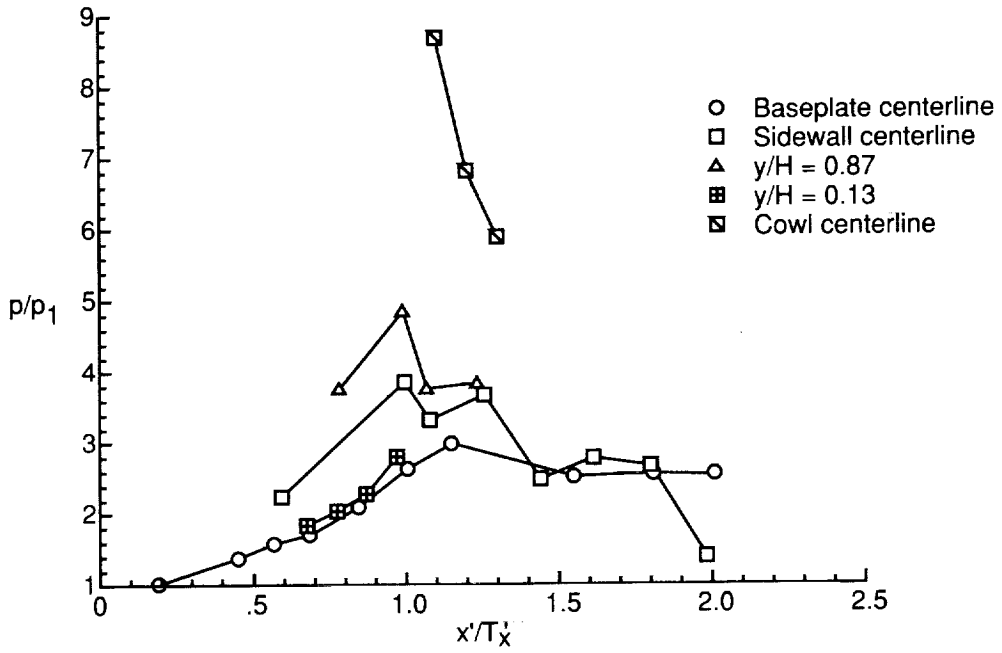

(g) Run 2281. CR = 3; 0-percent cowl; $N_{Re} = 5.50 \times 10^5$ per foot.

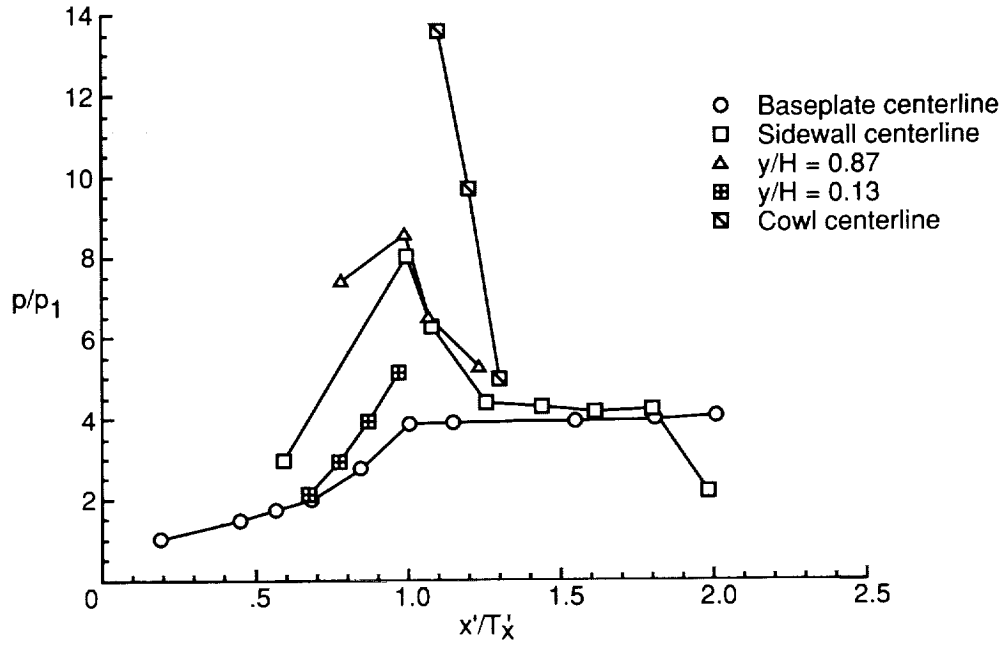

(h) Run 2282. CR = 5; 0-percent cowl; $N_{Re} = 5.50 \times 10^5$ per foot.

Figure 9. Continued.

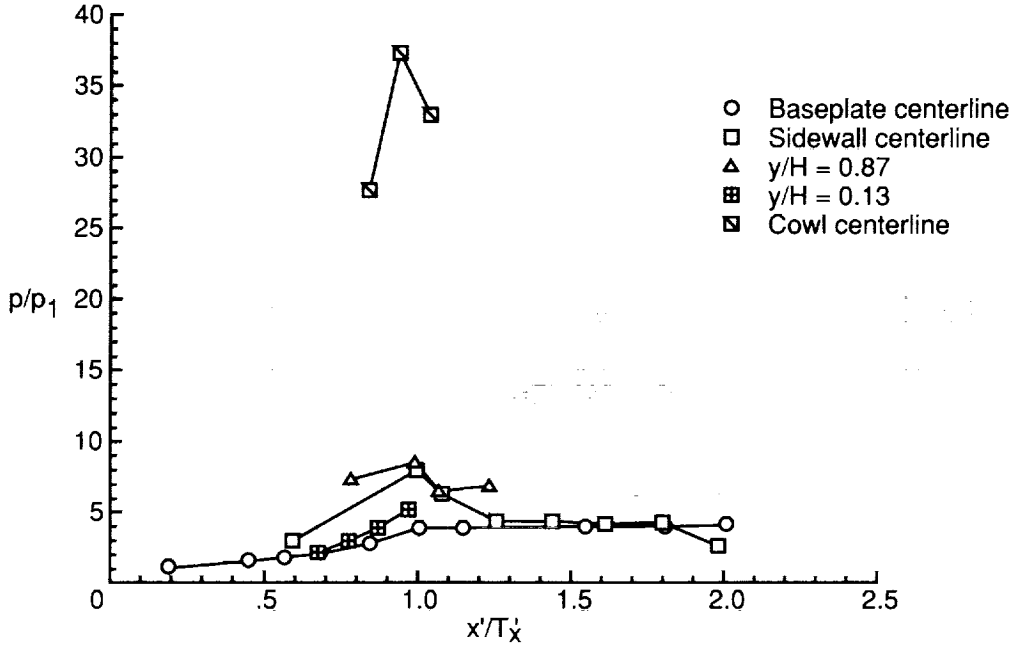

(i) Run 2284. CR = 5; 25-percent cowl; $N_{Re} = 5.50 \times 10^5$ per foot.

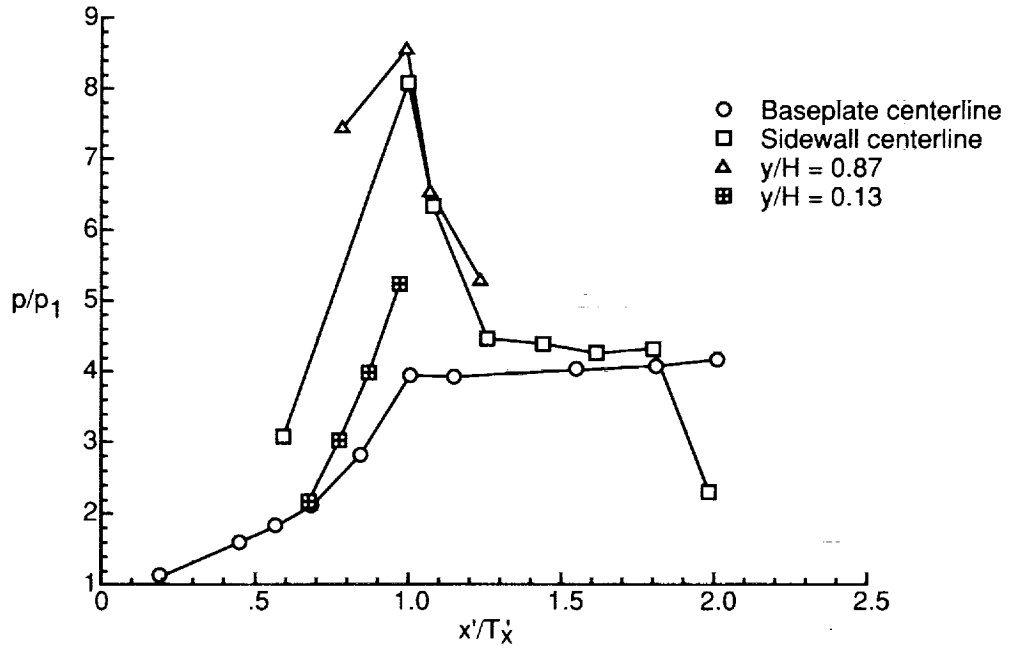

(j) Run 2285. CR = 5; no cowl; $N_{Re} = 5.50 \times 10^5$ per foot.

Figure 9. Continued.

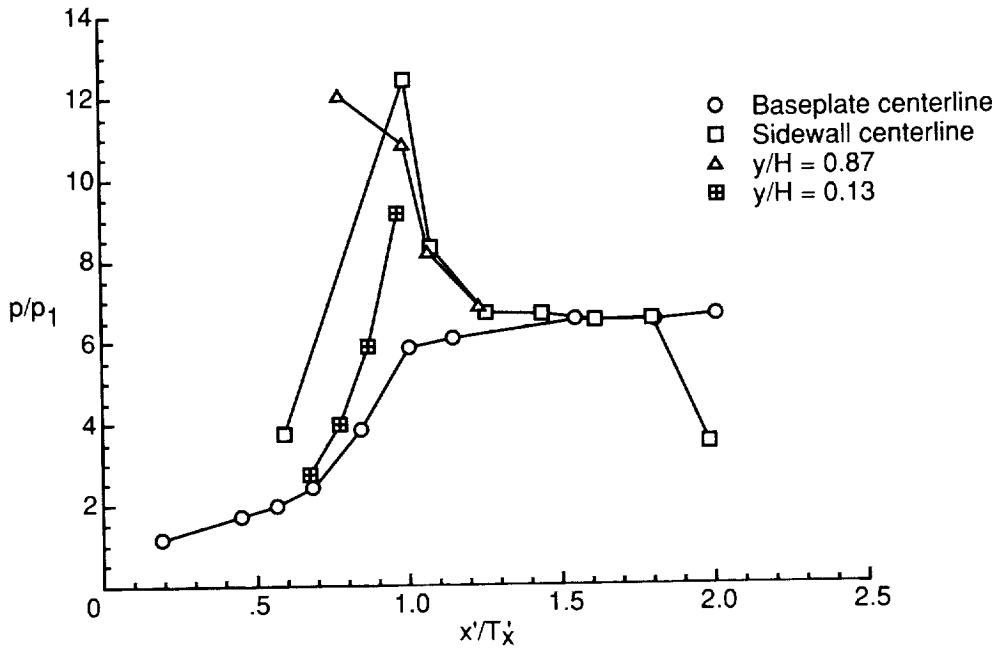

(k) Run 2286. CR = 9; no cowl; $N_{Re} = 5.50 \times 10^5$ per foot.

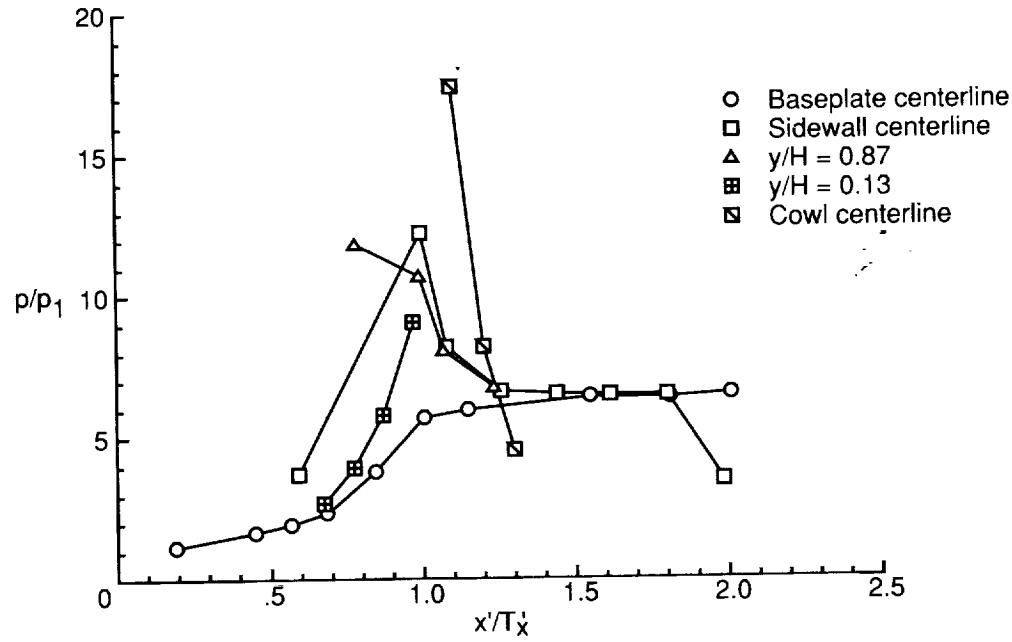

(l) Run 2287. CR = 9; 0-percent cowl; $N_{Re} = 5.50 \times 10^5$ per foot.

Figure 9. Continued.

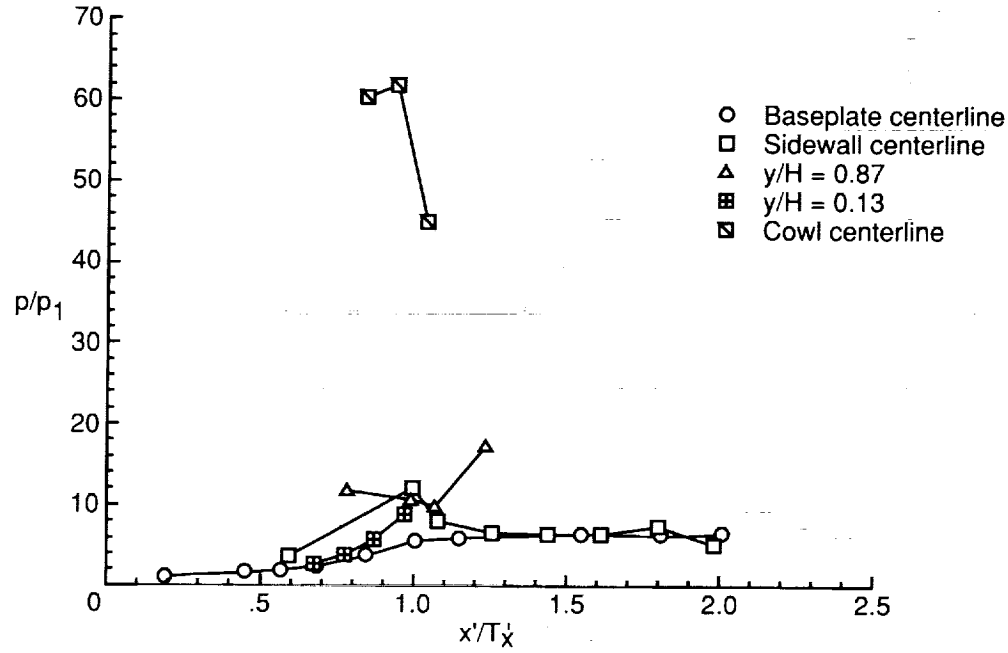

(m) Run 2288. CR = 9; 25-percent cowl; $N_{Re} = 5.50 \times 10^5$ per foot.

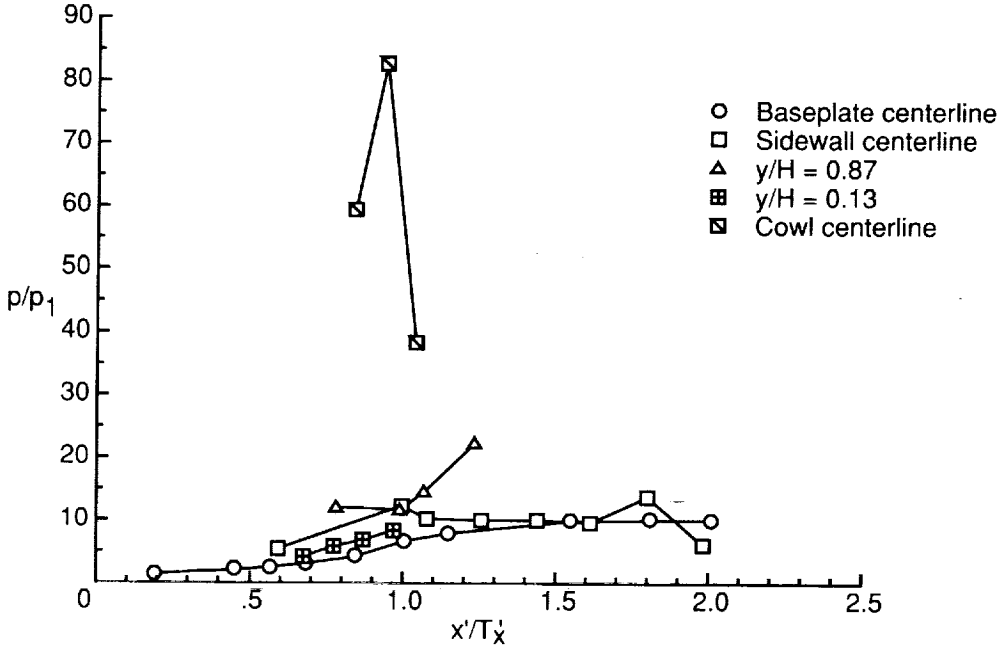

(n) Run 2289. CR = 9; 25-percent cowl; $N_{Re} = 0.89 \times 10^5$ per foot.

Figure 9. Continued.

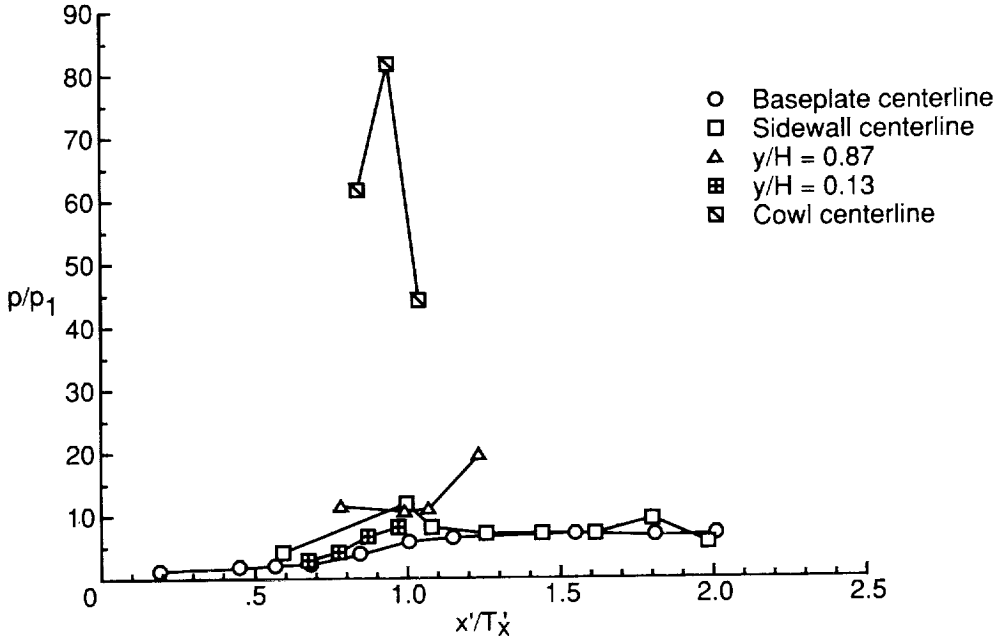

(o) Run 2290. CR = 9; 25-percent cowl; $N_{Re} = 2.85 \times 10^5$ per foot.

Figure 9. Concluded.

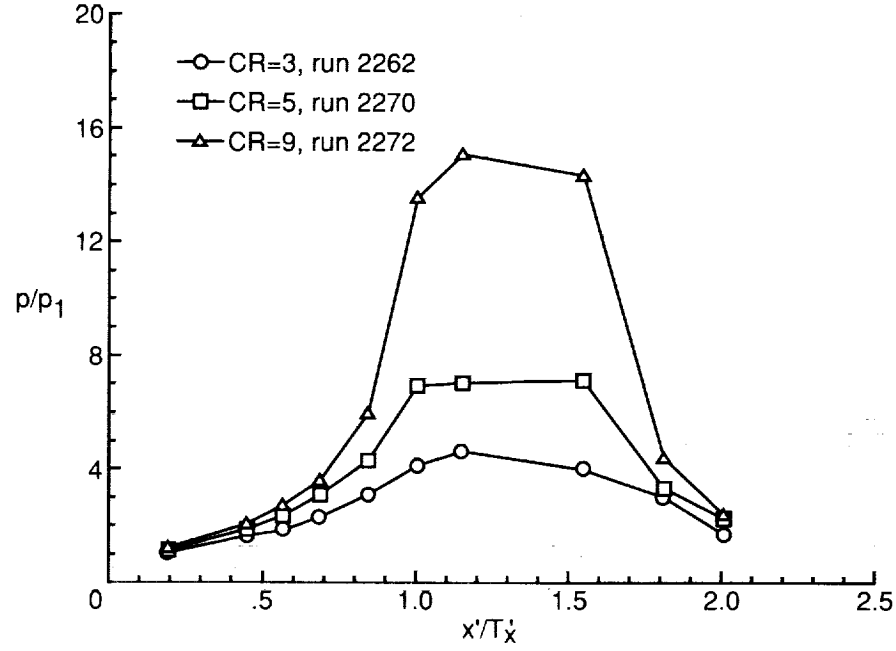

(a) Baseplate centerline.

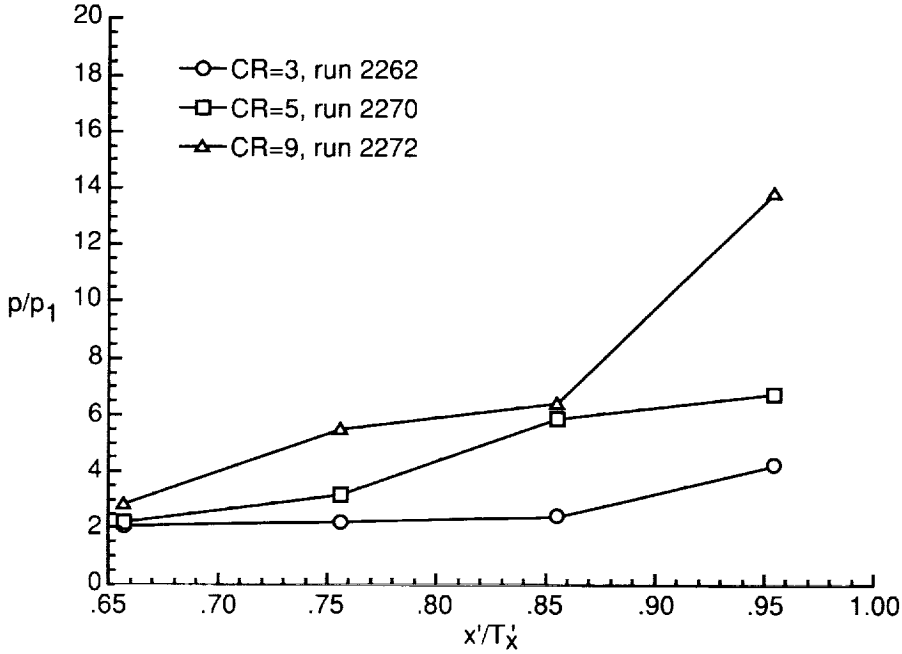

(b) Sidewall at $y/H = 0.13$.

Figure 10. Contraction ratio effects on pressure distributions of $\Lambda = 30°$ model with 0-percent cowl and $N_{Re} = 5.50 \times 10^5$ per foot.

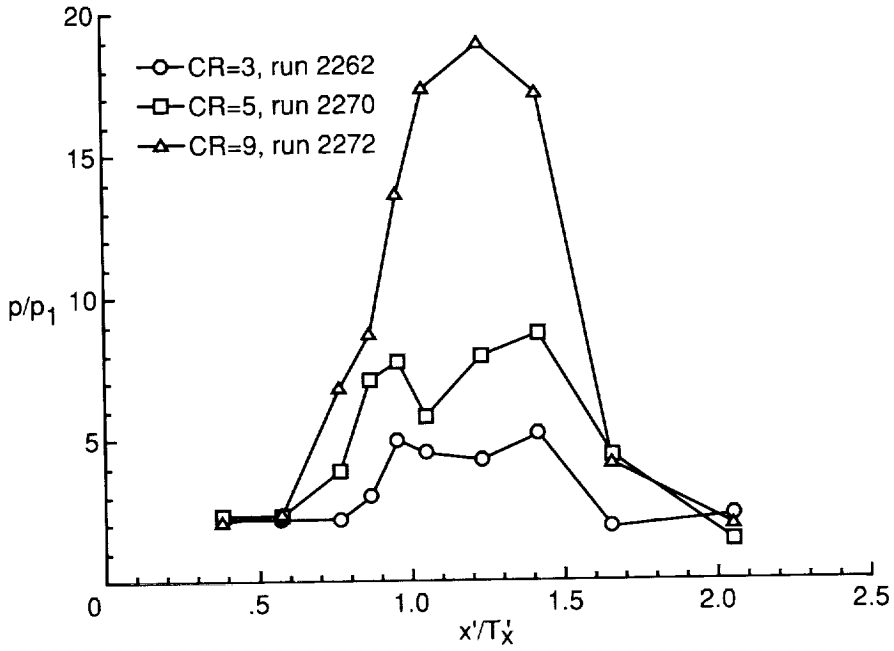

(c) Sidewall centerline.

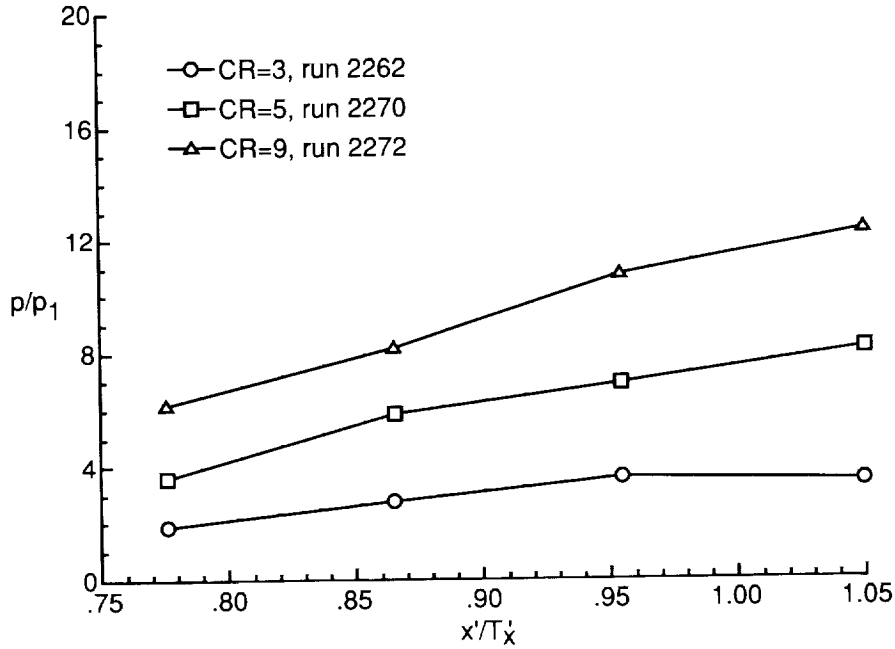

(d) Sidewall at $y/H = 0.87$.

Figure 10. Continued.

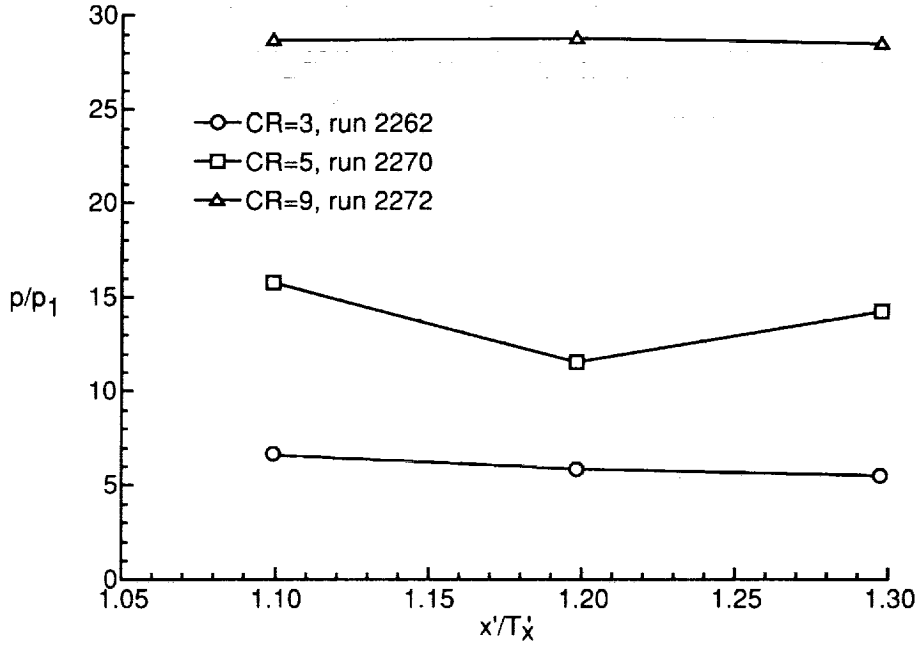

(e) Cowl centerline.

Figure 10. Concluded.

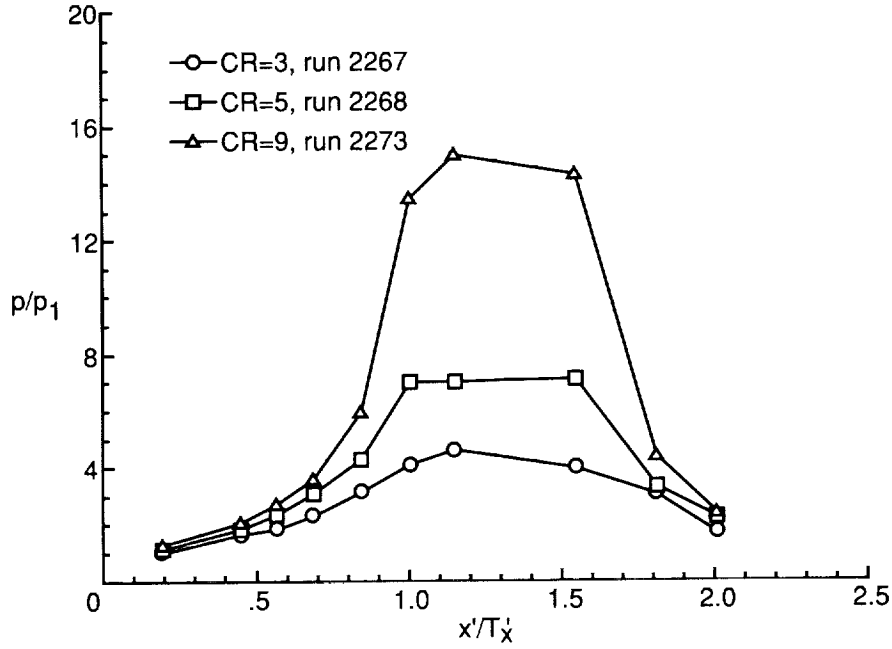

(a) Baseplate centerline.

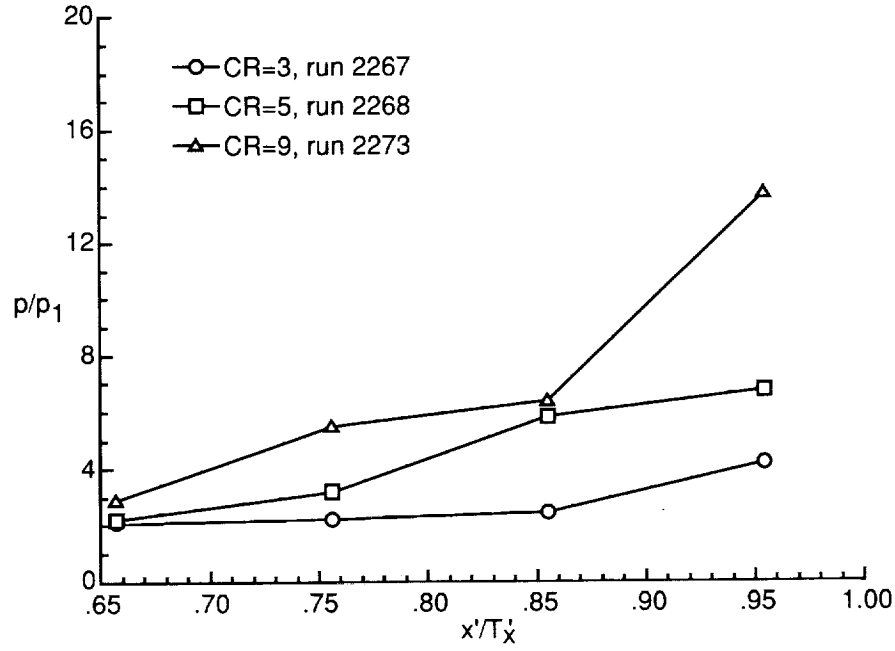

(b) Sidewall at $y/H = 0.13$.

Figure 11. Contraction ratio effects on pressure distributions of $\Lambda = 30°$ model with 25-percent cowl and $N_{Re} = 5.50 \times 10^5$ per foot.

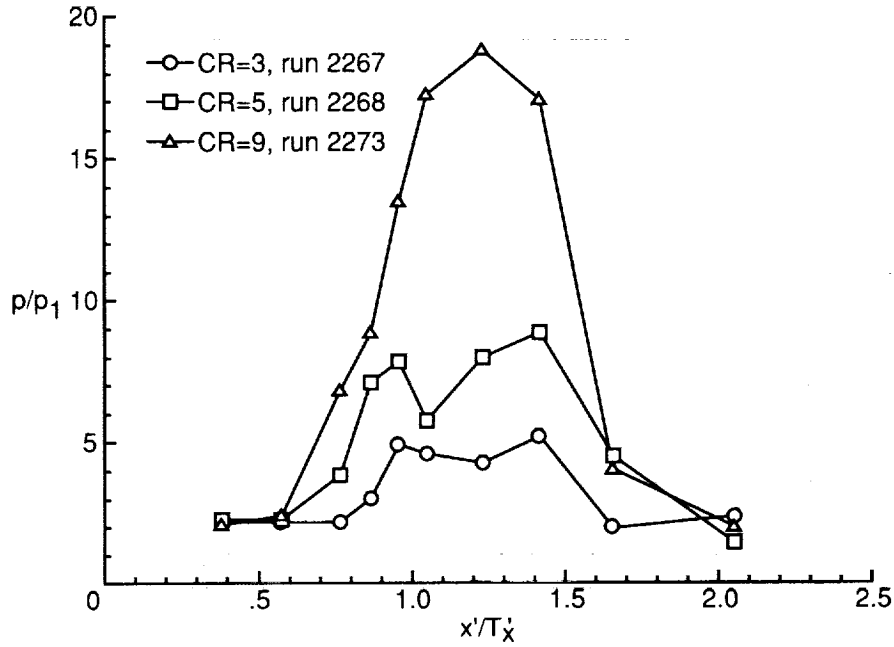

(c) Sidewall centerline.

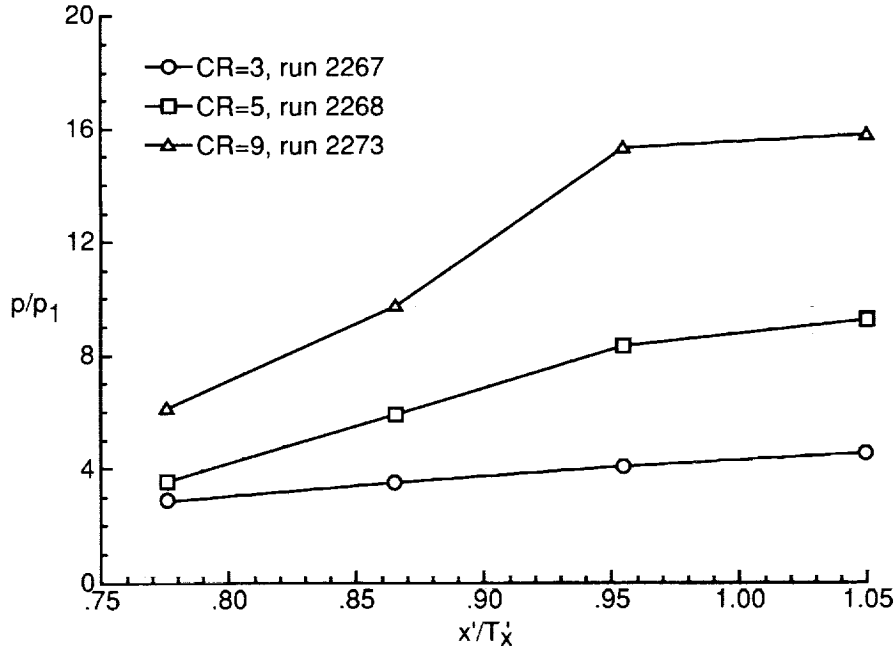

(d) Sidewall at $y/H = 0.87$.

Figure 11. Continued.

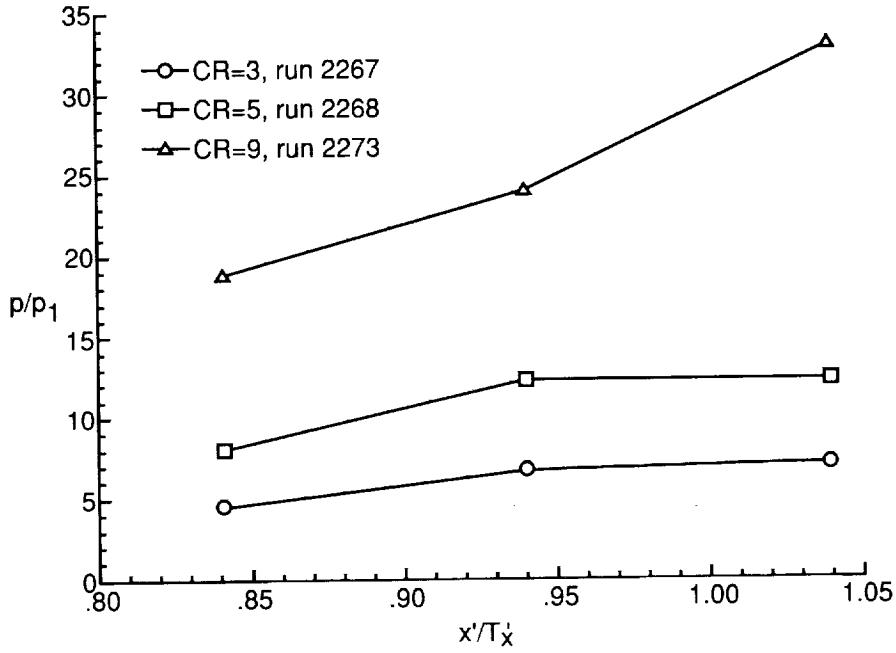

(e) Cowl centerline.

Figure 11. Concluded.

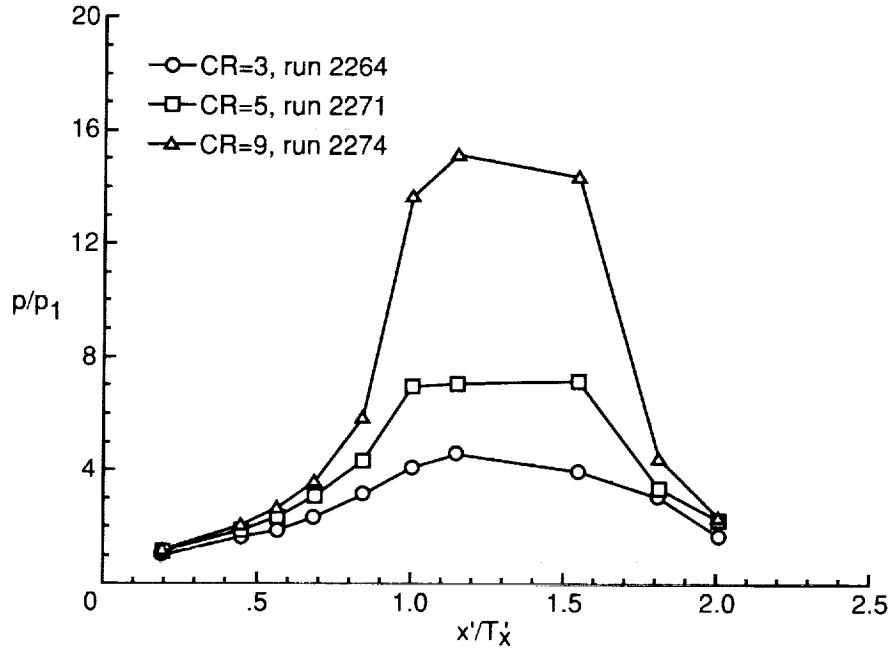

(a) Baseplate centerline.

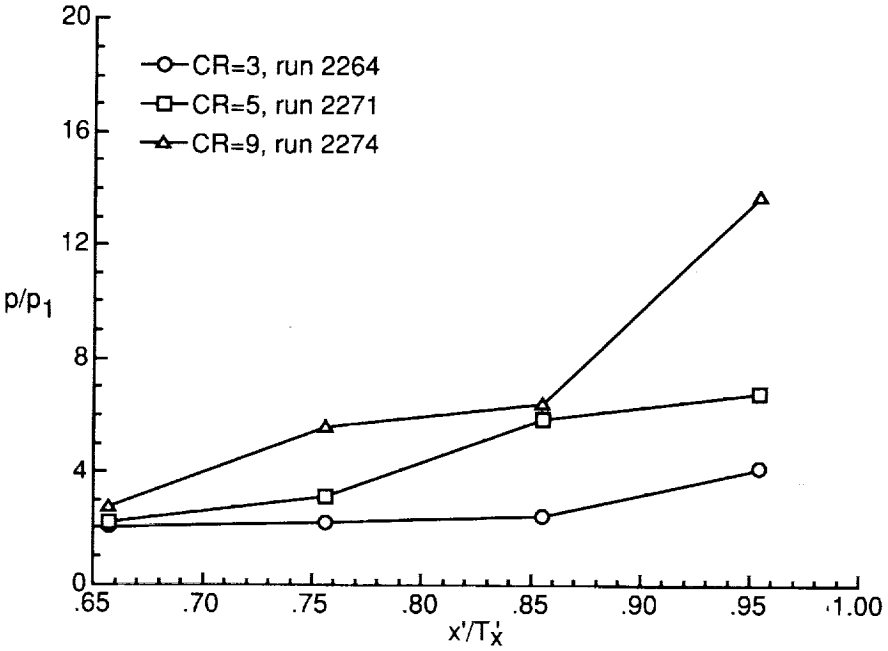

(b) Sidewall at $y/H = 0.13$.

Figure 12. Contraction ratio effects on pressure distributions of $\Lambda = 30°$ model with no cowl and $N_{Re} = 5.50 \times 10^5$ per foot.

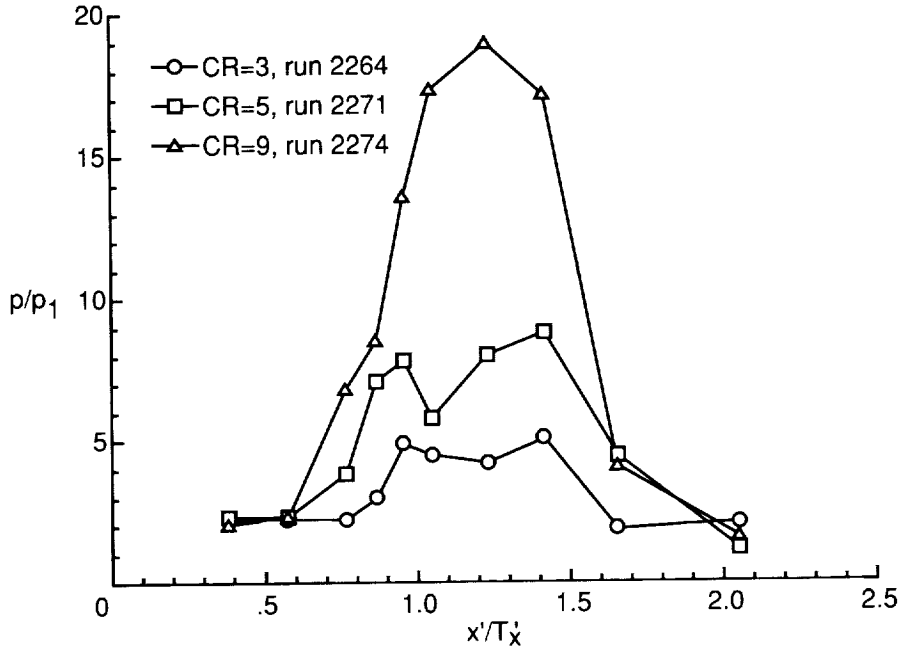

(c) Sidewall centerline.

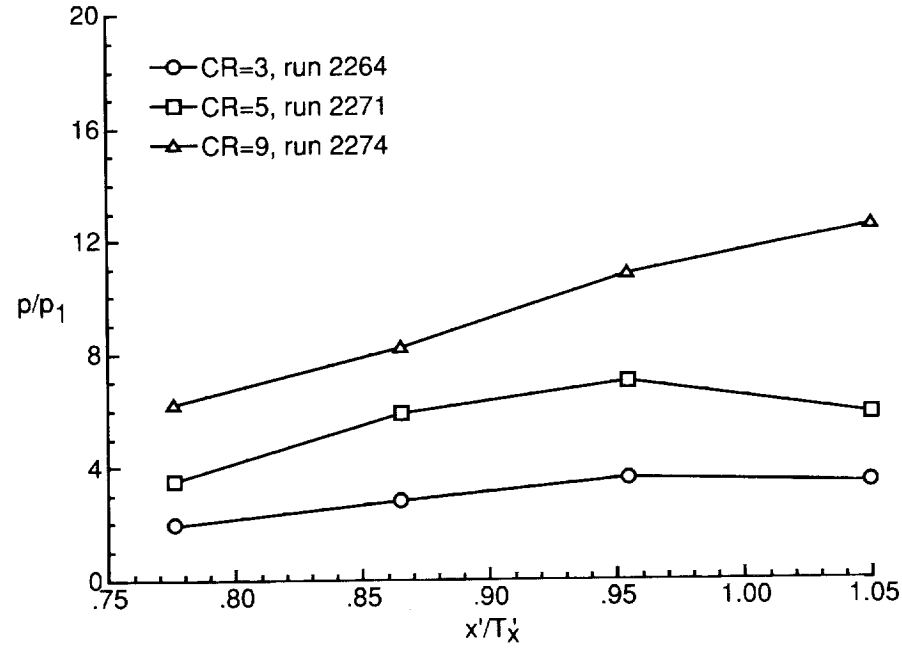

(d) Sidewall at $y/H = 0.87$.

Figure 12. Concluded.

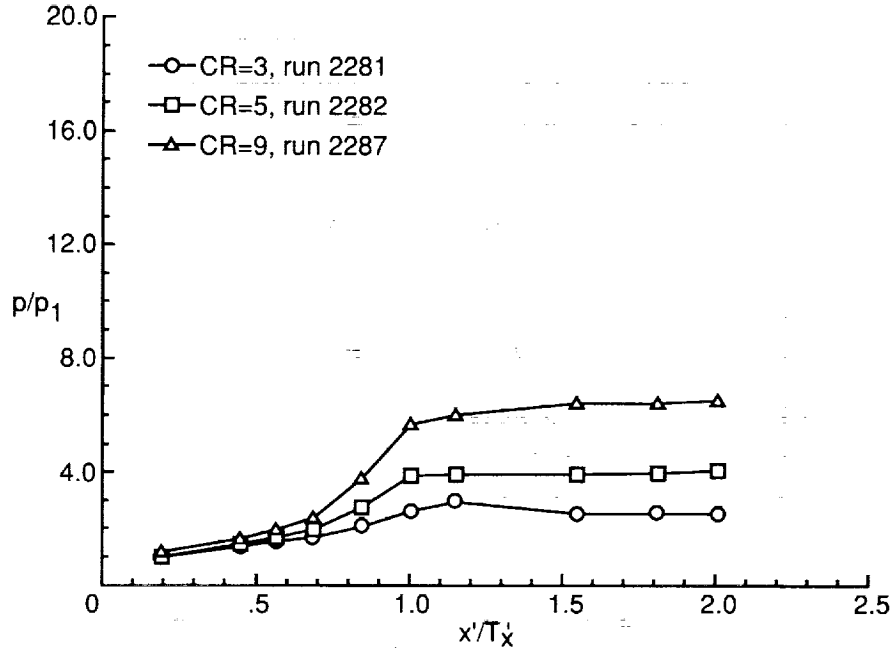

(a) Baseplate centerline.

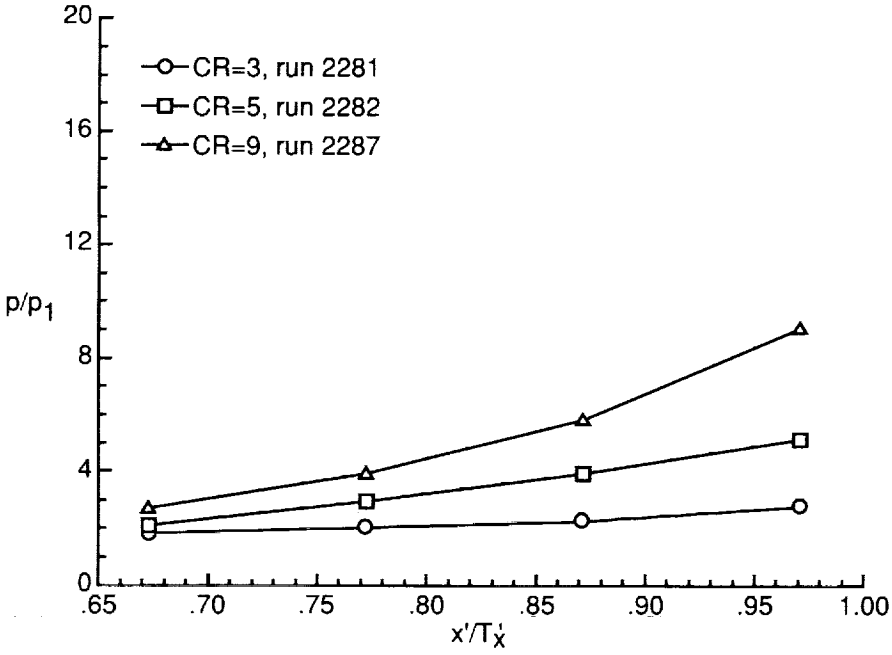

(b) Sidewall at $y/H = 0.13$.

Figure 13. Contraction ratio effects on pressure distributions of $\Lambda = 70°$ model with 0-percent cowl and $N_{Re} = 5.50 \times 10^5$ per foot.

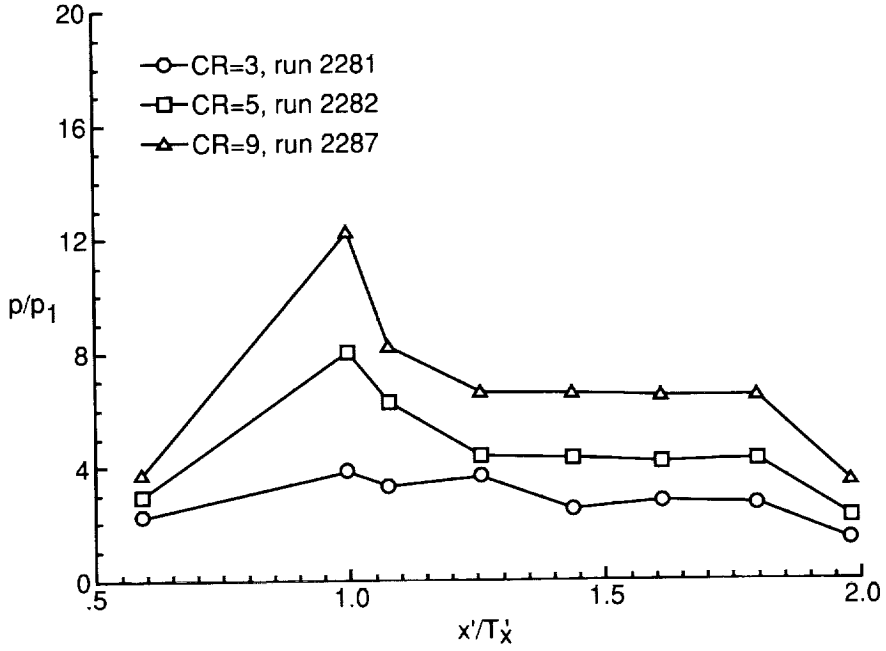

(c) Sidewall centerline.

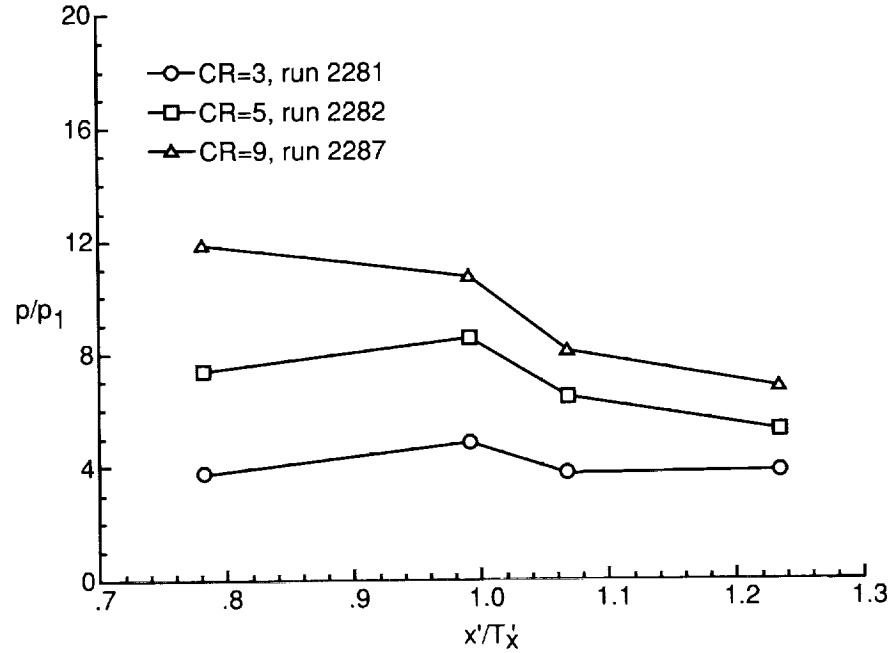

(d) Sidewall at $y/H = 0.87$.

Figure 13. Continued.

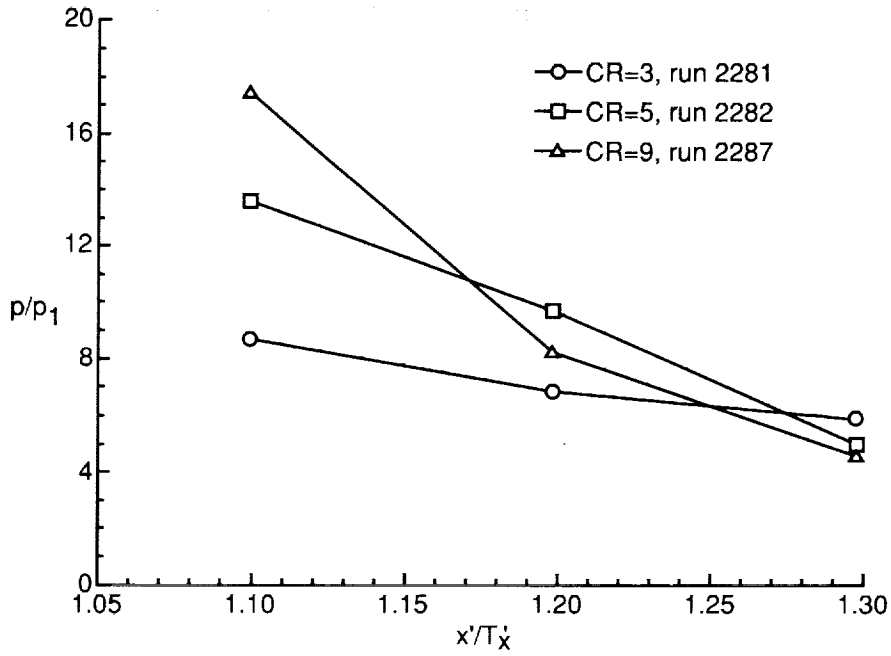

(e) Cowl centerline.

Figure 13. Concluded.

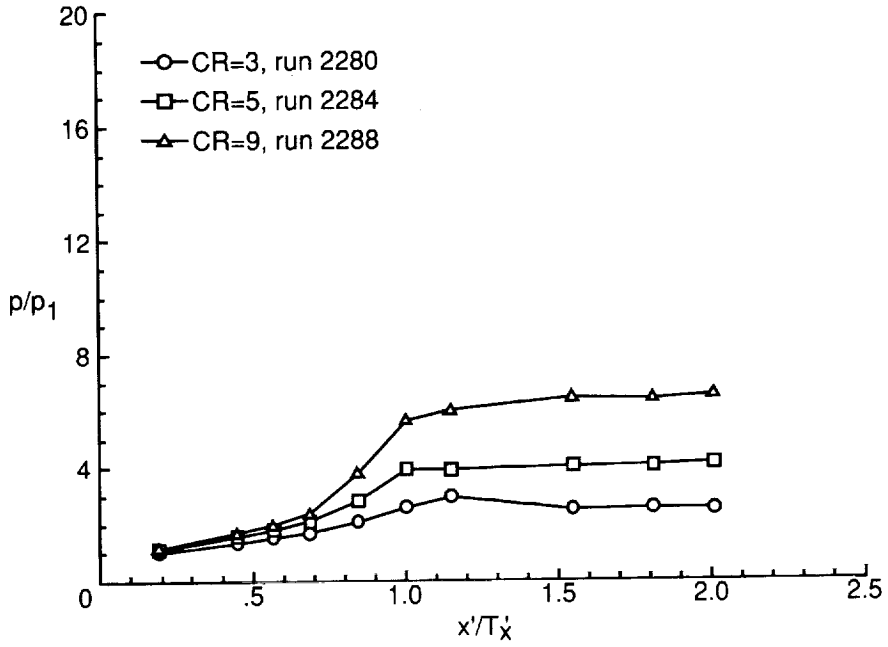

(a) Baseplate centerline.

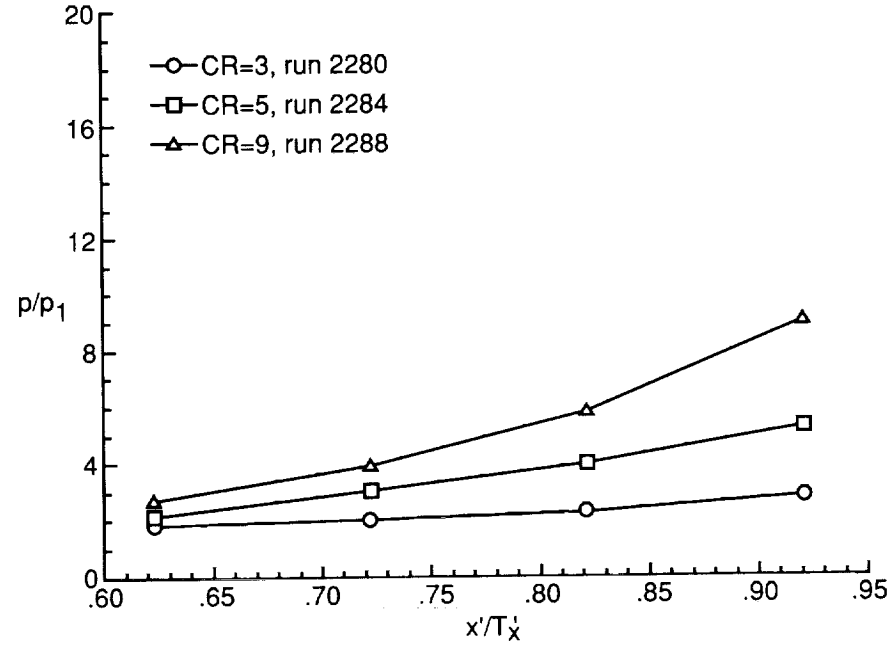

(b) Sidewall at $y/H = 0.13$.

Figure 14. Contraction ratio effects on pressure distributions of $\Lambda = 70°$ model with 25-percent cowl and $N_{Re} = 5.50 \times 10^5$ per foot.

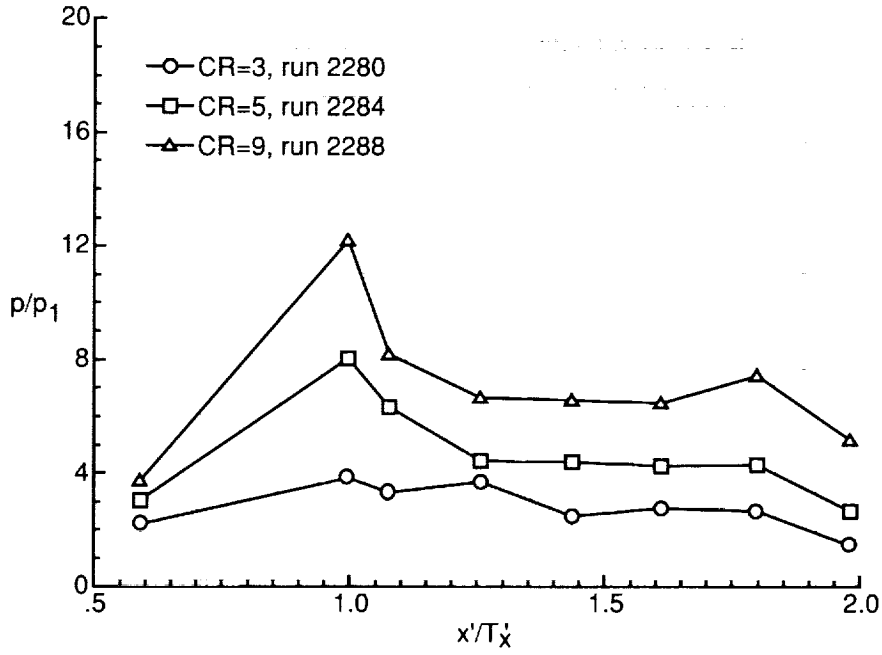

(c) Sidewall centerline.

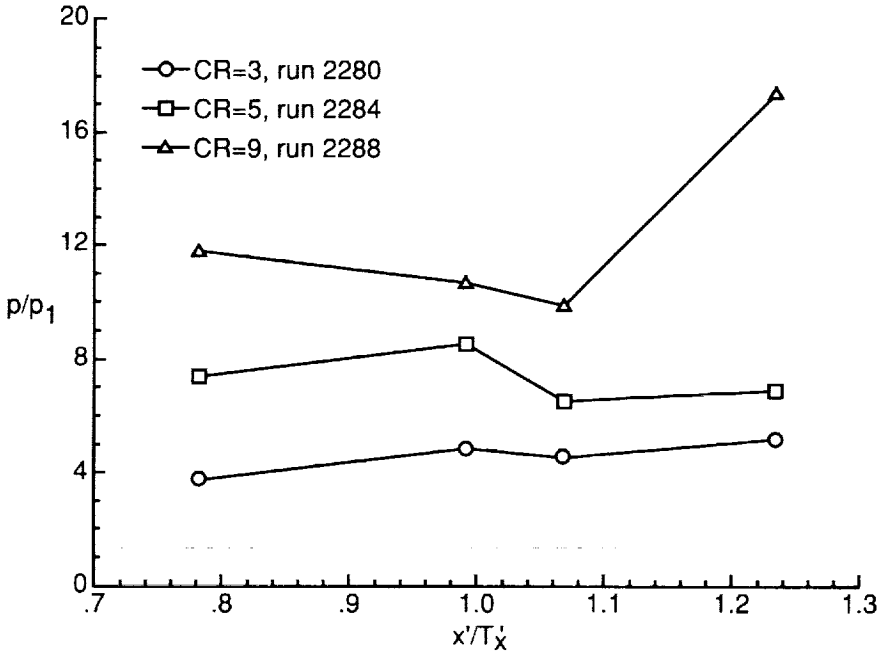

(d) Sidewall at $y/H = 0.87$.

Figure 14. Continued.

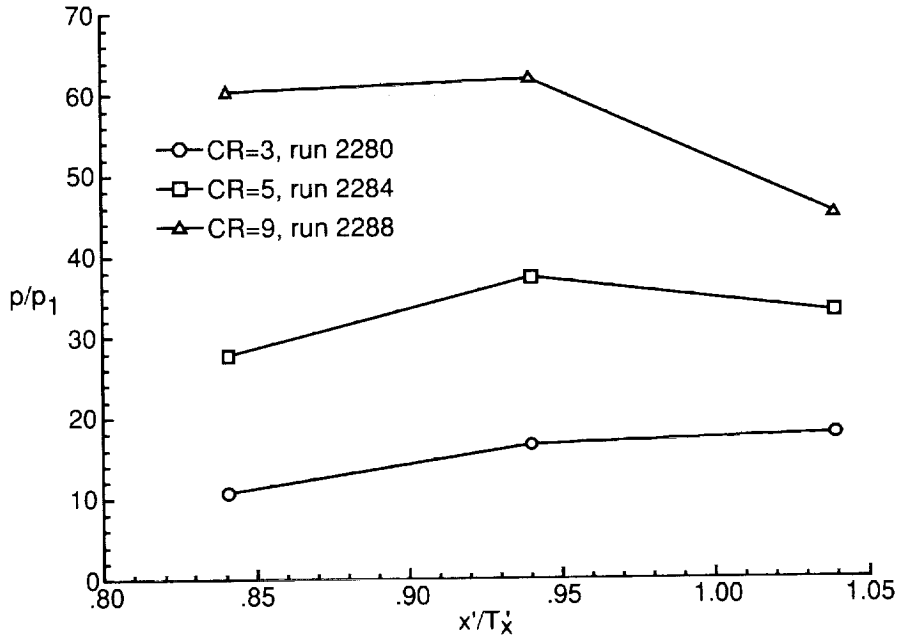

(c) Cowl centerline.

Figure 14. Concluded.

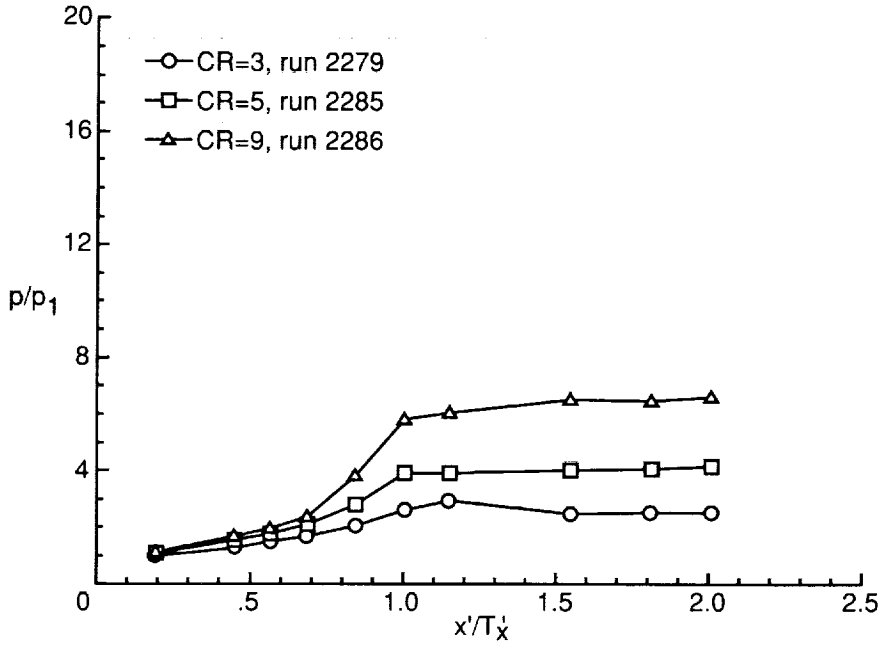

(a) Baseplate centerline.

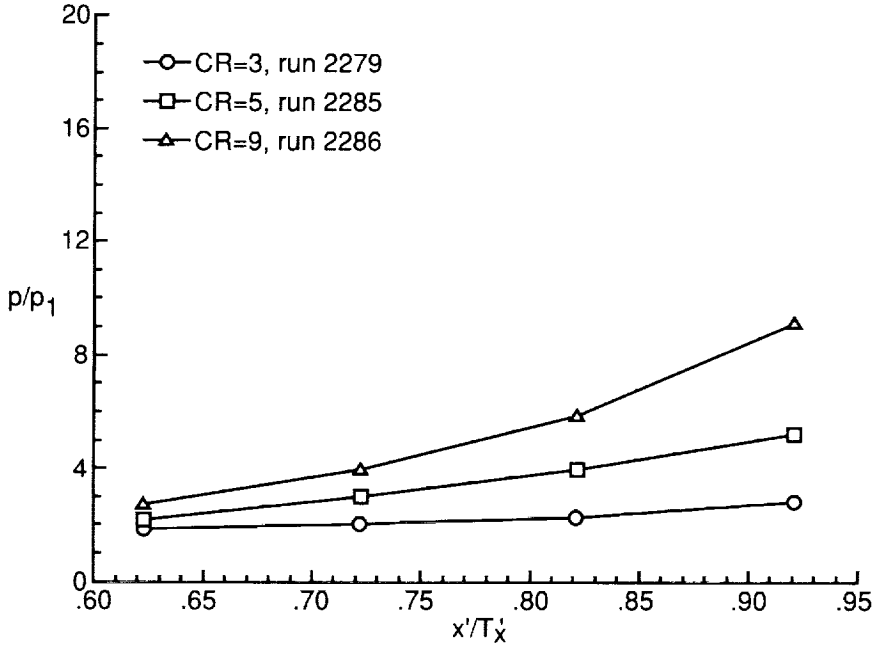

(b) Sidewall at $y/H = 0.13$.

Figure 15. Contraction ratio effects on pressure distributions of $\Lambda = 70°$ model with no cowl and $N_{Re} = 5.50 \times 10^5$ per foot.

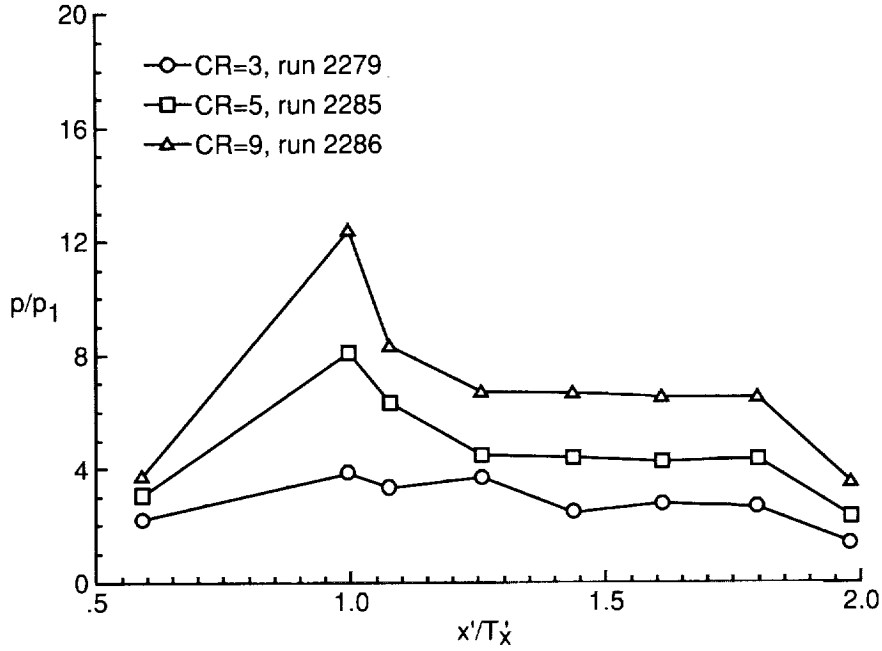

(c) Sidewall centerline.

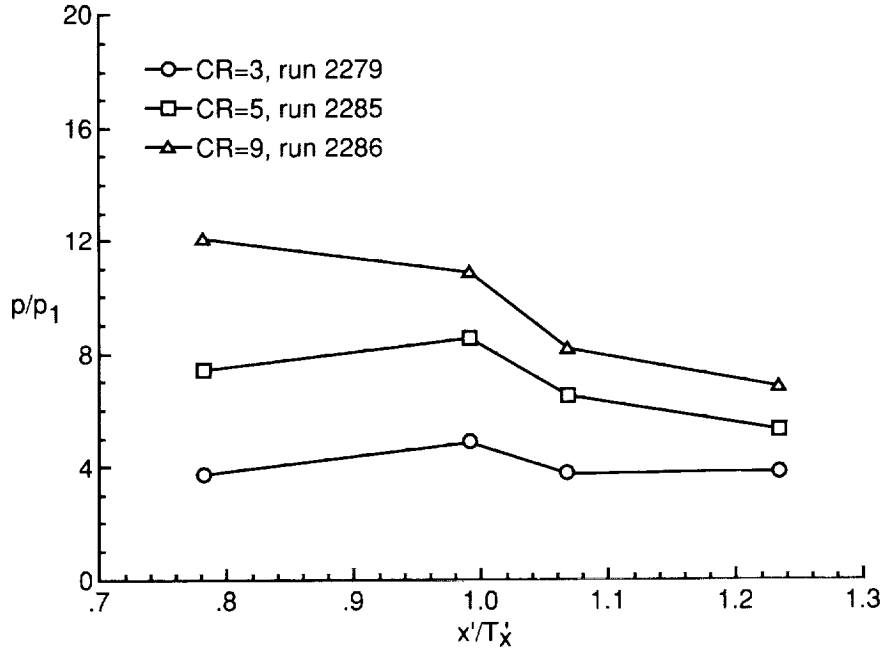

(d) Sidewall at $y/H = 0.87$.

Figure 15. Concluded.

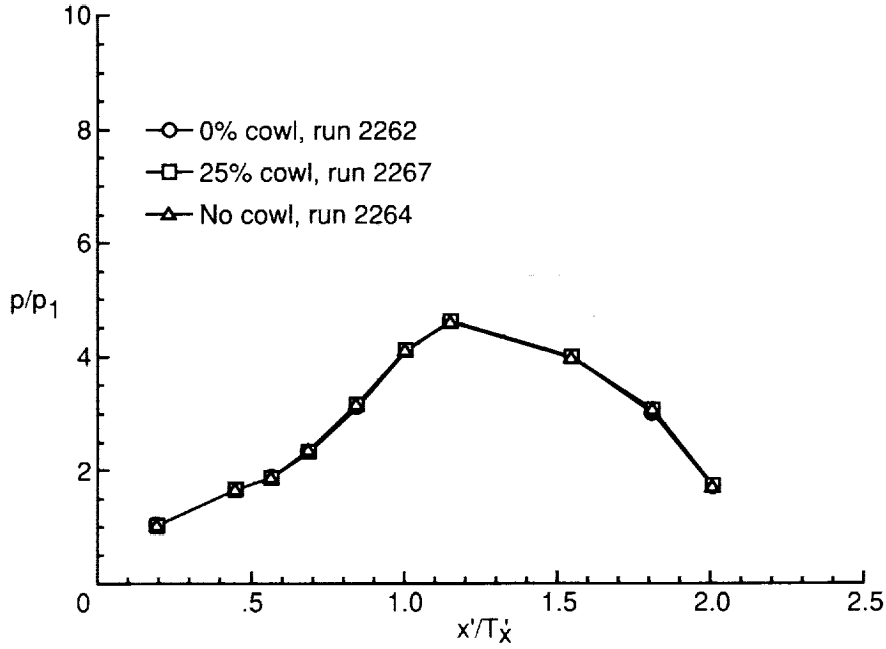

(a) Baseplate centerline.

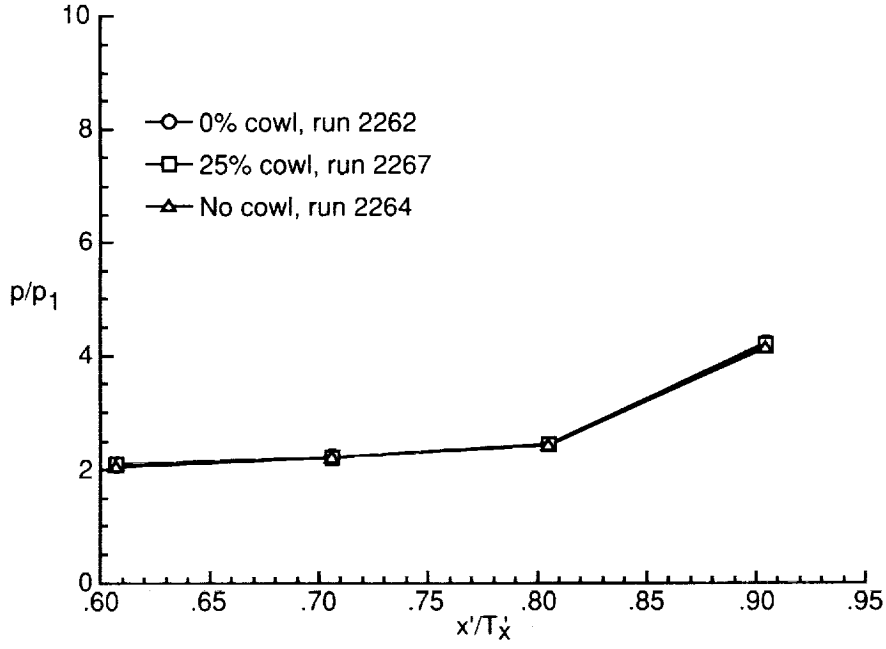

(b) Sidewall at $y/H = 0.13$.

Figure 16. Cowl position effects on pressure distributions of $\Lambda = 30°$ model with CR = 3 and $N_{Re} = 5.50 \times 10^5$ per foot.

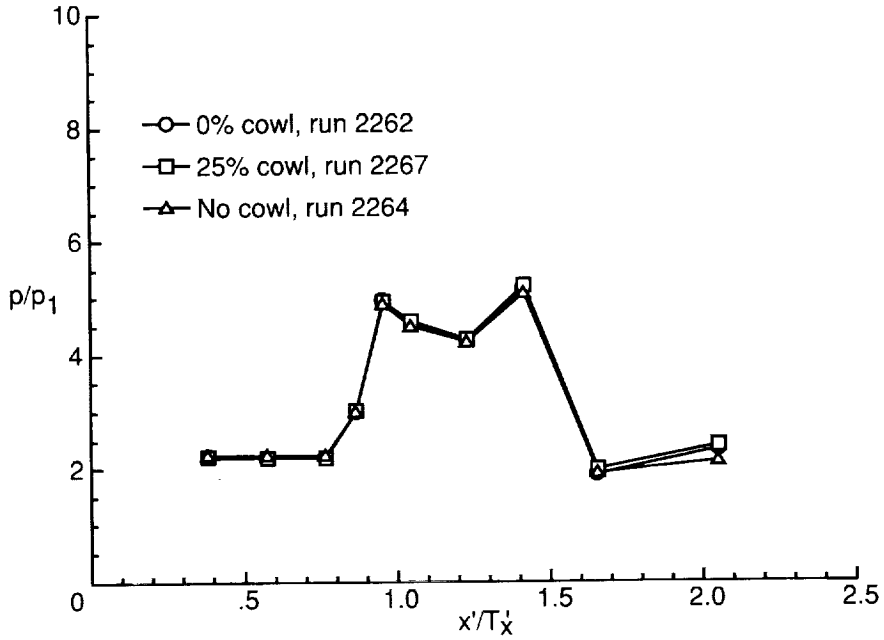

(c) Sidewall centerline.

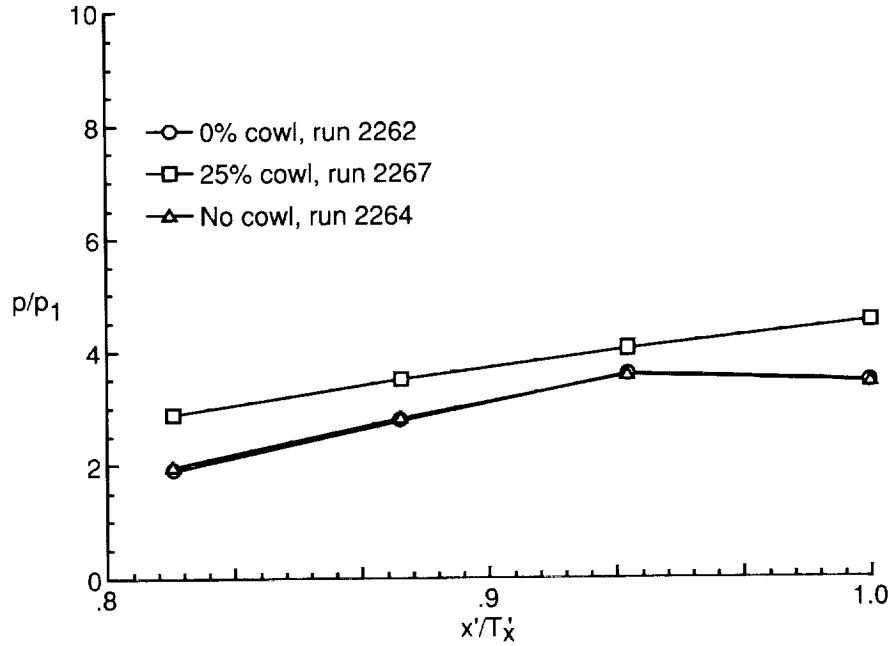

(d) Sidewall at $y/H = 0.87$.

Figure 16. Continued.

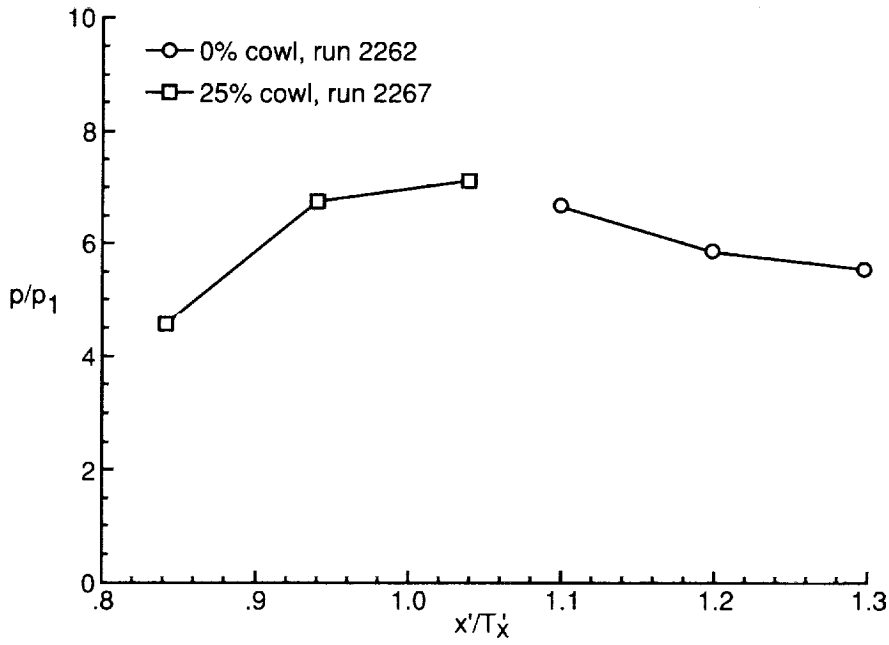

(e) Cowl centerline.

Figure 16. Concluded.

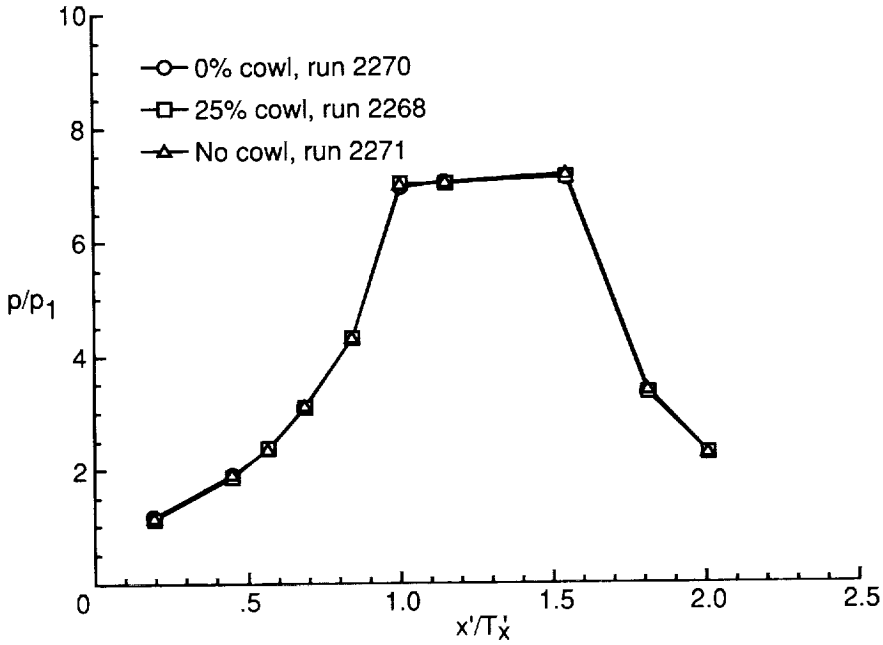

(a) Baseplate centerline.

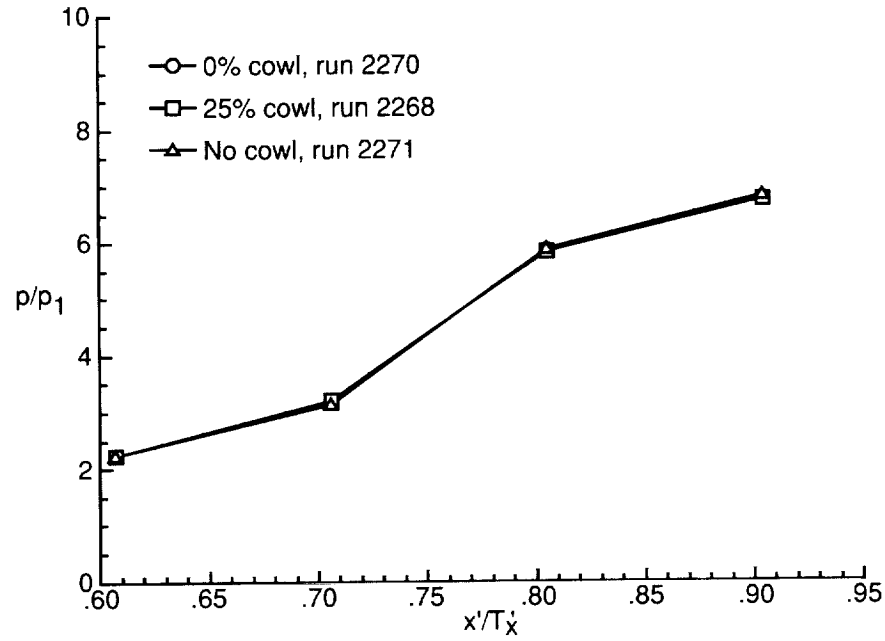

(b) Sidewall at $y/H = 0.13$.

Figure 17. Cowl position effects on pressure distributions of $\Lambda = 30°$ model with CR = 5 and $N_{Re} = 5.50 \times 10^5$ per foot.

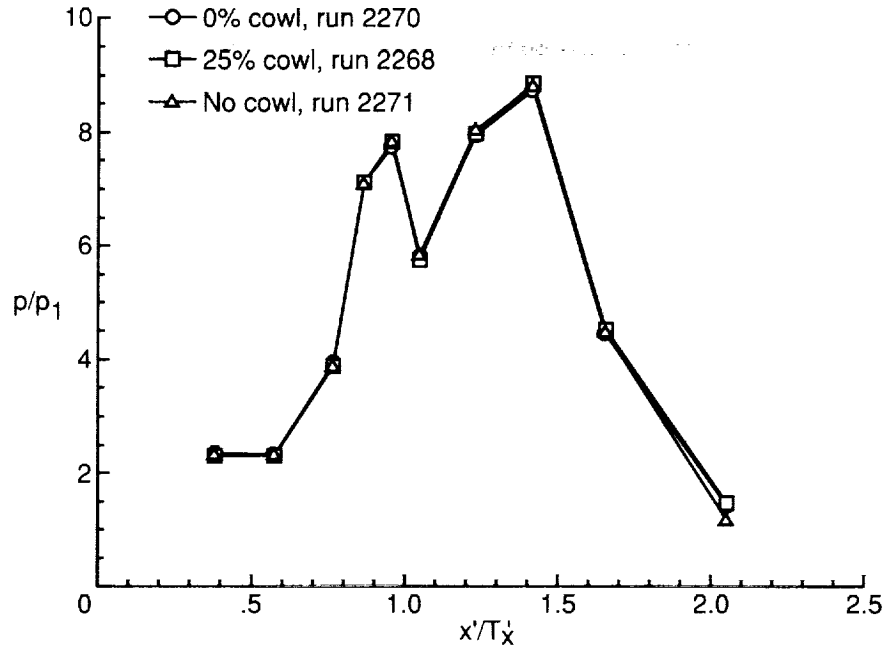

(c) Sidewall centerline.

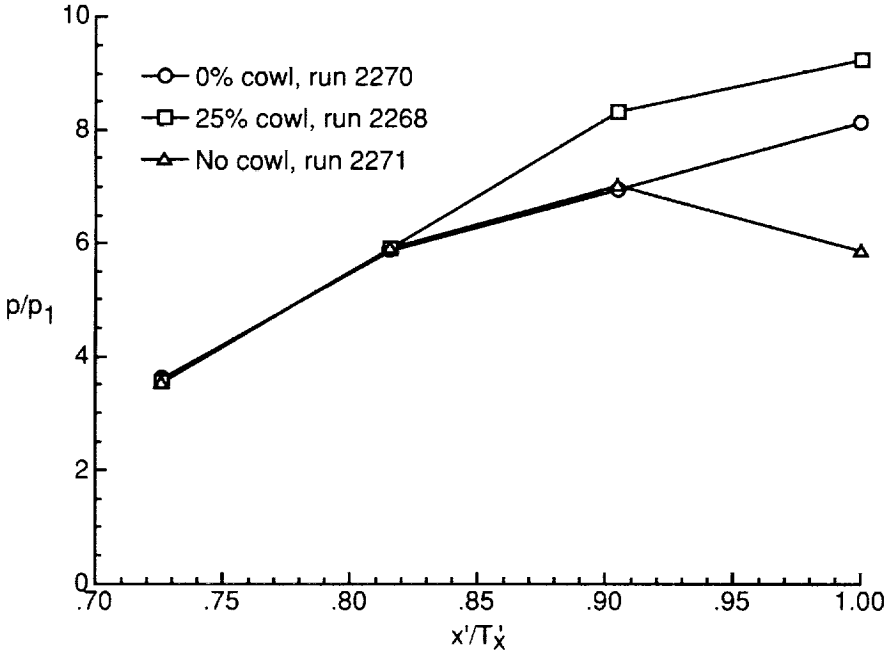

(d) Sidewall at $y/H = 0.87$.

Figure 17. Continued.

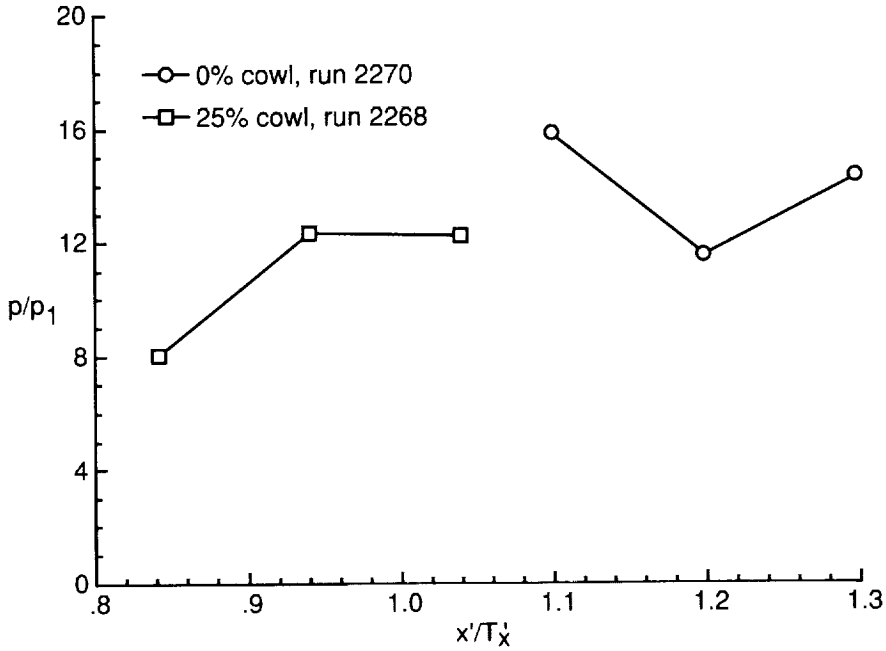

(e) Cowl centerline.

Figure 17. Concluded.

C-2

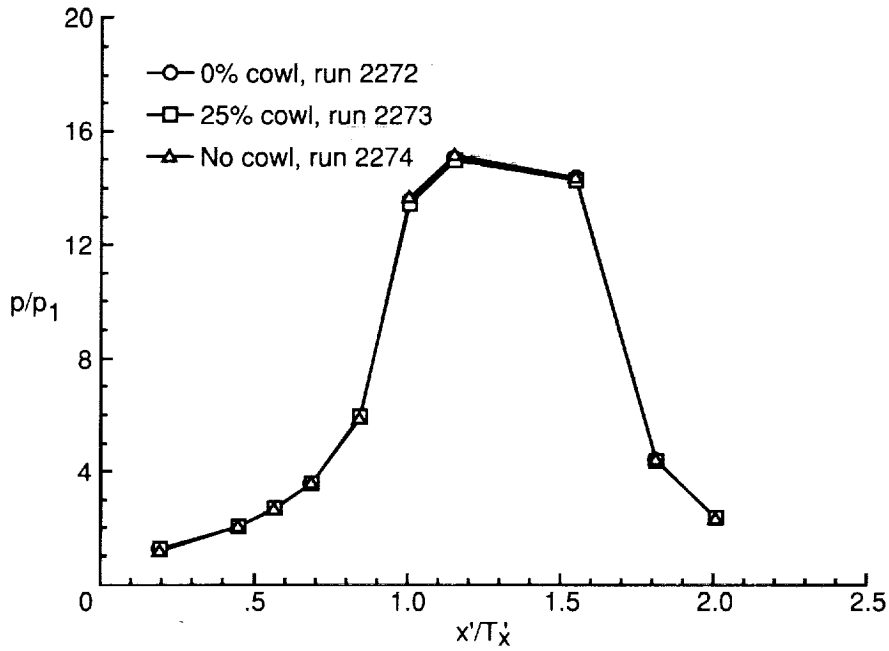

(a) Baseplate centerline.

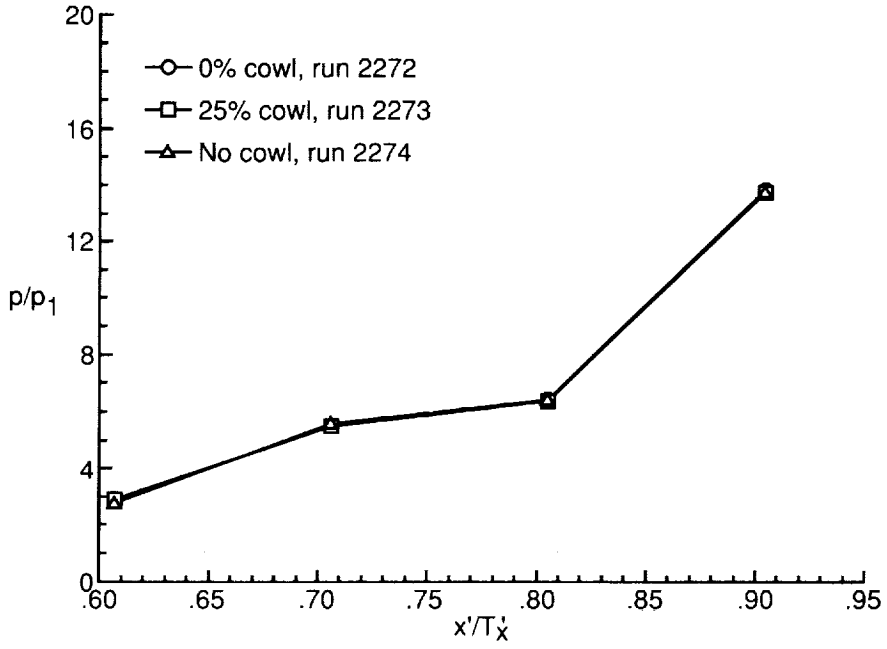

(b) Sidewall at $y/H = 0.13$.

Figure 18. Cowl position effects on pressure distributions of $\Lambda = 30°$ model with CR = 9 and $N_{Re} = 5.50 \times 10^5$ per foot.

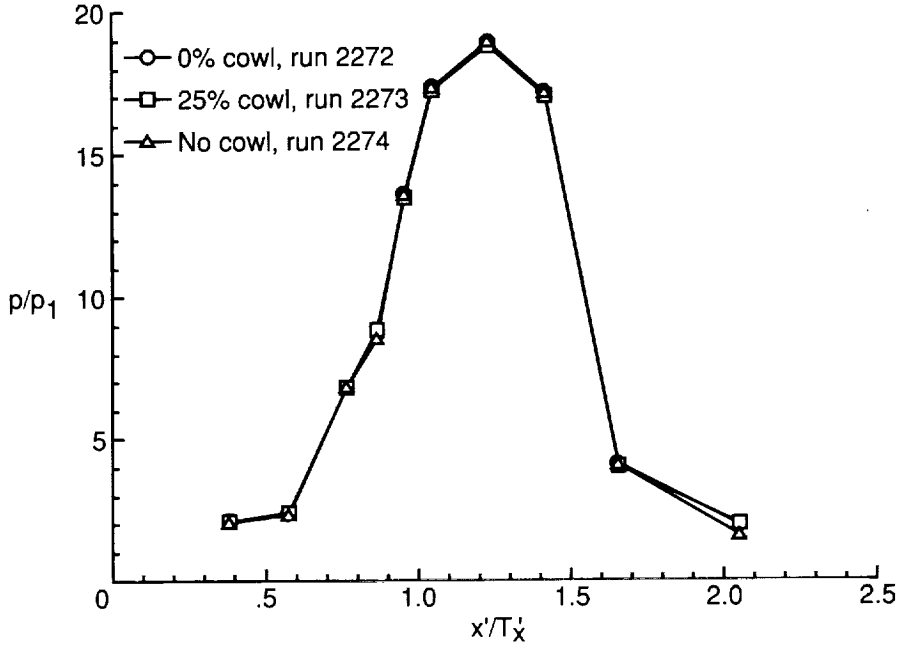

(c) Sidewall centerline.

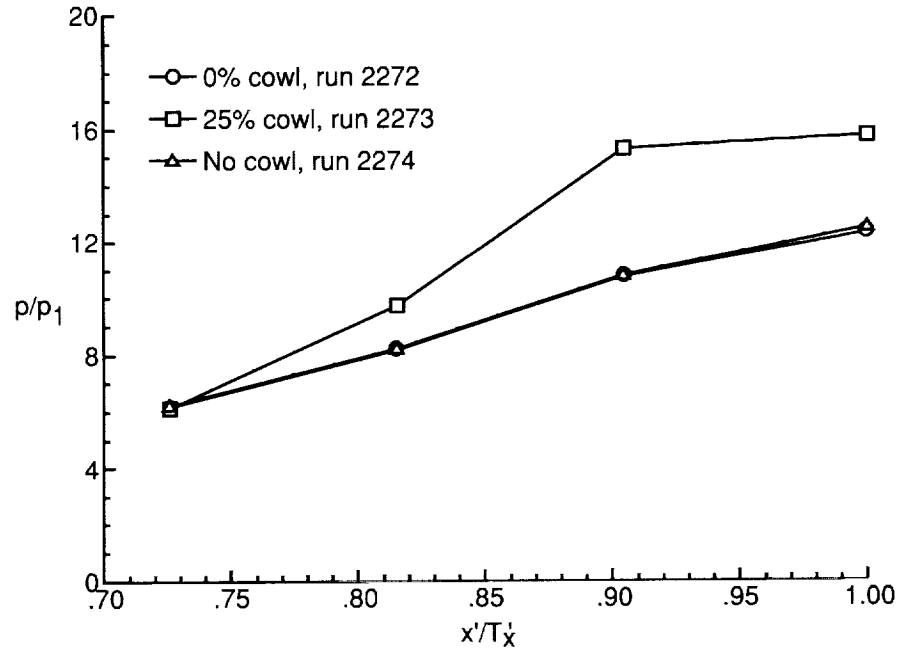

(d) Sidewall at $y/H = 0.87$.

Figure 18. Continued.

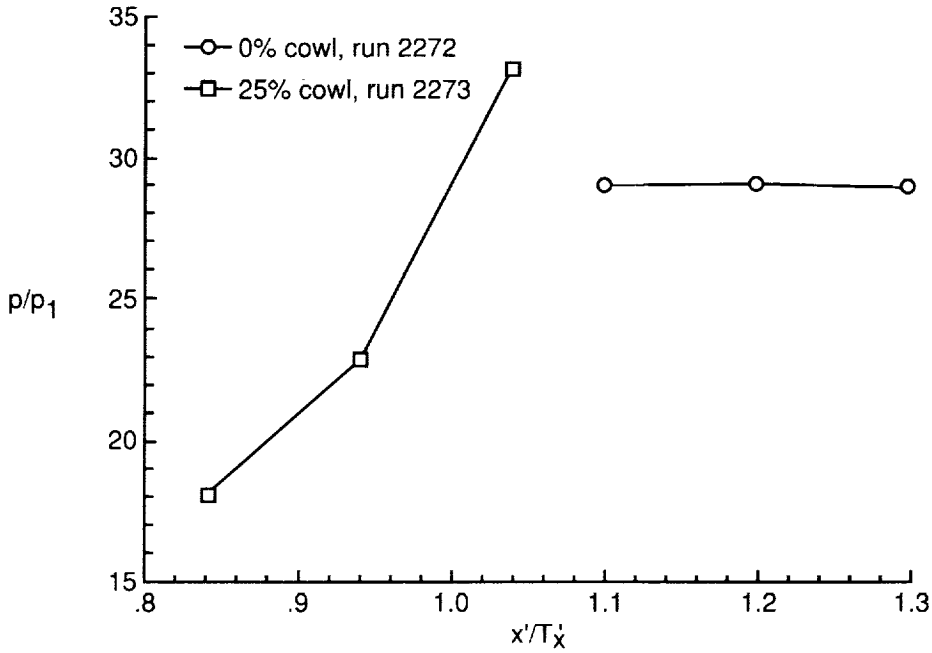

(e) Cowl centerline.

Figure 18. Concluded.

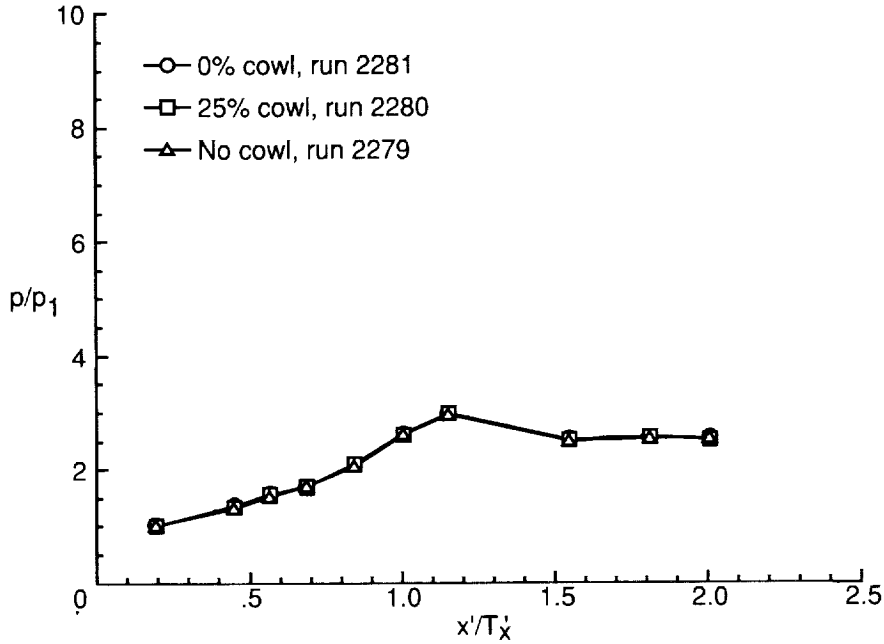

(a) Baseplate centerline.

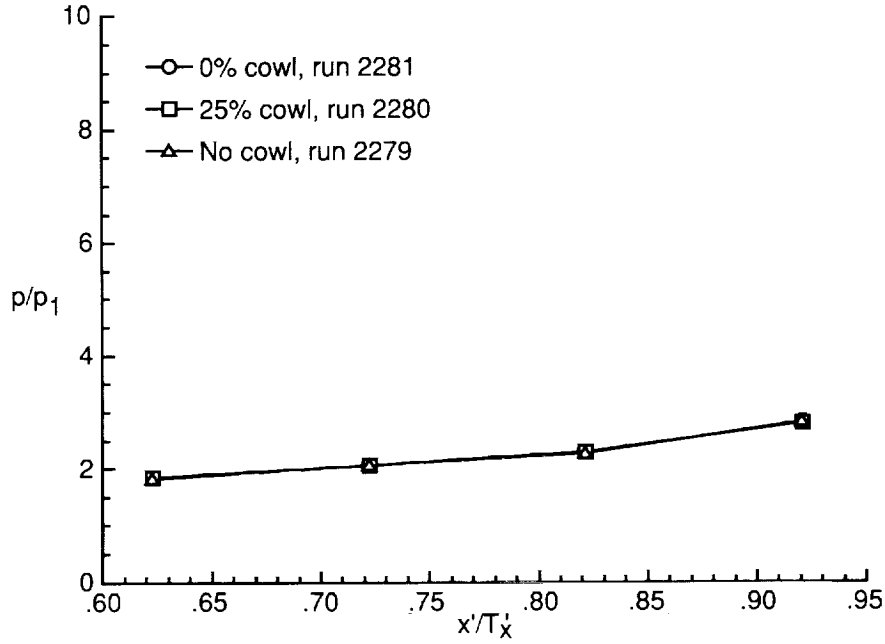

(b) Sidewall at $y/H = 0.13$.

Figure 19. Cowl position effects on pressure distributions of $\Lambda = 70°$ model with CR = 3 and $N_{Re} = 5.50 \times 10^5$ per foot.

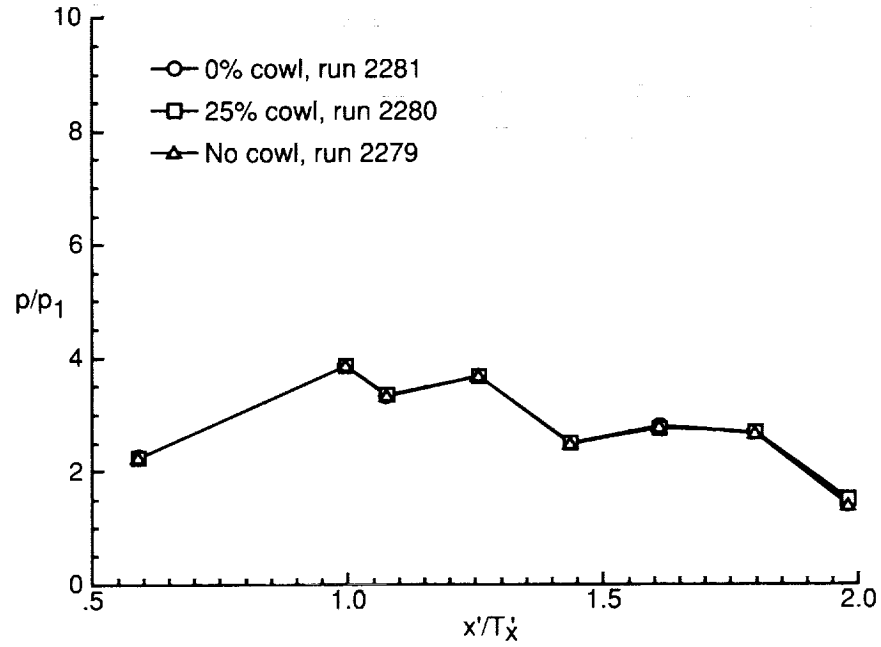

(c) Sidewall centerline.

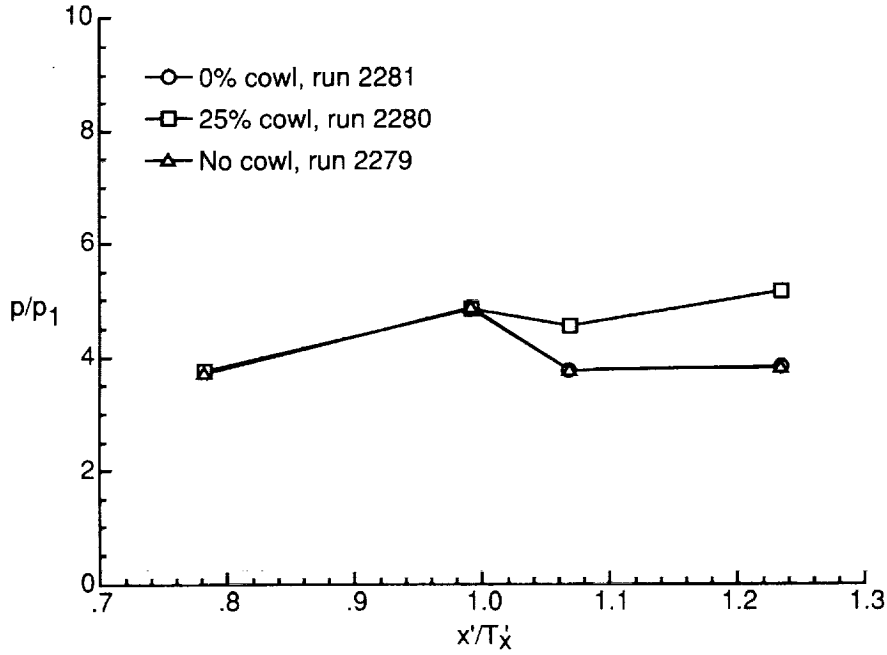

(d) Sidewall at $y/H = 0.87$.

Figure 19. Continued.

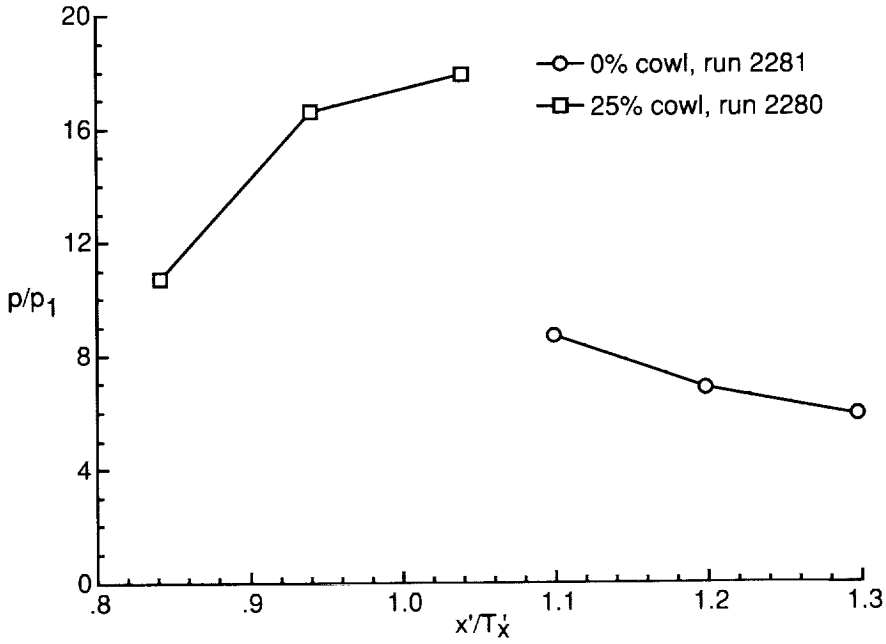

(c) Cowl centerline.

Figure 19. Concluded.

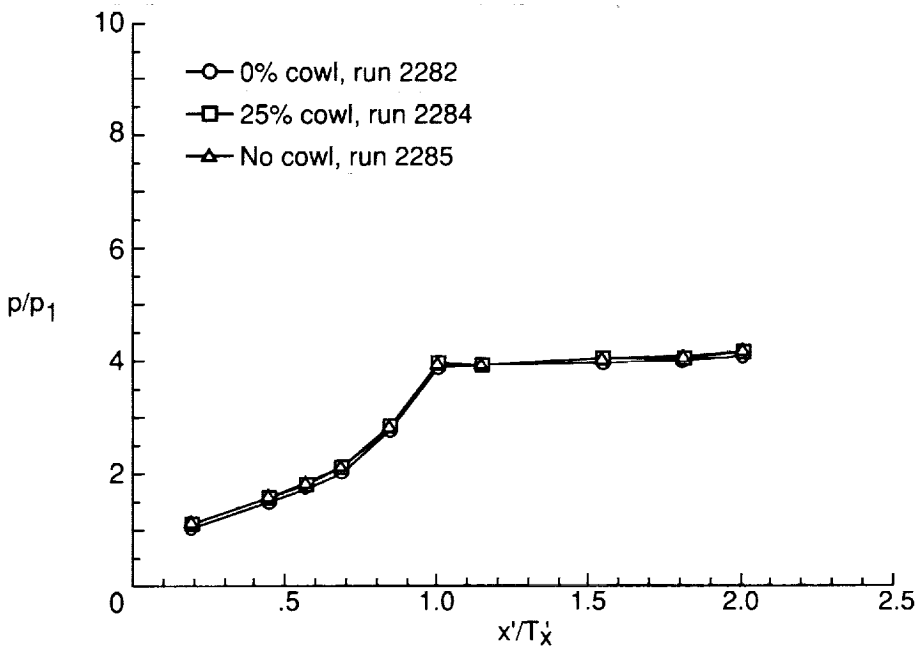

(a) Baseplate centerline.

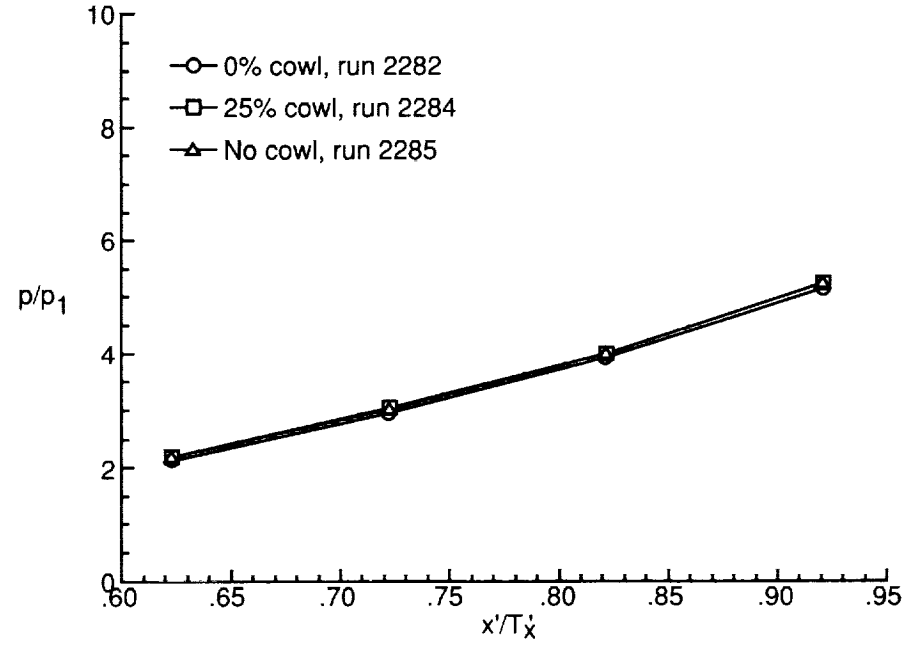

(b) Sidewall at $y/H = 0.13$.

Figure 20. Cowl position effects on pressure distributions of $\Lambda = 70°$ model with CR = 5 and $N_{Re} = 5.50 \times 10^5$ per foot.

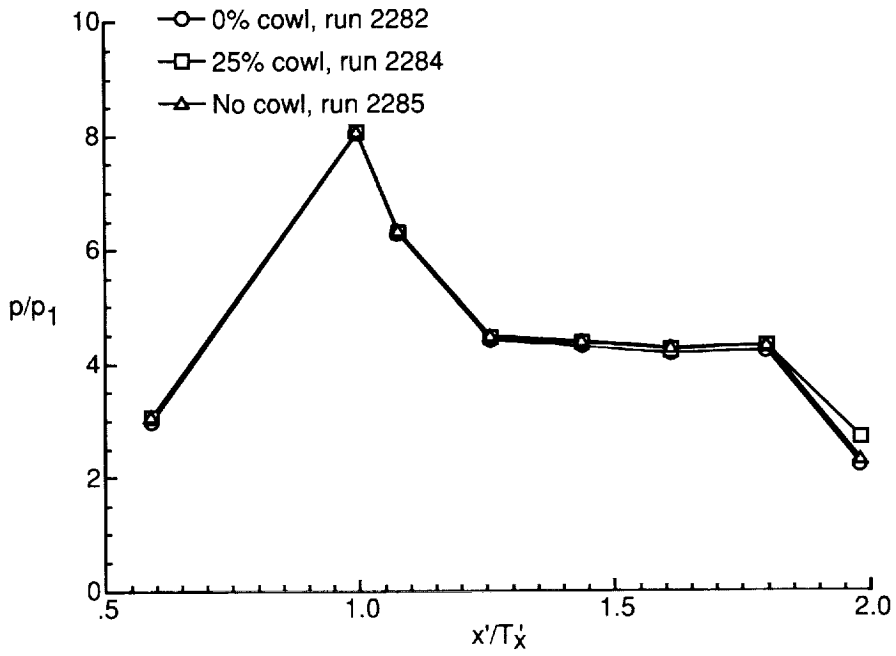

(c) Sidewall centerline.

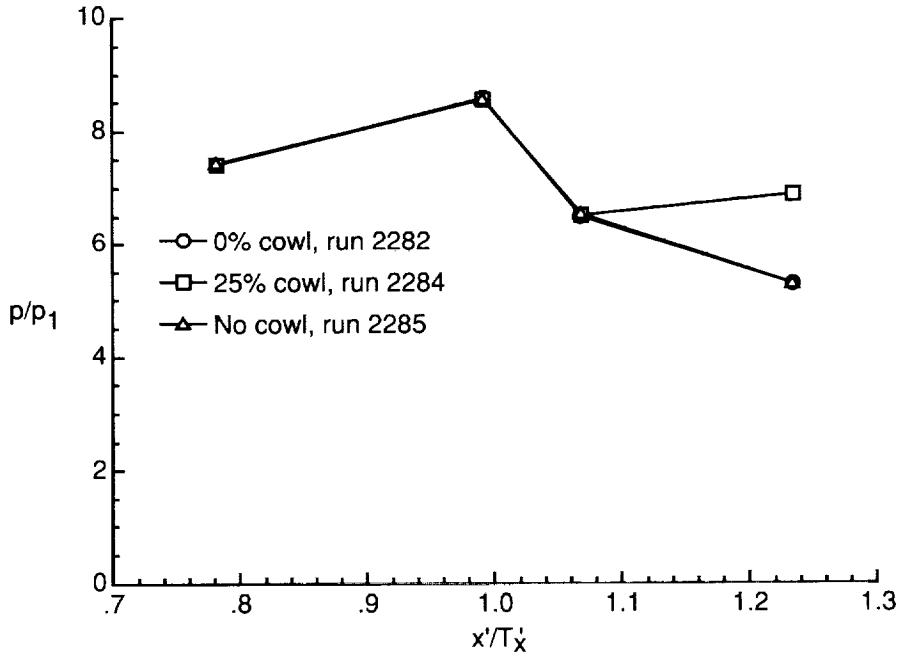

(d) Sidewall at $y/H = 0.87$.

Figure 20. Continued.

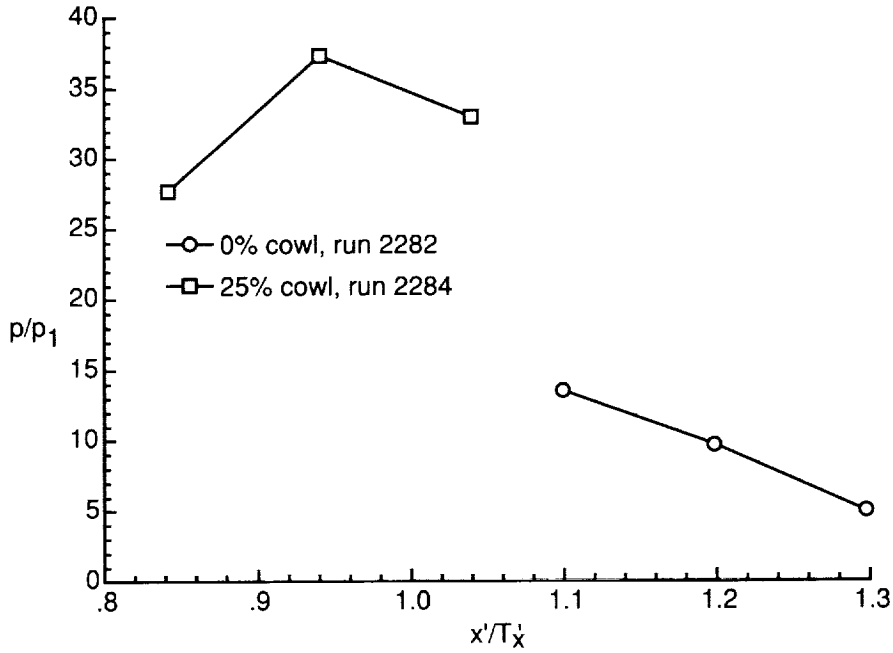

(e) Cowl centerline.

Figure 20. Concluded.

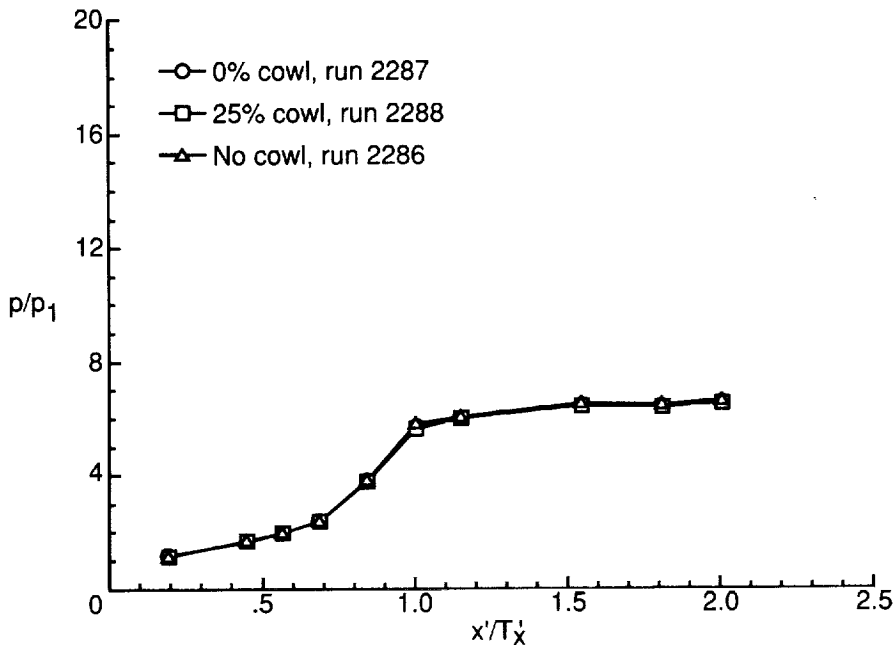

(a) Baseplate centerline.

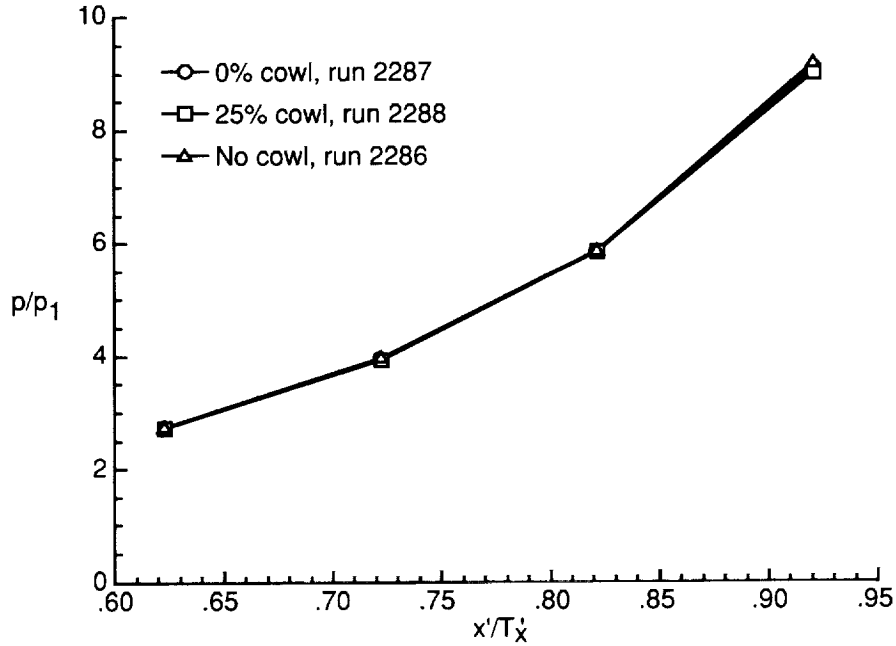

(b) Sidewall at $y/H = 0.13$.

Figure 21. Cowl position effects on pressure distributions of $\Lambda = 70°$ model with CR = 9 and $N_{Re} = 5.50 \times 10^5$ per foot.

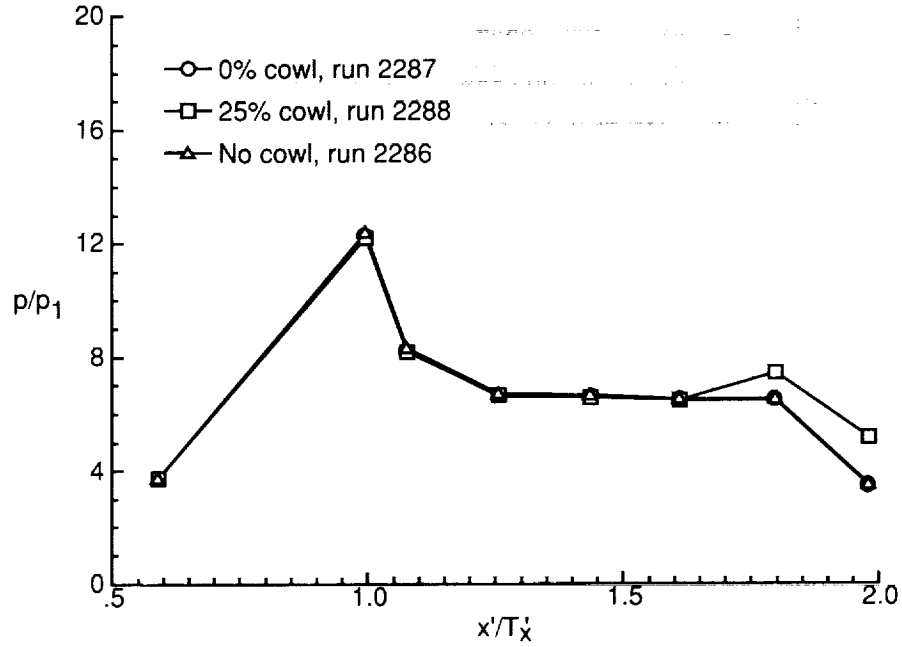

(c) Sidewall centerline.

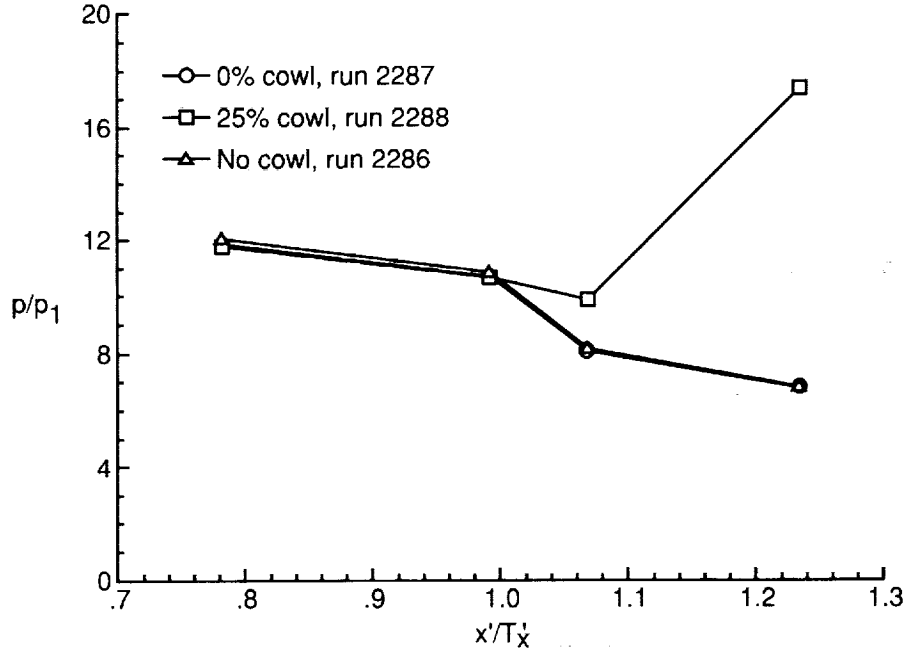

(d) Sidewall at $y/H = 0.87$.

Figure 21. Continued.

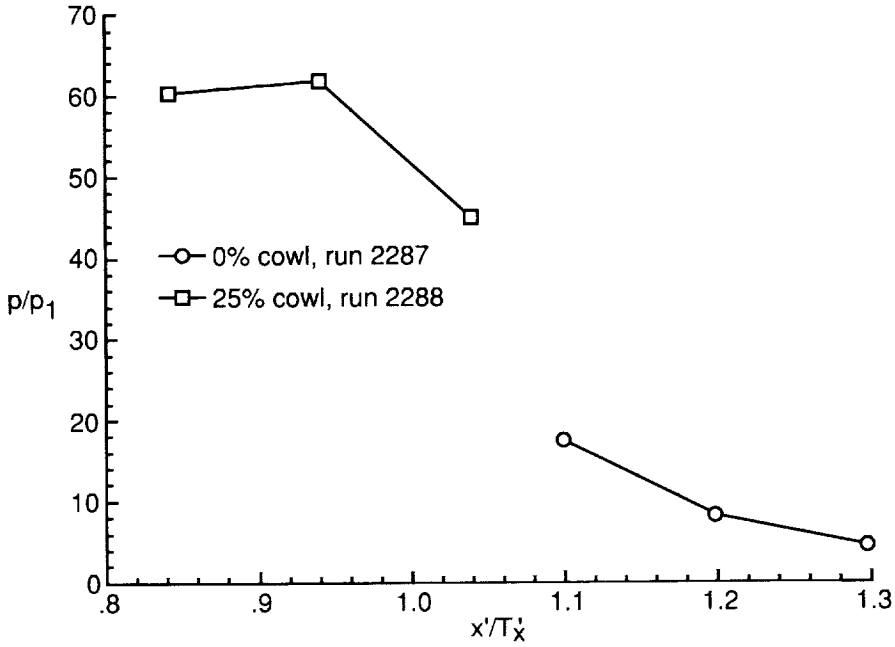

(e) Cowl centerline.

Figure 21. Concluded.

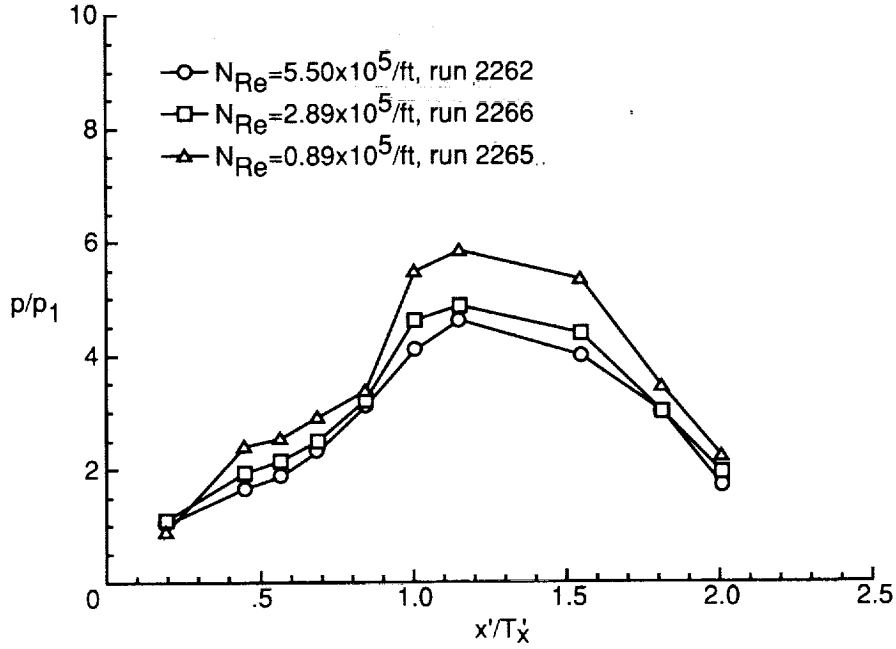

(a) Baseplate centerline.

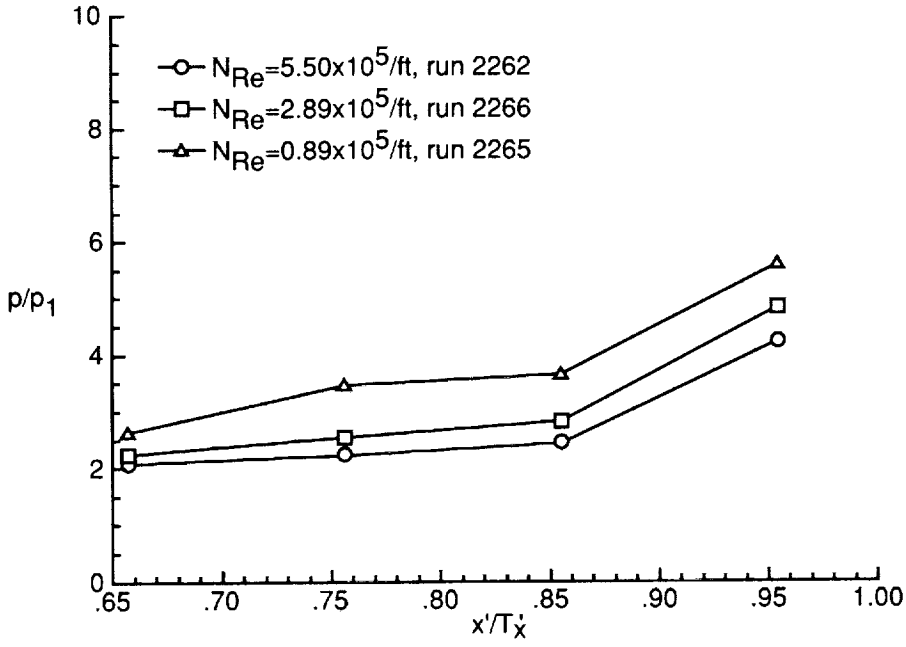

(b) Sidewall at $y/H = 0.13$.

Figure 22. Reynolds number effects on pressure distributions of $\Lambda = 30°$ model with CR = 3 and 0-percent cowl.

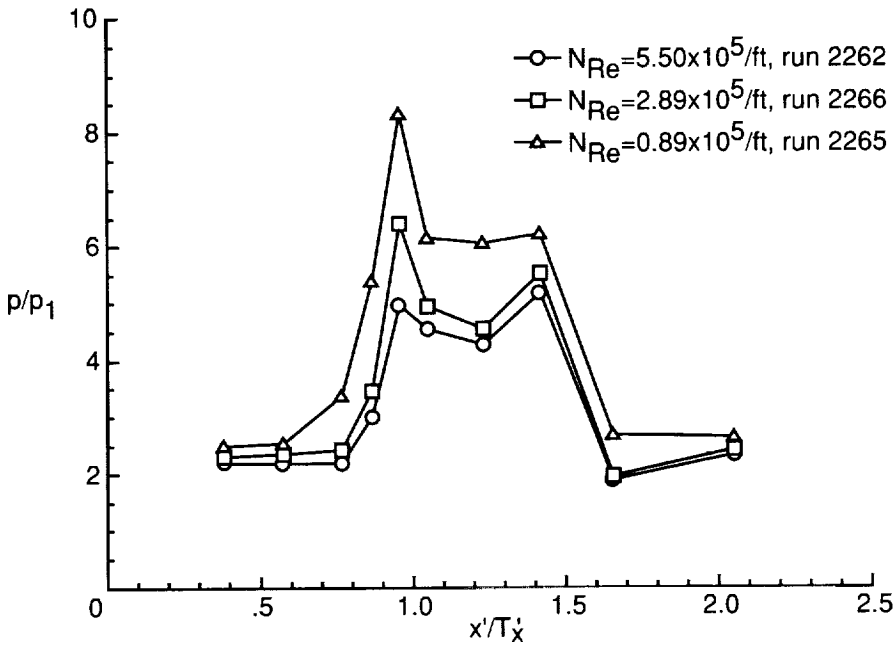

(c) Sidewall centerline.

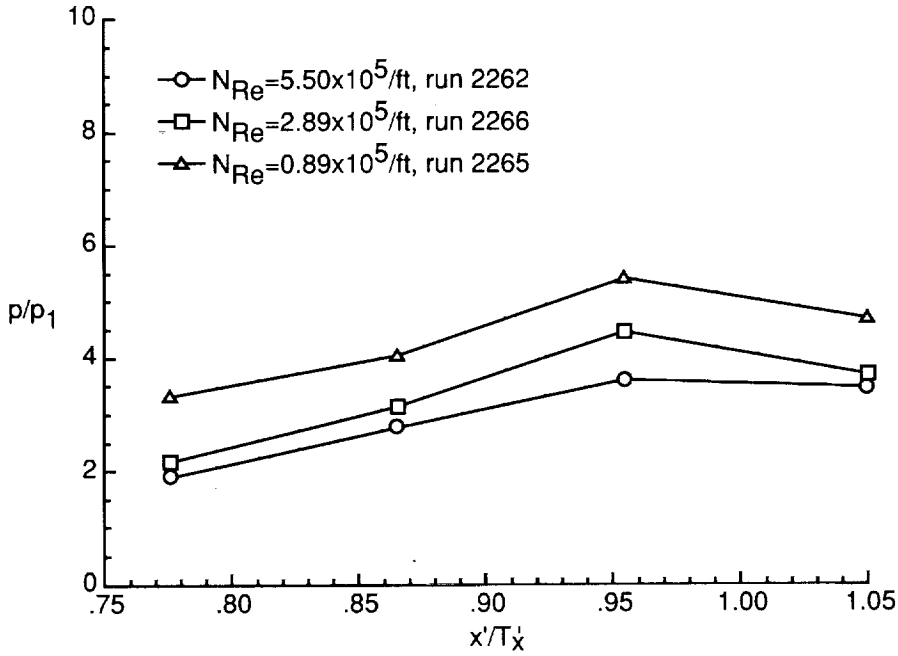

(d) Sidewall at $y/H = 0.87$.

Figure 22. Continued.

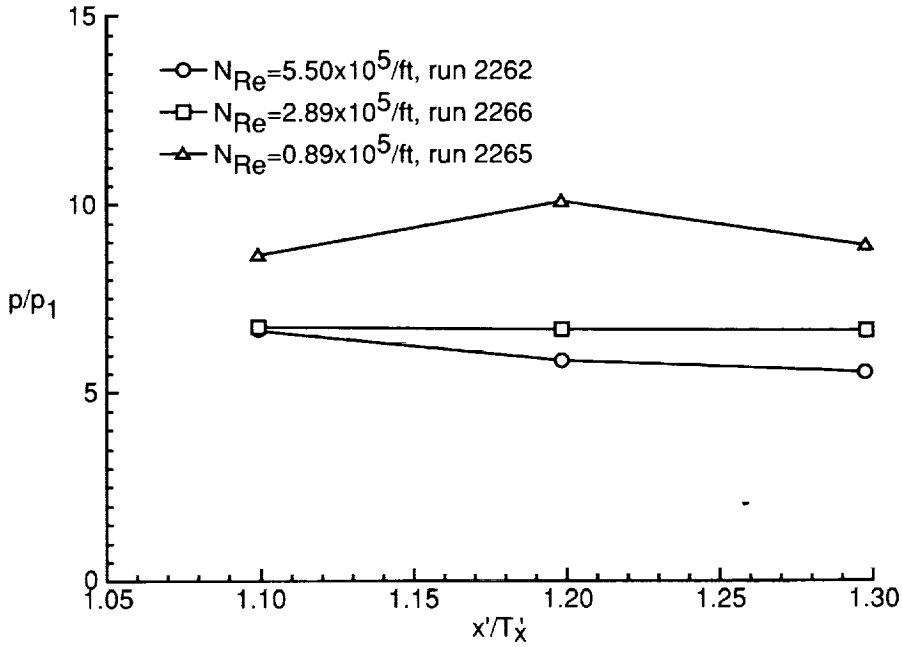

(c) Cowl centerline.

Figure 22. Concluded.

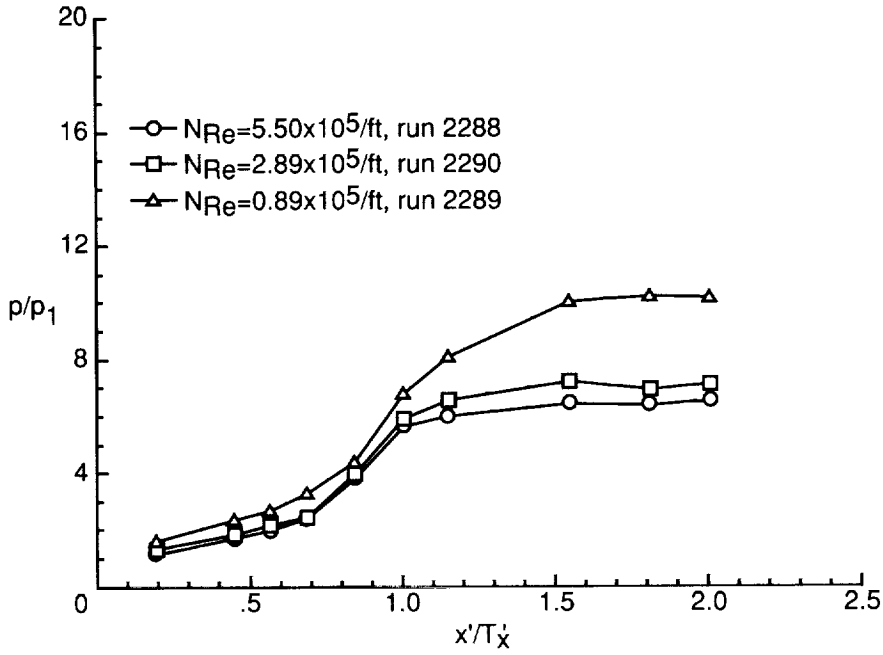

(a) Baseplate centerline.

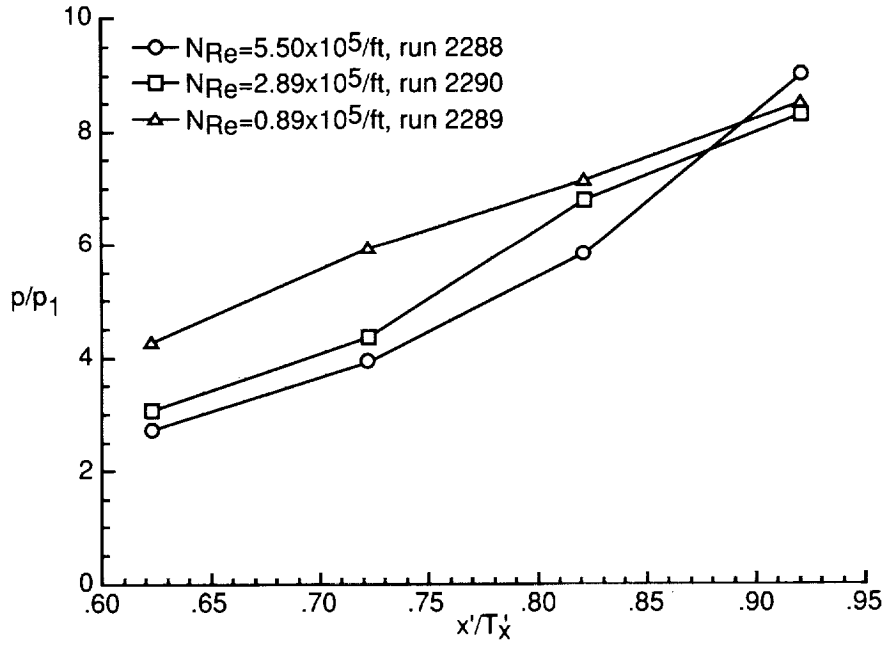

(b) Sidewall at $y/H = 0.13$.

Figure 23. Reynolds number effects on pressure distributions of $\Lambda = 70°$ model with CR = 9 and 25-percent cowl.

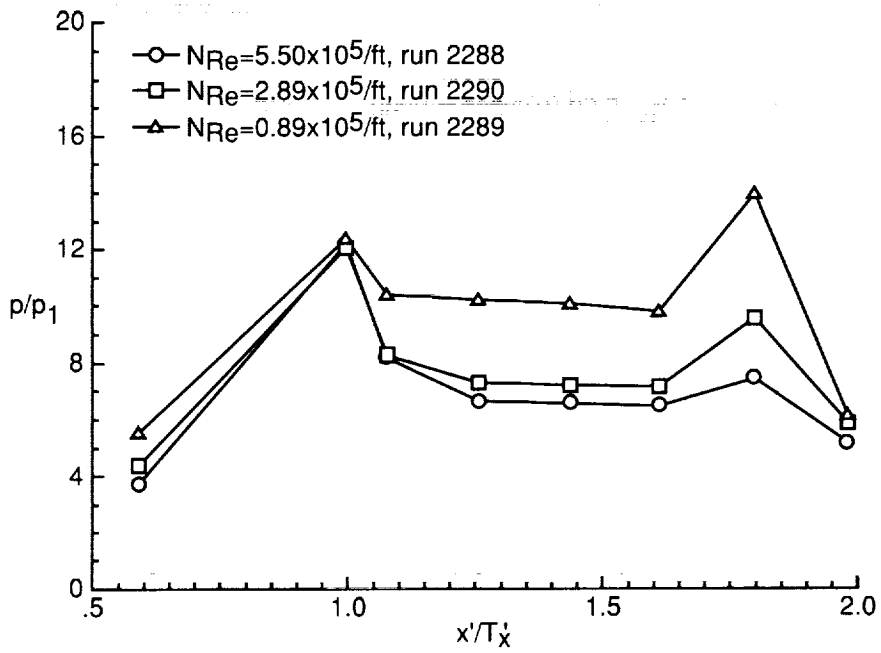

(c) Sidewall centerline.

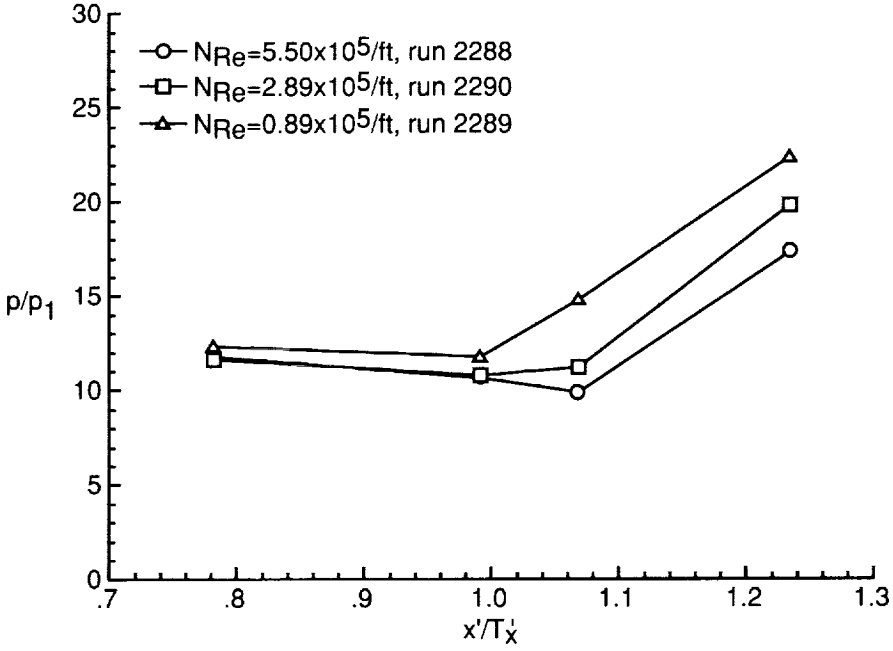

(d) Sidewall at $y/H = 0.87$.

Figure 23. Continued.

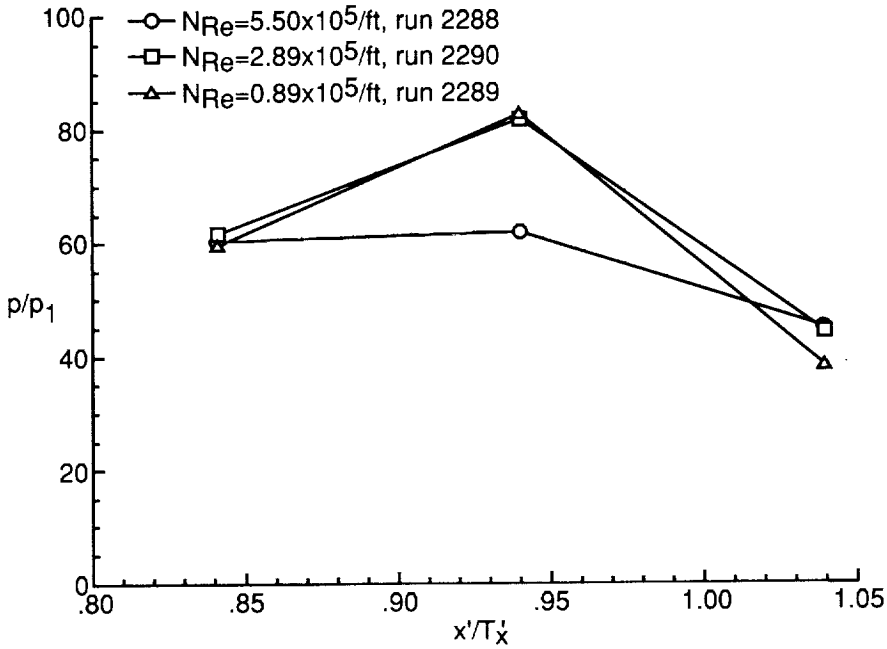

(e) Cowl centerline.

Figure 23. Concluded.

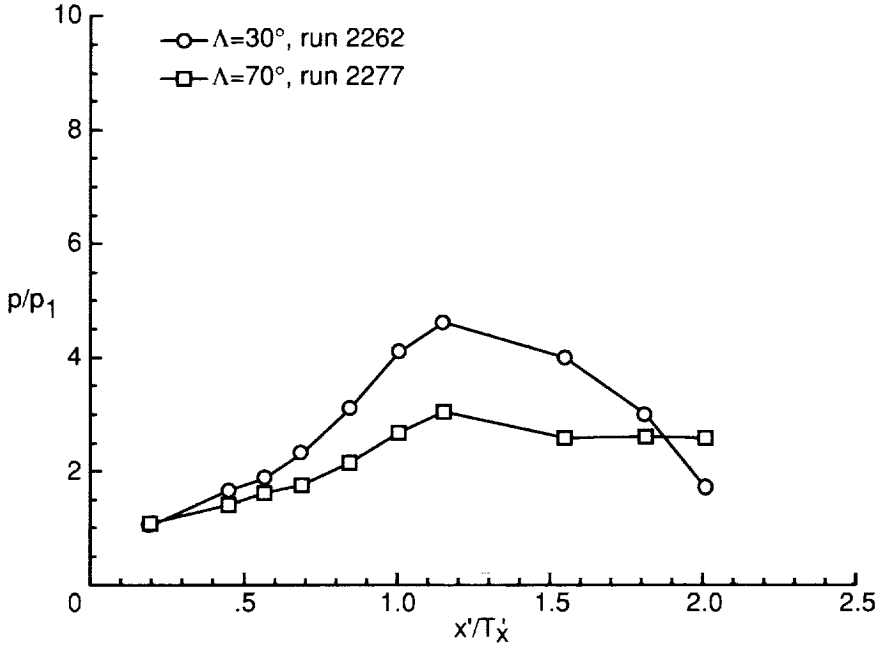

(a) Baseplate centerline.

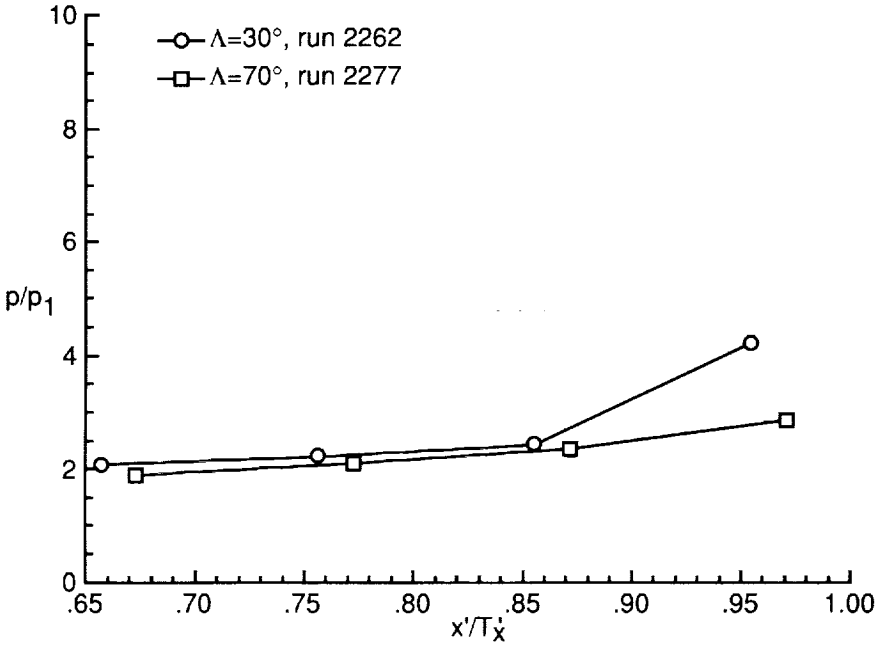

(b) Sidewall at $y/H = 0.13$.

Figure 24. Leading-edge sweep effects on pressure distributions of both models with CR = 3, 0-percent cowl, and $N_{Re} = 5.50 \times 10^5$ per foot.

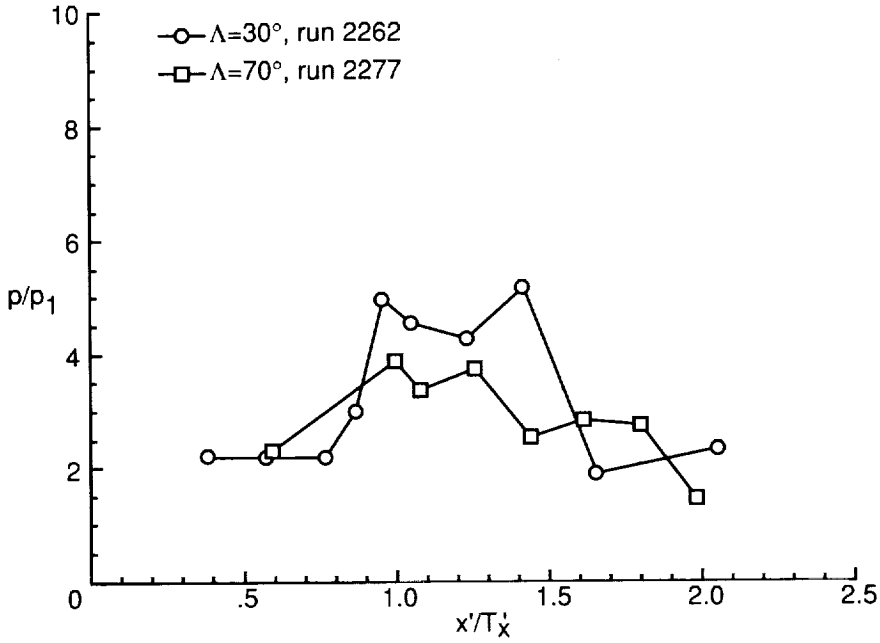

(c) Sidewall centerline.

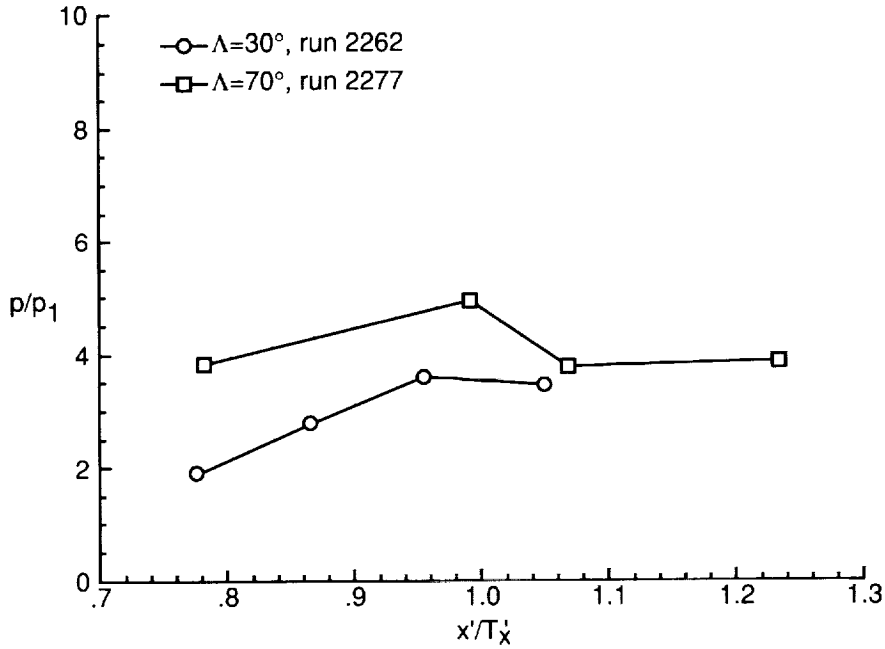

(d) Sidewall at $y/H = 0.87$.

Figure 24. Concluded.

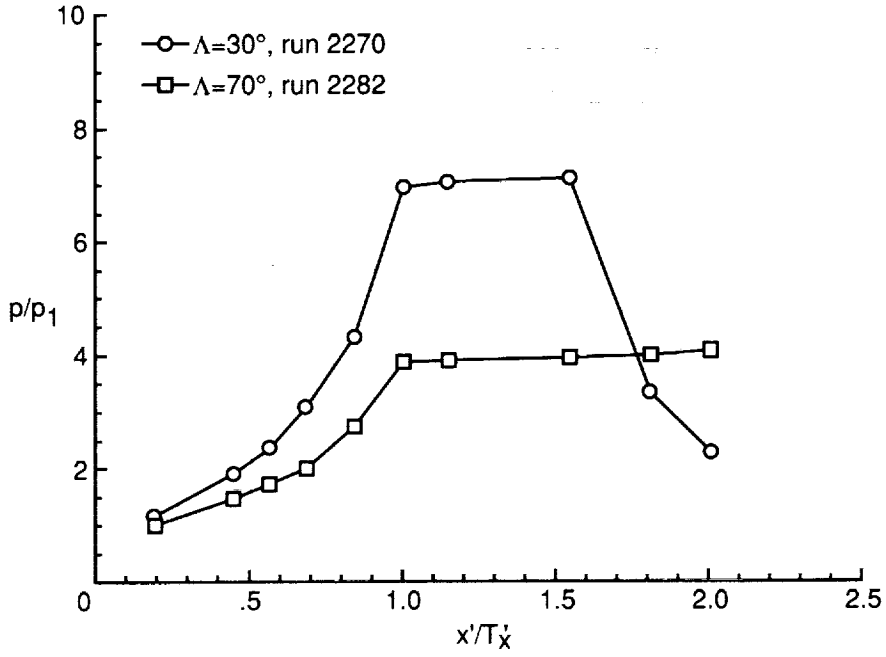

(a) Baseplate centerline.

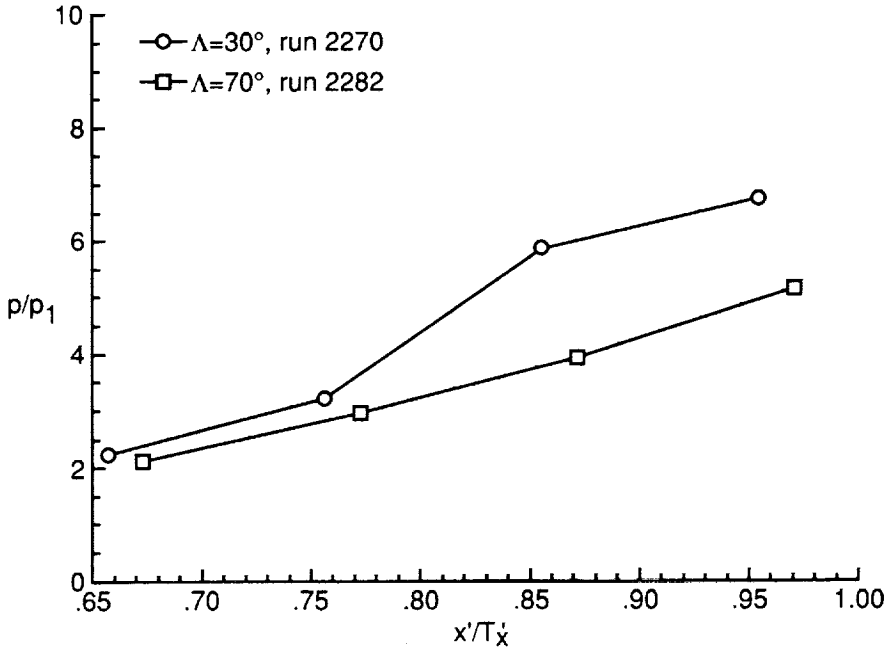

(b) Sidewall at $y/H = 0.13$.

Figure 25. Leading-edge sweep effects on pressure distributions of both models with CR = 5, 0-percent cowl, and $N_{Re} = 5.50 \times 10^5$ per foot.

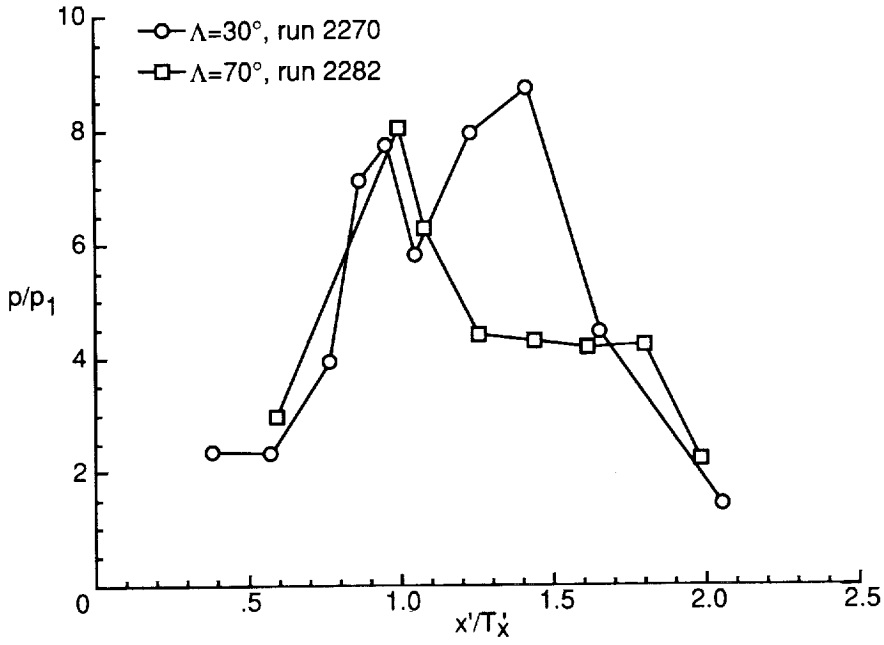

(c) Sidewall centerline.

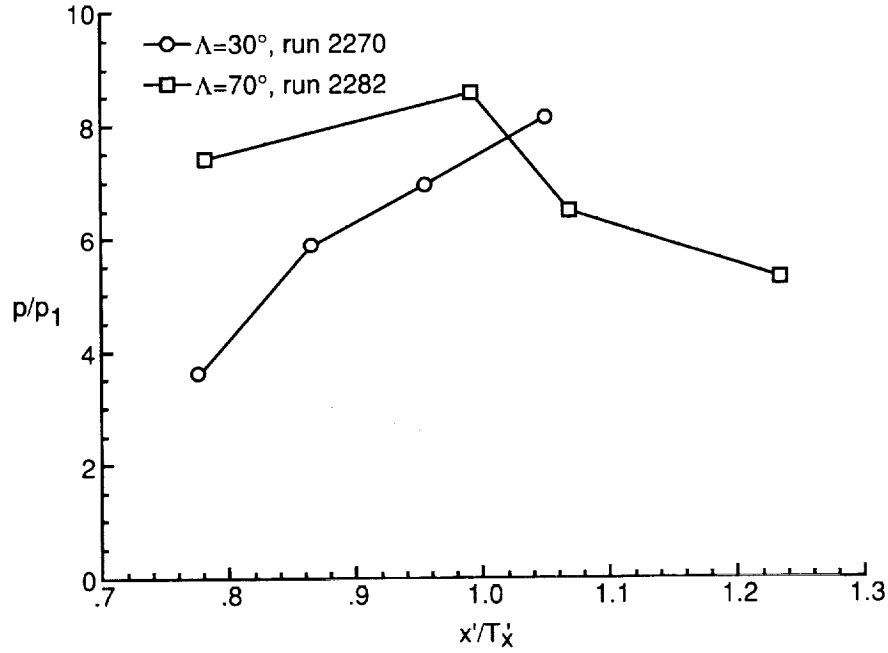

(d) Sidewall at $y/H = 0.87$.

Figure 25. Concluded.

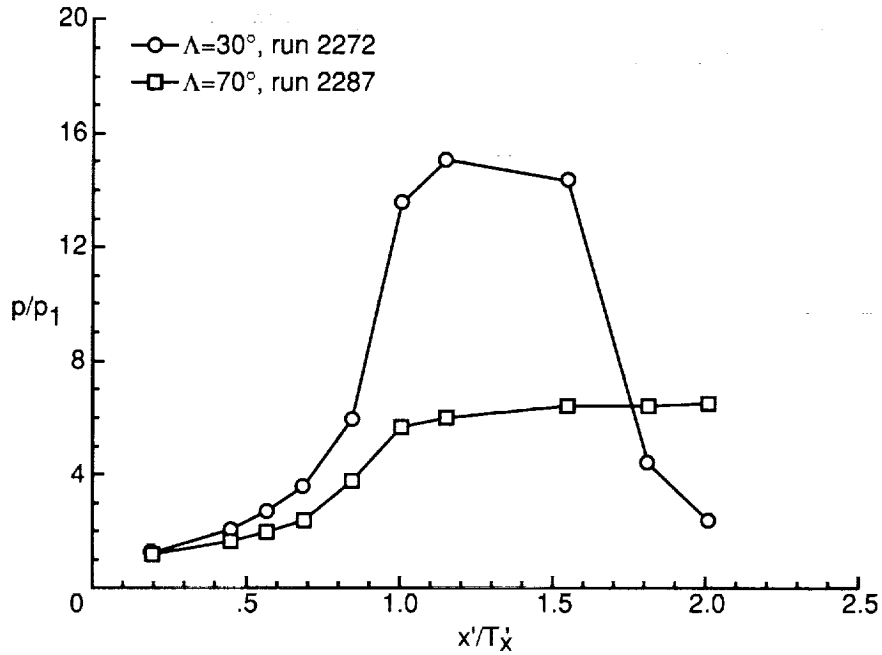

(a) Baseplate centerline.

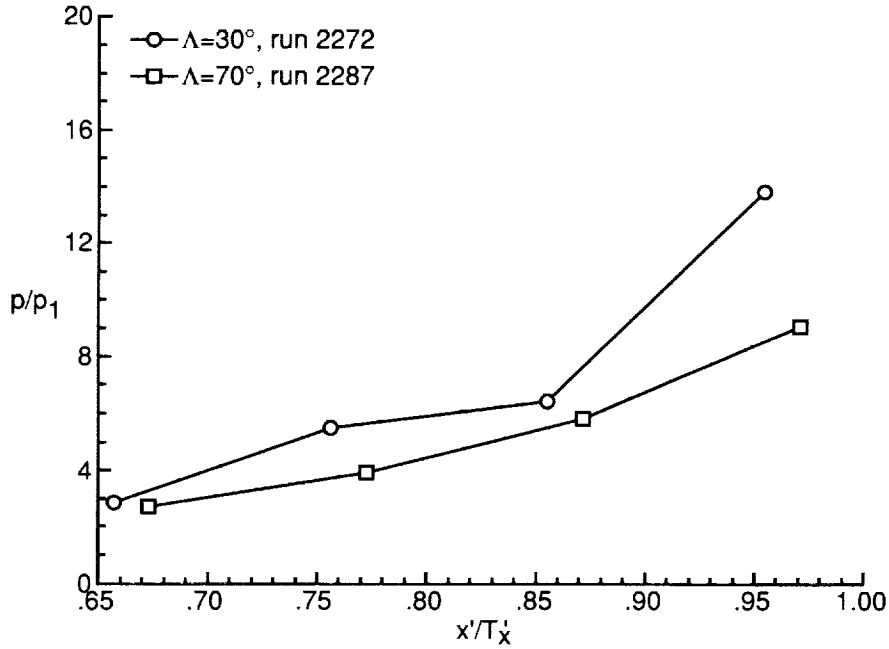

(b) Sidewall at $y/H = 0.13$.

Figure 26. Leading-edge sweep effects on pressure distributions of both models with CR = 9, 0-percent cowl, and $N_{Re} = 5.50 \times 10^5$ per foot.

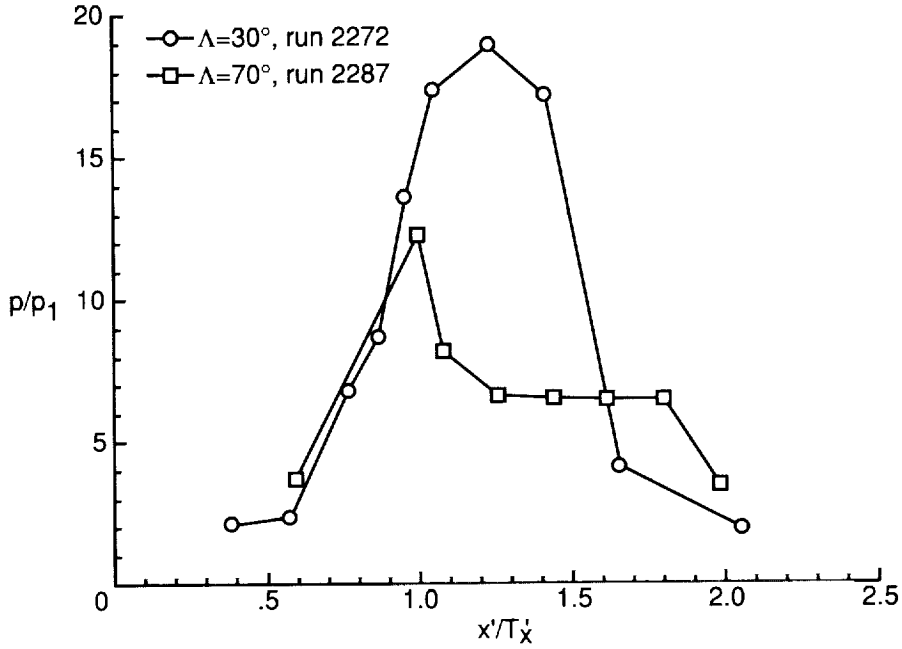

(c) Sidewall centerline.

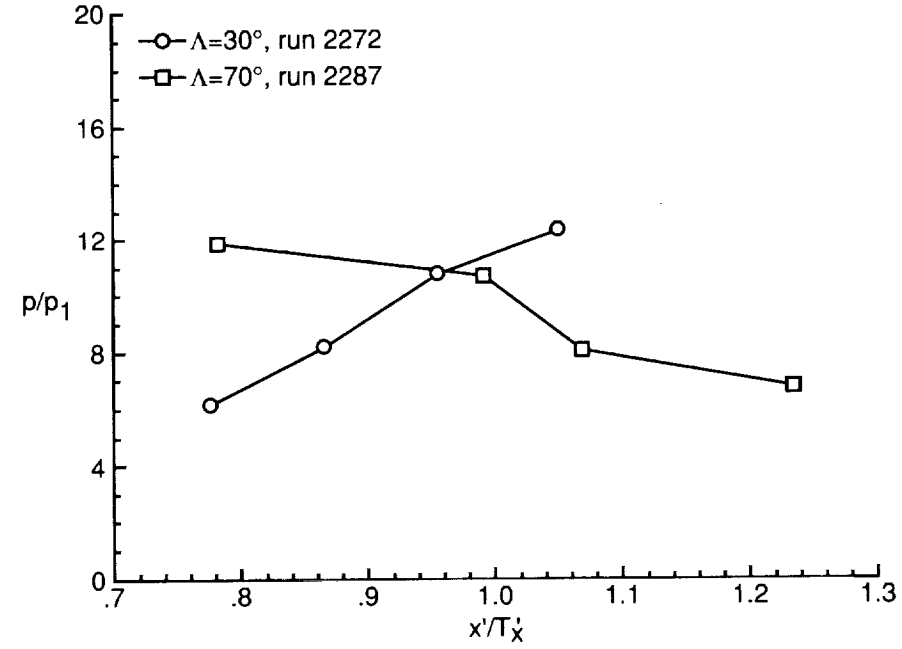

(d) Sidewall at $y/H = 0.87$.

Figure 26. Concluded.

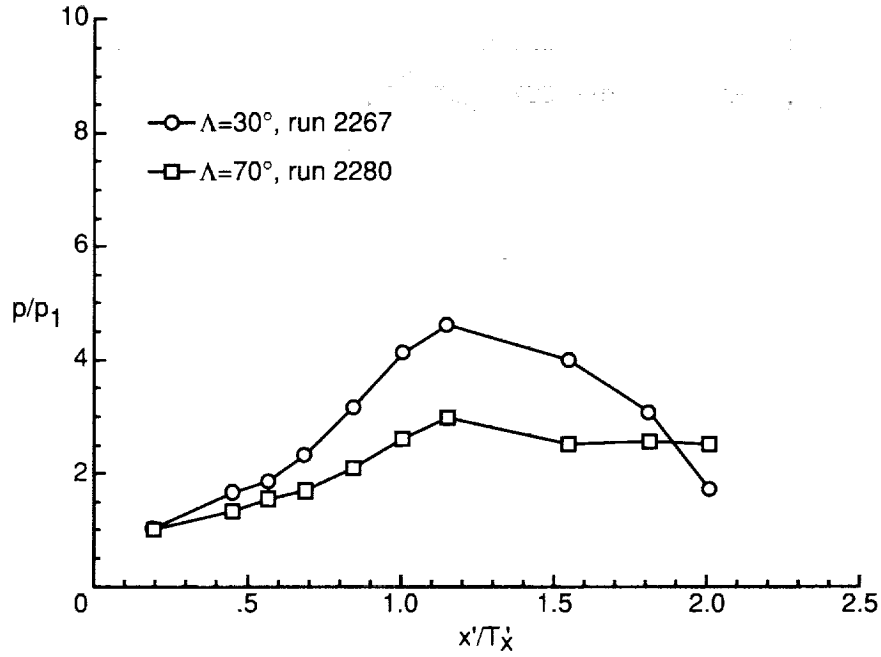

(a) Baseplate centerline.

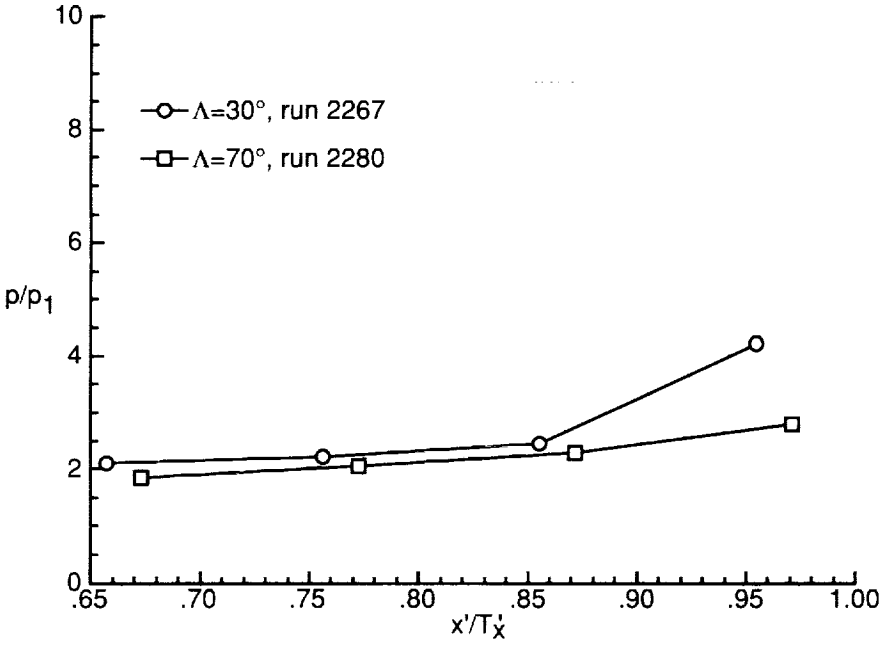

(b) Sidewall at $y/H = 0.13$.

Figure 27. Leading-edge sweep effects on pressure distributions of both models with CR = 3, 25-percent cowl, and $N_{Re} = 5.50 \times 10^5$ per foot.

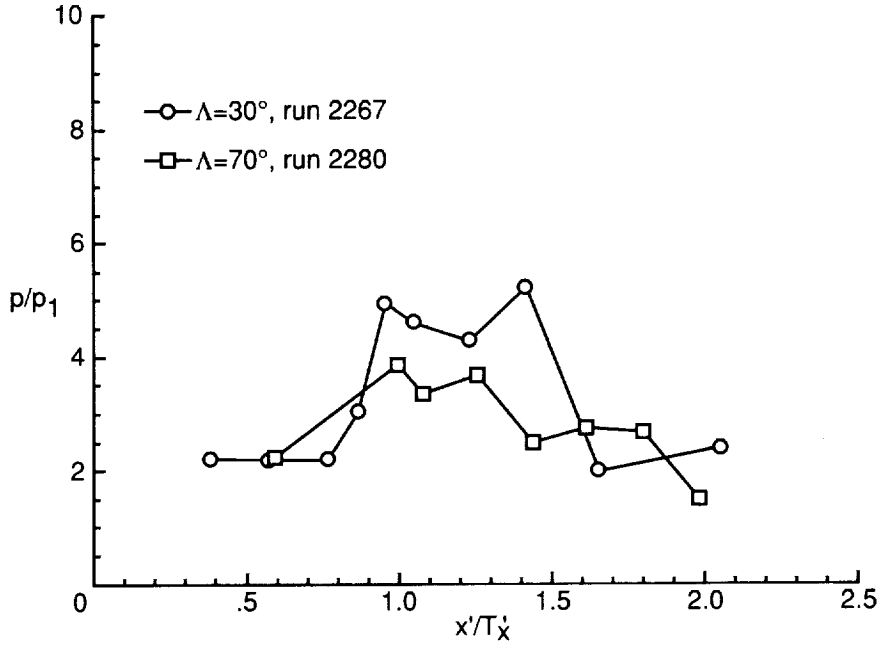

(c) Sidewall centerline.

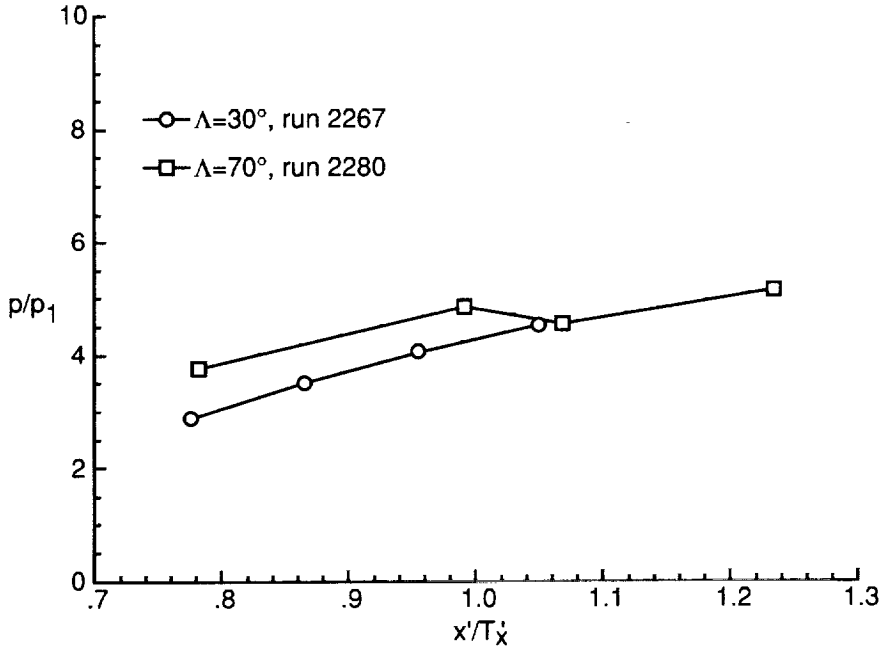

(d) Sidewall at $y/H = 0.87$.

Figure 27. Continued.

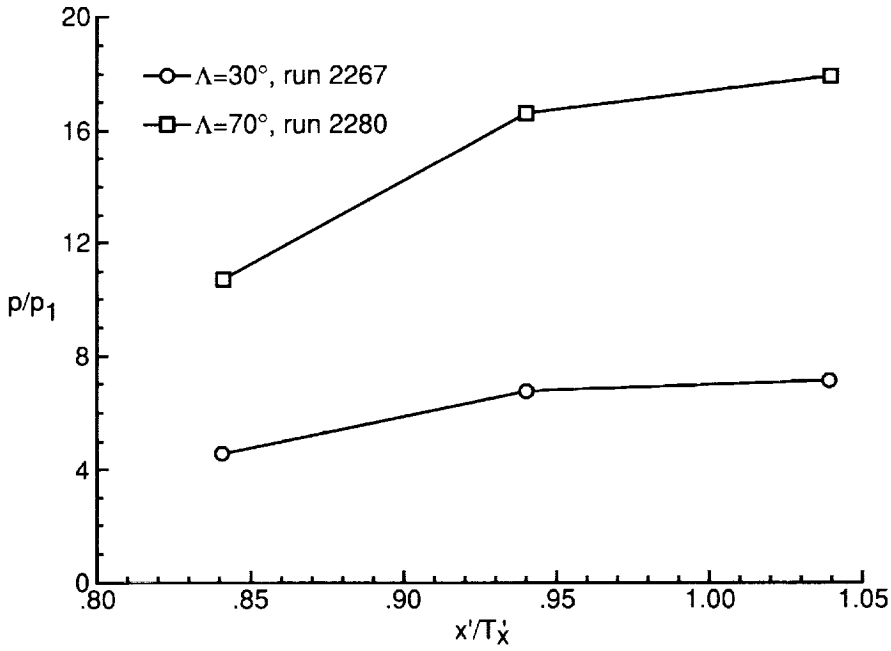

(e) Cowl centerline.

Figure 27. Concluded.

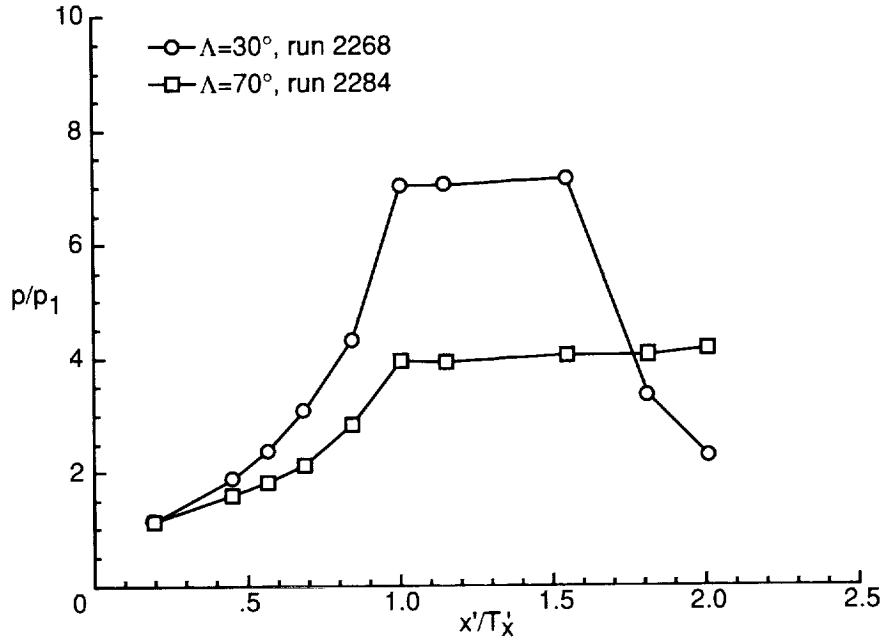

(a) Baseplate centerline.

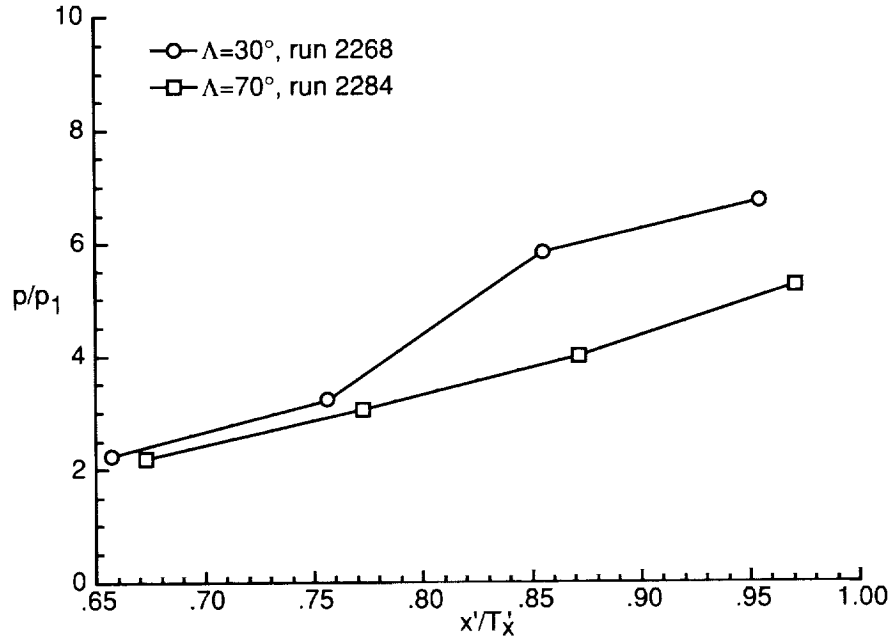

(b) Sidewall at $y/H = 0.13$.

Figure 28. Leading-edge sweep effects on pressure distributions of both models with CR = 5, 25-percent cowl, and $N_{Re} = 5.50 \times 10^5$ per foot.

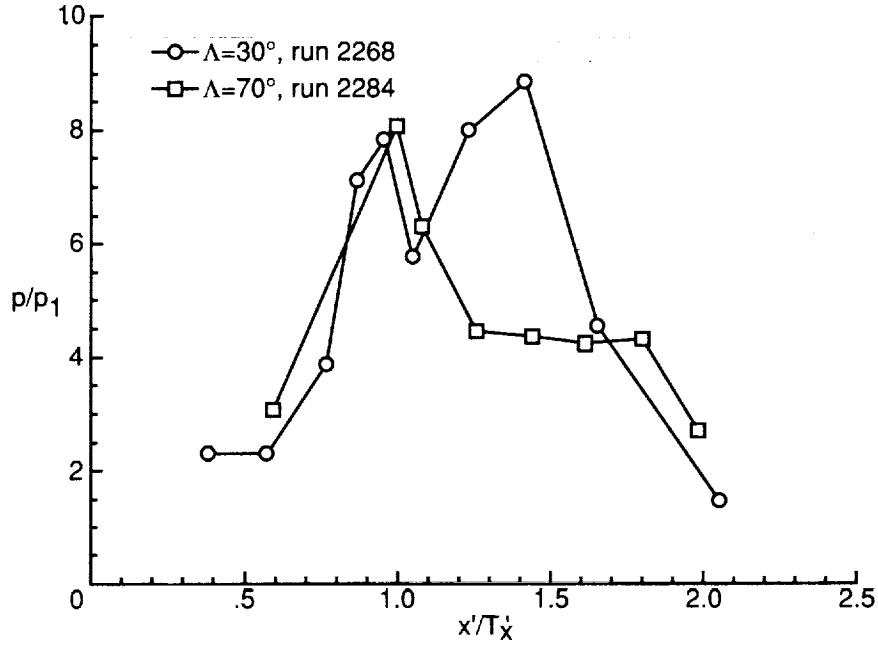

(c) Sidewall centerline.

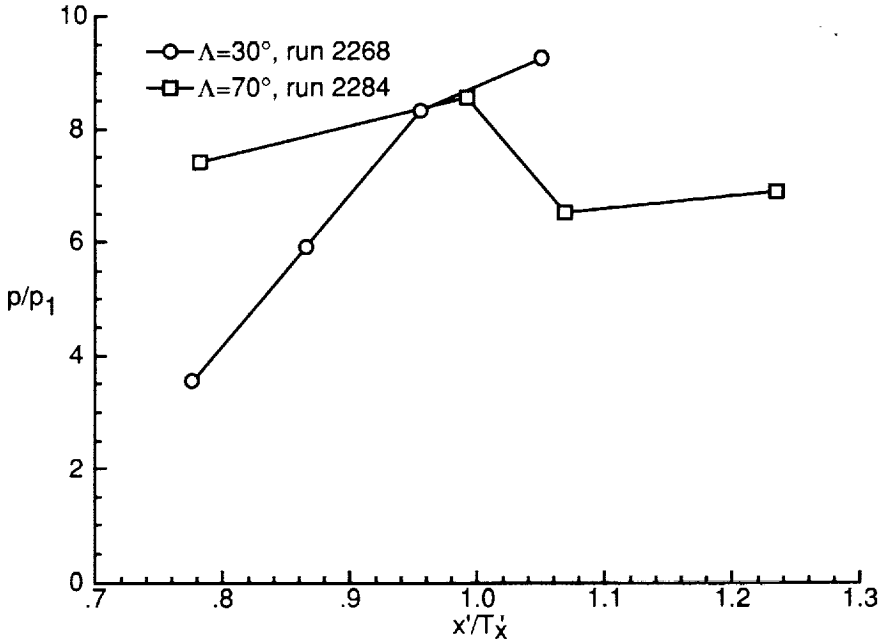

(d) Sidewall at $y/H = 0.87$.

Figure 28. Continued.

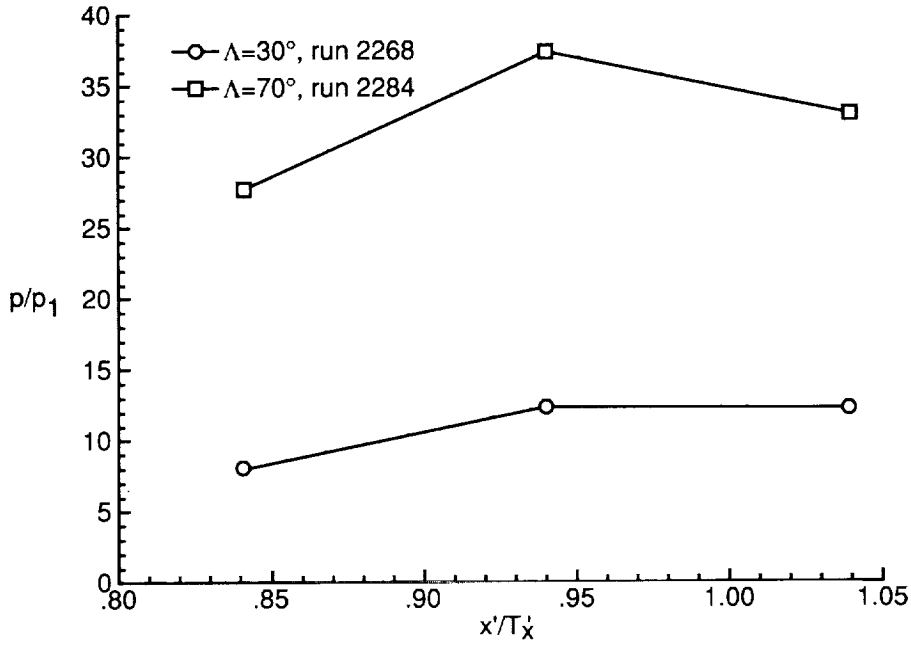

(e) Cowl centerline.

Figure 28. Concluded.

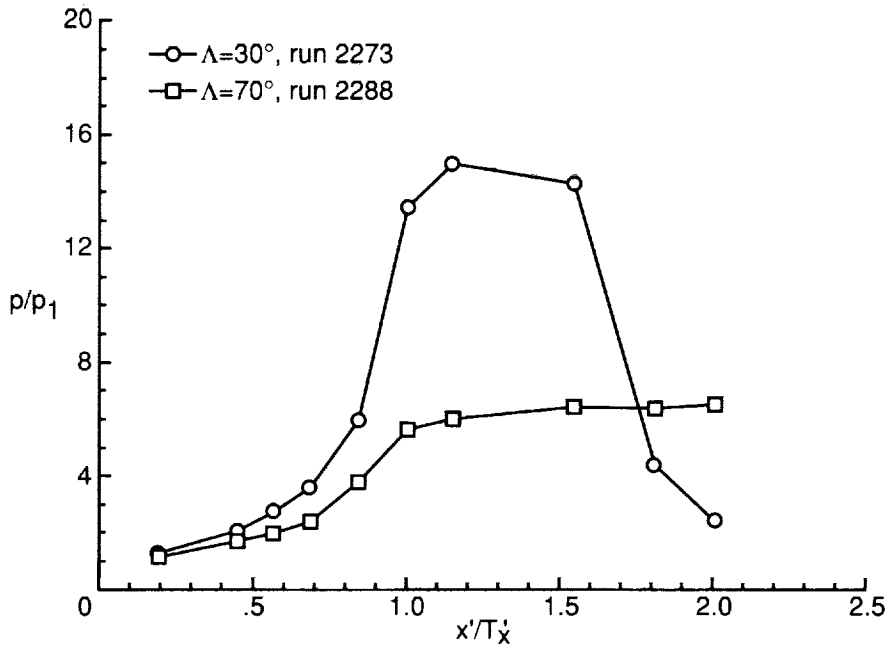

(a) Baseplate centerline.

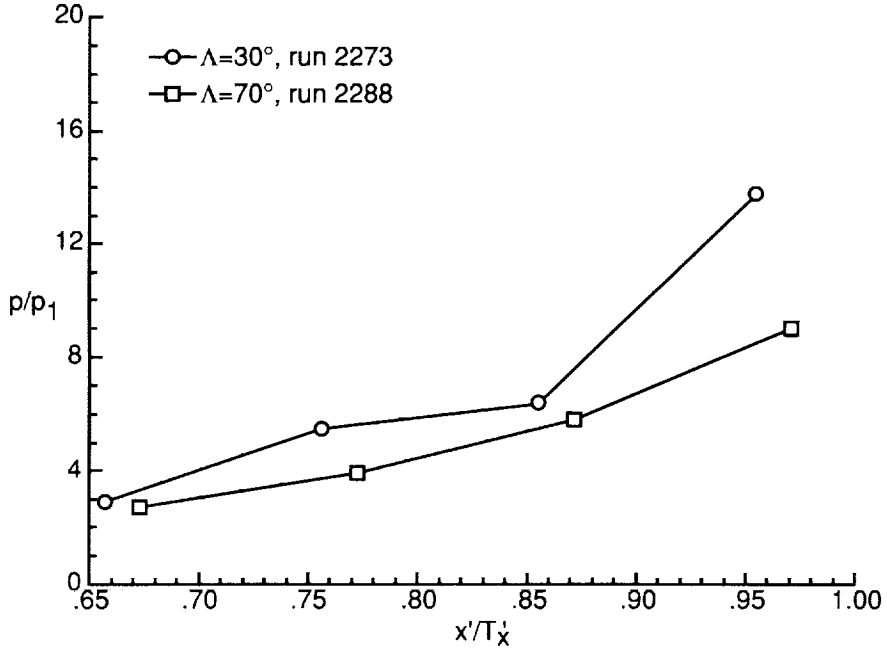

(b) Sidewall at $y/H = 0.13$.

Figure 29. Leading-edge sweep effects on pressure distributions of both models with CR = 9, 25-percent cowl, and $N_{Re} = 5.50 \times 10^5$ per foot.

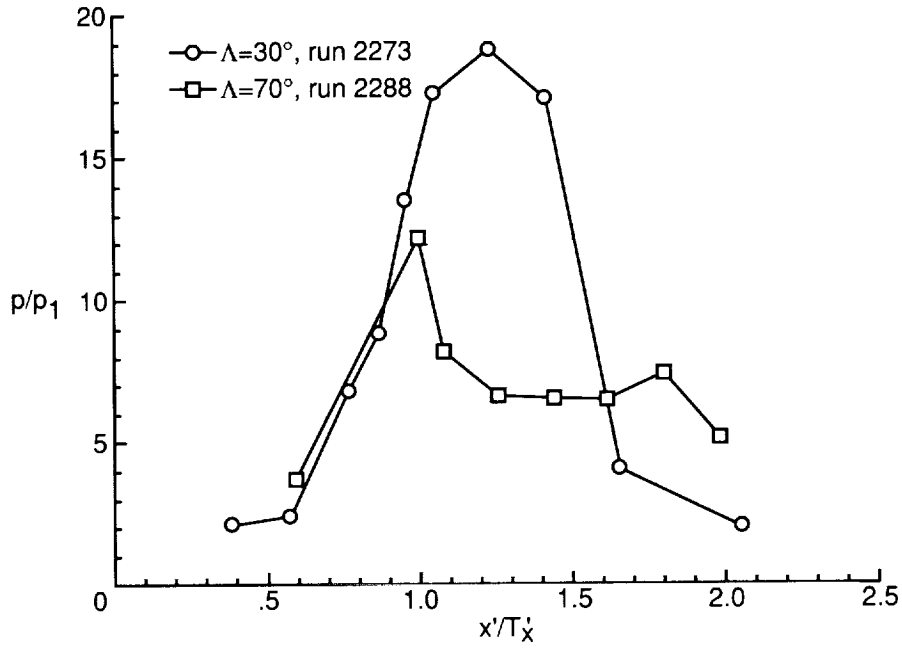

(c) Sidewall centerline.

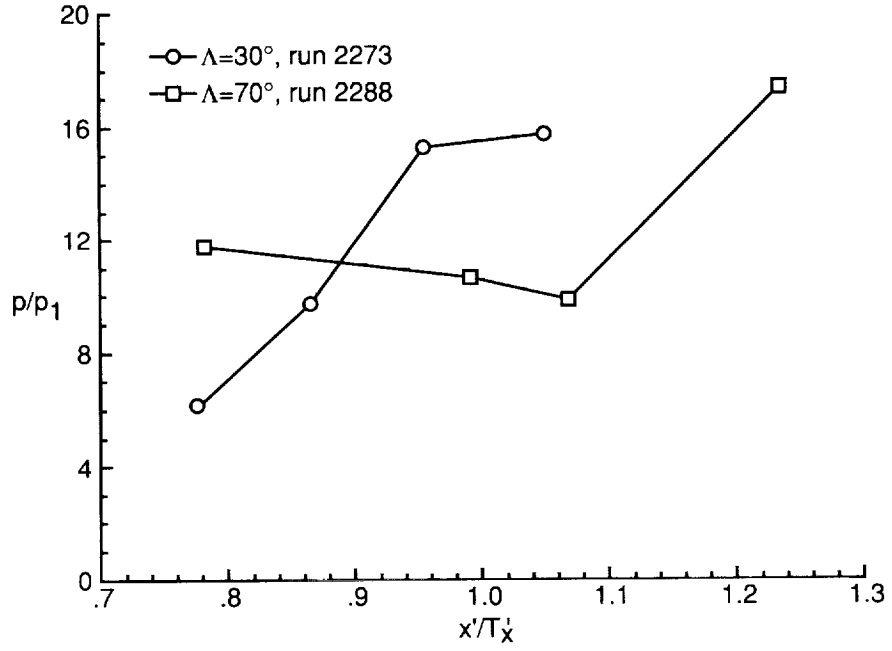

(d) Sidewall at $y/H = 0.87$.

Figure 29. Continued.

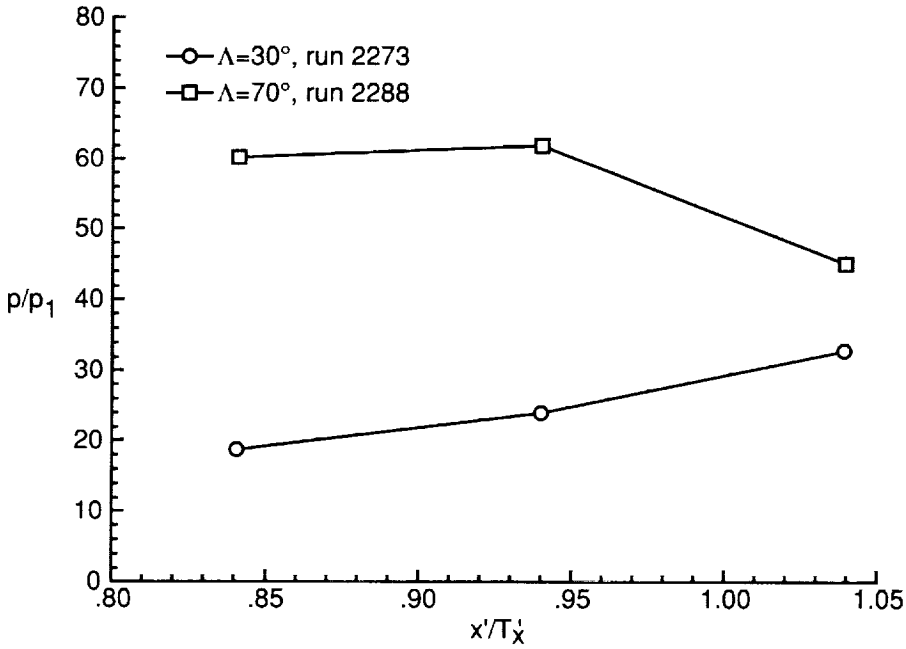

(e) Cowl centerline.

Figure 29. Concluded.

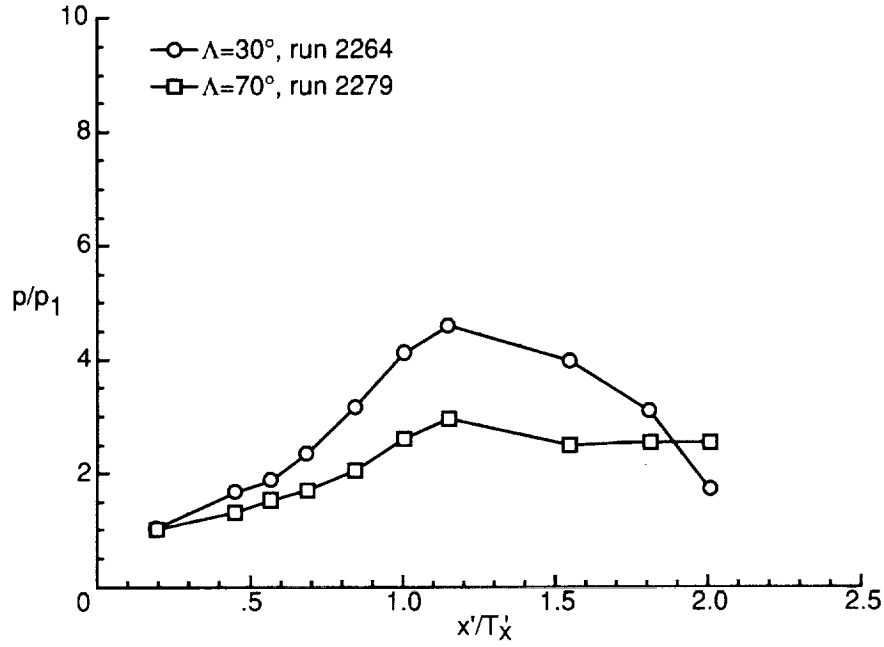

(a) Baseplate centerline.

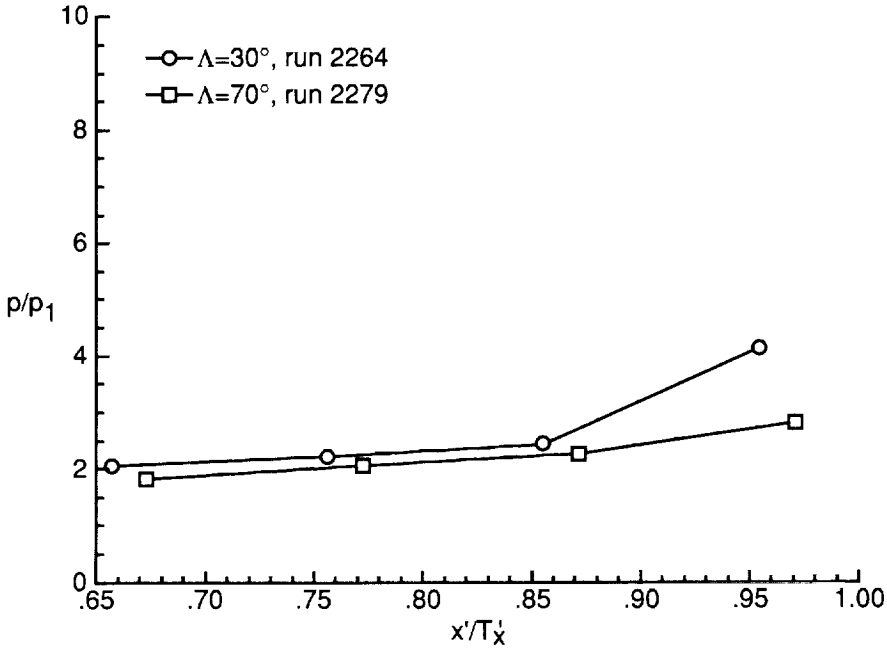

(b) Sidewall at $y/H = 0.13$.

Figure 30. Leading-edge sweep effects on pressure distributions of both models with CR = 3, no cowl, and $N_{Re} = 5.50 \times 10^5$ per foot.

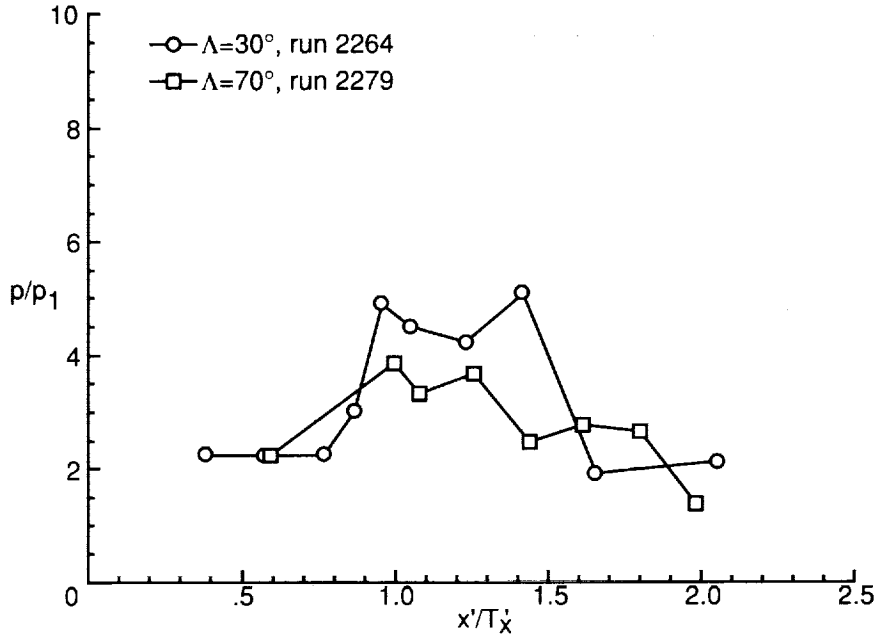

(c) Sidewall centerline.

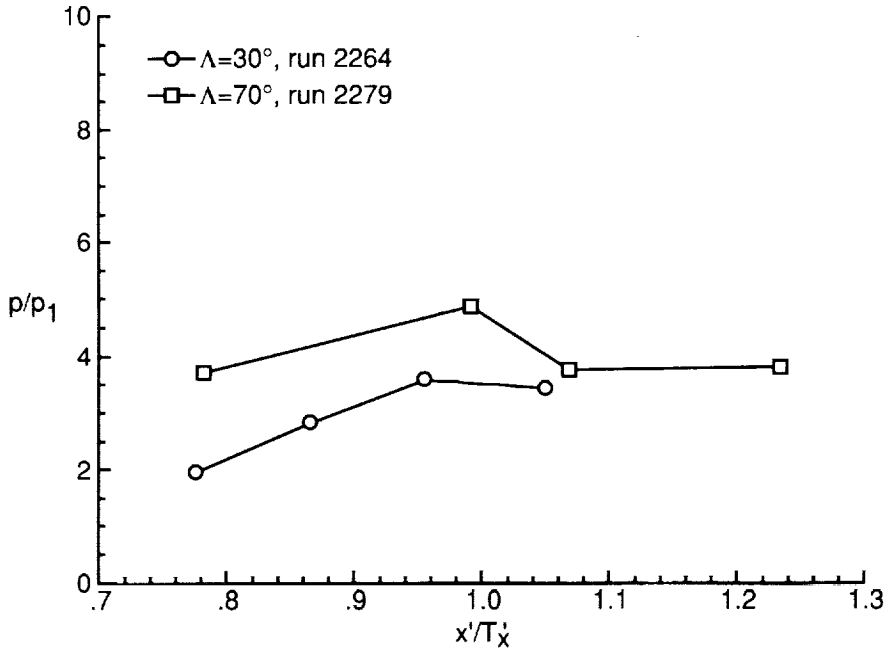

(d) Sidewall at $y/H = 0.87$.

Figure 30. Concluded.

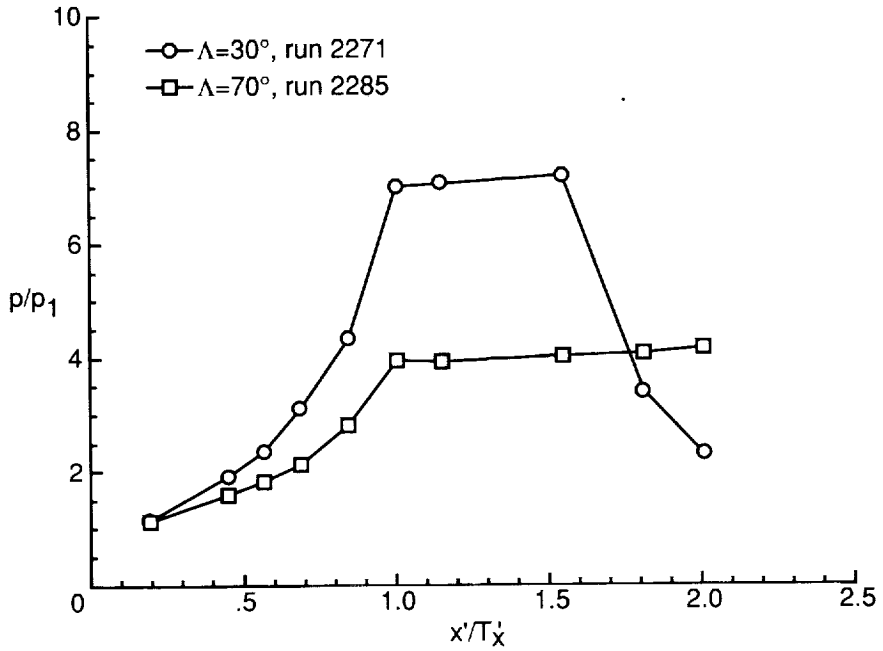

(a) Baseplate centerline.

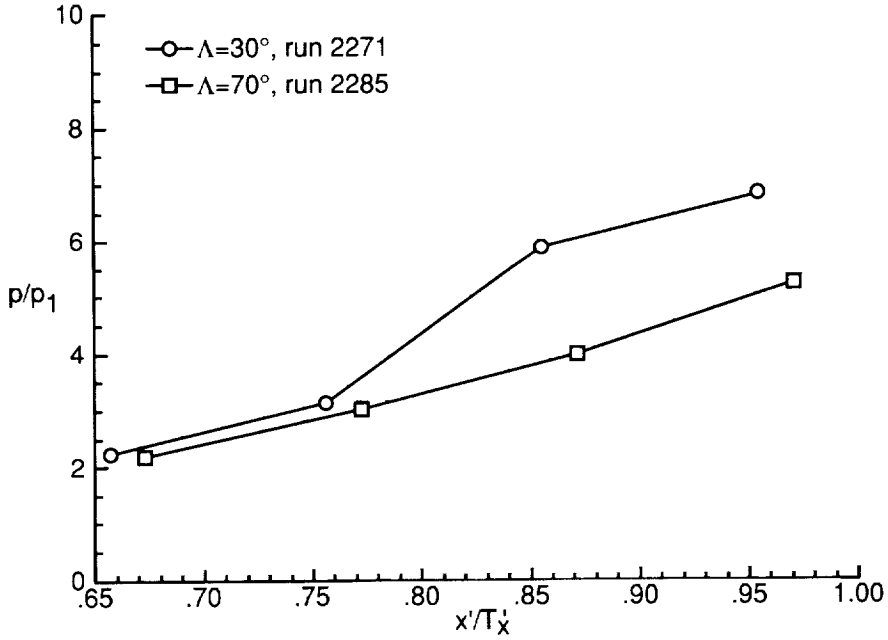

(b) Sidewall at $y/H = 0.13$.

Figure 31. Leading-edge sweep effects on pressure distributions of both models with CR = 5, no cowl, and $N_{Re} = 5.50 \times 10^5$ per foot.

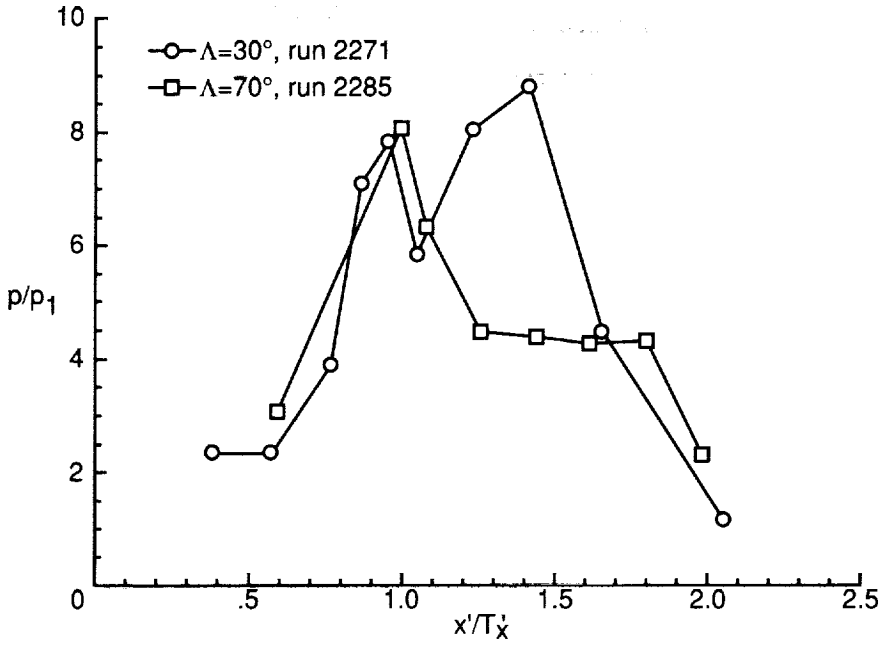

(c) Sidewall centerline.

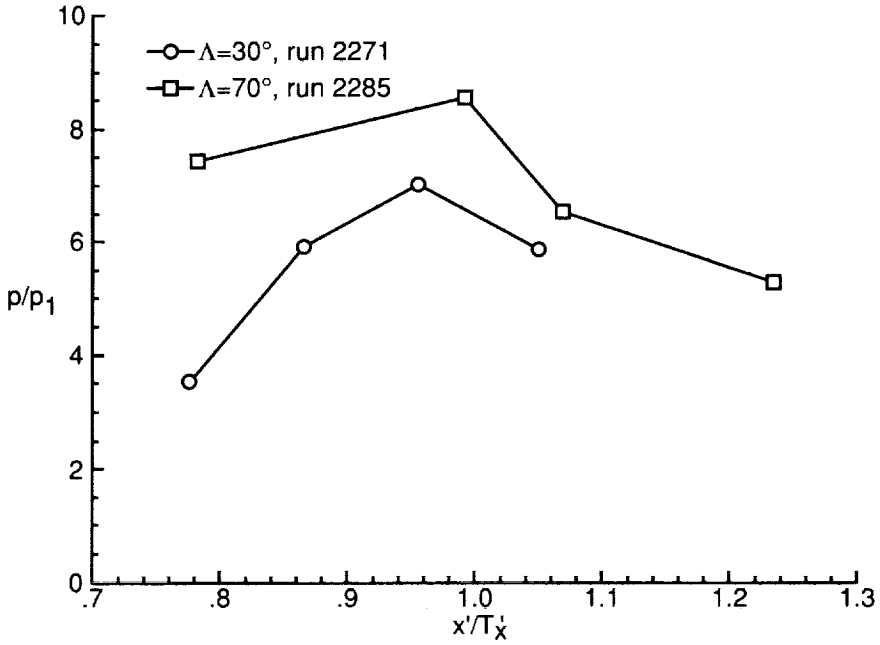

(d) Sidewall at $y/H = 0.87$.

Figure 31. Concluded.

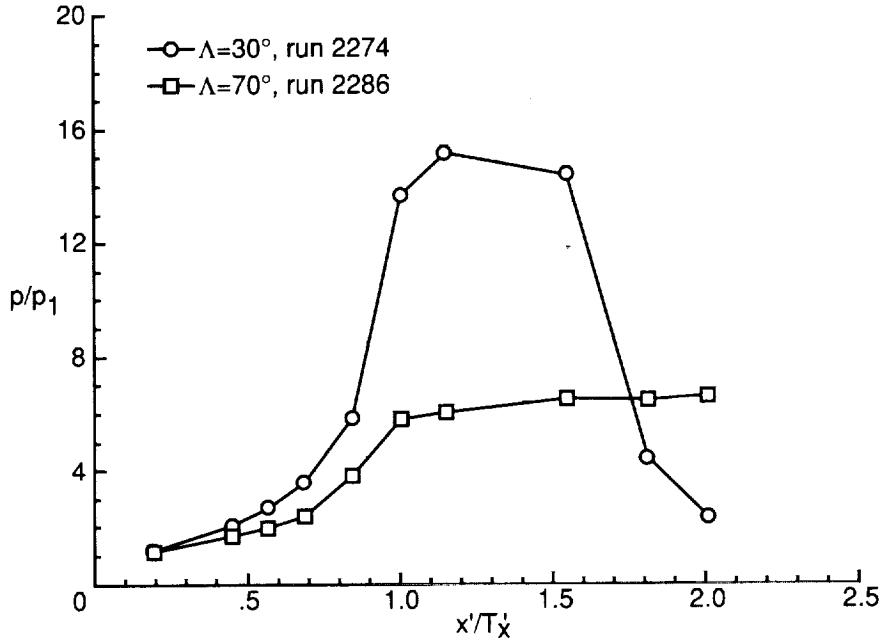

(a) Baseplate centerline.

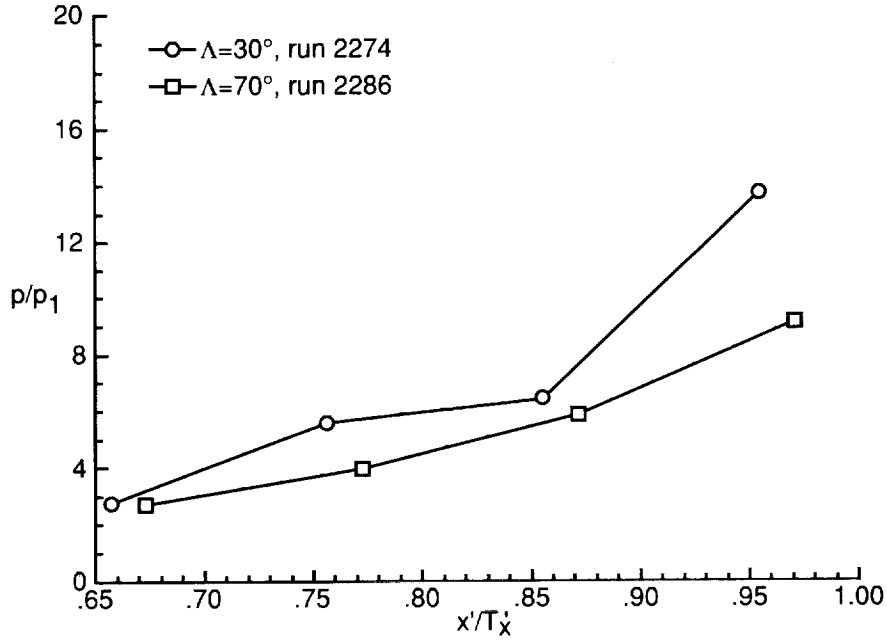

(b) Sidewall at $y/H = 0.13$.

Figure 32. Leading-edge sweep effects on pressure distributions of both models with CR = 9, no cowl, and $N_{Re} = 5.50 \times 10^5$ per foot.

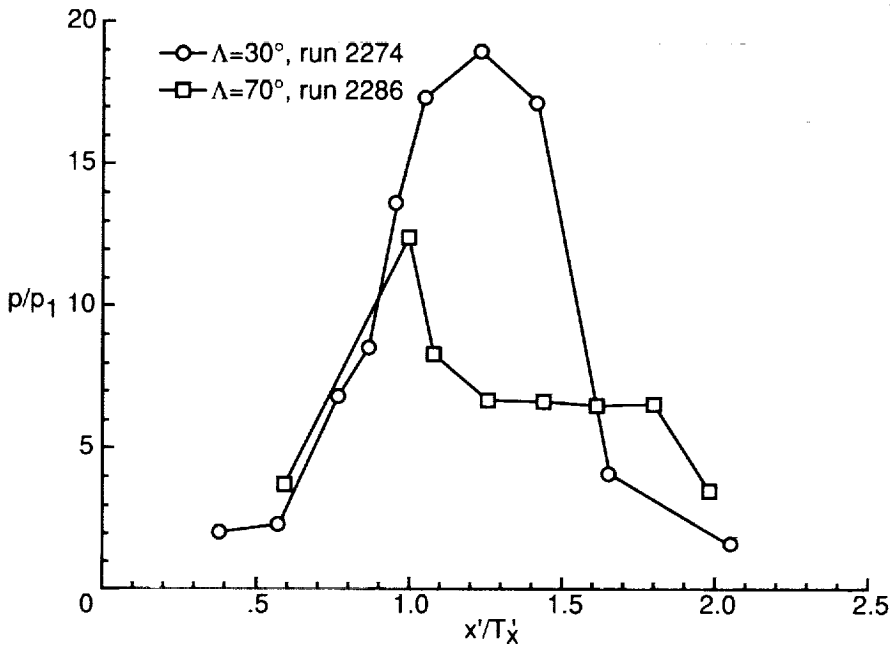

(c) Sidewall centerline.

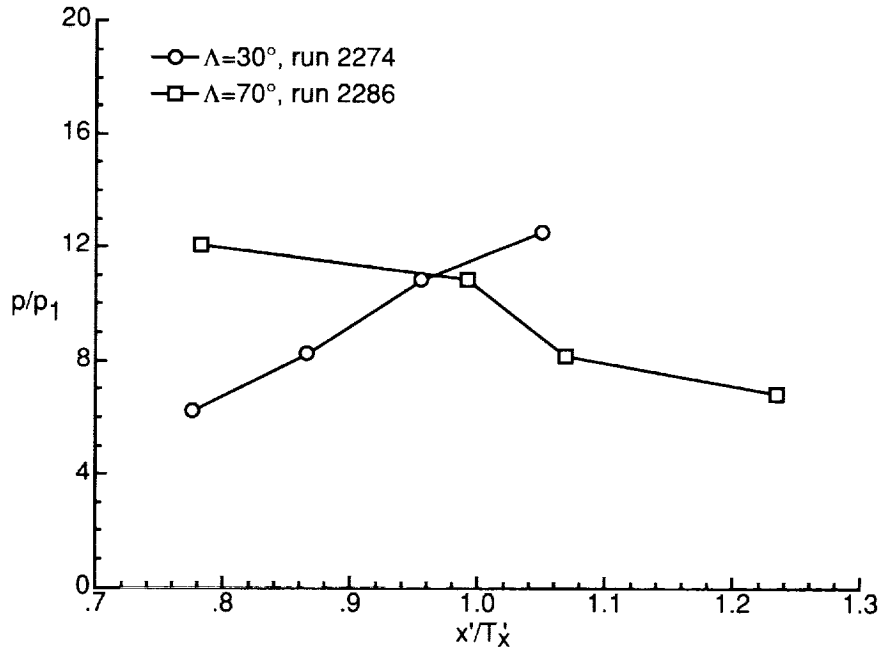

(d) Sidewall at $y/H = 0.87$.

Figure 32. Concluded.

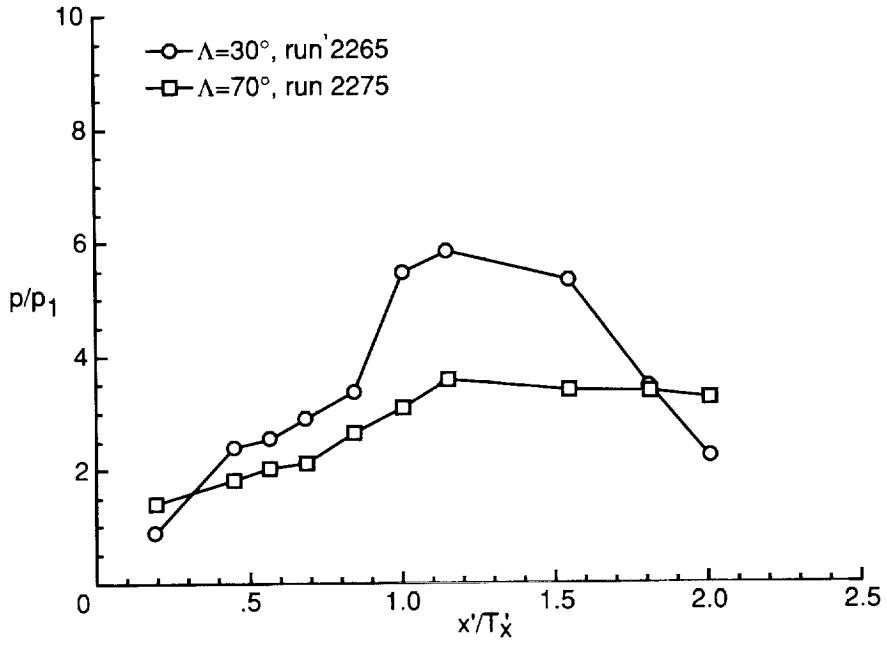

(a) Baseplate centerline.

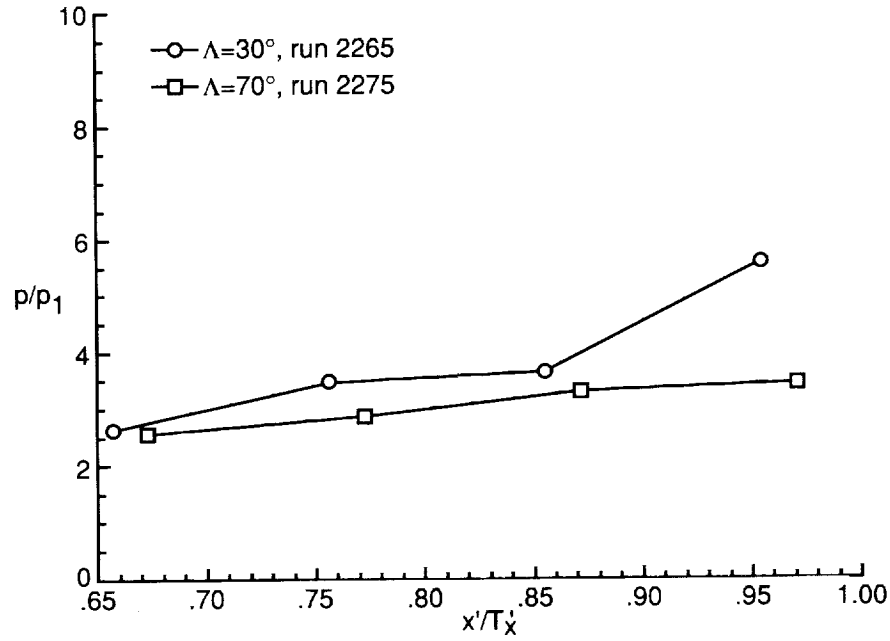

(b) Sidewall at $y/H = 0.13$.

Figure 33. Leading-edge sweep effects on pressure distributions of both models with CR = 3, 0-percent cowl, and $N_{Re} = 0.89 \times 10^5$ per foot.

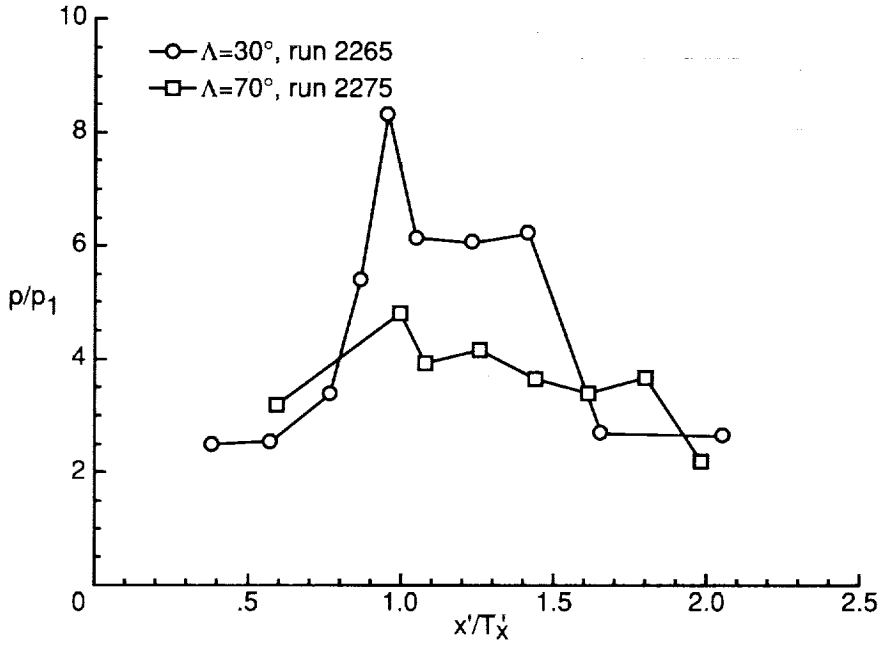

(c) Sidewall centerline.

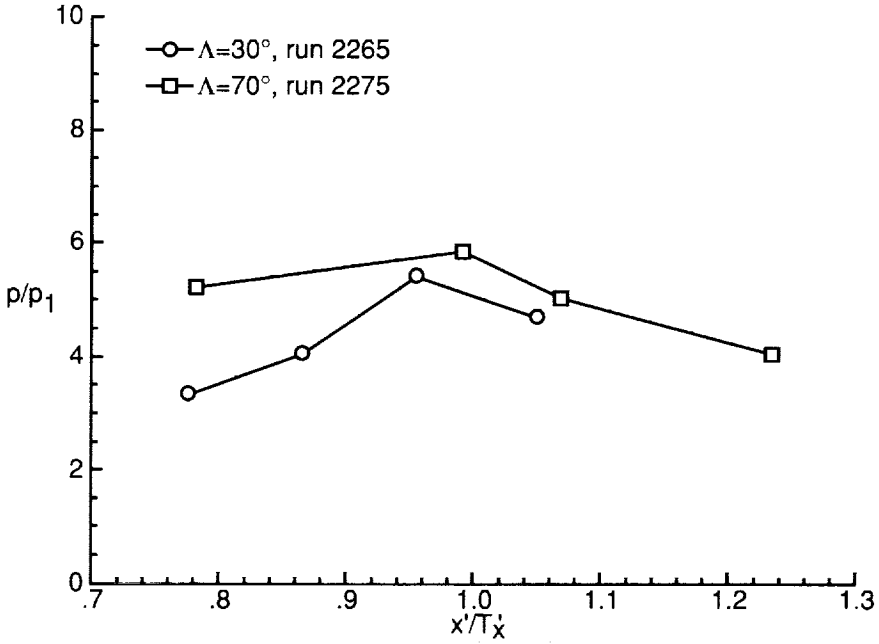

(d) Sidewall at $y/H = 0.87$.

Figure 33. Concluded.

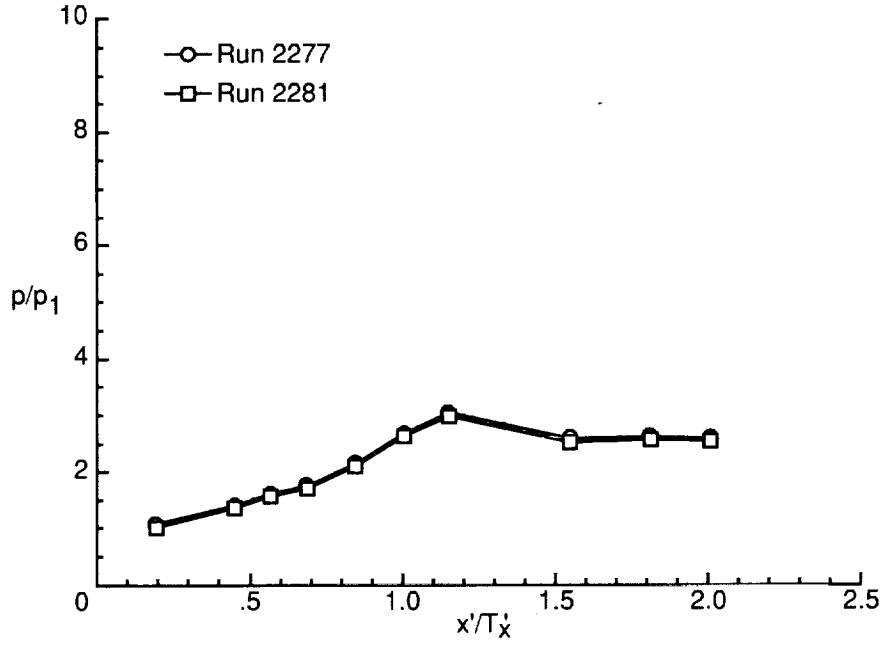

(a) Baseplate centerline.

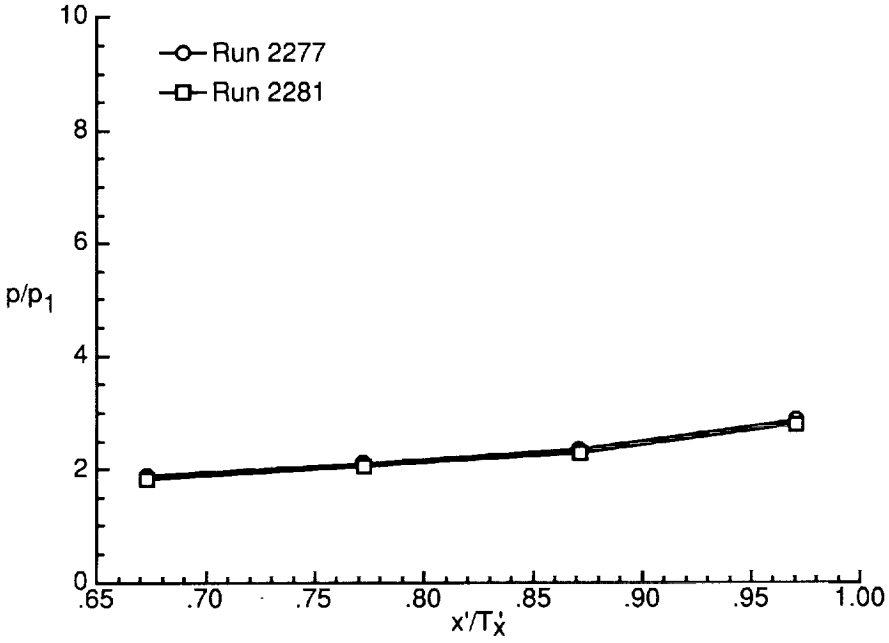

(b) Sidewall at $y/H = 0.13$.

Figure 34. Repeatability effects on pressure distributions of $\Lambda = 70°$ model with 0-percent cowl and $N_{Re} = 5.50 \times 10^5$ per foot.

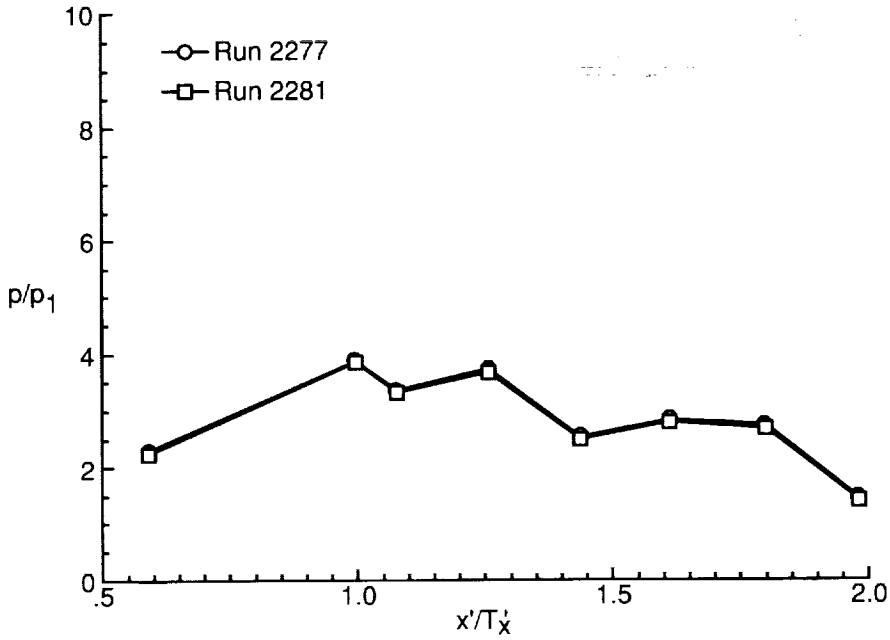

(c) Sidewall centerline.

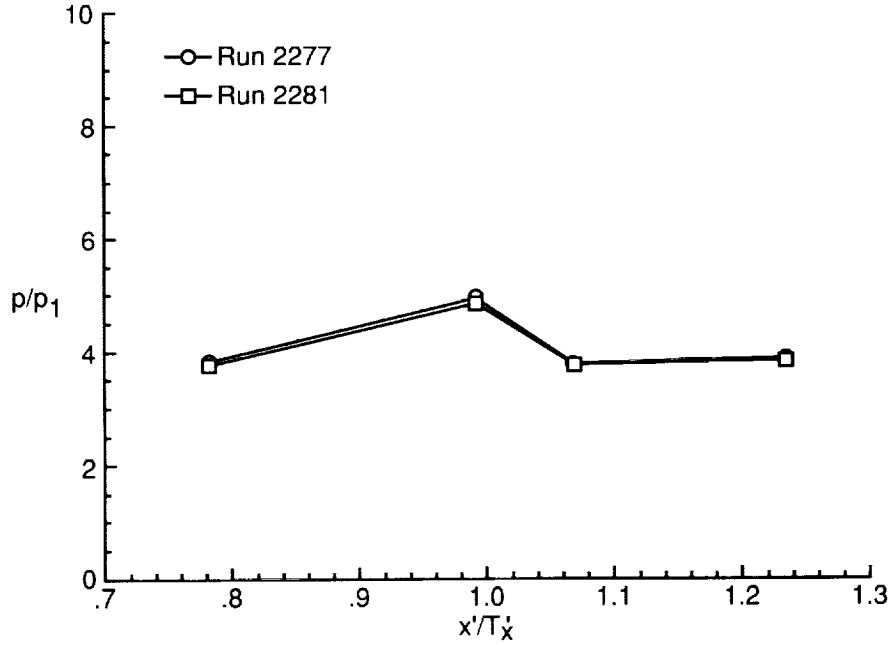

(d) Sidewall at $y/H = 0.87$.

Figure 34. Concluded.

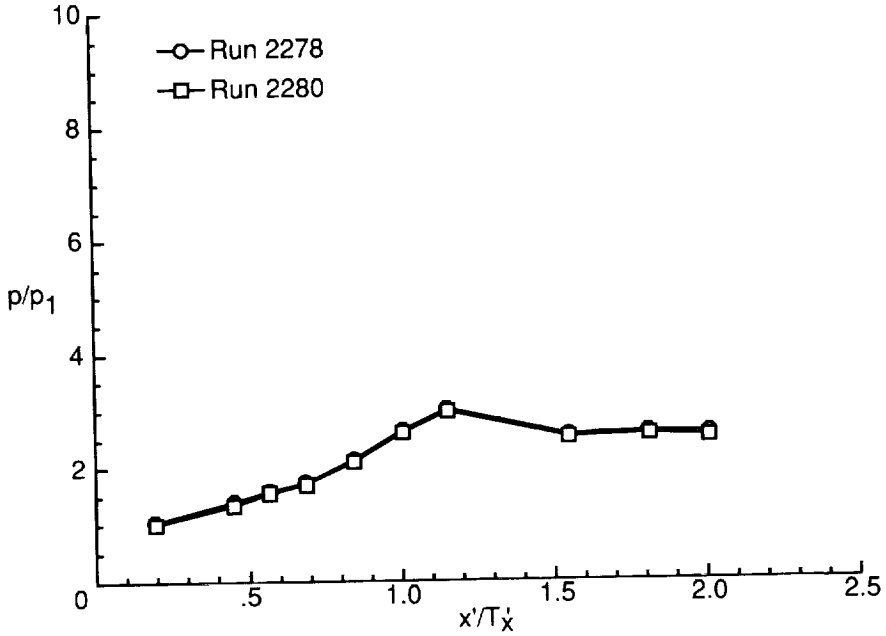

(a) Baseplate centerline.

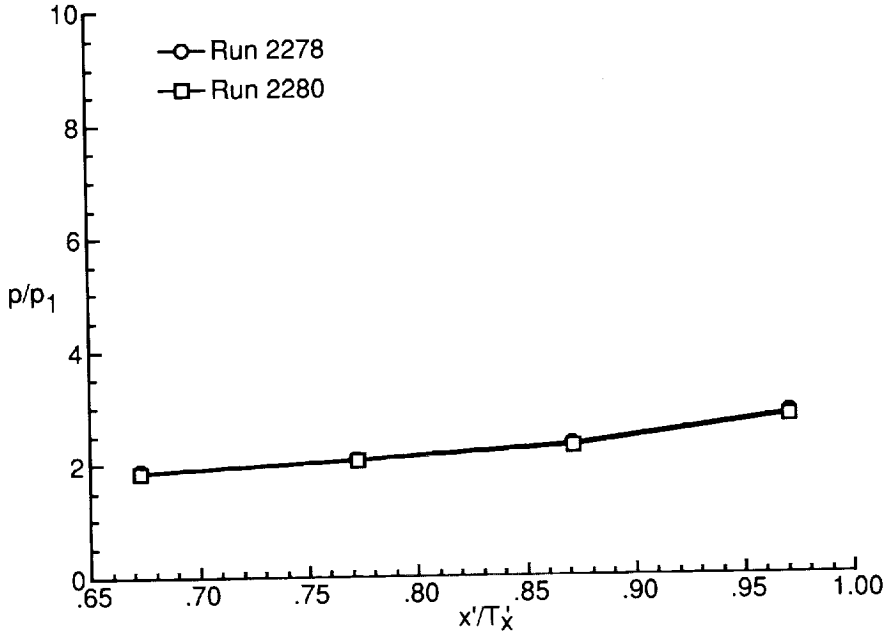

(b) Sidewall at $y/H = 0.13$.

Figure 35. Repeatability effects on pressure distributions of $\Lambda = 70°$ model with 25-percent cowl and $N_{Re} = 5.50 \times 10^5$ per foot.

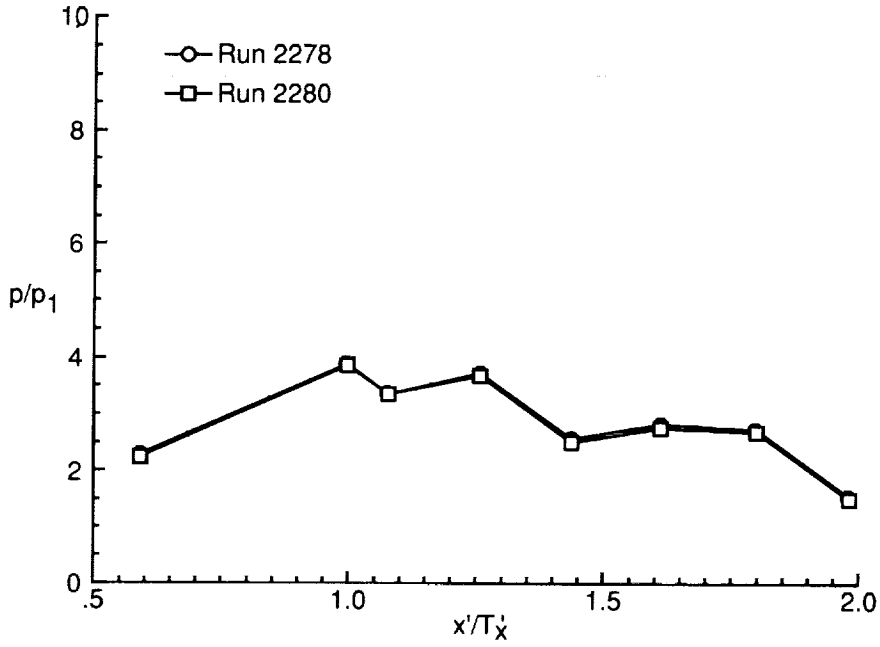

(c) Sidewall centerline.

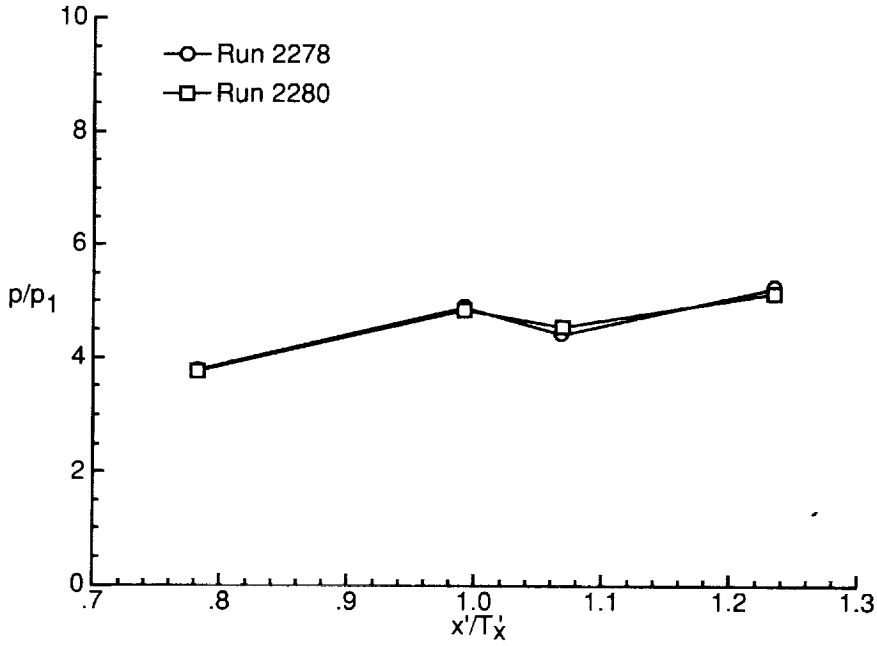

(d) Sidewall at $y/H = 0.87$.

Figure 35. Concluded.

REPORT DOCUMENTATION PAGE

Form Approved
OMB No. 0704-0188

1. AGENCY USE ONLY *(Leave blank)*	2. REPORT DATE	3. REPORT TYPE AND DATES COVERED
	August 1993	Technical Memorandum

4. TITLE AND SUBTITLE
Schlieren Photographs and Internal Pressure Distributions for Three-Dimensional Sidewall-Compression Scramjet Inlets at a Mach Number of 6 in CF_4

5. FUNDING NUMBERS
WU 506-40-41-02

6. AUTHOR(S)
Scott D. Holland

7. PERFORMING ORGANIZATION NAME(S) AND ADDRESS(ES)
NASA Langley Research Center
Hampton, VA 23681-0001

8. PERFORMING ORGANIZATION REPORT NUMBER
L-17206

9. SPONSORING/MONITORING AGENCY NAME(S) AND ADDRESS(ES)
National Aeronautics and Space Administration
Washington, DC 20546-0001

10. SPONSORING/MONITORING AGENCY REPORT NUMBER
NASA TM-4479

11. SUPPLEMENTARY NOTES

12a. DISTRIBUTION/AVAILABILITY STATEMENT
Unclassified Unlimited

Subject Category 34

12b. DISTRIBUTION CODE

13. ABSTRACT *(Maximum 200 words)*

Three-dimensional sidewall-compression scramjet inlets with leading-edge sweeps of 30° and 70° have been tested in the Langley Hypersonic CF_4 Tunnel at a Mach number of 6 and a free-stream ratio of specific heats of 1.2. The parametric effects of leading-edge sweep, cowl position, contraction ratio, and Reynolds number were investigated. The models were instrumented with static pressure orifices distributed on the sidewalls, baseplate, and cowl. Schlieren movies were made of selected tunnel runs for flow visualization of the entrance plane and cowl region. Although these movies could not show the internal flow, the effect of the internal flow on the external flow was evident by way of spillage. The purpose of the present report is to provide a preliminary data release for the investigation. The models, facility, and testing methods are described, and the test matrix and a tabulation of tunnel runs are provided. Line plots highlighting the stated parametric effects and a representative set of schlieren photographs are presented without analysis.

14. SUBJECT TERMS
Hypersonics; Inlets; Schlieren photographs; CF_4 tests; Pressure distributions

15. NUMBER OF PAGES
141

16. PRICE CODE
A07

17. SECURITY CLASSIFICATION OF REPORT	18. SECURITY CLASSIFICATION OF THIS PAGE	19. SECURITY CLASSIFICATION OF ABSTRACT	20. LIMITATION OF ABSTRACT
Unclassified	Unclassified		

NSN 7540-01-280-5500

Standard Form 298(Rev. 2-89)
Prescribed by ANSI Std. Z39-18
298-102